



Harnessing Visible Light for the Development of Novel Synthetic Strategies

Marco Michele Mastandrea

ADVERTIMENT. L'accés als continguts d'aquesta tesi doctoral i la seva utilització ha de respectar els drets de la persona autora. Pot ser utilitzada per a consulta o estudi personal, així com en activitats o materials d'investigació i docència en els termes establerts a l'art. 32 del Text Refós de la Llei de Propietat Intel·lectual (RDL 1/1996). Per altres utilitzacions es requereix l'autorització prèvia i expressa de la persona autora. En qualsevol cas, en la utilització dels seus continguts caldrà indicar de forma clara el nom i cognoms de la persona autora i el títol de la tesi doctoral. No s'autoritza la seva reproducció o altres formes d'explotació efectuades amb finalitats de lucre ni la seva comunicació pública des d'un lloc aliè al servei TDX. Tampoc s'autoritza la presentació del seu contingut en una finestra o marc aliè a TDX (framing). Aquesta reserva de drets afecta tant als continguts de la tesi com als seus resums i índexs.

ADVERTENCIA. El acceso a los contenidos de esta tesis doctoral y su utilización debe respetar los derechos de la persona autora. Puede ser utilizada para consulta o estudio personal, así como en actividades o materiales de investigación y docencia en los términos establecidos en el art. 32 del Texto Refundido de la Ley de Propiedad Intelectual (RDL 1/1996). Para otros usos se requiere la autorización previa y expresa de la persona autora. En cualquier caso, en la utilización de sus contenidos se deberá indicar de forma clara el nombre y apellidos de la persona autora y el título de la tesis doctoral. No se autoriza su reproducción u otras formas de explotación efectuadas con fines lucrativos ni su comunicación pública desde un sitio ajeno al servicio TDR. Tampoco se autoriza la presentación de su contenido en una ventana o marco ajeno a TDR (framing). Esta reserva de derechos afecta tanto al contenido de la tesis como a sus resúmenes e índices.

WARNING. Access to the contents of this doctoral thesis and its use must respect the rights of the author. It can be used for reference or private study, as well as research and learning activities or materials in the terms established by the 32nd article of the Spanish Consolidated Copyright Act (RDL 1/1996). Express and previous authorization of the author is required for any other uses. In any case, when using its content, full name of the author and title of the thesis must be clearly indicated. Reproduction or other forms of for profit use or public communication from outside TDX service is not allowed. Presentation of its content in a window or frame external to TDX (framing) is not authorized either. These rights affect both the content of the thesis and its abstracts and indexes.



UNIVERSITAT
ROVIRA I VIRGILI



Harnessing Visible Light for the Development of Novel Synthetic Strategies

Marco Michele Mastandrea



DOCTORAL THESIS
2020

UNIVERSITAT ROVIRA I VIRGILI

Harnessing Visible Light for the Development of Novel Synthetic Strategies

Marco Michele Mastandrea

UNIVERSITAT ROVIRA I VIRGILI

Harnessing Visible Light for the Development of Novel Synthetic Strategies

Marco Michele Mastandrea

Harnessing Visible Light for the Development of Novel Synthetic Strategies

Doctoral Thesis by
Marco Michele Mastandrea

Developed under the supervision of:
Prof. Miquel A. Pericàs



Departament de Química Analítica i Química Orgànica (URV)
Institut Català d'Investigació Química (ICIQ)

Tarragona
2020

UNIVERSITAT ROVIRA I VIRGILI

Harnessing Visible Light for the Development of Novel Synthetic Strategies

Marco Michele Mastandrea



UNIVERSITAT ROVIRA I VIRGILI



Prof. Miquel A. Pericàs Brondo, Group Leader and Director of the Institute of Chemical Research of Catalonia (ICIQ),

STATE, that the present Doctoral Thesis entitled: "**Harnessing Visible Light for the Development of Novel Synthetic Strategies**", presented by Marco M. Mastandrea to receive the degree of Doctor, has been carried out under my supervision at the Institute of Chemical Research of Catalonia (ICIQ).

Tarragona, 16th September 2020

Prof. Miquel A. Pericàs Brondo

UNIVERSITAT ROVIRA I VIRGILI

Harnessing Visible Light for the Development of Novel Synthetic Strategies

Marco Michele Mastandrea

Acknowledgments

First, I would like to express my gratitude to *Prof. Miquel Pericàs*, for giving me the opportunity to be part of his research group at ICIQ. During this period, he has always showed the deepest support for my research, but especially confidence in me as a person and a chemist.

I would also like to thank all the former and current lab mates of the Pericàs group. I will always be grateful to your joyful and helpful nature. I would like to emphasize the help of my co-workers, *Evgeny*, *Laura* and *Santi*. Last but not least, *Carles* for helping me day by day in this journey and being able to put a smile on my face even in the worst days.

During my PhD thesis, I have had the chance to perform a short stay at UCB Pharma. I would like to thank all the people that warmly welcomed me. In particular, I am grateful to *Teresa*, *Benedicte*, *Patrick*, *Matthieu* and *Dominique*.

Ci tengo a ringraziare tutti coloro che sono stati miei compagni di avventura durante il periodo trascorso qui a Tarragona per la loro sincera amicizia e l'affetto dimostratomi. Grazie *Benedetta*, *Daniele* e *Giandomenico* per tutto quello che avete fatto per me. Probabilmente non riuscirò mai ad esprimere a parole la mia gratitudine, ma avrò sempre un posto speciale per voi nei miei ricordi.

Voglio anche ringraziare i miei amici di sempre *Enrico*, *Francesco* (*Bob*) e *Giuseppe* semplicemente per esserci ed esserci stati.

Infine, la *mia famiglia* per tutto l'amore e il supporto incondizionato. Senza di voi tutto questo non sarebbe stato possibile.

UNIVERSITAT ROVIRA I VIRGILI

Harnessing Visible Light for the Development of Novel Synthetic Strategies

Marco Michele Mastandrea

Financial sources

The present doctoral thesis has been possible thanks to the funding received from ICIQ Foundation (ICIQ grant 2016/14) as well as from the following projects:

CERCA Programme/Generalitat de Catalunya, AEI/MINECO/FEDER (Grants: CTQ2015-69136-R and PID2019-109236RB-I00) and AGAUR (Grants: 2014SGR827 and 2017SGR1139)



Unión Europea

Fondo Europeo
de Desarrollo Regional
"Una manera de hacer Europa"



UNIVERSITAT ROVIRA I VIRGILI

Harnessing Visible Light for the Development of Novel Synthetic Strategies

Marco Michele Mastandrea

A mia madre

UNIVERSITAT ROVIRA I VIRGILI

Harnessing Visible Light for the Development of Novel Synthetic Strategies

Marco Michele Mastandrea

Table of Contents

List of Publications	III
Overall Goals	V
Summary	VII
CHAPTER I. General Introduction	1
I.1. Radicals in organic chemistry	3
I.2. Photoredox catalysis	5
I.2.1 General principles	7
I.2.2 Photoredox organocatalysis	13
I.2.3 Metallaphotocatalysis	23
I.3. Electron donor-acceptor complexes	32
I.3.1 Photophysical background	33
I.3.2 Synthetic applications	34
CHAPTER II. Asymmetric cross-dehydrogenative coupling of aldehydes with xanthenes	41
II.1. Introduction	43
II.1.1 Cross dehydrogenative coupling	43
II.1.2 Alkylation of benzylic C–H bonds	45
II.1.3 Asymmetric oxidative enamine catalysis	49
II.2. Objective	53
II.3. Asymmetric photoredox CDC of aldehydes with xanthenes	56
II.3.1 HTE screening and control experiments	56
II.3.2 Reaction scope	59
II.3.3 Mechanistic investigation	64
II.3.4 Conclusions	68
II.4. Supporting information	69
CHAPTER III. Decarboxylative hydroalkylation of alkynes	153
III.1. Introduction	155
III.1.1 Addition of C-centered radicals to alkynes	155
III.1.2 Double bond photoisomerization	157
III.1.3 Copper in visible-light photocatalysis	161
III.2. Objective	166
III.3. Dual Cu-photoredox catalyzed hydroalkylation of alkynes	168
III.3.1 HTE screening and control experiments	168
III.3.2 Reaction scope	170
III.3.3 Mechanistic investigation	174
III.3.4 Conclusions	178

III.4. Supporting information	180
CHAPTER IV. Anion-π interactions in light-induced reactions	225
IV.1. Introduction	227
IV.1.1 Anion- π interactions	227
IV.1.2 Anion- π catalysis	229
IV.1.3 Nitrogen-centered radicals	230
IV.1.4 Amidyl radicals	233
IV.2. Objective	241
IV.3. Anion- π interactions driven amidation of aromatic systems	244
IV.3.1 Preliminary studies and optimization	244
IV.3.2 Reaction scope	246
IV.3.3 Mechanistic investigation	249
IV.3.4 Conclusions	256
IV.4. Supporting information	257
CHAPTER V. Conclusions	281

List of Publications

The following publications are based on the work described in this thesis:

1. Evgeny Larionov, Marco M. Mastandrea and Miquel À. Pericàs
Asymmetric Visible-Light Photoredox Cross-Dehydrogenative
Coupling of Aldehydes with Xanthenes
ACS Catal. **2017**, *7*, 7008-7013.
2. Laura Buglioni, Marco M. Mastandrea, Antonio Frontera and Miquel À. Pericàs
Anion- π Interactions in Light-Induced Reactions: Role in the
Amidation of (Hetero)aromatic Systems with Activated *N*-
Aryloxyamides
Chem. Eur. J. **2019**, *25*, 11785-11790.
3. Marco M. Mastandrea, Santiago Cañellas, Xisco Caldentey and
Miquel À. Pericàs
Decarboxylative Hydroalkylation of Alkynes via Dual Copper-
Photoredox Catalysis
ACS Catal. **2020**, *10*, 6402-6408

UNIVERSITAT ROVIRA I VIRGILI

Harnessing Visible Light for the Development of Novel Synthetic Strategies

Marco Michele Mastandrea

Overall Goals

The main goal of the present thesis is the development of new synthetic strategies employing visible light as an economical and environmentally benign source of energy. Photoredox catalysis paradigm will be central in this manuscript, declined in its combination with organo- and metal-catalysis. Moreover, the participation of anion- π interactions in light-induced reactions will be explored in the amidation of aromatic systems with *N*-aryloxy amides.

Following these guidelines, the goals of each chapter are:

- **Chapter I.** Provide the background and fundamental concepts used in the following chapters. Photoredox catalysis principles, photoredox organocatalysis, metallaphotocatalysis and electron donor-acceptor complexes photochemistry will be disclosed herein.
- **Chapter II.** The merger of enamine and photoredox catalysis to enable the asymmetric coupling between xanthenes and aldehydes.
- **Chapter III.** The development of a dual copper and photoredox catalyzed decarboxylative hydroalkylation of terminal alkynes from carboxylic acids as radical sources and an organic photocatalyst.
- **Chapter IV.** The demonstration that the formation of an anion- π complex between inorganic anions and an electron-poor *N*-aryloxyamide can drive the photochemical amidation of aromatic substrates.
- **Chapter V.** Summarize the most important conclusions disclosed in the present thesis.

UNIVERSITAT ROVIRA I VIRGILI

Harnessing Visible Light for the Development of Novel Synthetic Strategies

Marco Michele Mastandrea

Summary

The first research project, included in Chapter II, shows the development of a methodology for the catalytic asymmetric cross-coupling of two C(sp³)-H bonds. Photoredox catalysis is used for the two-step oxidation of a diarylmethane to the corresponding cation, which is then trapped by an enamine intermediate generated in situ from an aldehyde and a secondary amine organocatalyst. Notably, this mild method is an ideal synthetic approach from the green chemistry point of view. It does not require preinstallation of functional groups, thereby constituting an atom economical, efficient transformation, and it allows the formation of a C-C bond with simultaneous installation of one or two new stereocenters in a highly enantio- and diastereoselective manner. Mechanistic studies by experimental and computational methods aid to clarify the origin of the observed enantioselectivity.

The second project, shown in Chapter III, illustrates a novel photoredox strategy for the synthesis of a wide range of allylic amines and ethers from carboxylic acids and alkynes. This approach relies on the activation of terminal alkynes through the formation and photoexcitation of copper acetylide intermediates. This process takes place through cooperative copper and organic photoredox catalysis and can be carried out in stereodivergent manner. Thus, a systematic multivariate HTE screening spotlighted that a switch in the stereochemical outcome can be provoked by choosing an appropriate combination of ligand and base. The developed methodology has been applied to the stereoselective coupling of primary, secondary and tertiary alkyl radicals with (hetero)aromatic terminal alkynes. As an additional practicality, similar reaction conditions allowed for the use of aromatic amines as radical precursors in a cross dehydrogenative coupling for the direct vinylation of inactivated C-H bonds.

Finally, Chapter IV shows the discovery of the participation of anion- π interactions in light-induced reactions. We demonstrated, in particular, how transient complexes formed through noncovalent anion- π interactions between electron-poor *N*-aryloxyamides and multiply-charged anions (such as carbonate or phosphate) can undergo facile light-promoted N-O cleavage, affording amidyl radicals that can subsequently be trapped by (hetero)aromatics.

UNIVERSITAT ROVIRA I VIRGILI

Harnessing Visible Light for the Development of Novel Synthetic Strategies

Marco Michele Mastandrea

UNIVERSITAT ROVIRA I VIRGILI

Harnessing Visible Light for the Development of Novel Synthetic Strategies

Marco Michele Mastandrea

CHAPTER I

General introduction

I.1. Radicals in organic chemistry	3
I.2. Photoredox catalysis	5
I.2.1. General principles	7
I.2.2. Photoredox organocatalysis	13
I.2.3. Metallaphotocatalysis	23
I.3. Electron donor-acceptor complexes	32
I.3.1. Photophysical background	33
I.3.2. Synthetic applications	34

UNIVERSITAT ROVIRA I VIRGILI

Harnessing Visible Light for the Development of Novel Synthetic Strategies

Marco Michele Mastandrea

CHAPTER I

General introduction

I.1. Radicals in organic chemistry

Nowadays, organic chemistry must face the growing demand of modern society for new industrial solutions and innovative products. The development of sustainable procedures involving natural raw materials and non-toxic chemicals in combination with strongly efficient processes has gained fundamental importance.¹ Thus, the need to accomplish these highly demanding requirements is constantly driving organic chemists to find new approaches in synthesis.

The synergy between organic synthesis and radical chemistry, emerged in the last three decades, produced an extensive toolkit of reactions and knowledge (*i.e.* reliable kinetic data and stereoselectivity models) that allowed radical reactions, previously perceived as uncontrollable, to be considered in retrosynthetic planning. Radical reactions main pros are mildness and functional group tolerance (protecting groups are often unnecessary). Moreover, the influence of solvation and aggregation state is often negligible and the characteristic early transition states make possible the construction of densely functionalized, quaternary centers. The latter aspect, combined with the easy implementation of cascade and radical-ion crossover reactions, suits for the step-economical synthesis of natural products and bio-active compounds. Finally, radical processes often follow

¹ a) Sheldon, R. A. *Top. Curr. Chem.* **1993**, *164*, 21-43; b) Anastas, P. T.; Warner, J. C. *Green Chemistry. Theory and Practice*, Oxford University Press, New York, **1998**; c) Trost, B. M. *Science* **1991**, *254*, 1471-1477; d) Trost, B. M. *Acc. Chem. Res.* **2002**, *35*, 695-705; e) Trnka, T. M.; Grubbs, R. H. *Acc. Chem. Res.* **2001**, *34*, 18-29.

General introduction

reaction pathways that are complementary to classical methods proceeding via ionic intermediates.²

The main issue that has thwarted the exploitation and appreciation of radical reactions is the classical approach used for radical intermediates generation. Traditionally, hazardous radical initiators have been employed in this task aided by toxic reagents (e.g., Bu₃SnH), and in many cases high-temperature or high-energy UV irradiation (Figure I-1, a). Initiators {e.g., AIBN [2,2'-azobis(isobutyronitrile)] and BEt₃ (triethylborane)} undergo homolysis induced by heat or UV light generating in turn radicals able to perform hydrogen or halogen-atom abstraction on suitable substrates. Besides the extreme efficiency of this strategy, the need for very reactive species or harsh conditions limited the selectivity and hampered the functional group tolerance of the ensuing radical processes. Methodologies later developed by Barton (Figure I-1, b)³ and Zard (Figure I-1, c),⁴ based on purposely designed stoichiometric reagents, furnished a solid milder alternative to traditional strategies but so far have not found a comparable level of utilization. An attractive alternative is the generation of radicals through redox chemistry. Radicals can emerge upon single electron oxidation of anions and electron-rich species (through fragmentation of the corresponding radical cation) (Figure I-1, d) or single electron reduction of cation and electron poor precursors (through fragmentation of the corresponding radical anion) (Figure I-1, e). Nevertheless, this approach

² a) Studer, A.; Chatgililoglu, C. *Encyclopedia of Radicals in Chemistry, Biology and Materials*, vol. 1 and 2, John Wiley & Sons, Chichester, **2012**; b) Renaud, P.; Sibi, M. P. *Radicals in Organic Synthesis*, vol. 1 and 2, Wiley-VCH, New York, **2001**; c) Gansäuer, A. *Radicals in Synthesis I & II, in Topics in Current Chemistry*, vol. 263 and 264, Springer, Heidelberg, **2006**; d) Curran, D.P.; Porter, N.A.; Giese, B. *Stereochemistry of Radical Reactions*, VCH, Weinheim. **1995**; e) Yan, M.; Lo, J. C.; Edwards, J. T.; Baran, P. S. *J. Am. Chem. Soc.* **2016**, *138*, 12692–12714.

³ a) Barton, D. H. R.; McCombie, S. W. *J. Chem. Soc. Perkin Trans. 1* **1975**, *16*, 1574-1585; b) Barton, D. H. R.; Crich, D.; Motherwell, W. B. *J. Chem. Soc., Chem. Commun.* **1983**, *17*, 939-941; c) Barton, D. H. R.; Zard, S. Z. *Pure Appl. Chem.* **1986**, *58*, 675-684.

⁴ a) Delduc, P.; Tailhan, C.; Zard, S. Z. *J. Chem. Soc., Chem. Commun.* **1988**, *4*, 308-310; b) Zard, S. Z. *Angew. Chem. Int. Ed.* **1997**, *36*, 672-685.

has generally relied upon the use of stoichiometric metals and harsh reaction conditions.

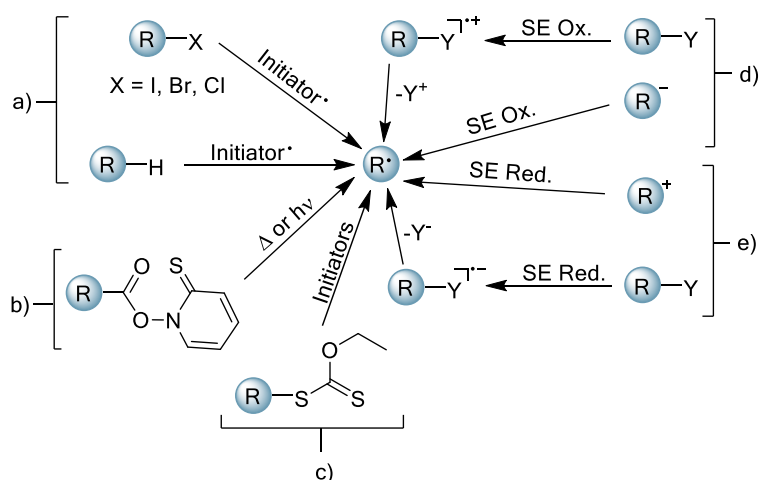


Figure I-1. Classic approach to radicals.

I.2. Photoredox Catalysis

The need to overcome the intrinsic limitation of classical radical chemistry pushed chemists to develop a new way to access radicals. The milestone of this novel approach to radical generation for chemical synthesis is the concept that visible light can be converted into chemical energy under controlled and mild conditions. In this sense, the translation of photoredox catalysis fundamental principles to organic synthesis has been an authentic revolution. For almost fifty years, photoredox catalysis has found widespread application in the areas of carbon dioxide reduction,⁵ watersplitting,⁶ solar-cell materials⁷ and only sporadically in organic

⁵ Takeda, H.; Ishitani, O. *Coord. Chem. Rev.* **2010**, *254*, 346-354.

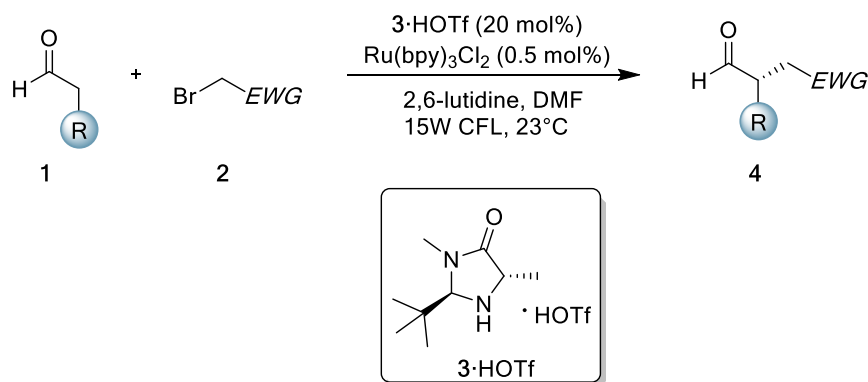
⁶ Graetzel, M. *Acc. Chem. Rev.* **1981**, *14*, 376-384.

⁷ Kalyanasundaram, K.; Grätzel, M. *Coord. Chem. Rev.* **1988**, *177*, 347-414.

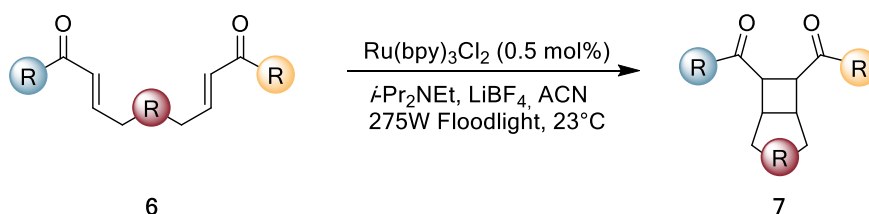
General introduction

synthesis.⁸

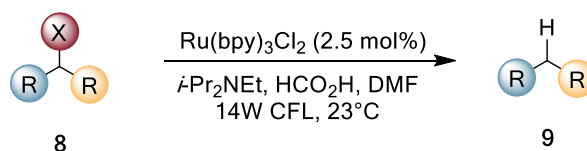
a) MacMillan, 2008



b) Yoon, 2008



c) Stephenson, 2009



Scheme I-1. a) Merger of organocatalysis with photoredox catalysis to promote the asymmetric α -alkylation of aldehydes; b) visible light photocatalysis of [2+2] enone cycloadditions; c) reductive dehalogenation using photoredox catalysis. X = Cl, Br.

⁸ a) Hedstrand, D. M.; Kruizinga, W. H.; Kellogg, R. M. *Tetrahedron Lett.* **1978**, *19*, 1255-1258; b) Van Bergen, T. J.; Hedstrand, D. M.; Kruizinga, W. H.; Kellogg, R. M. *J. Org. Chem.* **1979**, *44*, 4953-4962; c) Pac, C.; Ihama, M.; Yasuda, M.; Miyauchi, Y.; Sakurai, H. *J. Am. Chem. Soc.* **1981**, *103*, 6495-6497; d) Cano-Yelo, H.; Deronzier, A. *Tetrahedron Lett.* **1984**, *25*, 5517-5520; e) Cano-Yelo, H.; Deronzier, A. *J. Chem. Soc. Perkin Trans. 2* **1984**, 1093-1098; f) Goren, Z.; Willner, I. *J. Am. Chem. Soc.* **1983**, *105*, 7764-7765; g) Maidan, R.; Goren, Z.; Becker, J.Y.; Willner, I. *J. Am. Chem. Soc.* **1984**, *106*, 6217-6222; h) K. Hironaka, K.; Fukuzumi, S.; Tanaka, T. *J. Chem. Soc. Perkin Trans. 2* **1984**, 1705-1709.

However, after MacMillan (Scheme I-1, a),⁹ Yoon (Scheme I-1, b)¹⁰ and Stephenson (Scheme I-1, c)¹¹ groundbreaking reports on highly efficient visible light photoredox catalysis, last years have witnessed an authentic explosion in this field.¹²

1.2.1 General principles

Main actors in the renaissance of photoredox catalysis are organometallic polypyridyl transition metal complexes and organic dyes. Due to their peculiar photophysical and electrochemical properties, they exhibit high photocatalytic activity when irradiated with visible light. A well-studied example of transition-metal photocatalyst is Ru(bpy)₃²⁺. This complex shows a strong absorption band ($\lambda_{\text{max}} = 452 \text{ nm}$, $\epsilon = 14600 \text{ M}^{-1}\text{cm}^{-1}$) corresponding to a metal-to-ligand charge transfer (MLCT) transition. Irradiation at this wavelength results in the promotion of an electron from singlet ground state (**PC** ¹A₁) to one of the higher energy vibrational levels of the first singlet excited state (**PC*** ¹MLCT_n) (Figure I-2). This event is followed by rapid relaxation (internal conversion) to the lowest vibrational level of the first singlet excited state (**PC*** ¹MLCT₁). This state can regenerate the singlet ground state (*via* fluorescence or non-radiative pathway) or, more likely, undergo conversion to the lowest energy triplet excited state (**PC*** ³MLCT₁) through intersystem crossing (quantum yield to

⁹ Nicewicz, D. A.; MacMillan, D. W. C. *Science* **2008**, *322*, 77-80.

¹⁰ Ischay, M. A.; Anzovino, M. E.; Du, J.; Yoon, T. P. *J. Am. Chem. Soc.* **2008**, *130*, 12886-12887.

¹¹ Narayanam, J. M. R.; Tucker, J. W.; Stephenson, C. R. J. *J. Am. Chem. Soc.* **2009**, *131*, 8756-8757.

¹² (a) Narayanam, J. M. R.; Stephenson, C. R. J. *Chem. Soc. Rev.* **2011**, *40*, 102-113; (b) Xuan, J.; Xiao, W.-J. *Angew. Chem. Int. Ed.* **2012**, *51*, 6828-6838; (c) Reckenthäler, M.; Griesbeck, A. G. *Adv. Synth. Catal.* **2013**, *355*, 2727-2744; (d) Prier, C. K.; Rankic, D. A.; MacMillan, D. W. C. *Chem. Rev.* **2013**, *113*, 5322-5363; (e) Schultz, D. M.; Yoon, T. P. *Science* **2014**, *383*, 1239176(1-8); (f) Romero, N. A.; Nicewicz, D. A. *Chem. Rev.* **2016**, *116*, 10075-10166; (g) McAtee, R. C.; McClain, E. J.; Stephenson, C. R. J. *Trends in Chemistry* **2019**, *1*, 111-125.

General introduction

intersystem crossing $\Phi_{isc} \sim 1$ for $\text{Ru}(\text{bpy})_3^{2+}$ and vibrational relaxation. Since the transition of the triplet excited state to the singlet ground state is spin forbidden, the triplet excited state is reasonably long lived (triplet half-life $\tau_0 = 1100$ ns for $\text{Ru}(\text{bpy})_3^{2+}$) and can decay via radiative relaxation (phosphorescence) or non-radiative deactivation.

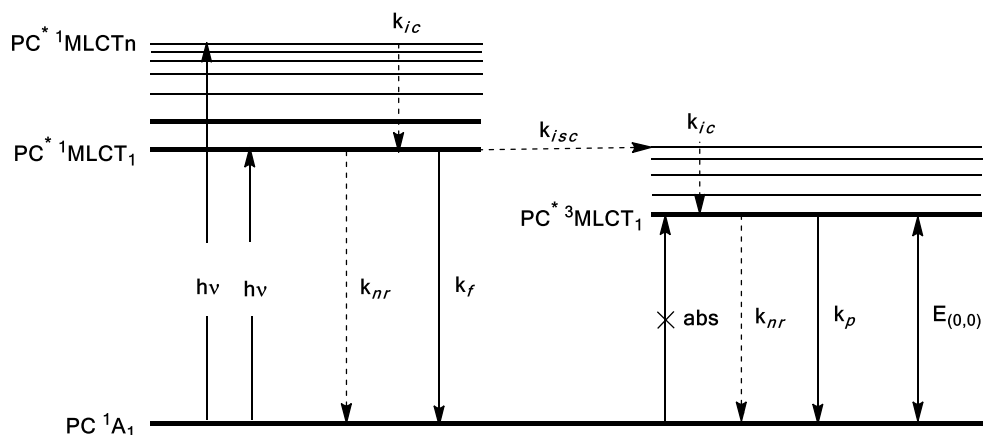
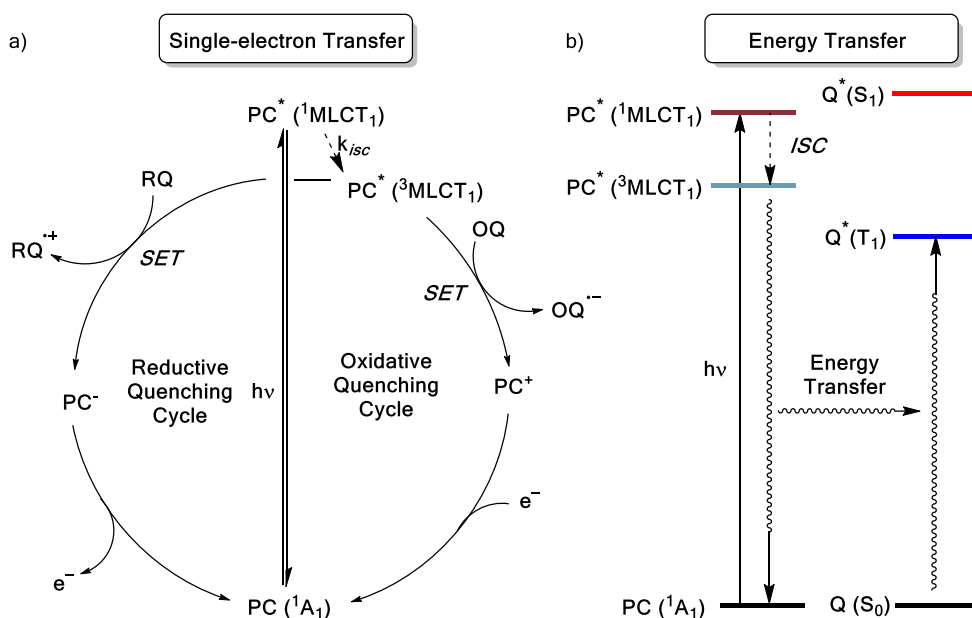


Figure I-2. Jablonski diagram for transition-metal photocatalyst. PC photocatalyst, k_{ic} rate of internal conversion, k_{isc} rate of intersystem crossing, k_{nr} rate of non-radiative deactivation, k_f fluorescence, k_p phosphorescence, $E_{(0,0)}$ = energy of emission from the triplet state.

Key concept for photocatalysis is that the long-lived triplet excited state can be quenched also in a bimolecular fashion *via* outer-sphere single electron transfer (SET) or energy transfer (EnT) processes involving suitable substrates. In the case of transition-metal centered photocatalyst, the coordinative saturation and conformation stability under reaction conditions make unlikely the binding between substrates and metal centers and, in turn, inner-sphere processes.

The depopulation of the photo-excited triplet state *via* electron transfer occurs through two different mechanisms: reductive quenching and oxidative quenching (Scheme I-2, a). In a reductive quenching process, the excited photocatalyst oxidizes an electron-rich substrate (**RQ**) to its

corresponding radical cation ($RQ^{\cdot+}$). The resulting reduced photocatalyst (PC^-) returns to the ground state donating an electron to a suitable acceptor while the radical cation can be engaged in a subsequent step. Conversely, in oxidative quenching the photocatalyst in the $PC^* {}^3MLCT_1$ state donates an electron to an electron-deficient substrate (OQ), delivering the oxidized photocatalyst (PC^+) and quencher radical anion ($OQ^{\cdot-}$). The return of the photocatalyst to the ground state is realized through oxidation of an electron-rich species while the radical anion ($OQ^{\cdot-}$) can follow different reaction pathways.



Scheme I-2. a) Photoredox catalytic cycle *via* single electron transfer (SET); b) photocatalytic cycle *via* energy transfer (EnT). PC photocatalyst, Q quencher: RQ reductive quencher, OQ oxidative quencher, *ISC* intersystem crossing. $Q(S_0)$ quencher singlet ground state, $Q^*(S_1)$ quencher first singlet excited state and $Q^*(T_1)$ quencher first triplet excited state.

The thermodynamic feasibility of each of the SET events depends upon the redox potentials of the species involved. Regarding the photocatalyst, the ground state redox potentials, $E_{1/2}(PC^+/PC)$ and $E_{1/2}(PC/PC^-)$ respectively, can be measured through cyclic voltammetry (CV). The corresponding

General introduction

oxidation and reduction potentials for excited states are more difficult to obtain and spectroscopic analysis must be applied to determine the difference in energy between $PC^* \text{ } ^3MLCT_1$ and 1A_1 which can be approximated to the maximum energy emission ($E_{0,0}$) (Figure I.2). The excited state oxidation and reduction potentials can then be estimated using the following equations¹³:

$$E_{1/2}(PC^+/PC^*) = E_{1/2}(PC^+/PC) - E_{0,0}(PC^*/PC) \quad (\text{Eq. 1})$$

$$E_{1/2}(PC^*/PC^-) = E_{1/2}(PC/PC^-) + E_{0,0}(PC^*/PC) \quad (\text{Eq. 2})$$

In an energy transfer process (Scheme I-2, b),¹⁴ the photo-excited triplet state interacts with a substrate having an energy triplet state comparable to the photocatalyst. As a result of the interaction, the photocatalyst returns to its ground state while the acceptor (**Q**) reaches its triplet state ($Q^* \text{ } T_1$) and is engaged in peculiar transformations.

Polypyridyl metal complexes (both homoleptic and heteroleptic) played a prominent role (and continue to do so) in the development of visible-light photoredox processes. The most common homoleptic photocatalysts are $[Ru(bpy)_3](PF_6)$ ($bpy = 2,2'$ -bipyridine) and *fac*- $Ir(ppy)_3$ ($ppy = 2$ -phenylpyridine) while the most common heteroleptic ones are $[Ir(ppy)_2(dtbbpy)](PF_6)$ ($dtbbpy = 4,4$ -di-*tert*-butyl- $2,2$ -bipyridine) and $[Ir(dF(CF_3)ppy)_2(dtbbpy)](PF_6)$ ($dF(CF_3)ppy = 2$ -($2,4$ -difluorophenyl)- 5 -trifluoromethylpyridine). A common feature of organometallic photocatalyst is that proper choosing of metal center and ligands allows to access a wide window of redox potentials.

Despite the great success of transition-metal based photocatalysts, the development of organic photocatalysts as sustainable and cheaper alternatives, has recently attracted enormous interest.^{12f} The photochemistry of organic dyes lacks the homogeneity described above for

¹³ Rehm, D.; Weller, A. *Isr. J. Chem.* **1970**, *8*, 259-271.

¹⁴ Strieth-Kalthoff, F.; James, M. J.; Teders, M.; Pitzer, L.; Glorius, F. *Chem. Soc. Rev.* **2018**, *47*, 7190-7202.

Ru- and Ir-based photocatalyst and is more structure-specific. Fukuzumi catalyst (9-mesityl-10-methyl acridinium) photochemistry, characterized by a charge-transfer excited state, will be here described in detail (Figure I-3).¹⁵ Upon visible light irradiation, the promotion of an electron into the LUMO (localized on the acridinium moiety) generates the S_1^{LE} state (I). This state quickly converts into the S_1^{CT} state (II) *via* intramolecular charge transfer from the mesityl group (HOMO). The longevity of this state (-6 ns) allows for bimolecular quenching processes.

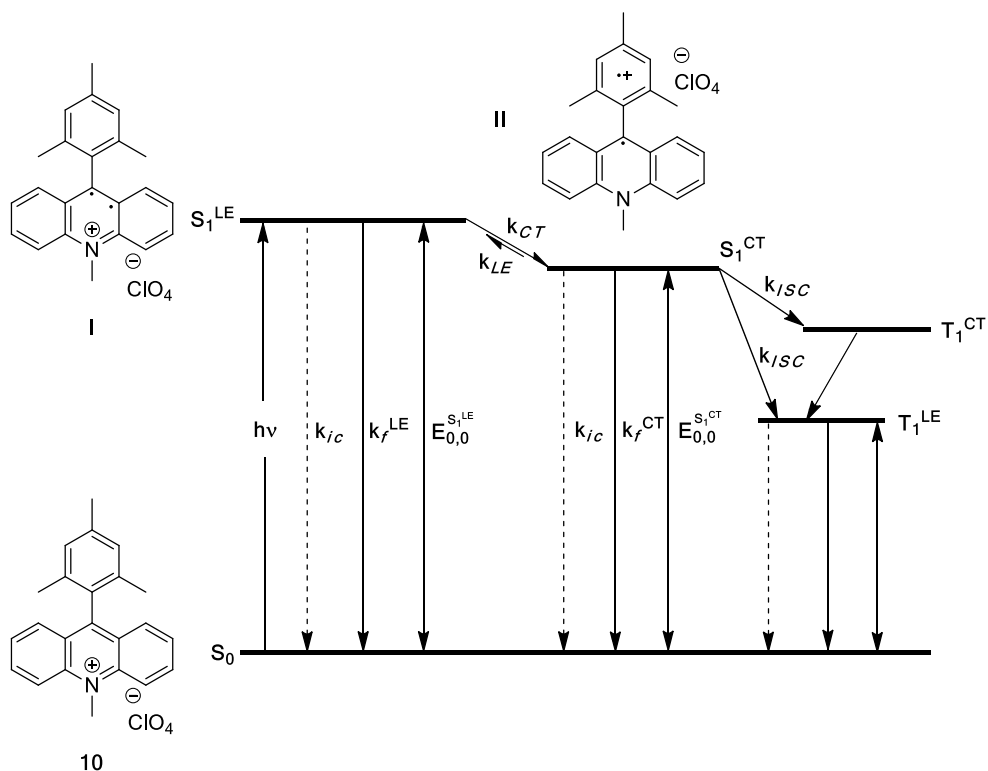


Figure I-3. Jablonski diagram for Fukuzumi photocatalyst. LE = local excitation complex, CT = charge transfer complex, k_{ct} = rate of intramolecular electron transfer.

¹⁵ a) Fukuzumi, S.; Kotani, H.; Ohkubo, K.; Ogo, S.; Tkachenko, N. V.; Lemmetyinen, H. *J. Am. Chem. Soc.* **2004**, *126*, 1600-1601; b) Benniston, A. C.; Harriman, A.; Li, P.; Rostron, J. P.; Ramesdonk, H. J. v.; Groeneveld, M. M.; Zhang, H.; Verhoeven, J. W. *J. Am. Chem. Soc.* **2005**, *127*, 16054-16064.

General introduction

Alternatively, the depopulation can happen through internal conversion or intersystem crossing to the triplet states (T_1^{CT} or T_1^{SE}) while fluorescence is a minor pathway. Nevertheless, it is possible to observe a fluorescence emission spectrum arising from decay from S_1^{LE} and S_1^{CT} witnessing the reversibility of the intramolecular electron transfer.

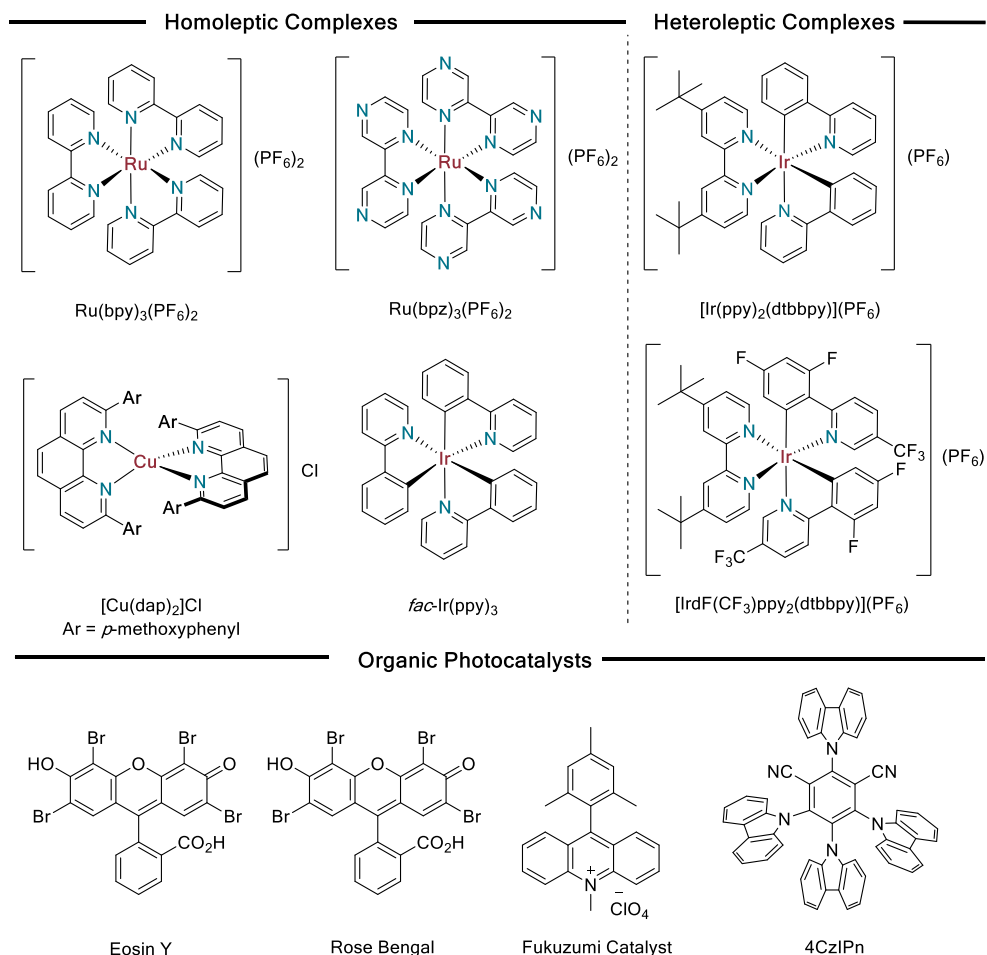


Figure I-4. Selection of homoleptic and heteroleptic transition-metal based photocatalysts and organic photocatalysts.

A representative list of organometallic photocatalysts and organic dyes is shown in Figure I-4.

1.2.2. Photoredox organocatalysis

Over the past two decades, organocatalysis emerged as a diverse and robust branch of contemporary organic synthesis. The typical activation modes of organocatalysis demonstrated to be extremely compatible with photoredox catalysis enabling remarkable reactions that are normally not accessible with either catalyst alone, thus paving the way to a most powerful exploitation of this dual activation mode.¹⁶ Organocatalysts can influence the photocatalytic step either by activating the substrate towards a SET process or by generating a transient species that could interact with the photocatalyst. Alternatively, the intermediate resulting from organocatalytic activation can react with species produced independently *via* photoredox processes.

Significant development of cooperative organo- and photocatalysis in asymmetric organic synthesis will be summarized according to a classification based on the organocatalytic activation mode.

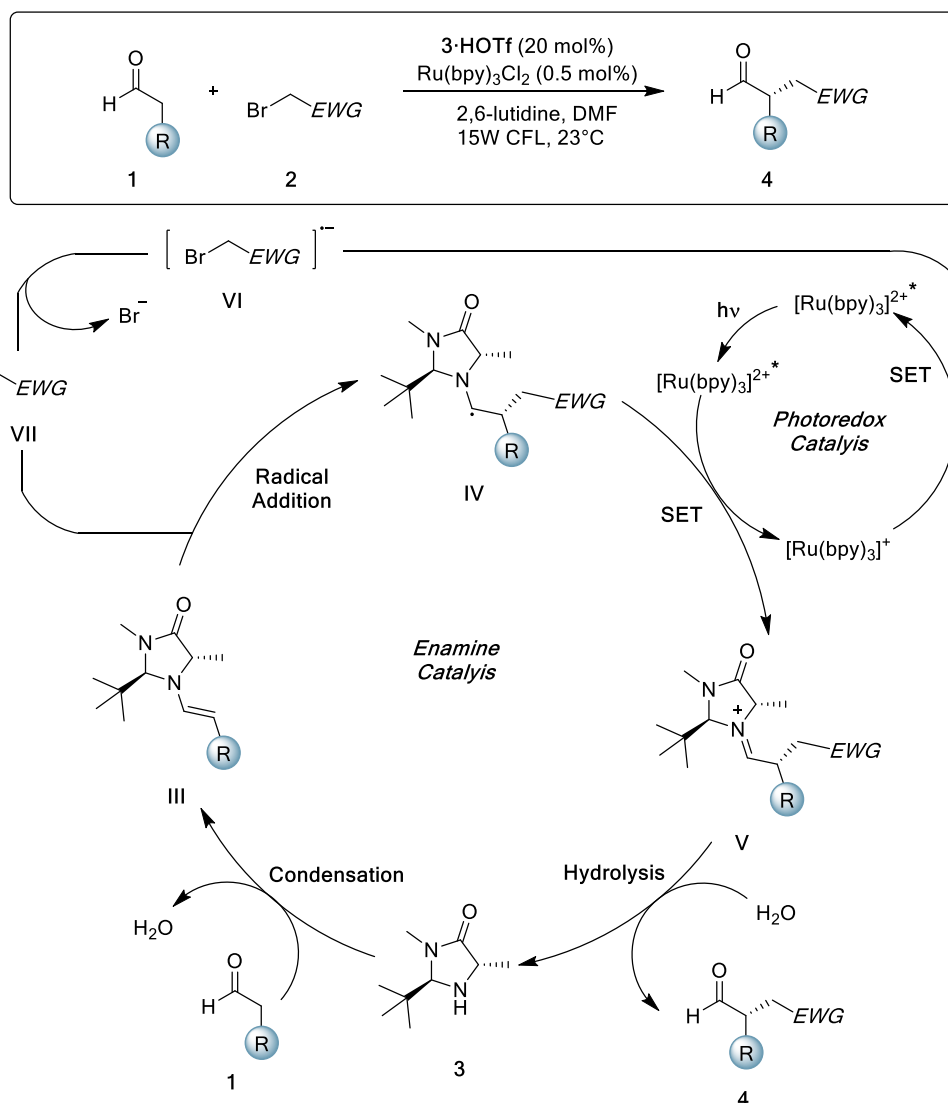
- **Enamine/Iminium Catalysis**

In MacMillan seminal work (Scheme I-1, a),⁹ the reactivity of enamines as acceptors of electrophilic radicals was investigated in order to develop the stereoselective α -alkylation of aldehydes, a long sought-after, yet hitherto elusive transformation in organic synthesis. Photoredox catalysis was employed as a novel method for the generation of radical intermediates which could be trapped by an enamine in an enantioselective fashion. The general mechanism for this reaction is depicted in Scheme I-3 and has

¹⁶ a) Hopkinson, M. N.; Sahoo, B.; Li, J.-L.; Glorius F. *Chem. Eur. J.* **2014**, *20*, 3874 - 3886;
b) Skubi, K. L.; Blum, T. R.; Yoon, T. P. *Chem. Rev.* **2016**, *116*, 10035–10074

General introduction

been proposed to be operative also for the addition of fluoroalkyl,¹⁷ α -cyanoalkyl¹⁸ and benzyl¹⁹ fragments.



Scheme I-3. Proposed mechanism for the α -alkylation of aldehydes with alkyl bromides.

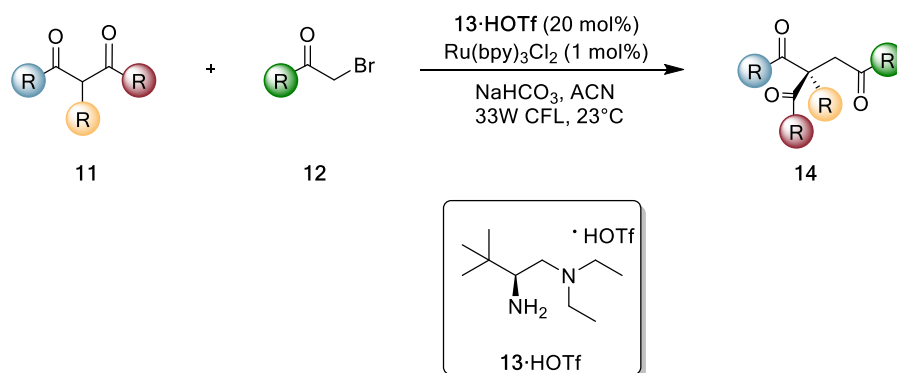
¹⁷ Nagib, D. A.; Scott, M. E.; MacMillan, D. W. C. *J. Am. Chem. Soc.* **2009**, *131*, 10875–10877.

¹⁸ Welin, E. R.; Warkentin, A. A.; Conrad, J. C.; MacMillan, D. W. C. *Angew. Chem., Int. Ed.* **2015**, *54*, 9668–9672.

¹⁹ Shih, H.-W.; Vander Wal, M. N.; Grange, R. L.; MacMillan, D. W. C. *J. Am. Chem. Soc.* **2010**, *132*, 13600–13603.

The condensation of organocatalyst **3** with an aldehyde (**1**) delivers chiral enamine **III**. A sacrificial amount of this species is oxidized by photoexcited $[\text{Ru}(\text{bpy})_3]^{2+}$ catalyst (not shown in Scheme 1.3), forming the strong reducing species $[\text{Ru}(\text{bpy})_3]^+$ which is able to transfer an electron to alkyl halide **2**. The resulting radical anion (**VI**) decomposes *via* mesolytic dehalogenation affording the electrophilic radical **VII**. SOMOphilic enamine (**III**) undergoes enantioselective radical attack from **VII** affording α -amino radical **IV**. This intermediate can be oxidized by either excited $[\text{Ru}(\text{bpy})_3]^{2+}$ or by another equivalent of **2** in a chain propagative manner.²⁰ Finally, the iminium ion **V** is hydrolyzed releasing the product **4** and organocatalyst **3**.

In 2014, Luo extended the dual enamine photoredox catalysis concept to the enantioselective α -alkylation of β -ketocarboxyls (Scheme I-4).²¹ The developed methodology allows the construction of a variety of acyclic, cyclic and spirocyclic quaternary stereocenters employing chiral diamine **13** as organocatalyst.



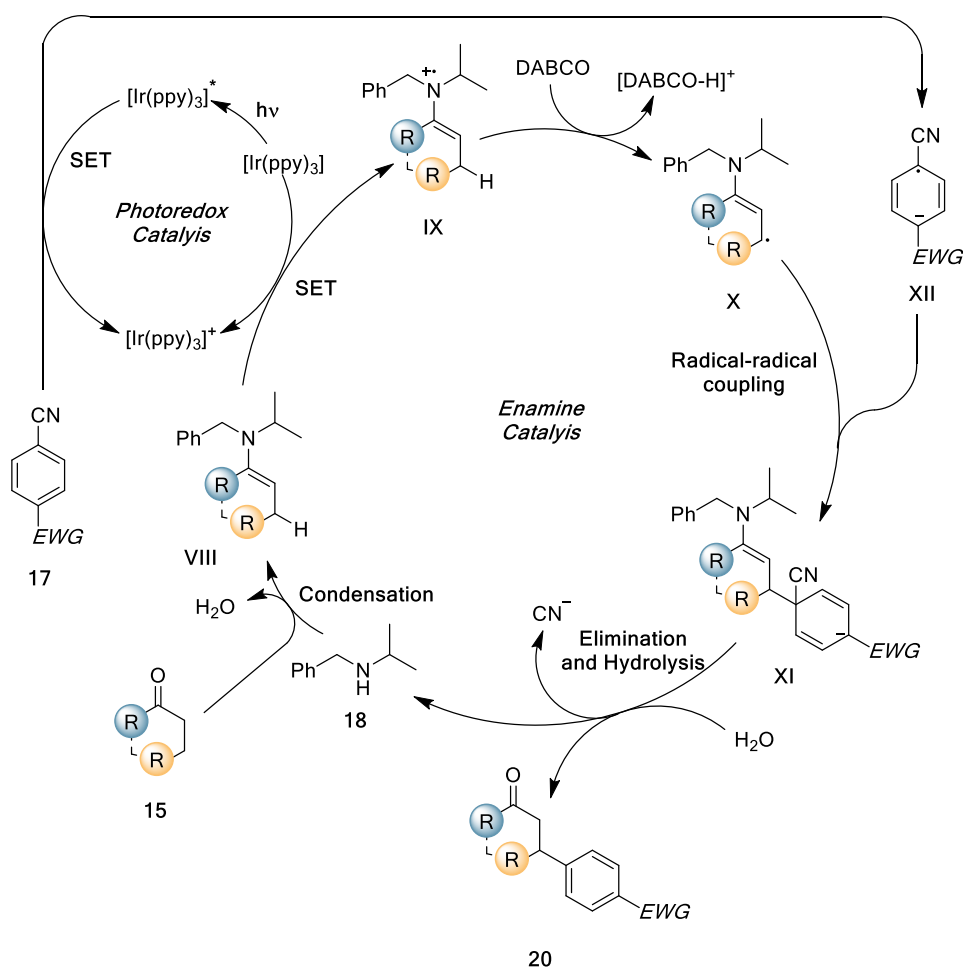
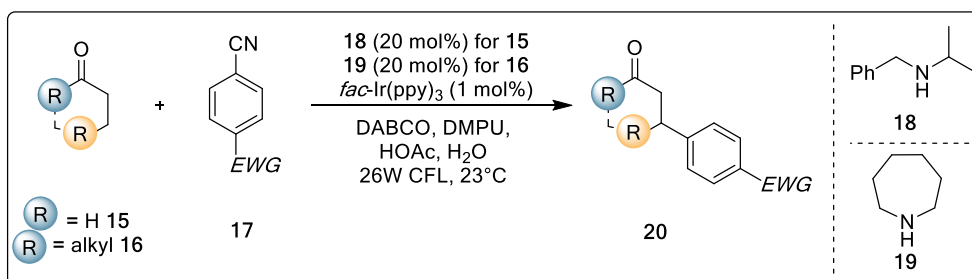
Scheme I-4. Catalytic asymmetric α -alkylation of β -ketocarboxyls.

²⁰ Cismesia, M. A.; Yoon, T. P. *Chem. Sci.* **2015**, *6*, 5426–5434.

²¹ Zhu, Y.; Zhang, L.; Luo, S. *J. Am. Chem. Soc.* **2014**, *136*, 14642–14645.

General introduction

An alternative reaction pathway for enamine radical cations was disclosed by MacMillan in 2013.²²



²² Pirnot, M. T.; Rankic, D. A.; Martin, D. B. C.; MacMillan, D. W. C. *Science* 2013, 339, 1593–1596.

The combination of photoredox and organocatalysis allowed the direct β -functionalization of saturated aldehydes (**15**) and ketones (**16**) with electrondeficient cyanoarenes (**17**) employing either secondary amines **18** or **19** as organocatalysts (Scheme I-5). The direct functionalization of carbonyl compounds in β position, a challenging task in organic synthesis, is accomplished through the generation of 5π -electron- β -enaminy radical (XI). A detailed mechanistic proposal is shown in Scheme I-5. Photoexcited catalyst $[\text{Ir}(\text{ppy})_3]^*$ reduces **17** delivering the corresponding radical anion XII and the oxidized form of the catalyst $[\text{Ir}(\text{ppy})_3]^+$. This Ir(IV) complex accepts an electron from the enamine VII regenerating the ground state photocatalyst and radical cation IX. Rather than undergoing radical attack from XII, this species is deprotonated by DABCO leading to the key β -enaminy radical (XI). Radical-radical coupling at this stage followed by loss of cyanide and hydrolysis affords β -arylated product (**20**).

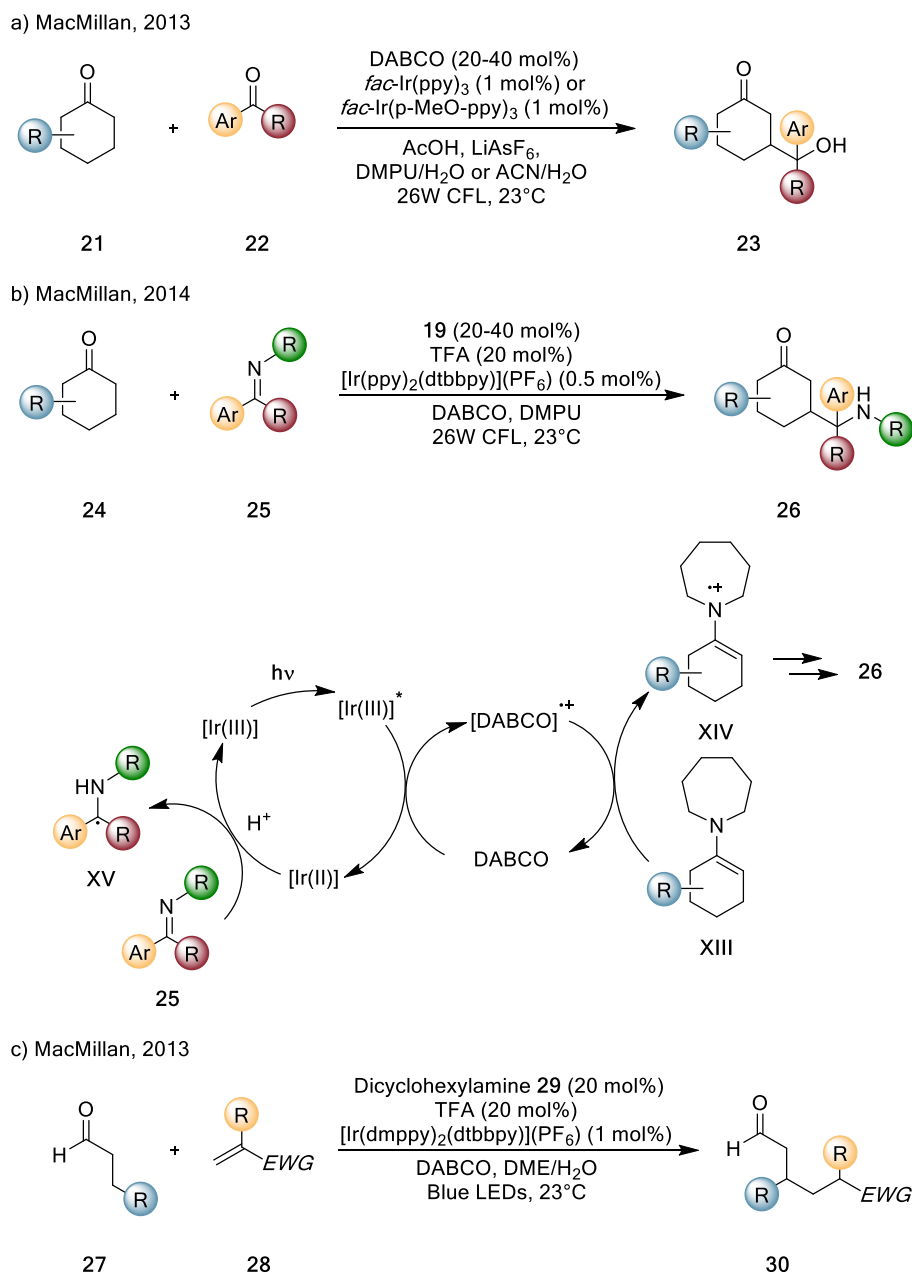
Next, this β -functionalization strategy was extended by replacing cyanoarenes with ketones (**22**) (Scheme I-6, a),²³ imines (**25**),²⁴ and electron-deficient alkenes (**28**) (Scheme I-6, c).²⁵ All these reactions share the fundamental intermediate π -electron- β -enaminy radical, even though for each coupling partner different organocatalysts, redox mediators and acids were required, reflecting variability in the mechanistic scenario. In the formal β -Mannich reaction (Scheme I-6, b), DABCO acts as a reductive quencher of the excited photocatalyst and the resultant radical cation oxidizes enamine XIII. Lewis (LiAsF_6) and Brønsted (TFA) acids are required for stabilizing the ketyl radical anions generated by SET reduction of ketones (Scheme I-6, a) and facilitate the reduction of the imines *via* PCET (proton-coupled electron transfer), respectively.

²³ Petronijević, F. R.; Nappi, M.; MacMillan, D. W. C. *J. Am. Chem. Soc.* **2013**, *135*, 18323–18326.

²⁴ Jeffrey, J. L.; Petronijević, F. R.; MacMillan, D. W. C. *J. Am. Chem. Soc.* **2015**, *137*, 8404–8407.

²⁵ Terrett, J. A.; Clift, M. D.; MacMillan, D. W. C. *J. Am. Chem. Soc.* **2014**, *136*, 6858–6861.

General introduction



Scheme I-6. a) β -Functionalization of cyclic ketones with aryl ketones; b) formal β -Mannich reaction; c) aldehyde β -alkylation via photoredox organocatalysis

In the coupling with electron-deficient alkenes, oxidation of the enamine is directly performed as SET quenching event delivering the β -enaminyll radical that could add to Michael acceptors (**28**). Reduction of the resulting radical and subsequent protonation affords the β -alkylated product **30**.

- **Nucleophilic Catalysis**

In 2012, Rovis demonstrated the feasibility of merging photoredox catalysis with chiral *N*-heterocyclic carbene (NHC) organocatalysis (Scheme I-7).²⁶ The developed methodology allows the enantioselective α -acylation of tertiary amines (**32**) with aldehydes (**31**). Addition of NHC **33** to aldehyde **31** leads to the formation of Breslow intermediate **XVII**. This nucleophilic species can trap iminium ion **XVI**, generated upon sequential SET oxidation and HAT from the corresponding amine **32**. The resulting intermediate (**XVIII**) undergoes fragmentation delivering α -amino ketones (**34**) and the NHC catalyst.

- **Chiral Brønsted Acid Catalysis**

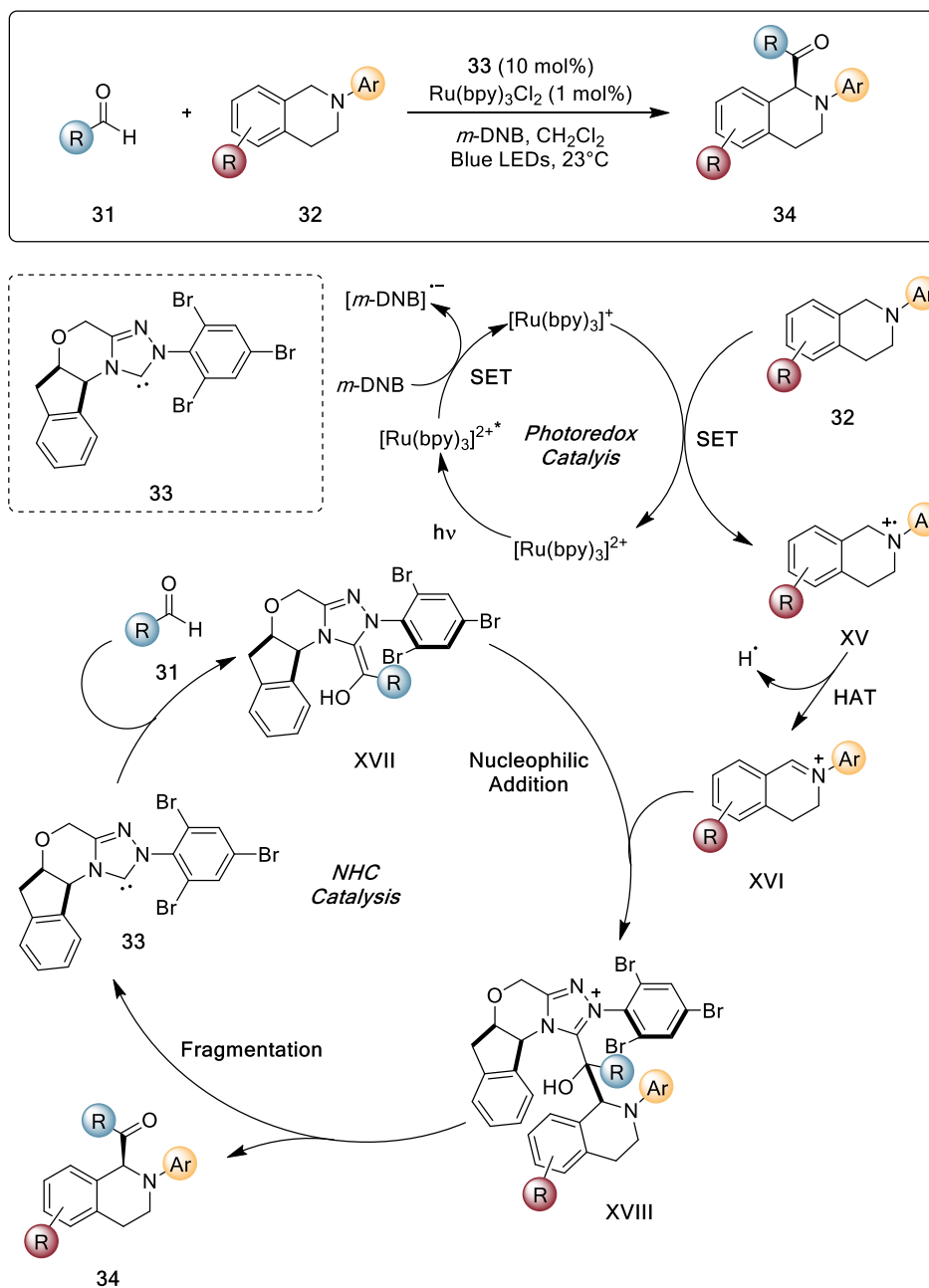
Lewis²⁷ and Brønsted acid catalysis have found widespread combination with photoredox catalysis due to the ability of such activation modes to impact the redox properties and reactivities of organic substrates. Brønsted acids can dramatically accelerate photo-reductive processes enabling proton-coupled electron transfer (PCET) pathway.²⁸

²⁶ DiRocco, D. A.; Rovis, T. *J. Am. Chem. Soc.* **2012**, *134*, 8094–8097.

²⁷ Fukuzumi, S.; Jieun Jung, J.; Lee, Y.-M.; Nam, W. *Asian J. Org. Chem.* **2017**, *6*, 397–409.

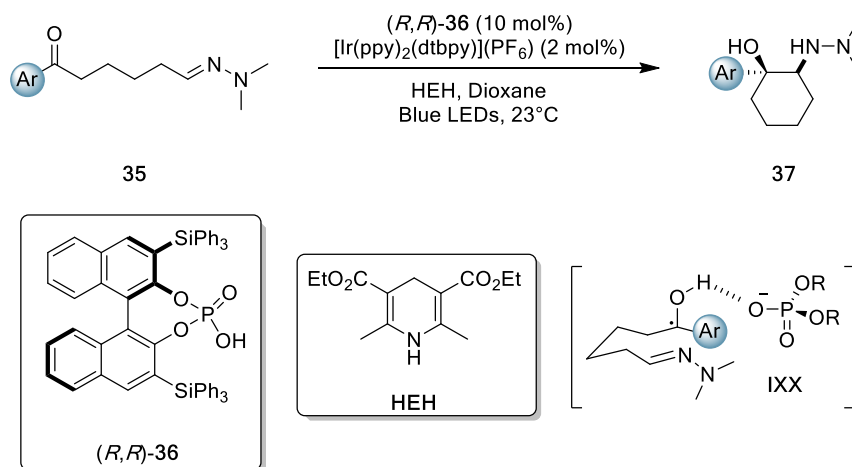
²⁸ a) Mayer, J. M *Annu. Rev. Phys. Chem.* **2004**, *55*, 363–390; b) Weinberg, D. R.; Gagliardi, C. J.; Hull, J. F.; Murphy, C. F.; Kent, C. A.; Westlake, B. C.; Paul, A.; Ess, D. H.; McCafferty, D. G.; Meyer, T. J. *Chem. Rev.* **2012**, *112*, 4016–4093; c) Yayla, H. G.; Knowles, R. R. *Synlett* **2014**, *25*, 2819–2826.

General introduction



Scheme I-7. Umpolung Reactivity Using Dual Photo/NHC Catalysis.
m-DNP = *m*-dinitrobenzene.

This activation strategy enables the generation of radical intermediates through concerted transfer of a proton and an electron to an organic substrate. However, Brønsted acid catalysis can also influence processes not strictly related with the photoredox cycle. Herein, we will comment only selected reports where the use of Brønsted acids had an impact on the overall stereochemical outcome of the transformation.²⁹



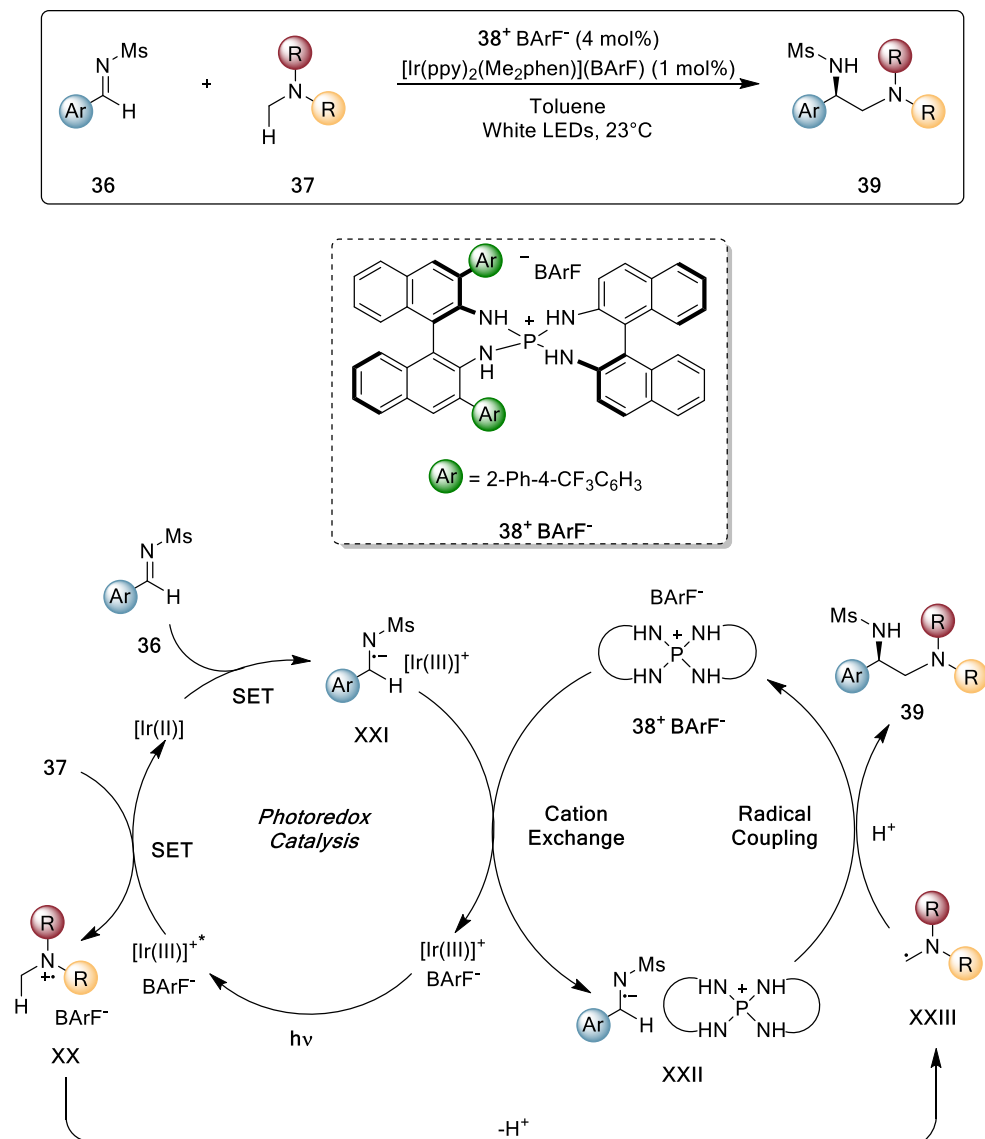
Scheme I-8. Catalytic asymmetric aza-pinacol cyclization reaction.

Knowles group investigations have focused efforts on the development of synthetic methods relying upon PCET for the generation of radical intermediates. In 2013 they reported an enantioselective intramolecular coupling of ketones and hydrazones (**35**) delivering valuable cyclic *syn*-1,2-amino alcohols (**37**) (Scheme I-8).³⁰ The combined use of $[\text{Ir}(\text{ppy})_2(\text{dtbbpy})](\text{PF}_6)$ as photocatalyst and chiral phosphoric acid (R,R)-**36** as organocatalyst, allowed the generation of the crucial ketyl radical intermediate **IXX** *via* PCET. Subsequent cyclization of this intermediate afforded aza-pinacol product (**37**) in enantioenriched form.

²⁹ Yin, Y.; Zhao, X.; Qiao, B.; Jiang, Z. *Org. Chem. Front.* **2020**, *7*, 1283-1296

³⁰ Rono, L. J.; Yayla, H. G.; Wang, D. Y.; Armstrong, M. F.; Knowles, R. R. *J. Am. Chem. Soc.* **2013**, *135*, 17735-17738.

General introduction



Scheme I-9. Redox neutral symmetric α -coupling of *N*-arylaminomethanes with aldimines

One example of Brønsted acid-based control of non-photochemical processes downstream of the photoactivation step was disclosed by Ooi (Scheme I-9).³¹ The concept of ion pairing was exploited to achieve a

³¹ Uraguchi, D.; Kinoshita, N.; Kizu, T.; Ooi, T. *J. Am. Chem. Soc.* **2015**, *137*, 13768–13771.

redox-neutral enantioselective coupling of aldimines (**36**) and N-arylaminomethanes (**37**).

The mechanistic proposal depicted in Scheme I-9 is based on reductive quenching of the excited Ir(III) photocatalyst affording radical cation **XX** and reduced Ir(II) complex. This species can reduce imine **36** to the corresponding radical anion **XXI**, which in turn exchanges its counterion in favor of the chiral aryl amino phosphonium **38**⁺. Ionic pair **XXII** then couples in an enantioselective fashion with radical **XXIII**, affording relevant 1,2-diamino products (**39**).

1.2.3. Metallaphotocatalysis

Recently, the merger of transition metal catalysis and photoredox catalysis, termed metallaphotocatalysis, has received great attention leading to the development of new strategies for forging C–C and C–heteroatom bond.³²

Most traditional cross coupling methodologies rely upon three two-electron elementary steps to forge bonds: oxidative addition, transmetallation and reductive elimination. Numerous mechanistic studies focused on cross coupling chemistry have revealed the influence of the metal catalyst and its ligand environment on the course of those reactions, but many challenges remain in this field.

Meanwhile, it has long been known that elementary transformations are faster for 17- and 19-electron transition metal complexes in comparison with their even-electron congeners.³³ Stoichiometric precedents in this area have been reported,³⁴ but only the development of photoredox catalysis

³² a) Vila, C. *ChemCatChem* **2015**, *7*, 1790-1793; b) Levin, M. D.; Kim, S.; Toste, F. D. *ACS Cent. Sci.* **2016**, *2*, 293-301 c) Twilton, J.; Le, C.; Zhang, P.; Shaw, M. H.; Evans, R. W.; MacMillan, D. W. C. *Nat. Rev. Chem.* **2017**, *1*, 0052.

³³ Stiegman, A. E.; Tyler, D. R. *Comments Inorg. Chem.* **1986**, *5*, 215-245.

³⁴ Halpern, J. *Acc. Chem. Res.* **1970**, *3*, 386-392.

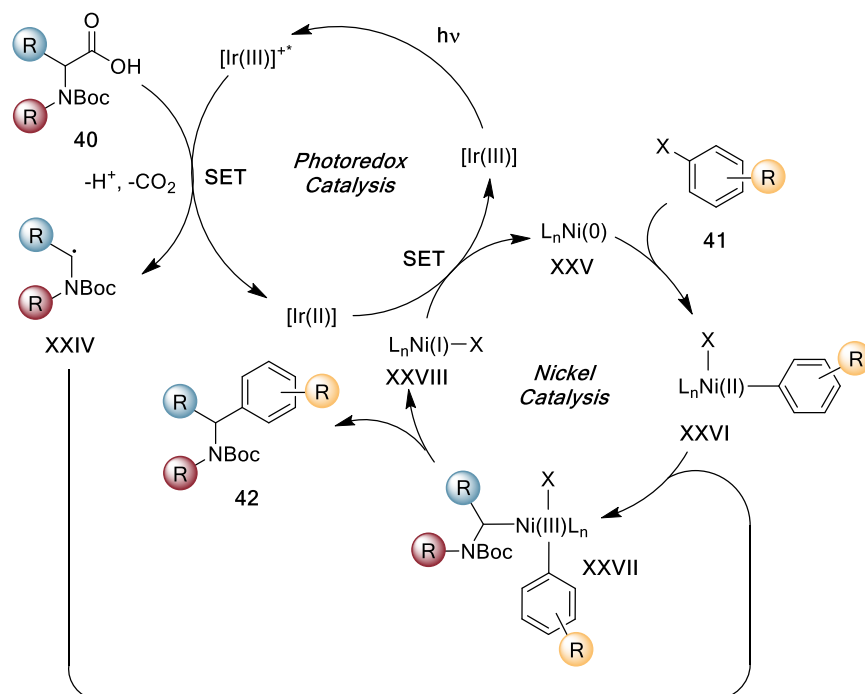
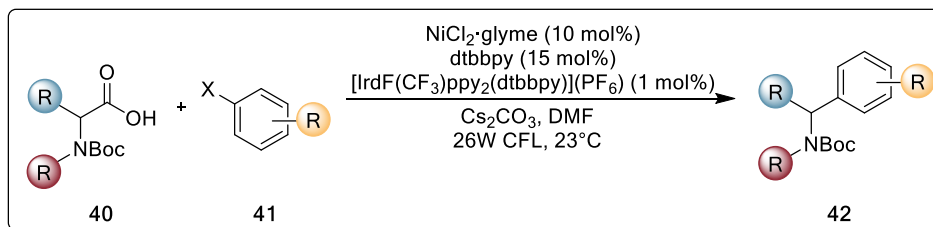
General introduction

allowed the switch to odd-electron organometallic reactivity in mild and catalytic conditions.

- **Nickel metallaphotocatalysis**

Nickel catalysis distinctive features in the field of cross coupling reactions include the ability of nickel complexes to undergo facile oxidative addition with alkyl electrophiles, providing solutions for the challenging coupling of C(sp³) fragments, and the reduced tendency to β-hydride elimination (compared with their palladium analogues) preventing undesired side reactions.³⁵

³⁵ a) Tasker, S. Z.; Standley, E. A.; Jamison, T. F. *Nature*, **2014**, *509*, 299-309; b) Hu, X. *Chem. Sci.*, **2011**, *2*, 1867-1886.



Scheme I-9. Coupling of α -carboxyl sp^3 -carbons with aryl halides. X = Br, I.

In this context, photoredox-mediated radical generation has revealed to be a powerful strategy for expanding the toolbox of nucleophilic coupling partners.

Several methodologies have relied upon the oxidative radical generation of the nucleophile and the first example of this strategy, enabling the cross

General introduction

coupling of carboxylic acids (**40**) and aryl halides (**41**), was reported by MacMillan in 2014 (Scheme I-9).³⁶

The proposed mechanism for this dual catalytic protocol is shown in Scheme I-9. Photoexcited iridium catalyst performs oxidative decarboxylation of **40** to radical **XXIV**. Concurrently Ni(0) complex **XXV** undergoes oxidative addition with an aryl halide affording a Ni(II) aryl complex (**XXVI**), which then traps **XXIV** affording Ni(III) complex **XXVII**. Subsequent reductive elimination results in the formation of the desired product (**42**) and Ni(I) complex (**XXVIII**). Electron exchange between **XXVIII** and Ir(I) restores the ground oxidation states of both catalysts.

Following this report, the same group disclosed the compatibility of this dual catalytic platform with vinyl halides³⁷ and alkyl halides.³⁸ This cross-coupling manifold is also prone to employment of other alkyl radical sources such as alkylbis(catecholato)silicates³⁹ and 4-alkyl-1,4-dihydropyridines.⁴⁰

A natural step forward in nickel metallaphotocatalysis has been the incorporation of strategies for radical generation from neutral and hydridic C–H bonds *via* Hydrogen Atom Transfer (HAT). Exploiting a previously reported HAT activation process,⁴¹ MacMillan group was able to develop a triple catalytic reaction platform that enables the selective arylation of electron-rich C–H bonds (Scheme I-10).⁴²

³⁶ Zuo, Z.; Ahneman, D. T.; Chu, L.; Terrett, J. A.; Doyle, A. G.; MacMillan, D. W. C. *Science* **2014**, *345*, 437–440.

³⁷ Noble, A.; McCarver, S. J.; MacMillan, D. W. C. *J. Am. Chem. Soc.* **2015**, *137*, 624–627

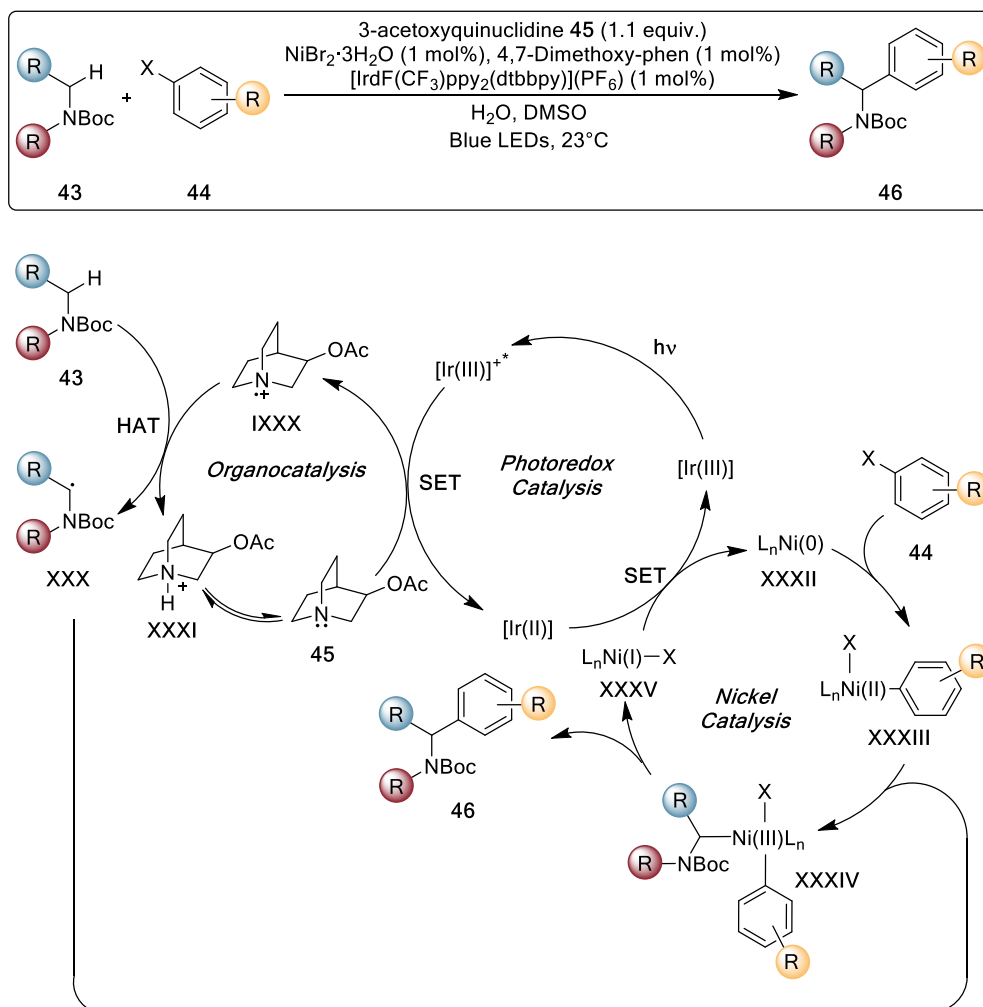
³⁸ Johnston, C. P.; Smith, R. T.; Allmendinger, S.; MacMillan, D. W. C. *Nature*, **2016**, *536*, 322–325.

³⁹ a) Jouffroy, M.; Primer, D. N.; Molander, G. A. *J. Am. Chem. Soc.*, **2016**, *138*, 475–478; b) Patel, N. R.; Kelly, C. B.; Jouffroy, M.; Molander, G. A. *Org. Lett.*, **2016**, *18*, 764–767.

⁴⁰ a) Nakajima, K.; Nojima, S.; Nishibayashi, Y. *Angew. Chem. Int. Ed.*, **2016**, *55*, 14106–14110; b) Gutiérrez-Bonet, Á.; Tellis, J. C.; Matsui, J. K.; Vara, B. A.; Molander, G. A. *ACS Catal.* **2016**, *6*, 8004–8008.

⁴¹ Jeffrey, J. L.; Terrett, J. A.; MacMillan, D. W. C. *Science* **2015**, *349*, 1532–1536.

⁴² Shaw, M. H.; Shurtleff, V. W.; Terrett, J. A.; Cuthbertson, J. D.; MacMillan, D. W. C. *Science*, **2016**, *352*, 1304–1308.



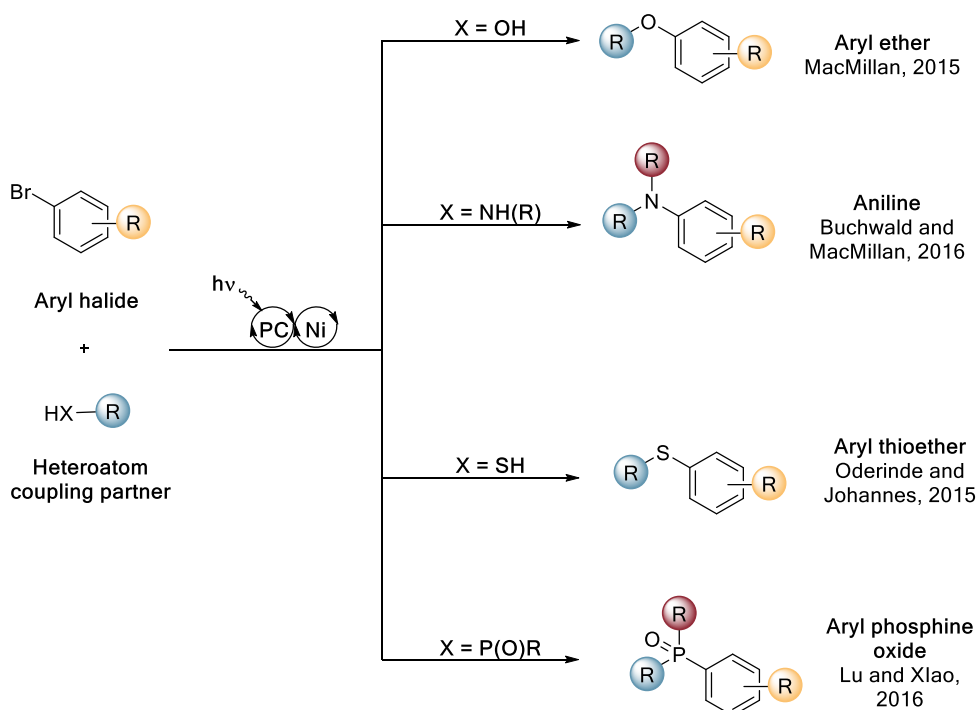
Scheme I-10 C–H arylation by dual nickel photoredox catalysis. X = Cl, Br.

The mechanism depicted in Scheme I-10 is somehow similar to the one proposed for the coupling of α -carboxyl sp^3 -carbons with aryl halides, the main difference standing in the reductive quencher of the excited photocatalyst. In this case, 3-acetoxyquinuclidine (**45**) undergoes oxidation yielding the corresponding radical cation (**IXXX**). This electrophilic radical intermediate abstracts a hydrogen atom selectively from **43** delivering α -

General introduction

amino radical **XXX**. The subsequent processes are likely to resemble the ones depicted in Scheme I-9.

The nickel metallaphotocatalysis unique ability to mediate challenging bond construction processes has been subsequently extended to the formation of valuable carbon–heteroatom bonds.



Scheme I-11. Visible light-enabled Ni-catalyzed C–X bond-forming reactions.

The most remarkable reports in this field have been summarized in Scheme I-11. Even if distinctive mechanistic features have been described, combination of nickel and photoredox catalysis allows for construction of $\text{C}(\text{sp}^2)\text{--O}$,⁴³ $\text{C}(\text{sp}^2)\text{--N}$,⁴⁴ $\text{C}(\text{sp}^2)\text{--S}$ ⁴⁵ and $\text{C}(\text{sp}^2)\text{--P}$ ⁴⁶ bonds.

⁴³ Terrett, J. A.; Cuthbertson, J. D.; Shurtleff, V. W.; MacMillan, D. W. C. *Nature* **2015**, *524*, 330–334.

⁴⁴ Corcoran, E. B.; Pirnot, M. T.; Lin, S.; Dreher, S. D.; DiRocco, D. A.; Davies, I. W.; Buchwald, S. L.; David W. C. MacMillan D. W. C. *Science* **2016**, *353*, 279–283.

- **Palladium metallaphotocatalysis**

After Osawa's seminal report (not described herein because the precise role of the photocatalyst was not determined),⁴⁷ in 2011 Sanford exploited a dual photoredox palladium catalyst system to accomplish C(sp²)-H arylation of 2-arylpyridines (**47**) with aryl diazonium salts (**48**) (Scheme I-12).⁴⁸ It's noteworthy that this transformation is accomplished at ambient temperature and in the absence of strong external oxidants, thereby providing great functional group tolerance. The key step in the mechanistic proposal is a concerted metallation-deprotonation of **47** by (Pd)(OAc)₂ affording palladacycle **XXXVII**. This intermediate, in turn, is intercepted by aryl radical **XXXVI** delivering the Pd(III) complex **XXXVIII**. Subsequent oxidation of this Pd(III) species by Ru(III) generates a high valency Pd(IV) complex **XXXIX** that undergoes rapid reductive elimination to yield **49**.

- **Gold metallaphotocatalysis**

Metallaphotoredox catalysis has demonstrated to be a powerful strategy enabling the addition of radicals to metal species that typically engage in polar oxidative additions. A long-standing challenge in gold homogeneous catalysis has been the difficulty of polar oxidative additions between Au(I) species and aryl halides.⁴⁹

⁴⁵ Oderinde, M. S.; Frenette, M.; Robbins, D. W.; Aquila, B.; Johannes, J. M. *J. Am. Chem. Soc.* **2016**, *138*, 1760-1763.

⁴⁶ Xuan, J.; Zeng, T.-T.; Chen, J.-R.; Lu, L.-Q.; Xiao, W.-J. *Chem. Eur. J.* **2015**, *21*, 4962-4965.

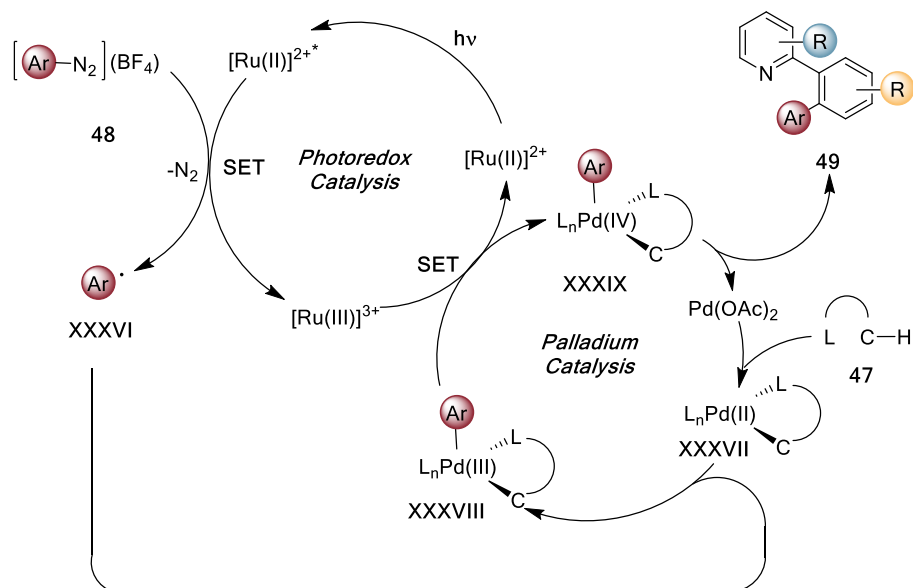
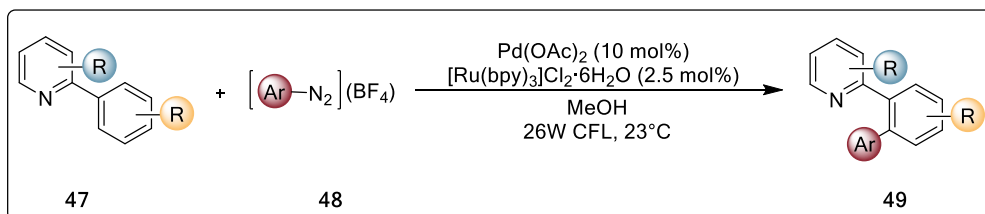
⁴⁷ Osawa, M.; Nagai, H.; Akita, M. *Dalton Trans.* **2007**, *8*, 827-829.

⁴⁸ Kalyani, D.; McMurtrey, K. B.; Neufeldt, S. R.; Sanford, M. S. *J. Am. Chem. Soc.* **2011**, *133*, 18566-18569.

⁴⁹ a) Joost, M.; Estévez, L.; Miqueu, K.; Amgoune, A.; Bourissou, D. *Angew. Chem. Int. Ed.* **2015**, *54*,

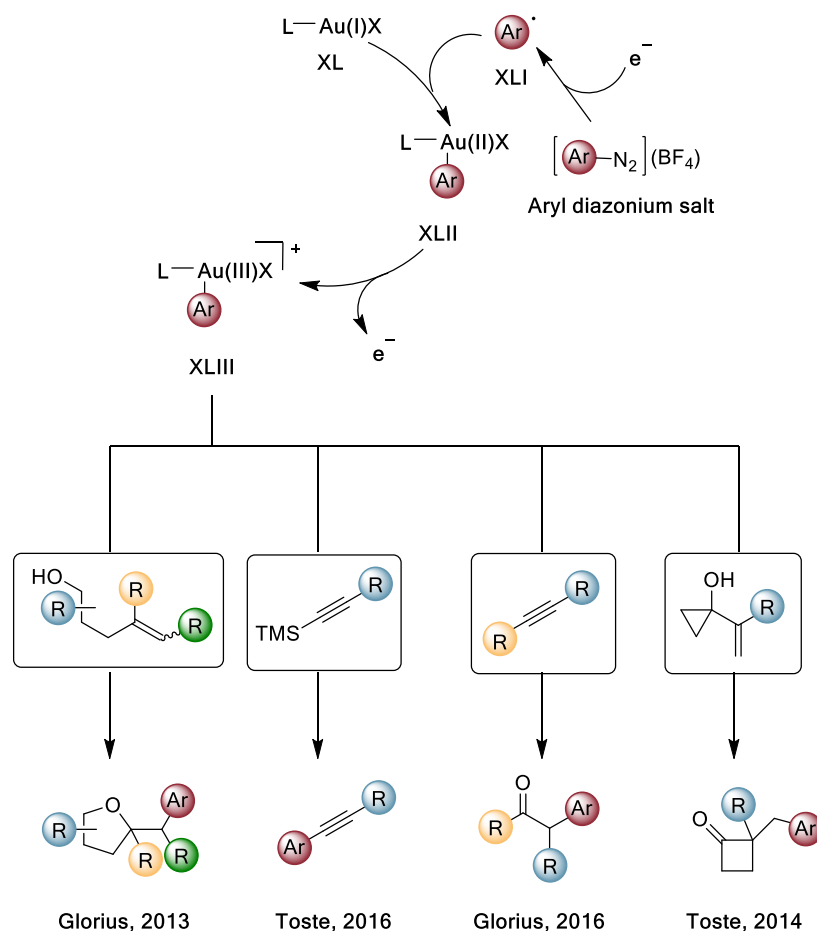
5236-5240; b) Wu, C.-Y.; Horibe, T.; Jacobsen, C. B.; Toste, F. D. *Nature* **2015**, *517*, 449-454.

General introduction



Scheme I-1. Merger of Pd-catalyzed C-H functionalization and visible-light photocatalysis.

Photoredox catalysis provided a solution addressing this issue (Scheme I-13). Thus, reductive generation of aryl radicals from the corresponding aryl diazonium salts and addition to Au(I) catalyst (**XL**) provides rapid access to Au(II) species (**XLII**). Subsequent oxidation either by oxidized photocatalyst or through a radical chain pathway affords the Au(III)-aryl complex (**XLIII**) that can react with double and triple C-C bonds.



Scheme I-13. Arylative functionalization mediated by dual gold photoredox catalysis.

The key intermediate **XLIII** has been a major actor in the most important applications of gold metallaphotocatalysis.⁵⁰

⁵⁰ a) Sahoo, B.; Hopkinson, M. N.; Glorius, F. *J. Am. Chem. Soc.* **2013**, *135*, 5505-5508; b) Kim, S.; Rojas-Martin, J.; Toste, F. D. *Chem. Sci.* **2016**, *7*, 85-88; c) Tlahuext-Aca, A.; Hopkinson, M. N.; Garza-Sanchez, R. A.; Glorius, F. *Chem. Eur. J.* **2016**, *22*, 5909-5913; d) Shu, X.-z.; Zhang, M.; He, Y.; Frei, H.; Toste, F. D. *J. Am. Chem. Soc.* **2014**, *136*, 5844-5847.

General introduction

1.3. Electron donor-acceptor complexes

Recently, a photochemical approach to radical generation intrinsically different from photoredox catalysis, since it does not require the use of an exogenous catalyst, has been developed by Melchiorre as a most practical synthetic tool.⁵¹ This strategy relies on the association of an electron acceptor substrate **A** and a donor molecule **D**, forming an aggregate in the ground state called an electron donor-acceptor complex (**EDA complex**) (Figure I-5).⁵²

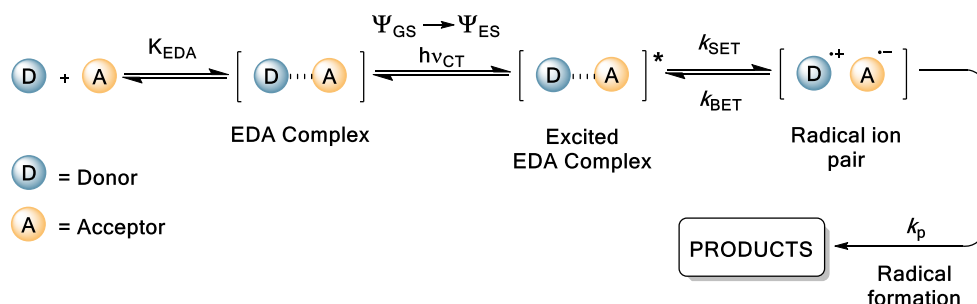


Figure I-5. Classical EDA complex theory. K_{EDA} : association constant for the formation of the EDA complex; k_{SET} , k_{BET} , k_p : kinetic constants; Ψ_{GS} : wave function associated with the ground state; Ψ_{ES} : wave function associated with the excited state.

EDA complexes usually absorb visible light, even if their constituents, the **A** and **D** molecules, are not able to do so. Excitation by visible light absorption

⁵¹ a) Arceo, E.; Jurberg, I. D.; Álvarez-Fernández, A.; Melchiorre, P. *Nat. Chem.* **2013**, *5*, 750-756; b) Arceo, E.; Bahamonde, A.; Bergonzini, G.; Melchiorre, P. *Chem. Sci.* **2014**, *5*, 2438-2442; c) Nappi, M.; Bergonzini, G.; Melchiorre, P. *Angew. Chem., Int. Ed.* **2014**, *53*, 4921-4925; d) Kandukuri, S. R.; Bahamonde, A.; Chatterjee, I.; Jurberg, I. D.; Escudero-Adán, E. C.; Melchiorre, P. *Angew. Chem., Int. Ed.* **2015**, *54*, 1485-1489; e) Wozniak, Ł.; Murphy, J. J.; Melchiorre, P. *J. Am. Chem. Soc.* **2015**, *137*, 5678-5681; f) Cao, Z.-Y.; Ghosh, T.; Melchiorre, P. *Nat. Commun.* **2018**, *9*, 3274.

⁵² Foster, R. *J. Phys. Chem.* **1980**, *84*, 2135-2141.

may result in an intramolecular SET event that can generate radical intermediates.⁵³ Photophysical properties of EDA complexes have been extensively studied since 1950s,⁵⁴ but only recently their photochemistry has started to be extensively exploited in synthetic chemistry.⁵⁵

1.3.1. Photophysical background

In 1952, Robert Mulliken proposed a quantum-mechanical theory to rationalize formation and behavior of EDA complexes. Mulliken charge-transfer theory is based on the association of an electron-rich substrate (a donor with a low ionization potential) with an electron-accepting molecule (an acceptor with high electronic affinity) resulting in the formation a new complex (Figure I-5). Electronic coupling of **D** and **A** frontier orbital results in the formation of new molecular orbitals and hence, a new absorption band appears. This charge-transfer band ($h\nu_{CT}$) is associated with the electronic transition $\Psi_{GS} \rightarrow \Psi_{ES}$ and can lie in the visible region range. Excitation of the ground-state EDA complex with the proper wavelength results in population of Ψ_{ES} , triggering an intramolecular electron transfer from **D** to **A** that results in the formation of a radical ion pair complex. This complex may ultimately furnish reactive radicals, unless an unproductive back electron transfer (**BET**) from the radical ion pair will take place. If the processes leading to radical generation (e.g. rearrangements, additions, eliminations) are

⁵³ Rosokha, S. V.; Kochi, J. K. *Acc. Chem. Res.* **2008**, *41*, 641–653.

⁵⁴ a) Hilinski, E. F.; Masnovi, J. M.; Amatore, C.; Kochi, J. K.; Rentzepis, P. M. *J. Am. Chem. Soc.* **1983**, *105*, 6167–6168; b) Singh, J. O.; Anunziata, J. D.; Silber, J. J. *Can. J. Chem.* **1985**, *63*, 903–907; c) Mulliken, R. S. *J. Am. Chem. Soc.* **1950**, *72*, 600–608; d) Mulliken, R. S. *J. Am. Chem. Soc.* **1952**, *74*, 811–824; d) Mulliken, R. S. *J. Phys. Chem.* **1952**, *56*, 801–822.

⁵⁵ a) Lima, C. G. S.; Lima, T. d. M.; Duarte, M.; Jurberg, I. D.; Paixao, M. W. *ACS Catal.* **2016**, *6*, 1389–1407; b) Yuan, Y.-Q.; Majumder, S.; Yang, M.-H.; Guo, S.-R. *Tetrahedron Lett.* **2020**, *61*, 151506; c) Crisenza, G. E. M.; Mazzarella, D.; Melchiorre, P. *J. Am. Chem. Soc.* **2020**, *142*, 5461–5476.

General introduction

kinetically not competitive with the BET, then the photoactivation of the EDA complex will be synthetically unproductive.

1.3.2. Synthetic applications

The competition of productive processes with BET, that hampered the development of synthetic processes based on EDA photochemistry,⁵⁶ was overcome in the seminal contributions to the field⁵⁷ adopting a common strategy (Figure I-6).

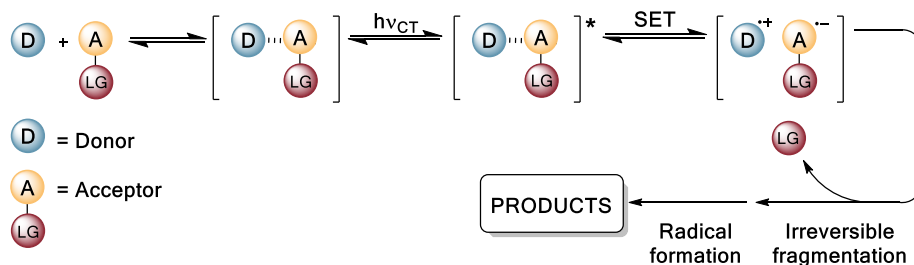


Figure I-6. A general strategy to make the EDA complex synthetically productive.

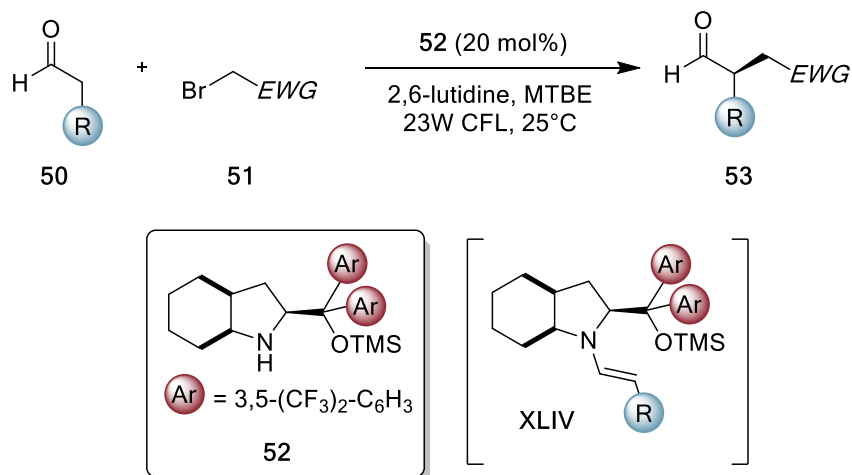
The presence of a suitable leaving group (LG) in the acceptor makes the fragmentation of the corresponding radical anion $A^{\cdot-}$ an irreversible event, fast enough to compete with the BET. This can afford two radical intermediates prone to be engaged in synthetically useful reactions.

These principles were used by Melchiorre in a seminal 2013 report where EDA complex photochemistry has been introduced as a mild and powerful radical generation strategy (Scheme I-14).^{51a} The key chiral EDA complex, exploited in the enantioselective alkylation of aldehydes (**50**) with electron-

⁵⁶ Rathore, R.; Kochi, J. K. *Adv. Phys. Org. Chem.* **2000**, *35*, 193–318.

⁵⁷ Cantacuzène, D.; Wakselman, C.; Dorme, R. *Chem. Soc., Perkin Trans. 1* **1977**, 1365–1371.

deficient benzyl and phenacyl bromides (**51**), is formed between enamines **XLIV** and the aromatic moiety of **51**.



Scheme I-14. Enantioselective catalytic α -alkylation of aldehydes enabled by irradiation of an enamine-based EDA complex

There are, however, some important drawbacks associated with the use of this approach. The most important one is the limitation in the diversity of the reaction products due to the need to select highly polarized reagents that will eventually end up in the product scaffold. One strategy to circumvent this limitation consists in the use of sacrificial donor compounds that are engaged by electron-poor substrates in the formation of an EDA complex (Figure I-7). After visible light triggered radical formation, the resulting reactive intermediate can be trapped by an external substrate that does not need specific electronic properties to elicit EDA complex formation.

General introduction

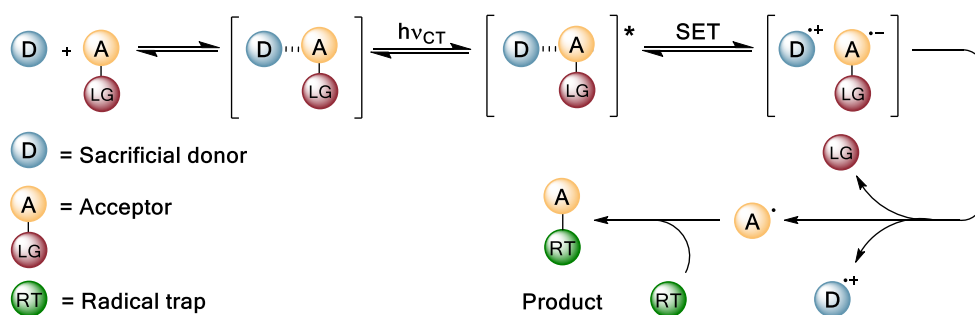
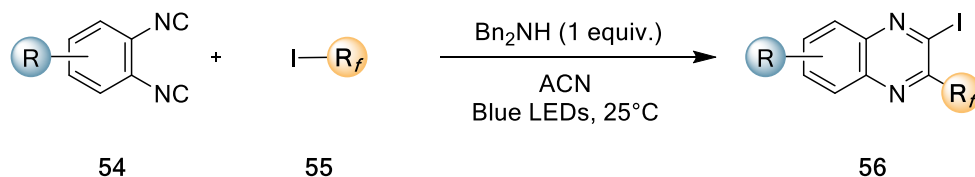


Figure I-7. General strategy for radical formation based on the use of a stoichiometric sacrificial donor to drive EDA complex formation.

An example of application of this strategy is depicted in Scheme I-15.⁵⁸ By employing dibenzylamine as a sacrificial donor to engage perfluoroalkyl iodides (**55**) in EDA complex formation, generation of perfluoroalkyl radical was accomplished under blue LEDs irradiation. The fluoroalkyl radicals have been then trapped by α -diisocyanoarenes (**54**) to give quinoxaline derivatives (**56**).



Scheme I-15. Photochemical generation of perfluoroalkyl radicals for the synthesis of quinoxalines. R_f = perfluoroalkyl residue.

Quantum yield measurement suggests that this reaction proceeds through a self-propagating radical chain mechanism. Thus, the photochemical activity of EDA served as an initiation to sustain a chain process.

So far, the discussed strategies rely upon the electronic bias of the substrates and the presence of a suitable fragmenting functionality.

⁵⁸ Sun, X.; Wang, W.; Li, Y.; Ma, J.; Yu, S. *Org. Lett.* **2016**, *18*, 4638–4641.

Generally, simple and easily available substrates with native functionalities (mostly organic halides) are fit for the purpose. This approach, albeit advantageous in terms of availability of the reagents, is still limited by strictly electronic requirements of the substrates main core. Thus, only highly polarized radicals are accessible by this strategy.

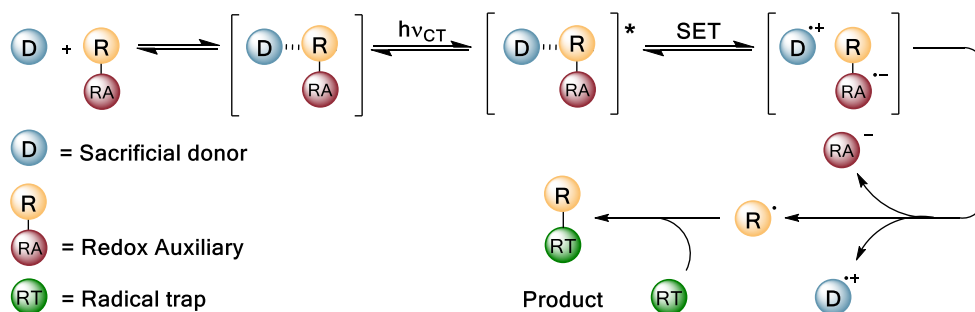


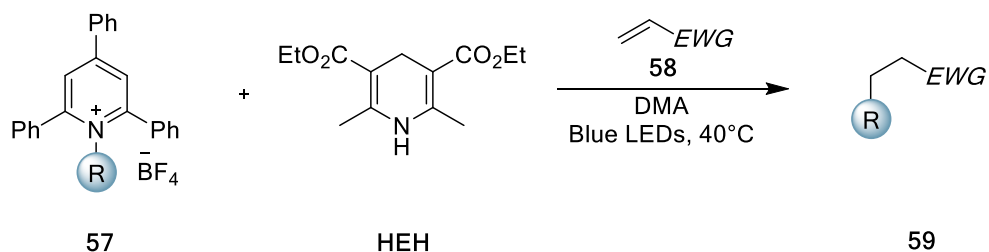
Figure I-8. General representation of the use of a redox auxiliary that drives both the formation of an EDA complex and the generation of an electronically unbiased radical.

A strategy overcoming the aforementioned limitation takes advantages of reaction partner bearing a purposely installed activating group (Figure I-8). It acts as both redox-auxiliary (RA) and leaving group, so that the substrate has not to fulfill any electronic requirements and the radical arising from fragmentation is therefore electronically unbiased.

An elegant demonstration of this approach was reported by Aggarwal (Scheme I-16).⁵⁹ Taking advantage of the electron-accepting properties of pyridinium salts **57**, easily prepared from amines, a Giese addition to electron-poor olefins **59** was developed. Pyridinium derivatives served as redox auxiliaries for EDA complex formation with Hantzsch ester (HEH), allowing the generation of alkyl radicals.

⁵⁹ Wu, J.; Grant, P. S.; Li, X.; Noble, A.; Aggarwal, V. K. *Angew. Chem., Int. Ed.* **2019**, *58*, 5697–5701.

General introduction



Scheme I-16. Pyridinium salts as redox auxiliaries for the activation of primary amines and the generation of alkyl radicals.

A further step in EDA photochemistry-driven reactions is the design of effective catalytic processes. The catalytic species must be involved only in the radical generation and efficiently undergo turnover. This strategy (Figure I-9) differs from the ones previously described in the fact that the donor radical cation can be reduced and hence be ready to engage another molecule of acceptor in an EDA complex.

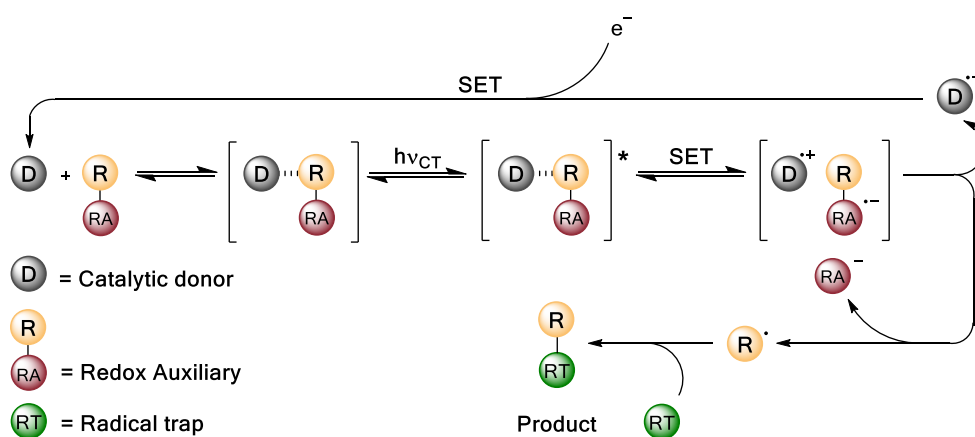
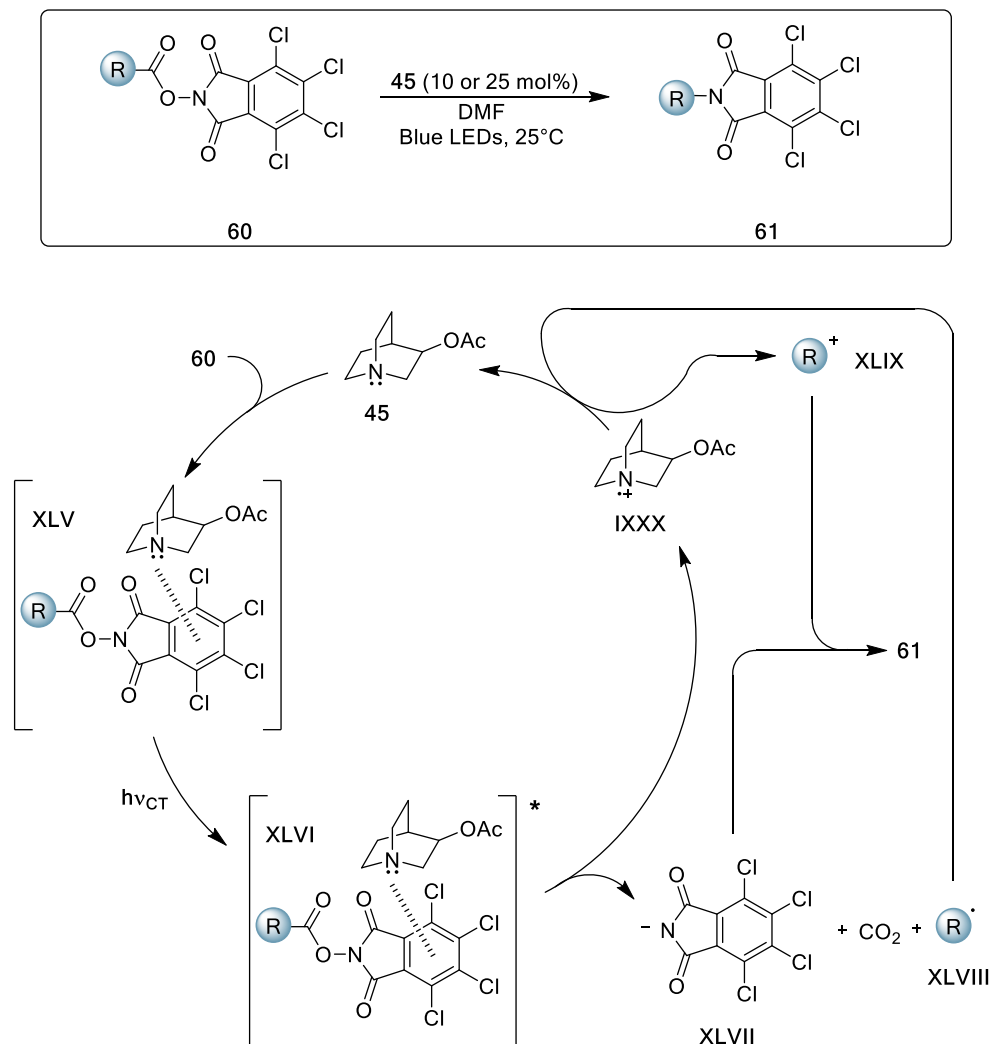


Figure I-9. General strategy for catalysis in EDA complex photochemistry

Bach reported an application of this concept demonstrating that 3-acetoxyquinuclidine (**45**) could be used as a catalytic electron donor Scheme (I-17).⁶⁰



Scheme I-17. Use of 3-acetoxyquinuclidine as an external electron-donor catalyst for visible-light-mediated radical processes via EDA complex formation.

⁶⁰ Bosque, I.; Bach, T. *ACS Catal.* **2019**, *9*, 9103–9109.

General introduction

Association with electron-poor tetrachlorophthalimide ester (**61**) affords the EDA complex **XLV**. Under visible light irradiation an intracomplex SET takes place between the **45** nitrogen-centered lone pair and the phthalimide moiety triggering the breakdown of the complex and leading to radical **XLVIII** through decarboxylation and to radical cation **IXXX**. The latter oxidizes **XLVIII**, turning the catalyst over, affording carbocation **XLIX**. Trapping of this intermediate with anion **XLVII** affords the desired product **61**.

CHAPTER II

Asymmetric cross-dehydrogenative coupling of aldehydes with xanthenes

II.1. Introduction	43
II.1.1. Cross dehydrogenative coupling	43
II.1.2. Alkylation of benzylic C–H bonds	45
II.1.3. Asymmetric oxidative enamine catalysis	49
II.2. Objective	53
II.3. Asymmetric photoredox CDC of aldehydes with xanthenes	56
II.3.1. HTE screening and control experiments	56
II.3.2. Reaction scope	59
II.3.3. Mechanistic investigation	64
II.3.4. Conclusions	68
II.4. Supporting information	69

UNIVERSITAT ROVIRA I VIRGILI

Harnessing Visible Light for the Development of Novel Synthetic Strategies

Marco Michele Mastandrea

CHAPTER II

Asymmetric cross-dehydrogenative coupling of aldehydes with xanthenes

II.1. Introduction

II.1.1. Cross dehydrogenative coupling

The term “cross dehydrogenative coupling (CDC)” was introduced by Li to define direct Y–Z bond formations from Y–H and Z–H bonds under oxidative conditions.¹ In particular, being the C–C bond one of the most abundant, versatile and important type of bond in nature, cross-coupling reaction between two C–H bonds has become a fundamental strategy in synthetic organic chemistry. In fact, cross dehydrogenative coupling strategies offer three main advantages (Figure II-1)²:

- no prefunctionalization is required, improving step economy;
- high atom efficiency is achieved, being molecular hydrogen the formal leaving group;
- direct and selective C–H activation is highly desirable on late-stage functionalization.

¹ a) Li, Z.; Li, C.-J. *J. Am. Chem. Soc.* **2004**, *126*, 11810-11811; b) Li, Z.; Li, C.-J. *J. Am. Chem. Soc.*, **2005**, *127*, 6968-6969; (c) Li, Z.; Bohle, D. S.; Li, C.-J. *Proc. Natl. Acad. Sci.*, **2006**, *103*, 8928- 8933.

² a) Li, C.-J. *Acc. Chem. Res.* **2009**, *42*, 335-344; b) Gulzar, N.; Schweitzer-Chaput, B.; Klussmann, M. *Catal. Sci. Technol.* **2014**, *4*, 2778-279; c) Girard, S. A.; Knauber, T.; Li, C.-J. *Angew. Chem., Int. Ed.* **2014**, *53*, 74-100; d) Li, C.-J. *Chem.* **2016**, *1*, 423-437; e) Varun, B. V.; Dhineshkumar, J.; Bettadapur, K. R.; Siddaraju, Y.; Alagiri, K.; Prabhu, K. R. *Tetrahedron Lett.* **2017**, *58*, 803-824.

Asymmetric cross-dehydrogenative coupling of aldehydes with xanthenes

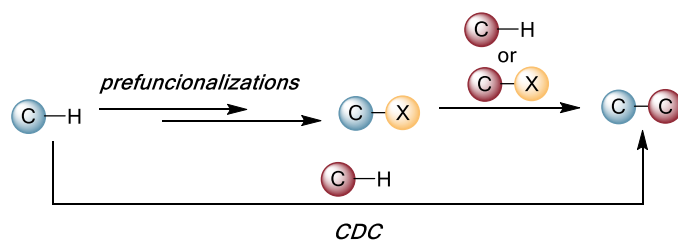


Figure II-1. Concept of CDC.

The two major challenges in CDC reactions design are: *how to activate the C-H bond* and *how to connect the C-H species*. The activation of a C-H bond can be achieved in several ways but not all of them are suitable for CDC, since it could affect the functional group tolerance, guide the regioselective outcome and ultimately determine the fate of the reaction. Activation strategies for C-H bonds applicable in CDC design can be categorized into six types (Figure II-2)³:

- hydrogen atom abstraction;
- α -heteroatom-driven hydride removal;
- tautomerization;
- single-electron arene/alkene oxidation;
- in situ* C-H functionalization;
- metal-catalyzed C-H activation.

Recognizing the intermediates generated in each strategy makes it easier to choose an appropriate coupling partner, leading to a rational CDC design.

The linking of different C-H fragments is intrinsically challenging given that multiple reactive C-H sites are present in any molecule. The desired regioselective outcome can be achieved with a judicious choice of activation systems and fine-tuned conditions. These two aspects allow for

³ Huang, C.-Y.; Kang, H.; Li, J.; Li, C.-J. *J. Org. Chem.* **2019**, *84*, 12705-12721.

exalting subtle differences on either electronics or sterics, thus achieving selectivity.

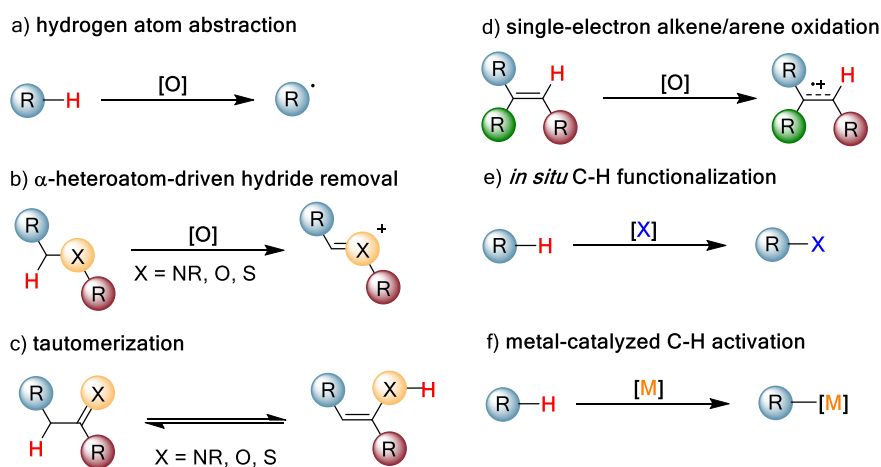


Figure II-2. Different approaches to generate active intermediates for CDCs.

II.1.2. Alkylation of benzylic C–H bonds *via* CDC

A particularly promising field of research within the realm of CDC is the coupling of benzylic C–H bonds with C(sp)–H, C(sp²)–H and C(sp³)–H bonds.⁴ It must be pointed out that, in contrast with the conventional methods depicted in Figure II-3, the CDC approach does not rely upon the use of highly reactive organometallic reagents, making the process more compatible with the presence of sensitive functional groups and minimizing waste generation.

Several methodologies allowing the benzylic alkylation *via* CDC, mainly at the α -position of carbonyl compounds, have been described.⁵ A selection of representative examples is reported in Scheme II-1.

⁴ Bosque, I.; Chinchilla, R.; Gonzalez-Gomez, J. C.; Gujjarro, D.; Alonso, F. *Org. Chem. Front.* **2020**, *7*, 1717-1742.

⁵ a) Li, Z.; L. Cao, L.; Li, C.-J. *Angew. Chem. Int. Ed.* **2007**, *46*, 6505-6507; b) N. Borduas, N.; Powell, D. A. *J. Org. Chem.* **2008**, *73*, 7822-7825; c) Correia, C. A.; Li, C.-J. *Tetrahedron*

Asymmetric cross-dehydrogenative coupling of aldehydes with xanthenes

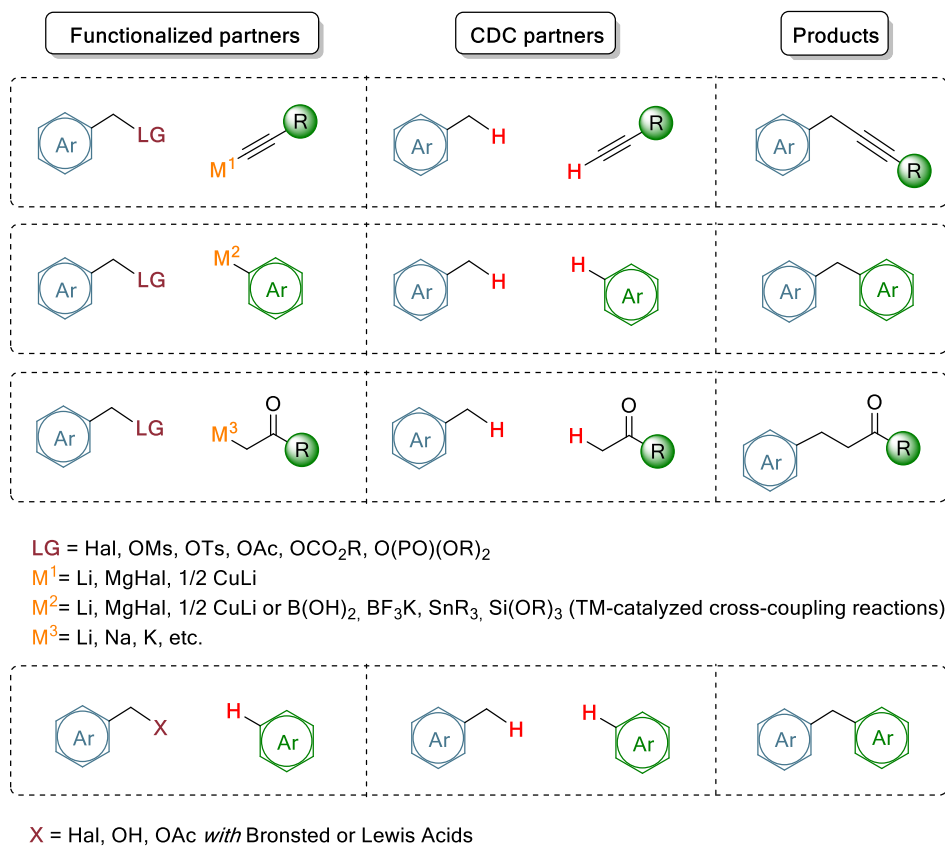
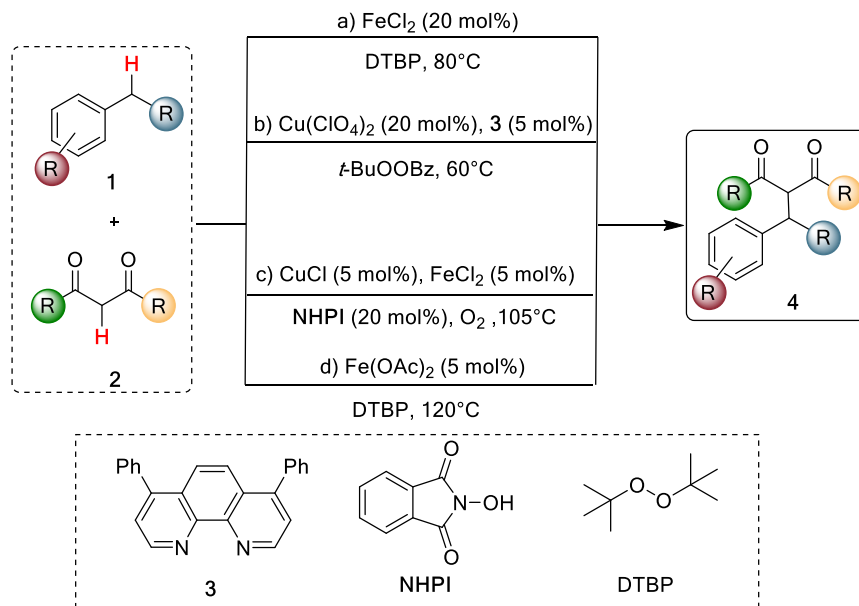


Figure II-3. Functionalized and CDC partners for the benzylation of different carbon centers.

In these reports, the benzylic reactive intermediate is generated by hydrogen atom abstraction by Fe(III) species or O-centered radicals formed upon homolysis of the corresponding peroxides. Harsher conditions are usually required in order to engage primary benzylic C–H bonds in abstraction processes (Scheme II-1, d). The activation of 1,3-dicarbonyl compounds (**2**) is instead achieved through the metal-assisted formation of the corresponding enolates.

All these protocols are generally based on the use of peroxides as terminal oxidants (except for Ref. 5c) in combination with high temperatures and are limited to 1,3-dicarbonyl substrates.

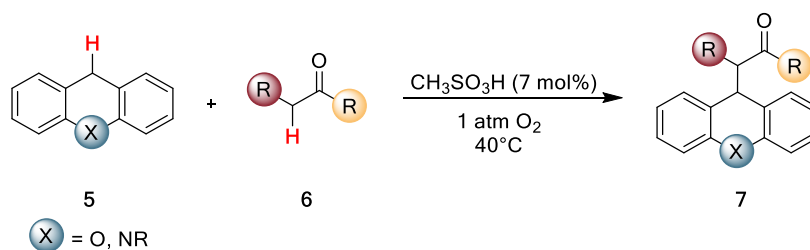


Scheme II-1. Cu- and Fe-mediated CDC reactions between 1,3-dicarbonyl compounds and toluene derivatives.

However, in the case of xanthenes or 9,10-dihydroacridines (**5**) milder conditions are required and the CDC can be accomplished under metal-free conditions (Scheme II-2).⁶ Moreover, the nucleophilic partner (**6**) does not need to fulfill specific requirements, being simple ketones, and only catalytic amounts of strong acid are needed to promote the reaction. The authors postulated the autoxidative formation of xanthene hydroperoxide, subsequently delivering the corresponding carbocation via acid-catalyzed C–O bond cleavage.

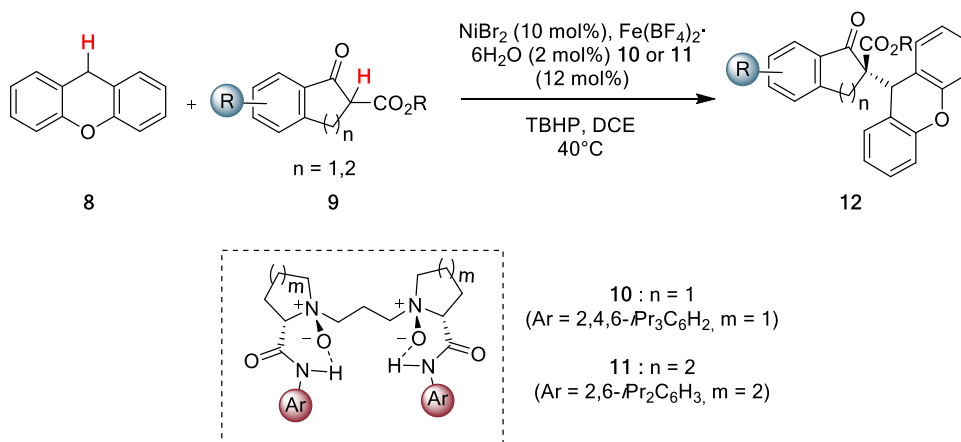
⁶ Pintér, Á.; Sud, A.; Sureshkumar, D.; Klusmann, M. *Angew. Chem. Int. Ed.* **2010**, *49*, 5004-5007.

Asymmetric cross-dehydrogenative coupling of aldehydes with xanthenes



Scheme II-2. Metal-free catalyzed CDC reactions between xanthene or 9,10-dihydroacridine derivatives and carbon nucleophiles.

In 2013, Feng reported an asymmetric CDC of 1-indanones and 1-tetralones (**9**) with xanthene, mediated by a Ni(II)/Fe(II) bimetallic catalytic system (Scheme II-3).⁷ Extensive optimization studies led to the synthesis of the desired products (**12**) in good yields and excellent enantioselectivity.



Scheme II-3 Cooperative bimetallic catalytic system for asymmetric CDC reactions between xanthene and 1-indanone or 1-tetralone derivatives.

This example shows the potential of asymmetric metal catalysis in the enantioselective alkylation of benzylic C–H bonds. Anyway, the most impressive progress in the field is due to the advent of asymmetric oxidative enamine catalysis.

⁷ Cao, W.; Liu, X.; Peng, R.; He, P.; Lin, L.; Feng, X. *Chem. Commun.* **2013**, *49*, 3470-3472.

II.1.3. Asymmetric oxidative enamine catalysis

The classical enamine catalytic process involves the reaction of a nucleophilic enamine intermediate with an electrophile for C–C or C–X bond formation.⁸ Beyond their nucleophilic character, enamine intermediates have interesting redox properties, in particular they could be readily oxidized *via* single-electron transfer or in a two-electron process coupled with deprotonation.⁹

Recently, exploration of oxidative strategies in enamine catalysis has enabled the coupling with nucleophiles, thus expanding the scope of typical enamine catalysis (Figure II-4).¹⁰ In this framework, three strategies emerged:

- a) oxidation of the nucleophile into an electrophile, then engaged in a typical enamine cycle (Figure II-4, a);
- b) single-electron oxidation of the enamine into electrophilic radical cation species, able to couple with nucleophiles delivering α -functionalized products (Figure II-4, b);
- c) dehydrogenative process to the corresponding iminium ion intermediate. Subsequent Michael addition affords β -substituted products (Figure II-4, c).

⁸ a) Matos Paz, B.; Jiang, H.; Jørgensen, K. A. *Chem. Eur. J.* **2015**, *21*, 1846-1853; b) Donslund, B. S.; Johansen, T. K.; Poulsen, P. H.; Halskov, K. S.; Jørgensen, K. A. *Angew. Chem., Int. Ed.* **2015**, *54*, 13860-13874; c) Jiang, H.; Albrecht, L.; Jørgensen, K. A. *Chem. Sci.* **2013**, *4*, 2287-2300; d) Li, J.-L.; Liu, T.-Y.; Chen, Y.-C. *Acc. Chem. Res.* **2012**, *45*, 1491-1500; e) Mukherjee, S.; Yang, J. W.; Hoffmann, S.; List, B. *Chem. Rev.* **2007**, *107*, 5471-5569.

⁹ a) Fritsch, J. M.; Weingarten, H.; Wilson, J. D. *J. Am. Chem. Soc.* **1970**, *92*, 4038-4046; b) Schoeller, W.; Niemann, J. *J. Chem. Soc., Perkin Trans. 2* **1988**, *3*, 369-373; c) Zhu, J.; Liu, J.; Ma, R.; Xie, H.; Li, J.; Jiang, H.; Wang, W. A. *Adv. Synth. Catal.* **2009**, *351*, 1229-1232; d) Liu, J.; Zhu, J.; Jiang, H.; Wang, W.; Li, J. *Chem. Asian J.* **2009**, *4*, 1712-1716; e) Xiao, J. *ChemCatChem* **2012**, *4*, 612-615.

¹⁰ Zhu, L.; Wang, D.; Jia, Z.; Lin, Q.; Huang, M.; Luo, S. *ACS Catal.* **2018**, *8*, 5466-5484.

Asymmetric cross-dehydrogenative coupling of aldehydes with xanthenes

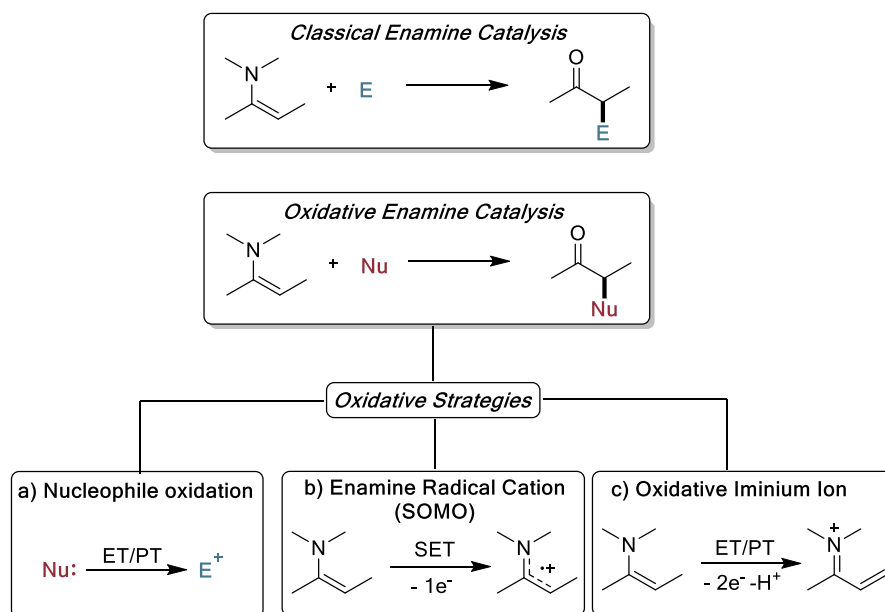


Figure II-4. Working modes for asymmetric oxidative enamine catalysis.

In this epigraph we will focus on application of the first oxidative strategy, being closely related with the topic of the chapter. In particular, among the various approaches to achieve enantioselective CDC reactions, enamine catalysis turned out to be a powerful strategy when aldehydes and ketones are involved.

When independent oxidation of the nucleophile is implemented, the main concern is the oxidative tolerability of the redox-active enamine species and amine catalyst.

Overcoming this issue has been relatively easy in the enantioselective CDC of tertiary amines and benzylic cyclic ethers (Figure II-5). The general strategy depicted in Figure II-5 is based on the α C-H oxidation of amines and ethers and trapping of the resulting electrophilic species with enamines. In 2012, Chi employed cooperative Cu(II) and secondary amine catalysis to achieve enantioselective CDC of tertiary amines and aldehydes

(Figure II-5, a).¹¹ TBHP was chosen as the oxidant and in these conditions (catalyst **15**) desired products were generally obtained in high enantioselectivity but low diastereoselectivity. Later on, Wang was able to extend the applicability of this strategy to cyclic ketones, using DDQ as an oxidant and L-phenylalanine (**16**) (Figure II-5, b).¹² The observed stereoselectivity is postulated to arise from a chiral ion pair between the carboxylate and iminium ion intermediate.

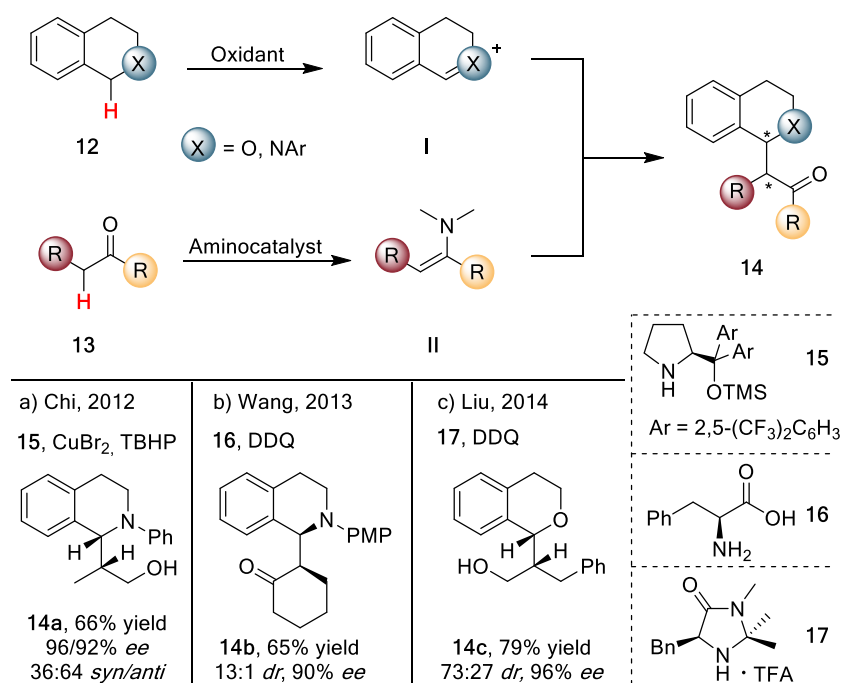


Figure II-5. Enantioselective CDC of amines and ethers with enamine through chemical oxidation. TBHP = *tert*-butyl hydroperoxide; DDQ = 2,3-dichloro-5,6-dicyano-*p*-benzoquinone.

In 2014, Liu reported an enantioselective enamine-CDC reaction between aldehydes and benzylic cyclic ethers (Figure II-5, c).¹³ Catalyst **17**, in

¹¹ Zhang, J.; Tiwari, B.; Xing, C.; Chen, X.; Chi, Y. R. *Angew. Chem. Int. Ed.* **2012**, *51*, 3649-3652.

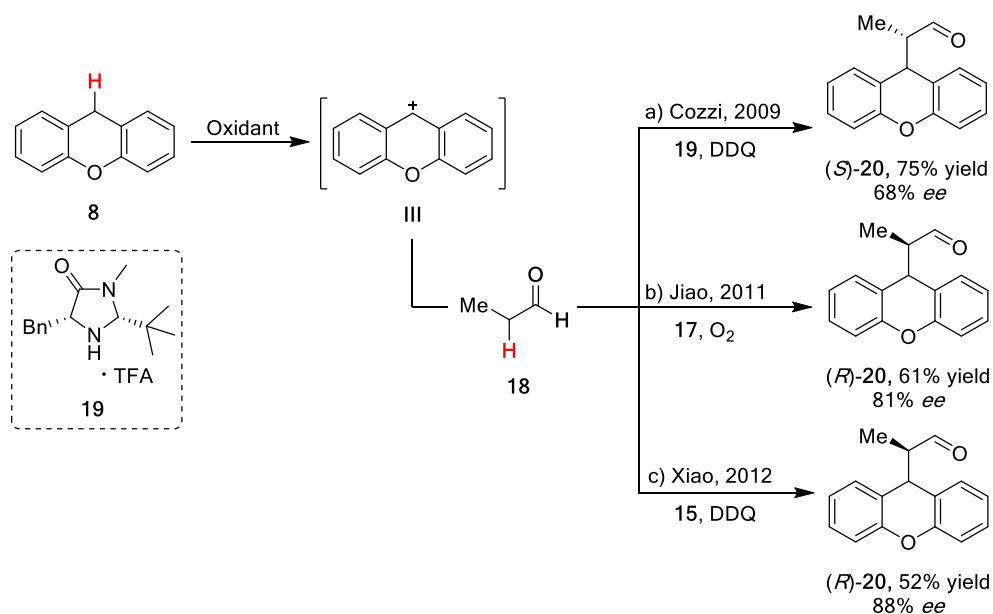
¹² Zhang, G.; Ma, Y.; Wang, S.; Kong, W.; Wang, R. *Chem. Sci.* **2013**, *4*, 2645-2671.

¹³ Meng, Z.; Sun, S.; Yuan, H.; Lou, H.; Liu, L. *Angew. Chem. Int. Ed.* **2014**, *53*, 543-547.

Asymmetric cross-dehydrogenative coupling of aldehydes with xanthenes

combination with DDQ, was identified to promote the reaction in a highly stereoselective fashion.

The oxidation of unfunctionalized benzylic substrates is instead more problematic due to their higher oxidation potential. Up to date, asymmetric oxidative enamine catalysis has been applied to the functionalization of conjugated benzyl compounds such as xanthene, 1,3,5-cycloheptatriene, flavanoids and indole derivatives.



Scheme II-4. Enantioselective oxidative α -benzylation of aldehydes.

Relevant to resume and compare the progress done in the field is the enantioselective oxidative CDC between xanthene (**8**) and propanal (**18**) (Scheme II-4). The common intermediate **III** is formed under oxidative conditions from **8** and then coupled with the enamine resulting from condensation of **18** with an aminocatalyst. In 2009, Cozzi reported an asymmetric α -benzylation reaction of aldehydes catalyzed by **19** with DDQ

as the oxidant (Scheme II-4, a).¹⁴ Under these conditions, product (*S*)-**20** is obtained in moderate yield and enantioselectivity. Next, Jiao¹⁵ and Xiao¹⁶ developed a similar transformation delivering (*R*)-**20** and employing catalysts **17** and **15**, respectively (Scheme II-4, b and c). These protocols guaranteed higher levels of stereocontrol, albeit with significant lowering in yields.

II.2. Objective

The direct functionalization of inert C–H bonds has emerged in recent years as a powerful tool in synthetic organic chemistry.¹⁷ The cross-dehydrogenative coupling (CDC) reactions represent one of the most successful examples of mild and selective C–C bond formations from C–H bonds. Compared with non-asymmetric CDC reactions, only limited examples of enantioselective protocols for the C–C coupling *via* C(sp³)–H activation have been reported so far. In this context, it has been verified that chiral aminocatalysis is a powerful tool in CDC reactions with aldehydes and ketones. These reactions were generally carried out with stoichiometric or excess amounts of strong oxidants, but the stability of aminocatalysts under oxidative conditions remains an issue.

¹⁴ Benfatti, F.; Capdevila, M. G.; Zoli, L.; Benedetto, E.; Cozzi, P. G. *Chem. Commun.* **2009**, 5919-5921.

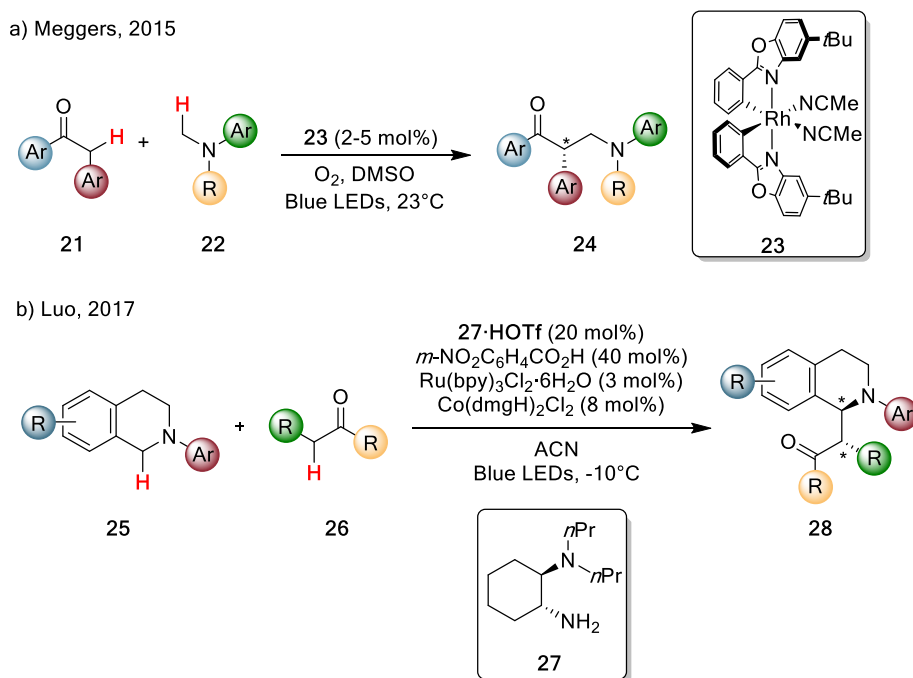
¹⁵ Zhang, B.; Xiang, S.-K.; Zhang, L.-H.; Cui, Y.; Jiao, N. *Org. Lett.* **2011**, *13*, 5212-5215.

¹⁶ Huang, F.; Xu, L.; Xiao, J. *Chin. J. Chem.* **2012**, *30*, 2721-2725.

¹⁷ a) Labinger, J. A.; Bercaw, J. E. *Nature* **2002**, *417*, 507-514; b) Godula, K.; Sames, D. *Science* **2006**, *312*, 67-72; c) Bergman, R. G. *Nature* **2007**, *446*, 391-393; d) Zhang, S.-Y.; Zhang, F.-M.; Tu, Y.-Q. *Chem. Soc. Rev.* **2011**, *40*, 1937-1949; e) Kuhl, N.; Hopkinson, M. N.; Wencel-Delord, J.; Glorius, F. *Angew. Chem. Int. Ed.* **2012**, *51*, 10236-10254; f) Zheng, C.; You, S.-L. *RSC Adv.* **2014**, *4*, 6173-6214.

Asymmetric cross-dehydrogenative coupling of aldehydes with xanthenes

To overcome this oxidative constraint, photoredox catalysis is a promising alternative since it enables the generation of reactive intermediates under mild conditions. Moreover, the synergistic combination of photoredox with asymmetric organocatalysis has emerged as a powerful approach to discover novel reactivities. However, application of photoredox catalysis to asymmetric CDC reactions remains a formidable challenge, and few examples have been described in literature so far (Scheme II-5).¹⁸ In both the examples depicted in Scheme II-5, the electrophilic intermediate involved is an iminium ion generated from **22** or **25** upon SET oxidation and subsequent hydrogen atom abstraction from amine radical cation.

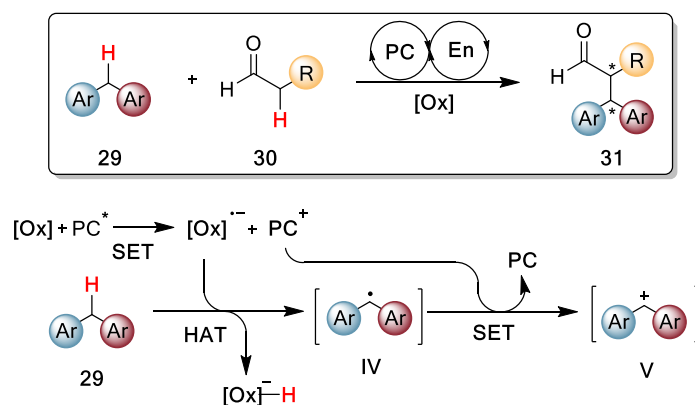


Scheme II-5. a) Photoinduced asymmetric dehydrogenative C–C bond formation; b) enantioselective CDC via photoredox multiple catalysis.

¹⁸ a) Tan, Y.; Yuan, W.; Gong, L.; Meggers, E. *Angew. Chem., Int. Ed.* **2015**, *54*, 13045-13048; b) Yang, Q.; Zhang, L.; Ye, C.; Luo, S.; Wu, L.-Z.; Tung, C.-H. *Angew. Chem. Int. Ed.* **2017**, *56*, 3694-3698.

Despite the great progress in enantioselective photoredox α -alkylation of aldehydes using alkyl bromides,¹⁹ there are few reports on the corresponding photoredox CDC reactions with non-functionalized C(sp³)–H bonds. Therefore, the main aim of this project is combining enamine and photoredox catalysis to enable an asymmetric coupling between diarylsubstituted CH₂ units and aldehydes (Scheme II-6).

Compared with the aforementioned enantioselective CDC coupling (Scheme II-5), we had to face different challenges in reaction planning. Since diarylmethanes **29** are lacking heteroatom lone pairs, their oxidation to the corresponding carbocations **V** or radical cations is harder to achieve. Thus, a two-step oxidation process needed to be implemented. The excited state photocatalyst should undergo oxidative quenching generating a species ([Ox]⁻) able to abstract a hydrogen atom from **29**. The benzylic radical **IV** should then be able to reduce PC⁺ and couple with the chiral enamine arising from **30**.²⁰



Scheme II-1. Asymmetric visible-light photoredox cross-dehydrogenative coupling of aldehydes with diarylmethanes. PC = photocatalyst; En = enamine; [Ox] = oxidant.

¹⁹ a) Nagib, D. A.; Scott, M. E.; MacMillan, D. W. C. *J. Am. Chem. Soc.* **2009**, *131*, 10875-10877; b) Meggers, E. *Chem. Commun.* **2015**, *51*, 3290-3301.

²⁰ This project has been conducted in collaboration with Dr. Evgeny Larionov.

Asymmetric cross-dehydrogenative coupling of aldehydes with xanthenes

II.3. Asymmetric photoredox CDC of aldehydes with xanthenes

II.3.1. HTE screening and control experiments

We commenced our study by investigating the asymmetric CDC between xanthene (**1a**) and pentanal (**2a**) under visible-light photoredox conditions in presence of **cat.1** as the catalyst (Figure II-6).

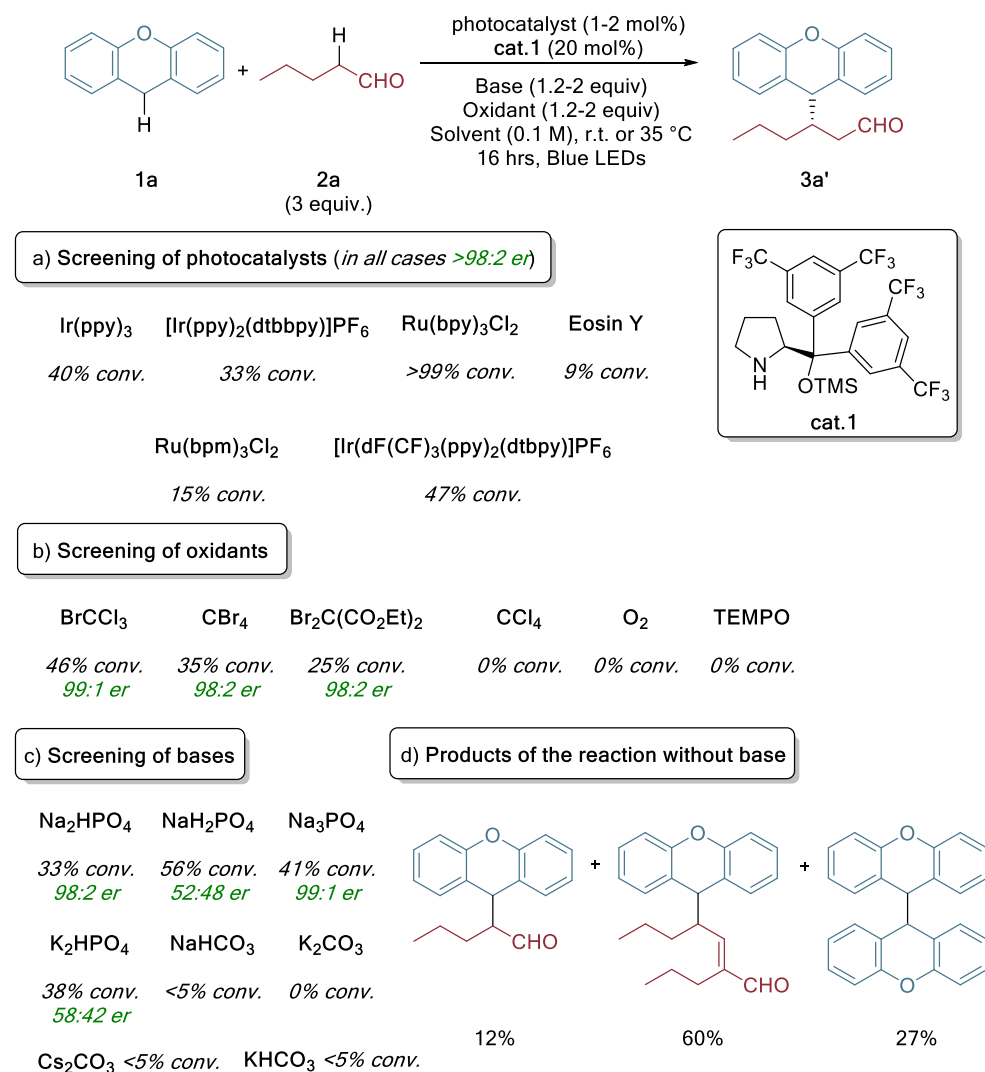


Figure II-6. HTE screening of reaction conditions (photocatalysts and bases); screening of oxidants (0.2 mmol scale). a) Photocatalyst (1 mol%), Na_3PO_4 (2

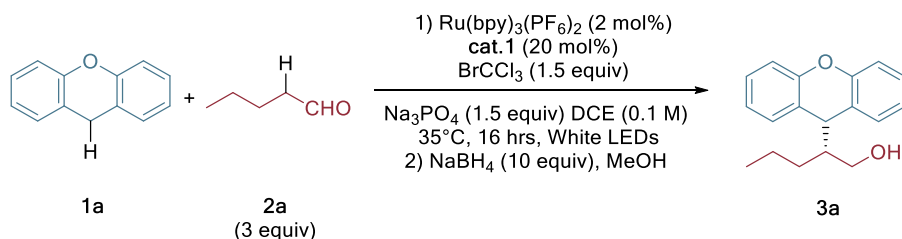
equiv), BrCCl_3 (1.2 equiv), DCM, rt.; b) $\text{Ru}(\text{bpy})_3\text{Cl}_2$ (2 mol%), Na_3PO_4 (1.2 equiv), 35°C ; c) $\text{Ir}(\text{ppy})_3$ (1 mol%), base (2 equiv), BrCCl_3 (3 equiv), ACN; d) standard conditions from Table II-1.

The use of high-throughput experimentation (Figure II-6 a and c; see Section II.4.3.3. for more details) allowed us to rapidly screen reaction conditions. We used a 96-well-plate reactor engineered to allow each reaction to be irradiated independently by a single light-emitting diode (LED) to evaluate important reaction parameters. Screening of solvents (see Section II.4.3.3. for details) and photocatalysts (Figure II-6, a) allowed us to identify DCE and $\text{Ru}(\text{bpy})_3\text{Cl}_2$ as an optimal solvent and photocatalyst, respectively. We did not observe any reasonable correlation between the reactivity and oxidation/reduction potentials of tested photocatalysts. The $\text{Ru}(\text{bpy})_3$ complex seems to have both potentials matching the corresponding electrochemical properties of reagents/intermediates (*vide infra*). Due to a better solubility, $\text{Ru}(\text{bpy})_3(\text{PF}_6)_2$ gave slightly better conversion when the reaction was performed on a catalytic scale (0.2 mmol). Screening of different oxidants showed that the presence of a weak C–Br bond is crucial for the sought reactivity: among different bromoalkanes that were tested BrCCl_3 gave the highest conversion to the product. In contrast, other oxidants (O_2 , CCl_4) showed no conversion to the desired product (Figure II-6, b).

Control experiments (Table II-1, entries 3-6) showed that light, photocatalyst, base and oxidant are all crucial for achieving an appreciable conversion to the product. Notably, base is required in order to scavenge HBr - a stoichiometric product of the reaction. In support of this hypothesis, in the absence of any base mostly self-condensation products of aldehyde **2a** along with 12% of the desired product were observed in the reaction crude (Figure II-1, d; see Section II.4.3.4. for further details). Other mild phosphate bases (e.g. NaH_2PO_4 , Na_2HPO_4) also gave a reasonable conversion, whereas stronger carbonate bases (such as K_2CO_3 , Cs_2CO_3)

Asymmetric cross-dehydrogenative coupling of aldehydes with xanthenes

were ineffective in the studied reaction (Figure II-6, c). During the screening of organocatalysts (Table II-1, bottom) we found that MacMillan's catalysts **cat.2** and **cat.3** are active in the studied reaction; however, lower enantioselectivities were observed with these species. Comparison of different prolinol derivatives **cat.4**–**cat.6** highlights the importance of both TMS protecting group and bis(trifluoromethyl)phenyl substituent for reactivity and enantioselectivity. The loading of **cat.1** can be lowered to 10 mol% without affecting the reaction yield and enantioselectivity (Table II-1, entry 2). Finally, when the reaction was performed in the presence of a radical scavenger (Table II-1, entry 7), much lower conversion to product was achieved, thus indicating a radical nature of the process (*vide infra*).



Entry	Deviation from standard conditions	Conv. (%) ^[a]	Yield (%) ^[b]	er ^[c]
1	None	78	65	97:3
2	cat.1 (10 mol%)	76	63	97:3
3	Dark	0	n.d.	n.d.
4	No $\text{Ru}(\text{bpy})_3(\text{PF}_6)_2$	4	n.d.	97:3
5	No Na_3PO_4	10	n.d.	97:3
6	No BrCCl_3	0	n.d.	n.d.
7	With 1.1 equiv Galvinoxyl	26	n.d.	97:3

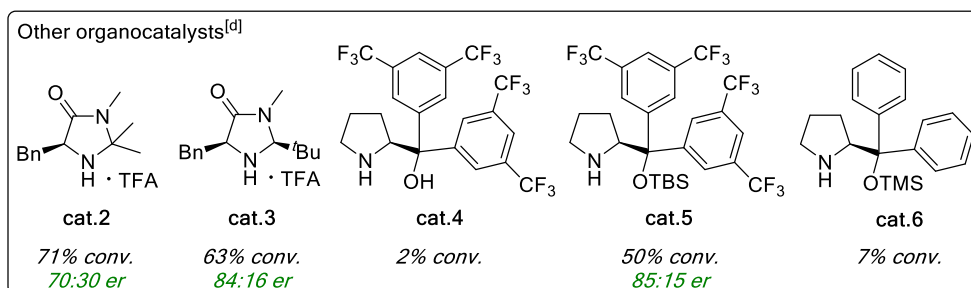


Table II-1. Optimization of reaction conditions and control experiments. Reactions performed on 0.2 mmol scale. ^[a]Conversion was determined by GC analysis. ^[b]Yield of isolated product. ^[c]Determined by HPLC analysis using a chiral stationary phase. ^[d]Results for **cat.2-cat.6** with no variation from standard conditions. n.d.= not determined.

II.3.2. Reaction scope

The scope of the enantioselective CDC of xanthene with various aldehydes was then extensively investigated under the optimized reaction conditions (Figure II-7).

Asymmetric cross-dehydrogenative coupling of aldehydes with xanthenes

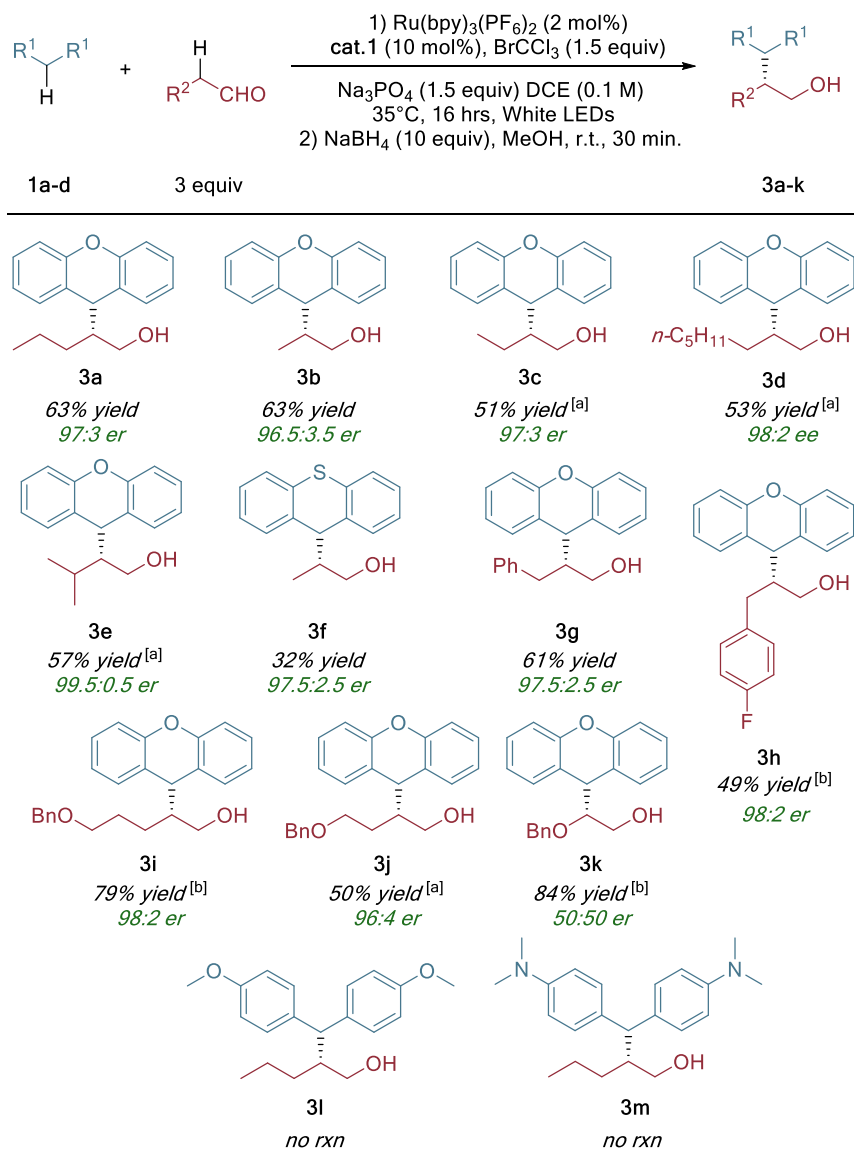


Figure II-7. Scope of aldehydes and diarylmethanes in the asymmetric photoredox CDC. Reactions performed on 0.2 mmol scale. ^[a] 2 mol% of Ru(bpy)₃Cl₂. ^[b] 20 mol% of cat. 1.

Aliphatic aldehydes delivered products in good yields and excellent enantioselectivities (3a-d). The more sterically hindered isobutyraldehyde (2e) gave product 3e in 57% yield and 99.5:0.5 er. Thioxanthene (1b) was

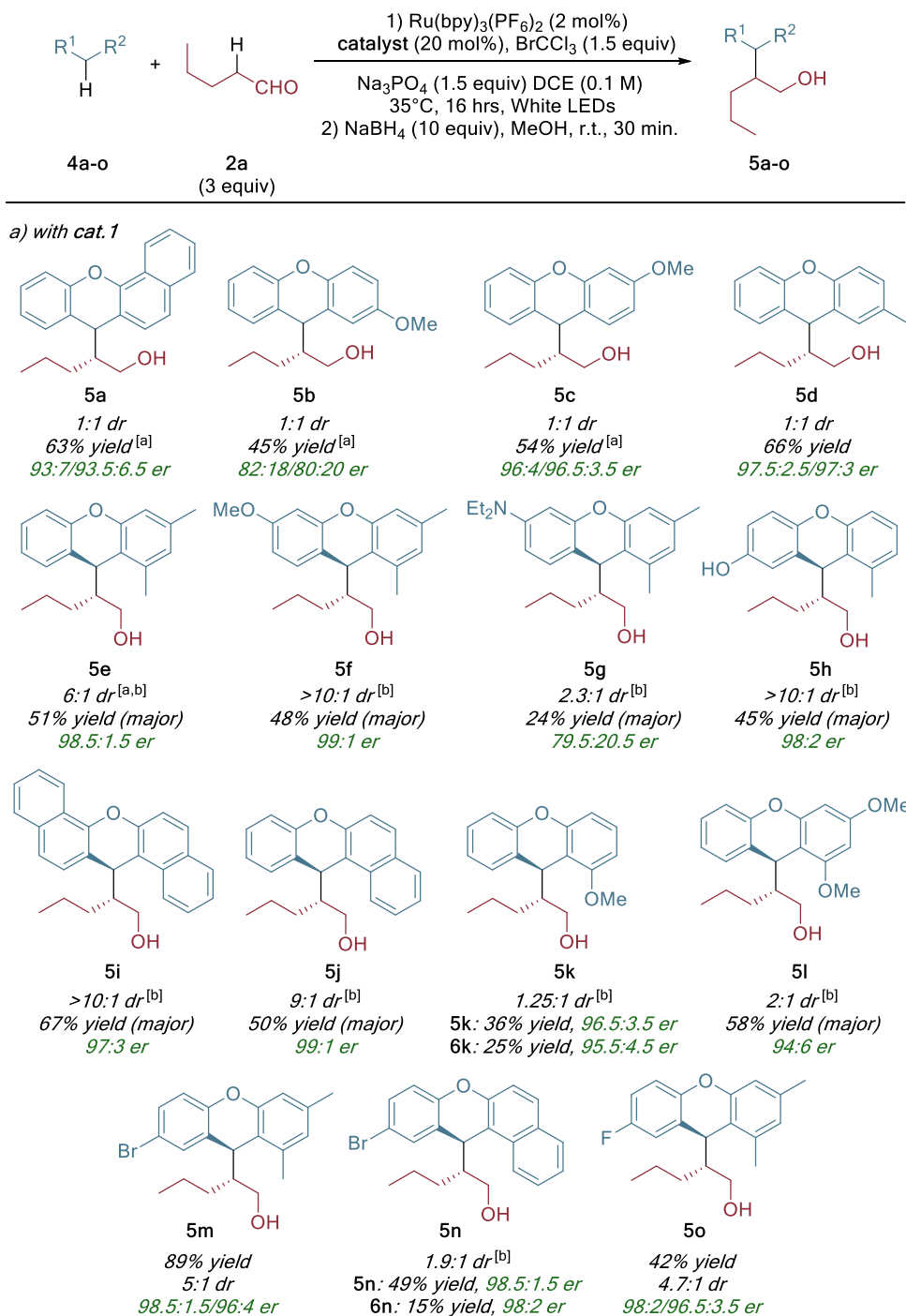
well tolerated in the CDC reaction (**3f**). Substituted phenylpropanals as well as benzyloxy-substituted aldehydes were compatible with the catalytic system (**3g-k**). Surprisingly, product **3k** with a benzyloxy substituent directly attached to the α -carbon of the aldehyde reactant (*i.e.*, to the β -carbon of the enamine intermediate) was obtained as a racemic mixture.²¹ Non-conformationally restricted, electron-rich diarylmethanes (**1l,m**) unfortunately did not give the desired products.

Next, different substituted xanthenes were subjected to the photoredox CDC with pentanal (Figure II-8, a).²² 2-, 3- and 4-substituted xanthenes delivered the corresponding products in good yields and high enantioselectivities (up to 97.5:2.5 er), but eventually as 1:1 mixtures of diastereomers (**5a-d**). To our delight, the reaction with 1-methyl-substituted xanthenes gave much higher diastereoselectivities (up to 10:1) and in many cases single diastereomers could be easily isolated (**5e-h, m-o**). Products derived from benzo-fused xanthenes (**5i-j, n**) were obtained in good yields and excellent diastereo- and enantioselectivities. On the other side, 1-methoxyxanthenes gave the corresponding products with lower diastereoselectivities (**5k-l**) allowing, however, the isolation of both diastereomers in moderate yields and high enantiomeric purities.

²¹ We think the highly electron-rich nature of the enamine intermediate could be responsible for this behavior by triggering a non-enantioselective pathway with participation of the derived radical-cation.

²² Substituted xanthenes were prepared according to: B6b, E.; Hillringhaus, T.; Nitsch, J.; Klusmann, M. *Org. Biomol. Chem.* **2011**, *9*, 1744-1748.

Asymmetric cross-dehydrogenative coupling of aldehydes with xanthenes



b) with *cat.2*

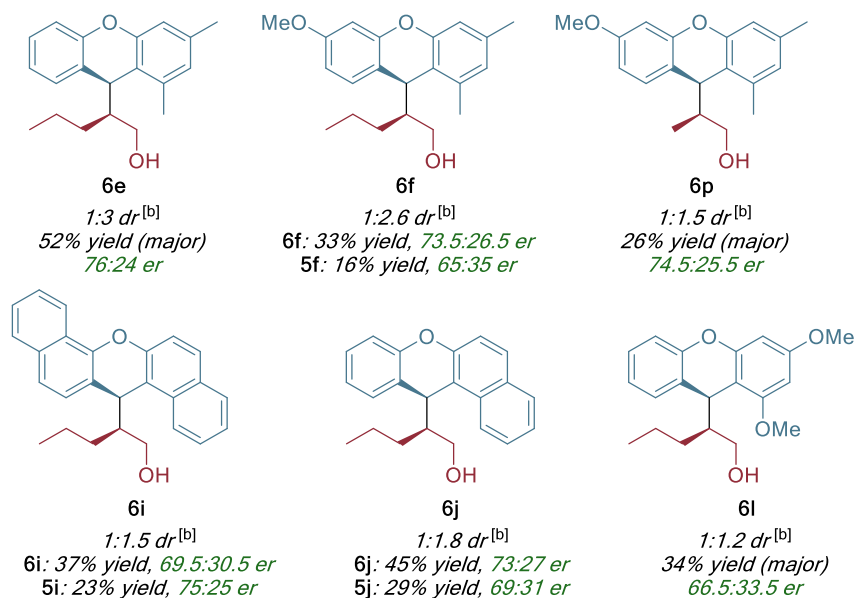


Figure II-8. Scope of substituted xanthenes in the asymmetric photoredox CDC.

Reactions performed on 0.2 mmol scale. ^[a] Carried out with 10 mol% **cat.1**.

^[b]Diastereomeric ratio determined by NMR analysis of the crude reaction mixture, given as **5/6** ratio.

The reaction tolerates different functional groups, such as methoxy, phenolic hydroxyl, diethylamino, bromo and fluoro. This could open up possibilities for the orthogonal functionalization of products by cross-coupling (**5m-n**) or etherification (**5h**). Interestingly, we found that switching from the Jørgensen-Hayashi's catalyst **cat.1** to MacMillan's catalyst **cat.2** allowed to switch the diastereoselectivity in favor of a different diastereomer, where the configuration of the α -carbon had been inverted (Figure II-8, b).²³ Several substrate combinations were tested with **cat.2**, affording moderate to good yields of the corresponding products (up to 74%

²³ Although catalysts **cat.1**, **cat.2** and **cat.3** gave the same configuration of the α -carbon atom in the product **3a** (Table II-1), an opposite configuration of the α -carbon atom in products **5** and **6** was observed when catalyst **cat.2** was employed (Figure II-8). This side-differentiation change could be caused by the increased size of the substituents at the xanthenes partner.

Asymmetric cross-dehydrogenative coupling of aldehydes with xanthenes

combined yield of diastereomers). Due to the lower diastereoselectivity achieved with this catalyst, the yields of individual diastereomers were relatively moderate. Enantioselectivities with **cat.2** reached the modest level of 76:24 er (for **6e**), and further screening of imidazolinones did not significantly improve this result (*e.g.*, 79:21 er for **6e** with **cat.3**, see II.4.3.5. for more details). In general, in the studied transformation the **cat.1** is more selective in terms of enantio- and diastereoselectivity, compared with imidazolinones **cat.2** and **cat.3**. In the case of 1-substituted xanthenes **4e-o** it leads to a stronger catalyst control of diastereoselectivity by **cat.1**, whereas the reaction in presence of **cat.2** is substrate controlled. The absolute configuration of product **5e** was determined by single-crystal X-ray diffraction of its ferrocene derivative. The second diastereomer (**6e**) was crystallized as a racemate, which allowed us to determine its relative configuration (Figure II-9).



Figure II-9. X-ray structure of ferrocene derivative of **5e** (left) and (*rac*)-**6e** (right).

II.3.3. Mechanistic investigation

The proposed mechanism for the studied transformation is shown in Figure II-10. In the photoredox cycle, bromotrichloromethane ($E_{1/2}^{\text{red}} = -0.18 \text{ V vs}$

SCE)²⁴ is first reduced by the excited state of the Ru(II) complex ($E_{1/2}$ Ru(II)^{*}/Ru(III) = -0.81 V vs SCE)²⁵ to the CCl₃ radical (oxidative quenching), which then abstracts a hydrogen atom from **1a** to generate the xanthyl radical INT1.²⁶ Suppression of the catalytic reaction in the presence of a radical scavenger (*vide supra*) gave the first evidence for the radical nature of the process. Secondly, an experimentally measured kinetic isotope effect (KIE) of 4.0 (see Section II.4.6.) indicates that C–H bond cleavage occurs during the rate-limiting step. This was additionally confirmed by DFT study of the reaction mechanism (see Section II.4.8.1. for more details).²⁷ Calculations show that the hydrogen abstraction step by the CCl₃ radical through transition state TS1 is rate-limiting with an activation barrier $\Delta G^\ddagger = 8.3$ kcal/mol (Figure II-10). Moreover, the KIE predicted by computations (4.3) is in a perfect agreement with the experimental value of 4.0. Quenching studies (see Section II.4.7. for details) show significant quenching of the excited Ru(bpy)₃²⁺ by BrCCl₃ (quenching rate $k_q = 1.5 \times 10^8$ M⁻¹ s⁻¹) which is in agreement with the proposed mechanism.²⁸ At this point we cannot exclude a radical chain mechanism where radical INT1

²⁴ Murayama, E.; Kohda, A.; Sato, T. *J. Chem. Soc., Perkin Trans.* **1980**, *1*, 947-949.

²⁵ Kalyanasundaram, K. *Coord. Chem. Rev.* **1982**, *46*, 159-244.

²⁶ The second product of this step, CHCl₃ was detected in the crude reaction mixture (see Sec. II.4.5.).

²⁷ a) DFT calculations have been performed by Dr. Evgeny Larionov. DFT method: PCMDCE-B2PLYP-D3/6-311+G(d,p)//B3LYP/6-31G(d); b) Frisch, M. J.; Trucks, G. W.; Schlegel, H. B.; Scuseria, G. E.; Robb, M. A.; Cheeseman, J. R.; Scalmani, G.; Barone, V.; Mennucci, B.; Petersson, G. A.; Nakatsuji, H.; Caricato, M.; Li, X.; Hratchian, H. P.; Izmaylov, A. F.; Bloino, J.; Zheng, G.; Sonnenberg, J. L.; Hada, M.; Ehara, M.; Toyota, K.; Fukuda, R.; Hasegawa, J.; Ishida, M.; Nakajima, T.; Honda, Y.; Kitao, O.; Nakai, H.; Vreven, T.; Montgomery, J. A., Jr.; Peralta, J. E.; Ogliaro, F.; Bearpark, M.; Heyd, J. J.; Brothers, E.; Kudin, K. N.; Staroverov, V. N.; Kobayashi, R.; Normand, J.; Raghavachari, K.; Rendell, A.; Burant, J. C.; Iyengar, S. S.; Tomasi, J.; Cossi, M.; Rega, N.; Millam, J. M.; Klene, M.; Knox, J. E.; Cross, J. B.; Bakken, V.; Adamo, C.; Jaramillo, J.; Gomperts, R.; Stratmann, R. E.; Yazyev, O.; Austin, A. J.; Cammi, R.; Pomelli, C.; Ochterski, J. W.; Martin, R. L.; Morokuma, K.; Zakrzewski, V. G.; Voith, G. A.; Salvador, P.; Dannenberg, J. J.; Dapprich, S.; Daniels, A. D.; Farkas, Ö.; Foresman, J. B.; Ortiz, J. V.; Cioslowski, J.; Fox, D. J. *Gaussian 09*, Revision D.01; Gaussian, Inc., Wallingford, CT, 2009.

²⁸ From the other side, a significant quenching rate k_q by xanthene **1a** (2.3×10^8 M⁻¹ s⁻¹) was observed. It can be caused by the fast oxidation of **1a** to the corresponding radical cation but it is unlikely to have an overall relevance due to the high value of the corresponding potential: $E_{1/2}^{ox} = 1.55$ V vs SCE. (see Ref. 29 and Section II.4.8.1. for further details).

Asymmetric cross-dehydrogenative coupling of aldehydes with xanthenes

($E_{1/2}^{ox} = 0.12 \text{ V vs SCE}$)²⁹ would directly reduce BrCCl_3 to a CCl_3 radical.³⁰ In this case photocatalyst is only required in the first cycle as initiator. The CCl_3 radical is then regenerated in a chain propagation step ($\Delta G_{rxn} = +6.9 \text{ kcal/mol}$, see Section II.4.8.2.).³¹

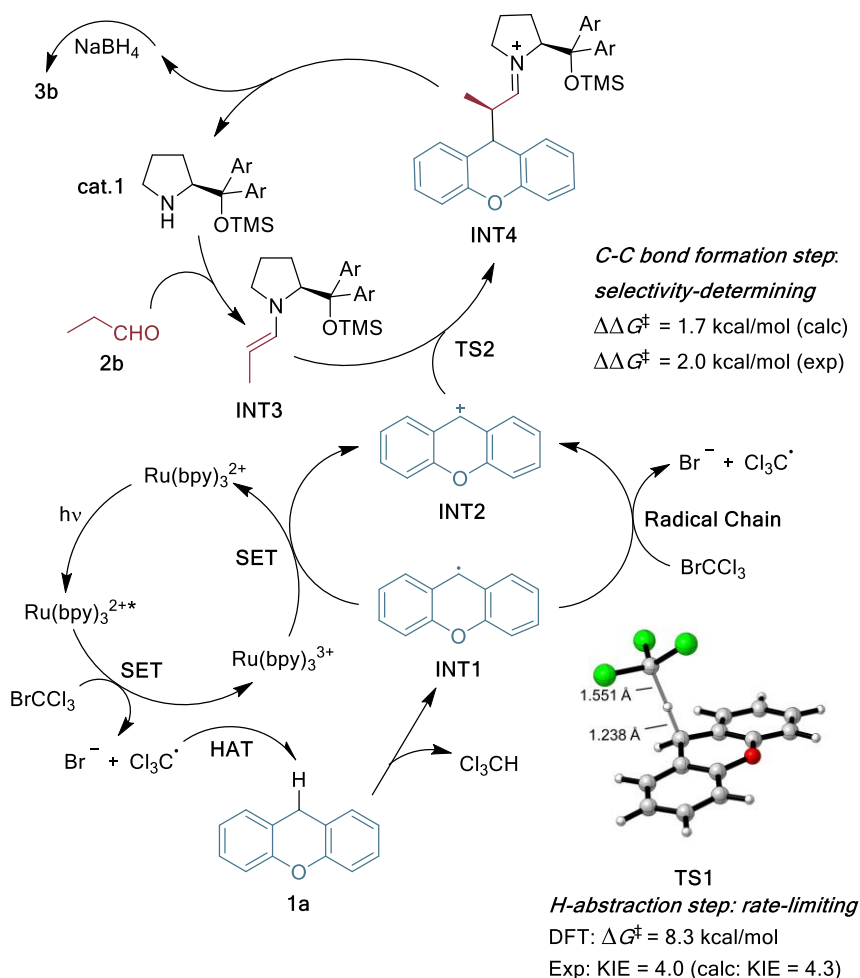


Figure II-10. Mechanistic proposal and DFT results.

²⁹ Zhu, X.-Q.; Dai, Z.; Yu, A.; Wu, S.; Cheng, J.-P. *J. Phys. Chem. B* **2008**, *112*, 11694-11707.

³⁰ The quantum yield measurements would be helpful to clarify this scenario, but they were not possible to perform due to the heterogeneity of the reaction mixture.

³¹ Alternative radical chain pathway *via* the addition of radical **INT1** onto enamine **INT3**, followed by the reduction of BrCCl_3 by the formed intermediate, is also feasible. However, according to further discussion this pathway would have a higher activation barrier (20.6 kcal/mol, Pathway A on Figure II-11).

In the computational study of the C–C bond forming step we considered different possibilities, such as attack of radical **INT1** onto enamine **INT3** (Pathway A in Figure II-10, $\Delta G^\ddagger = 20.6$ kcal/mol) or oxidation of enamine **INT3** to the corresponding radical-cation ($E_{1/2}^{\text{ox}} = 0.49$ V vs SCE)³² followed by the attack of **INT1** (Pathway B in Figure II-11, $\Delta G^\ddagger = 30.9$ kcal/mol).

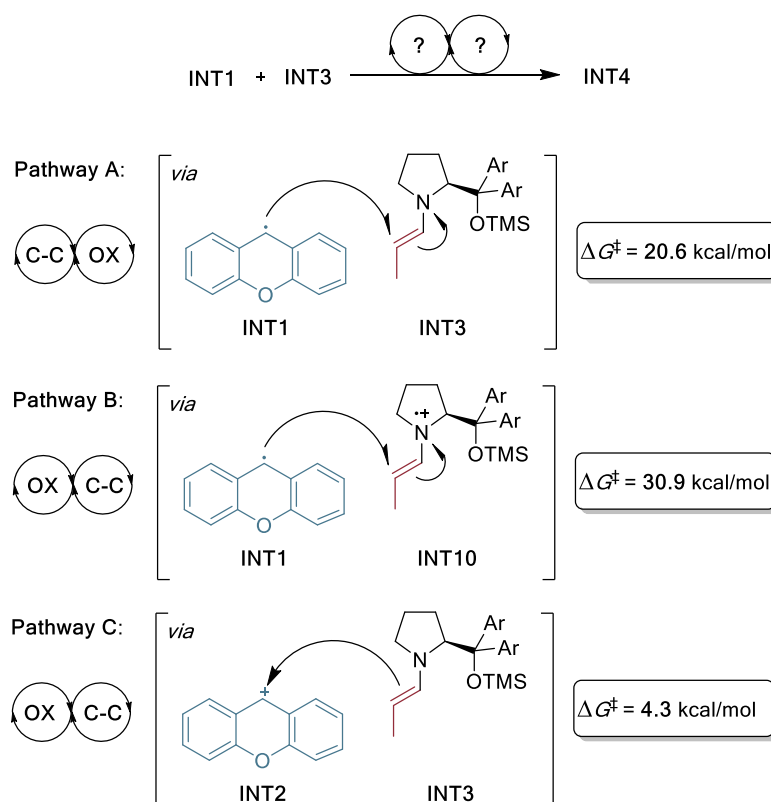


Figure II-11. Possible pathways of the C-C bond forming step.

However, the most energetically favorable pathway was found to be an oxidation of xanthyl radical **INT1** to cation **INT2** by the Ru(III) complex ($E_{1/2}$ Ru(III)/Ru(II) = 1.29 V vs SCE), followed by the attack of so-generated cation on enamine **INT3** *via* transition state **TS2** (Pathway C in Figure II-10, $\Delta G^\ddagger = 4.3$ kcal/mol). The latter step is the selectivity-determining, deciding

³² Oxidation potential from DFT calculations, see Section II.4.8.3.

Asymmetric cross-dehydrogenative coupling of aldehydes with xanthenes

which diastereomer of **INT4** and, correspondingly, enantiomer of product **3b**, is formed. Computed energy difference between diastereomeric transition states (*R*)-**TS2** and (*S*)-**TS2** ($\Delta\Delta G^\ddagger = 1.7$ kcal/mol) is in a perfect agreement with the experimental data ($\Delta\Delta G^\ddagger = 2.0$ kcal/mol). We also considered an alternative pathway *via* the reductive quenching of excited Ru(II) species ($E_{1/2} \text{Ru(II)}^*/\text{Ru(I)} = 0.77$ V *vs* SCE) by enamine **INT3** ($E_{1/2}^{\text{ox}} = 0.49$ V *vs* SCE). This redox step is therefore energetically favorable (see Sec. II.4.8.3.). The next step, attack on the corresponding radical-cation by radical **INT1**, has however a high activation barrier (Pathway B in Figure II-10, $\Delta G^\ddagger = 30.9$ kcal/mol). This pathway is thus less favorable than the oxidative quenching pathway.

II.3.4. Conclusions

In conclusion, we have developed a unique catalytic asymmetric cross-dehydrogenative coupling of xanthenes with aldehydes using visible light as a sustainable source of energy. The reaction features high enantioselectivities, good yields and wide functional group tolerance. The method was extended to the coupling of non-symmetrical xanthenes, which give CDC products with high diastereoselectivities, thus allowing isolation of single diastereomers in good yields and with high enantiomeric purities. Mechanistic studies by experimental and computational methods have shown that the reaction proceeds *via* the rate-limiting hydrogen abstraction followed by single-electron transfer and selectivity-determining attack of enamine on carbocation.

II.4. Supporting information

II.4.1. Table of contents

II.4.2. General information	70
II.4.3. Experimental details and procedures	71
II.4.3.1. General procedures for the synthesis of xanthenes	71
II.4.3.2. General procedure for the asymmetric photoredox CDC	72
II.4.3.3. Optimization of the reaction conditions by HTE	73
II.4.3.4. Further optimization of the reaction conditions	82
II.4.3.5. Screening of catalysts for the asymmetric CDC of 4e	86
II.4.4. Product characterization	87
II.4.5. Detection of CHCl_3 in the reaction mixture	125
II.4.6. KIE measurements	127
II.4.7. Quenching studies	130
II.4.8. Computational details	133
II.4.8.1. Photoredox cycle	134
II.4.8.2. Radical chain mechanism	140
II.4.8.3. C–C bond formation	142
II.4.9. References	150

II.4.2. General information

Unless otherwise stated, all reactions were conducted under air. All catalytic reactions were carried out under an inert atmosphere of nitrogen using a *Pure Lab* glovebox. All commercial reagents were used as received except the aldehydes that were distilled before the use. Bromotrichloromethane was distilled before the use and subsequently stored in the glove box. 3-(4-Fluorophenyl)propanal (**2h**),¹ 5-(benzyloxy)pentanal (**2i**)² and 4-(benzyloxy)butanal (**2j**)³ were prepared according to literature procedures. Solvents were dried over activated alumina columns and further degassed by three successive "freeze-pump-thaw" cycles if necessary. The experiments under microwave irradiation were carried out in a CEM Discover microwave reactor. Conversion and yield in HTE experiments were determined by UHPLC using an ACQUITY UPLC H-Class System from Waters. The ee in HTE experiments was measured by SFC chromatography using an Acquity UPC2 System from Waters. Flash chromatography was carried out using 60 mesh silica gel and dry-packed columns. Thin layer chromatography was carried out using Merck TLC Silicagel 60 F254 aluminum sheets. Components were visualized by UV light ($\lambda = 254$ nm) and stained with phosphomolybdic acid dip.

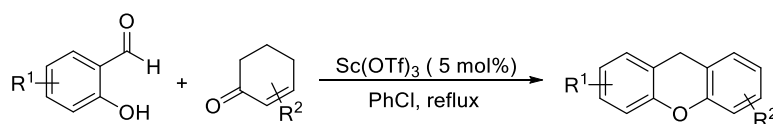
NMR spectra were recorded at 298 K on a Bruker Avance 400 Ultrashield or a Bruker Avance 500 Ultrashield spectrometer. ¹H NMR spectroscopy chemical shifts are quoted in ppm relative to tetramethylsilane (TMS). CDCl₃ was used as internal standard for ¹³C{¹H} NMR spectra. Chemical shifts are given in ppm and coupling constants in Hz. IR spectra were recorded on a Bruker Tensor 27 FT-IR spectrometer and are reported in wavenumbers (cm⁻¹). High performance liquid chromatography (HPLC) was performed on Agilent Technologies chromatographs (1100 and 1200 Series), using Daicel Chiralpak IA, IB, IC, AS-H and AD-H columns and

guard columns. Specific optical rotation measurements were carried out on a Jasco P-1030 polarimeter.

UV-Vis measurements were carried out on a Shimadzu UV-2401PC spectrophotometer equipped with a photomultiplier detector, double beam optics and D2 and W light sources. Fluorescence measurements were carried out on a Fluorolog Horiba Jobin Yvon spectrofluorimeter equipped with photomultiplier detector, double monochromator and Xenon light source.

II.4.3. Experimental details and procedures

II.4.3.1. General procedures for the synthesis of xanthenes



Scheme II-7. Preparation of xanthenes.

General procedure for the synthesis of xanthenes with conventional heating (GP1):

Ketone (1 equiv) was added to a solution of scandium(III) triflate (5 mol%) and *o*-salicylaldehyde (1.1 equiv) in PhCl (0.25 M) in a Young-valve Schlenk tube. The reaction mixture was refluxed for 40 hours (oil bath temperature 180 °C) and allowed to cool to room temperature. DCM (10 mL/mmol) and saturated aqueous NaHCO₃ (10 mL/mmol) were added to the reaction mixture, and the two layers were separated. The aqueous phase was extracted with DCM (3 × 10 mL/mmol) and the combined organic layers were dried over MgSO₄, filtered, and the solvent was removed by a rotary evaporator. Crude xanthene was purified by flash chromatography using *n*-pentane:EtOAc.

Asymmetric cross-dehydrogenative coupling of aldehydes with xanthenes

General procedure for the synthesis of xanthenes with microwave heating (GP2):

Ketone (1 equiv) was added to a solution of scandium(III) triflate (5 mol%) and *o*-salicylaldehyde (1.1 equiv) in PhCl (0.25 M) in a microwave tube. The reaction mixture was heated in a microwave oven at 180 °C for 30 min and allowed to cool to room temperature. DCM (10 mL/mmol) and saturated aqueous NaHCO₃ (10 mL/mmol) were added to the reaction mixture, and the two layers were separated. The aqueous phase was extracted with DCM (3 × 10 mL/mmol) and the combined organic layers were dried over MgSO₄, filtered, and the solvent was removed by a rotary evaporator. Crude xanthene was purified by flash chromatography using *n*-pentane:EtOAc.

II.4.3.2. General Procedure for the Asymmetric Photoredox CDC

General procedure GP3:

10 mL vial was charged with xanthene (0.2 mmol, 1.0 equiv), Ru(bpy)₃(PF₆)₂ (3.4 mg, 4.0 μmol, 2 mol%), **cat.1** (11.9 mg, 0.02 mmol, 10 mol%), Na₃PO₄ (49.2 mg, 0.3 mmol, 1.5 equiv) and 6 glass balls. DCE (2.0 mL) was added to the vial in the glovebox, followed by aldehyde (0.6 mmol, 3.0 equiv) and bromotrichloromethane (29.6 μL, 0.3 mmol, 1.5 equiv). The vial was sealed and the reaction mixture was irradiated by white LEDs at 35°C for 16 hours (irradiation setup depicted in Figure II-12). MeOH (1 mL) was then added to the reaction mixture, followed by portionwise addition of NaBH₄ (76 mg, 2.0 mmol) at 0 °C. The reaction mixture was stirred at room temperature for 0.5 hours and subsequently quenched with water (1 mL) and HCl (1 M). The combined organic phase was separated and the aqueous solution was extracted with CH₂Cl₂ (3 × 5 mL). Organic phase was dried over MgSO₄ and concentrated in vacuum to provide a crude mixture.

Purification by flash column chromatography (ethyl acetate:*n*-pentane mixture) gave desired product. The enantiomeric excess was determined by HPLC with chiral stationary phase using *n*-hexane/*i*-PrOH mixture as eluent..



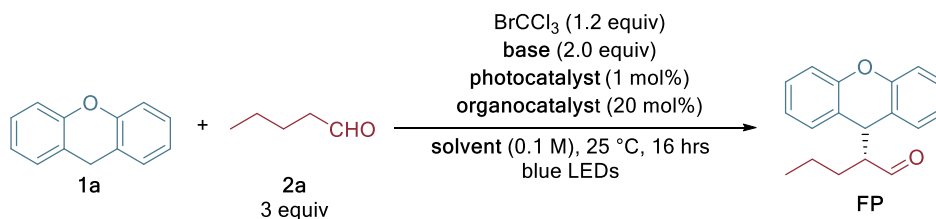
LEDs were purchased from luxeonstar (<http://www.luxeonstar.com>).

1. White LEDs:
<http://www.luxeonstar.com/neutral-white-20mm-star-coolbase-led-230lm>
Measured emission intensity at 800 mA:
175 mW/cm².

2. Royal blue LEDs:
<http://www.luxeonstar.com/royal-blue-20mm-star-coolbase-led-910mw>
Measured emission intensity at 800 mA:
70 mW/cm²

Figure II-12. Irradiation setup.

II.4.3.3. Optimization of the Reaction Conditions by HTE



Scheme II-8. HTE optimization of model reaction.

Asymmetric cross-dehydrogenative coupling of aldehydes with xanthenes

Procedure:

Experiments were set inside a glovebox under a nitrogen atmosphere. Screening reaction was carried out in 0.75 mL glass vials (8 × 30mm) in a 96-well aluminum block (equipment available from Analytical Sales and Services). Chemicals were dosed using multi-channel or single-channel pipettors as solutions.

- Organocatalysts were predosed (2 μmol) into the corresponding reaction vials (50 μL, 0.04 M MeOH or DCE).
- Substrate and photocatalysts were added to all reaction vials:
- Photocatalyst (0.2 μmol) (50 μL, 0.004 M DCE).
- Xanthene **1a** (10 μmol) (50 μL, 0.2 M DCE).
- The solvent was removed to dryness using GeneVac.
- Base (15 μmol) (37.5 μL, 0.4 M THF) was dosed as a slurry into vials.
- The solvent was removed to dryness using GeneVac and Teflon®-coated stirring bars were then added to each reaction vial.
- Pentanal (30 μmol/reaction) and BrCCl₃ (15 μmol/reaction) were then dosed together into each reaction vial as a solution in a reaction solvent (100 μL, 0.15 M in BrCCl₃ and 0.3 M in aldehyde).
- The 96-well plate was then sealed and stirred under irradiation of blue LEDs for 16 hours (22.1 V, 0.153 A) with fan cooling. During the course of the reaction the temperature reached 25°C.

Upon opening the plate to air, 500 μL of a solution of 1,3,5-trimethoxybenzene (used as internal standard to measure UPLC yields) in acetonitrile (0.02 M) was added into each vial. The plate was covered again

and the vials were stirred to ensure good homogenization, followed by centrifugation for 20 min. Into a separate 96-well LC block 500 μL of acetonitrile were added, followed by 20 μL of the diluted reaction mixtures. The LC block was then sealed with a silicon-rubber storage mat and mounted on an automated UPLC instrument for analysis. The reactions that gave some FP (final product) were analyzed in the UPC2 to determine the ee.

SFC-UPC2 conditions for the determination of ee: Column Chiralpak IC-3 (100 \times 4.6 \times 3mm), *SC*-CO₂/IPA 95:5, 3 mL/min, 1500 psi, column temperature: 35.0 $^{\circ}\text{C}$, detection at 240 nm;

$t_{\text{major}} = 2.40 \text{ min}$; $t_{\text{minor}} = 2.63 \text{ min}$ (Figure II-12).

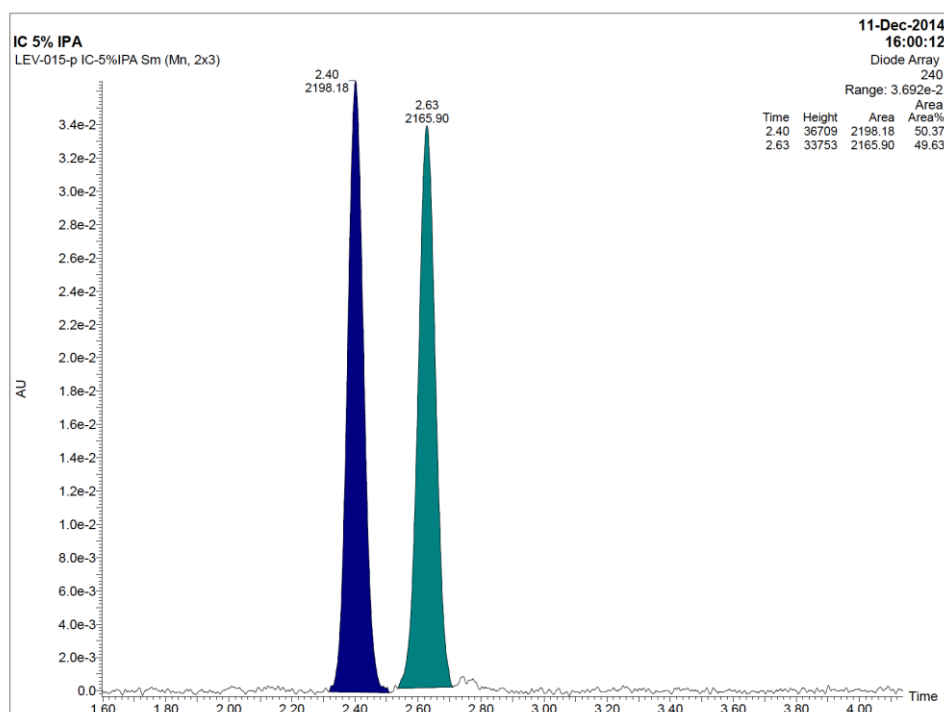
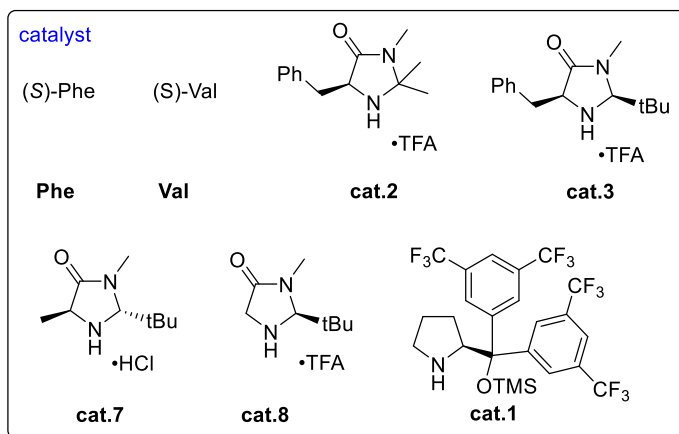
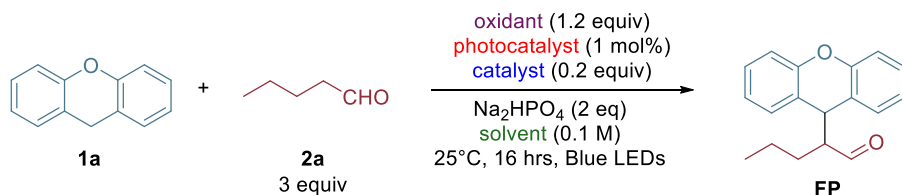


Figure II-13. SFC-UPC2 traces of the racemic sample of FP.

Asymmetric cross-dehydrogenative coupling of aldehydes with xanthenes

HTE screening 1:

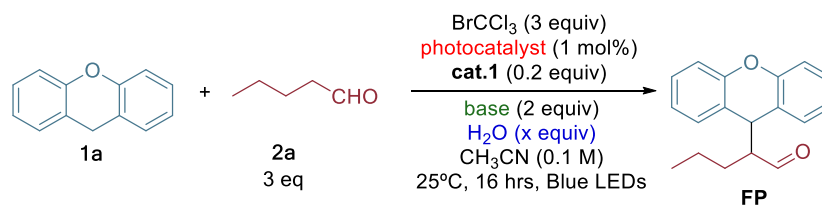


Oxidant	Photocatalyst	Solvent	No cat	Phe	Val	Cat.2	Cat.3	Cat.1	Cat.7	Cat.8
CBrCl ₃	Ir(ppy) ₂ (dtbbpy)PF ₆	CH ₃ CN		58			66	66		10
		DMF		7						
		CH ₂ Cl ₂		69		6	8	37		
Ph ₃ CClO ₄	-	CH ₃ CN	9	102						9
		DMF		10	10	76	87	27	85	77
		CH ₂ Cl ₂								

Scheme II-9. HTE screening 1. Legend: number (size of circle) = Conversion to FP; color of circle - enantioselectivity (blue - high, red - low).

Best hit: cat.1 in CH₃CN with BrCCl₃ as oxidant.

HTE screening 2:



Scheme II-9. HTE screening 2.

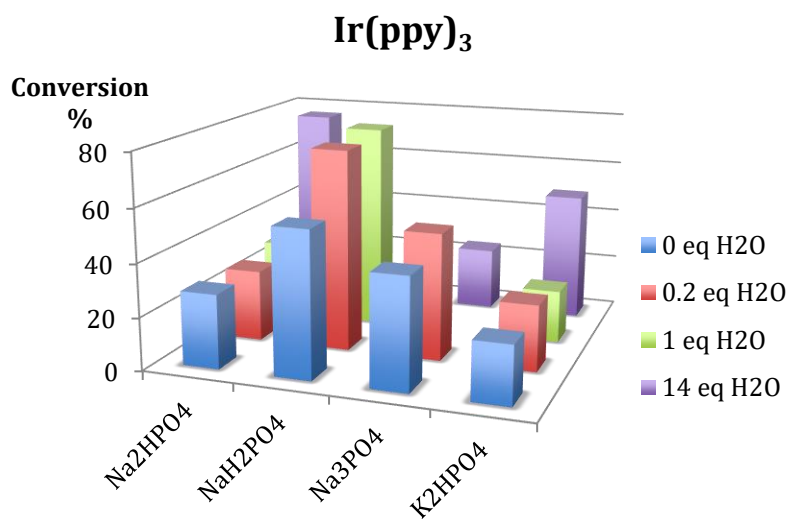


Figure II-14. Influence of water equivalents and base on conversion with $\text{Ir}(\text{ppy})_3$.

Asymmetric cross-dehydrogenative coupling of aldehydes with xanthenes

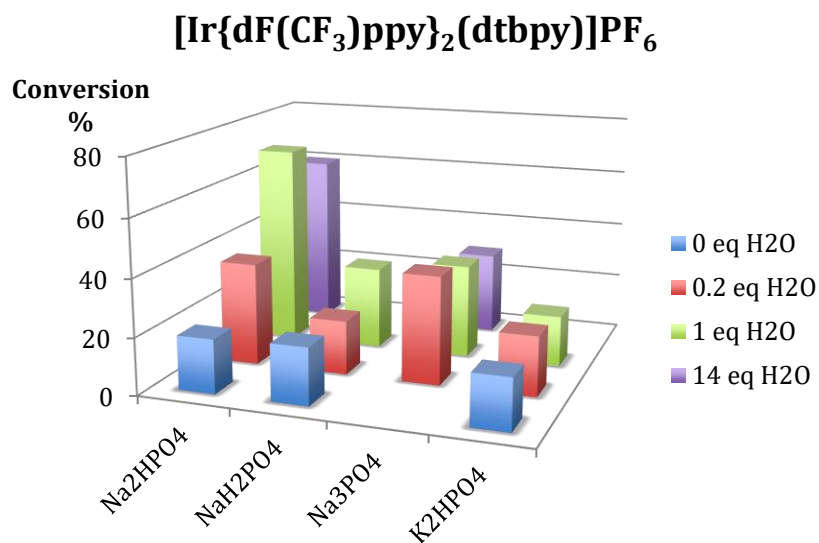


Figure II-15. Influence of water equivalents and base on conversion with $[\text{Ir}\{\text{dF}(\text{CF}_3)\text{ppy}\}_2(\text{dtbpy})]\text{PF}_6$.

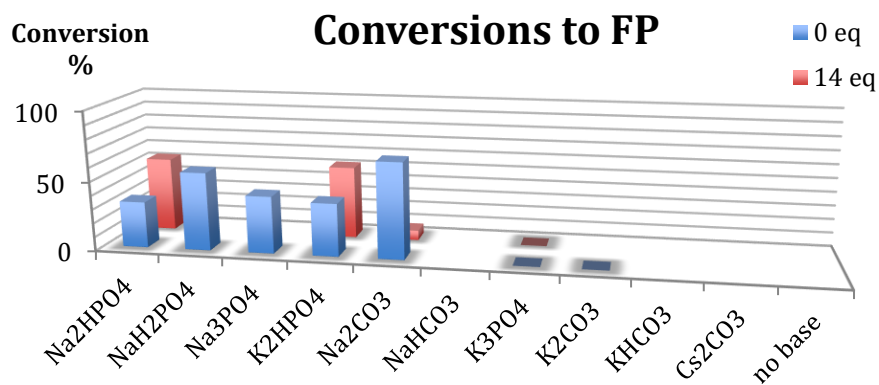


Figure II-16. Influence of water equivalents and other bases on conversion with $\text{Ir}(\text{ppy})_3$.

Enantioselectivities

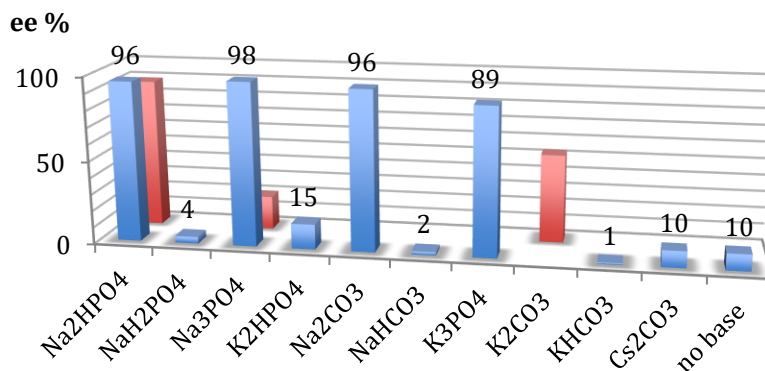
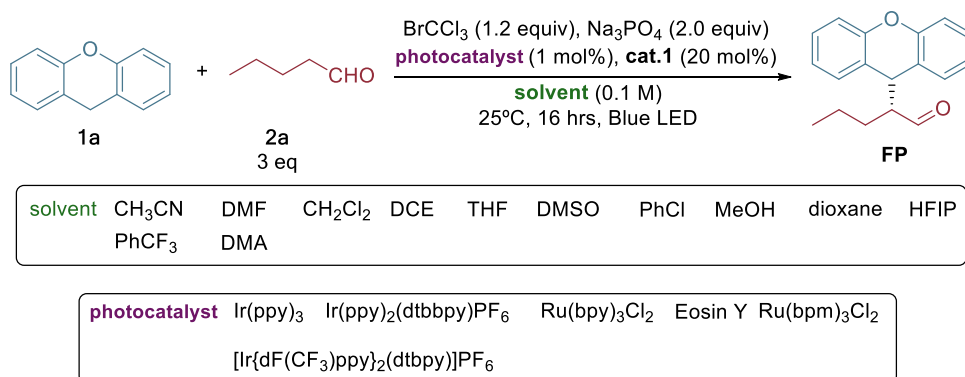


Figure II-17. Influence of water equivalents and base on enantioselectivity with Ir(ppy)₃.

Best hits:

- Ir(ppy)₃, Na₂HPO₄, 14 equivalents H₂O: 76% conv, 96% ee (these conditions are not well reproducible on a larger scale of 0.2 mmol)
- Ir(ppy)₃, Na₃PO₄, 0 equivalents H₂O: 42% conv, 98% ee.

HTE screening 3:



Scheme II-10. HTE screening 3 (solvents and photocatalysts).

Asymmetric cross-dehydrogenative coupling of aldehydes with xanthenes

	ACN	DMF	DCM	DCE	THF	DMSO	PhCl	MeOH	Diox.	HFIP	PhCF ₃	DMA
Ir(ppy)₃	56	100	35	42	56	100	88	100	46	100	53	40
Ir(ppy)₂(dtbbpy)PF₆	61	78	82	80	89	81	100	100	100	74	100	74
Ru(bpy)₃Cl₂	94	100	83	68	22	100	31	85	24	100	9	67
Eosin Y	40	87	23	-	27	61	32	94	93	39	29	50
Ru(bpm)₃Cl₂	26	27	18	-	4	34	18	18	20	61	19	19
[Ir(dFCF₃)ppy]₂(dtbbpy)]PF₆	47	55	46	-	100	78	90	100	66	100	74	67
-	21	8	7	-	13	33	7	9	7	8	4	5

Table II-2. Consumption of SM, %.

	ACN	DMF	DCM	DCE	THF	DMSO	PhCl	MeOH	Diox.	HFIP	PhCF ₃	DMA
Ir(ppy)₃	19	73	40	45	-	-	86	-	15	92	26	13
Ir(ppy)₂(dtbbpy)PF₆	18	47	33	19	11	9	24	-	24	50	20	22
Ru(bpy)₃Cl₂	42	99	100	88	17	10	22	-	12	69	-	25
Eosin Y	13	-	9	-	-	8	-	-	-	-	-	-
Ru(bpm)₃Cl₂	15	6	15	-	-	12	-	-	6	25	8	-
[Ir(dFCF₃)ppy]₂(dtbbpy)]PF₆	12	19	47	-	-	12	28	-	24	73	27	11
-	9	-	24	-	-	-	-	-	-	-	-	-

Table II-3. Conversions to FP, %.

	ACN	DMF	DCM	DCE	THF	DMSO	PhCl	Me OH	Diox.	HFIP	PhC F ₃	D M A
Ir(ppy) ₃	-	-	-	80	-	-	64	-	-	24	-	-
Ir(ppy) ₂ (dtbbpy)PF ₆	-	-	97	-	-	-	-	-	-	39	-	-
Ru(bpy) ₃ Cl ₂	98	48	100	94	-	-	-	-	-	33	-	-
Eosin Y	-	-	-	-	-	-	-	-	-	-	-	-
Ru(bpm) ₃ Cl ₂	-	-	-	-	-	-	-	-	-	69	-	-
[Ir(dF(CF ₃)ppy) ₂ (dtbbpy)]PF ₆	-	-	97	-	-	-	97	-	-	29	-	-
-	-	-	-	-	-	-	-	-	-	-	-	-

Table II-4. Enantioselectivities (ee, %).

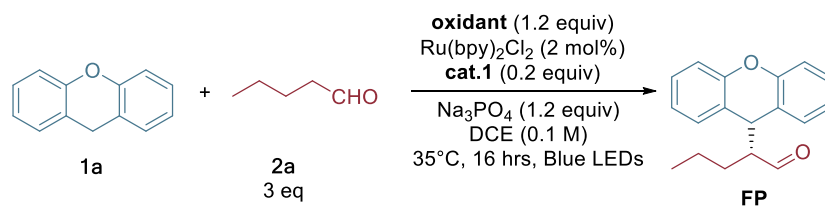


Figure II-18. Heat map for the HTE screening 3.

Best hit: Ru(bpy)₃Cl₂ in DCE or DCM.

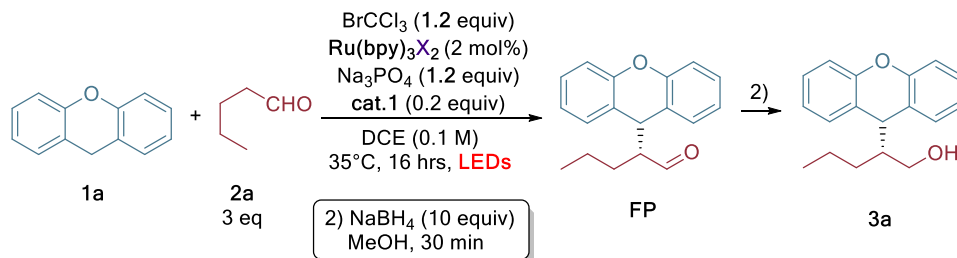
Asymmetric cross-dehydrogenative coupling of aldehydes with xanthenes

II.4.3.4. Further optimization of the reaction conditions



Oxidant	Conversion to FP	er
BrCCl ₃	48%	99:1
BrCH ₂ COOEt	1%	
BrCH(COOEt) ₂	11%	
CBr ₄	35%	98:2
CCl ₄	0%	
Br ₂ C(COOEt) ₂	20%	98.5:1.5
BrCH ₂ COPh	5%	
O ₂	0%	
TEMPO	0%	
<i>m</i> -dinitrobenzene	0%	

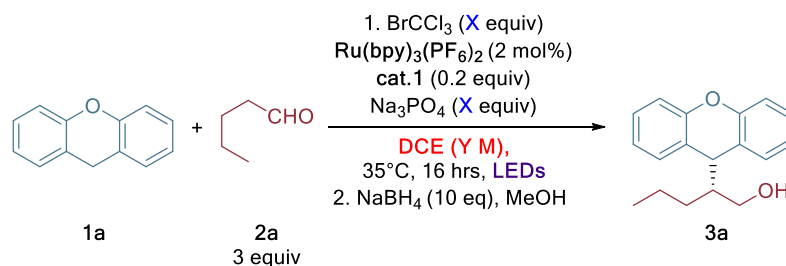
Scheme II-11. Screening of oxidants (0.2 mmol scale).



X	LEDs	Conversion to FP (by GC)	er 3a	Isolated yield 3a
Cl	blue LEDs	63%	97.5:2.5	53%
Cl	white LEDs	51%	98:2	
PF ₆	blue LEDs	62%	98:2	50%
PF ₆	white LEDs	64%	96.5:3.5	60%

Scheme II-12. Screening of photocatalyst counterion and source of light.

- PF₆ salt gives slightly better result than Cl salt
- White LEDs are better than blue LEDs.

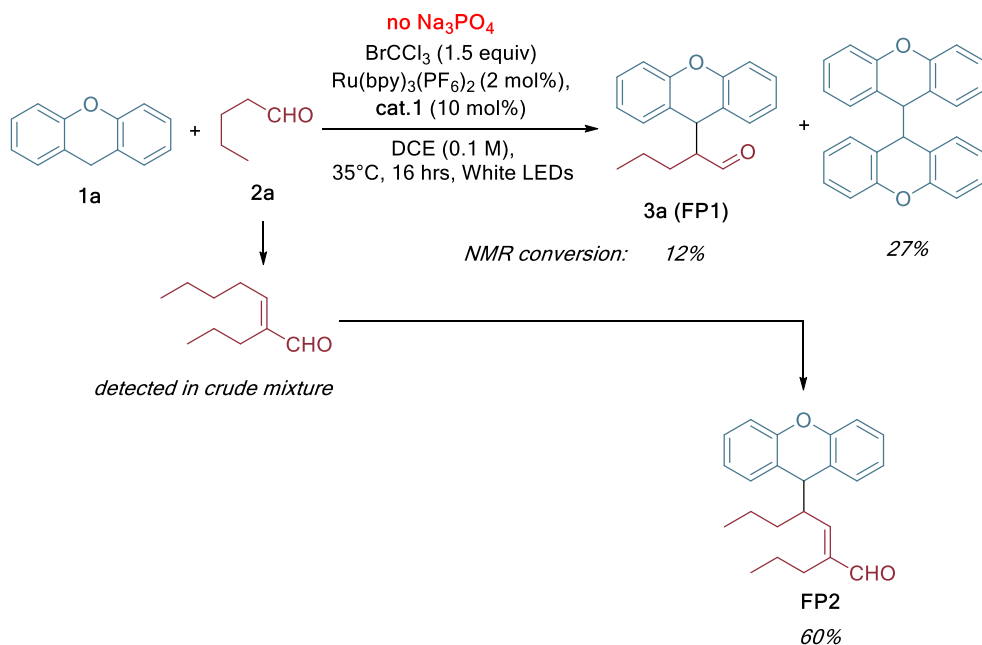


LEDs	X	Y	3a (yield, er)
white LEDs	1.2	0.2	60% yield, 96.5:3.5 er
white LEDs	1.5	0.2	61% yield, 97.5:2.5 er
white LEDs	1.8	0.2	53% yield, 97.5:2.5 er
white LEDs	2.0	0.2	51% yield, 97.5:2.5 er
white LEDs	1.5	0.1	65% yield, 97:3 er
white LEDs	1.8	0.1	58% yield, 97.5:2.5 er
blue LEDs	1.2	0.2	50% yield, 98:2 er
blue LEDs	1.5	0.2	53% yield, 97.5:2.5 er
blue LEDs	1.8	0.2	56% yield, 97.5:2.5 er
blue LEDs	1.5	0.1	59% yield, 97:3 er

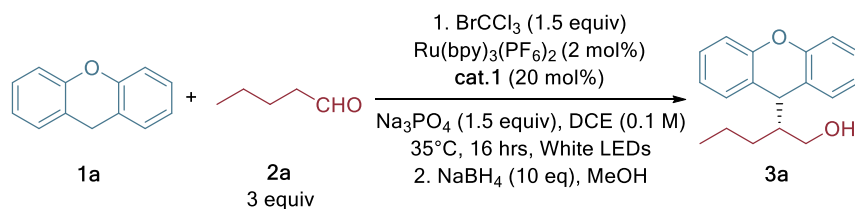
Scheme II-13. Screening of LED, stoichiometry and concentration.

- 1.5 equivalents of base and oxidant is optimal
- Dilution to 0.1 M increases the yield of **3a**.

Asymmetric cross-dehydrogenative coupling of aldehydes with xanthenes



Scheme II-14. Reaction performed without the addition of base.



Entry	Variation from standard conditions	Conversion ^[a] , %	Yield ^[b] , %	er ^[c]
1	-	78	65	97:3
2	10 mol% of cat. 1	76	63	97:3
3	1 mol% of Ru	58	51	97:3
4	DCE (0.05 M)	57	<i>n.d.</i>	75:25
5	DCE (0.2 M)	66	61	96:4
6	Blue LED	73	59	97:3

7	At 25°C	44	<i>n.d.</i>	96:4
8	1.8 equiv BrCCl ₃ ^[d]	75	58	97:3
9	With 10 mol% of TBAB	59	48	96:4
10	With 1.1 equiv of galvinoxyl	26	<i>n.d.</i>	97:3
11	No light	0	<i>n.d.</i>	<i>n.d.</i>
12	No Ru	4	<i>n.d.</i>	97:3
13	No Na ₃ PO ₄	12	<i>n.d.</i>	97:3
14	No BrCCl ₃	0	<i>n.d.</i>	<i>n.d.</i>

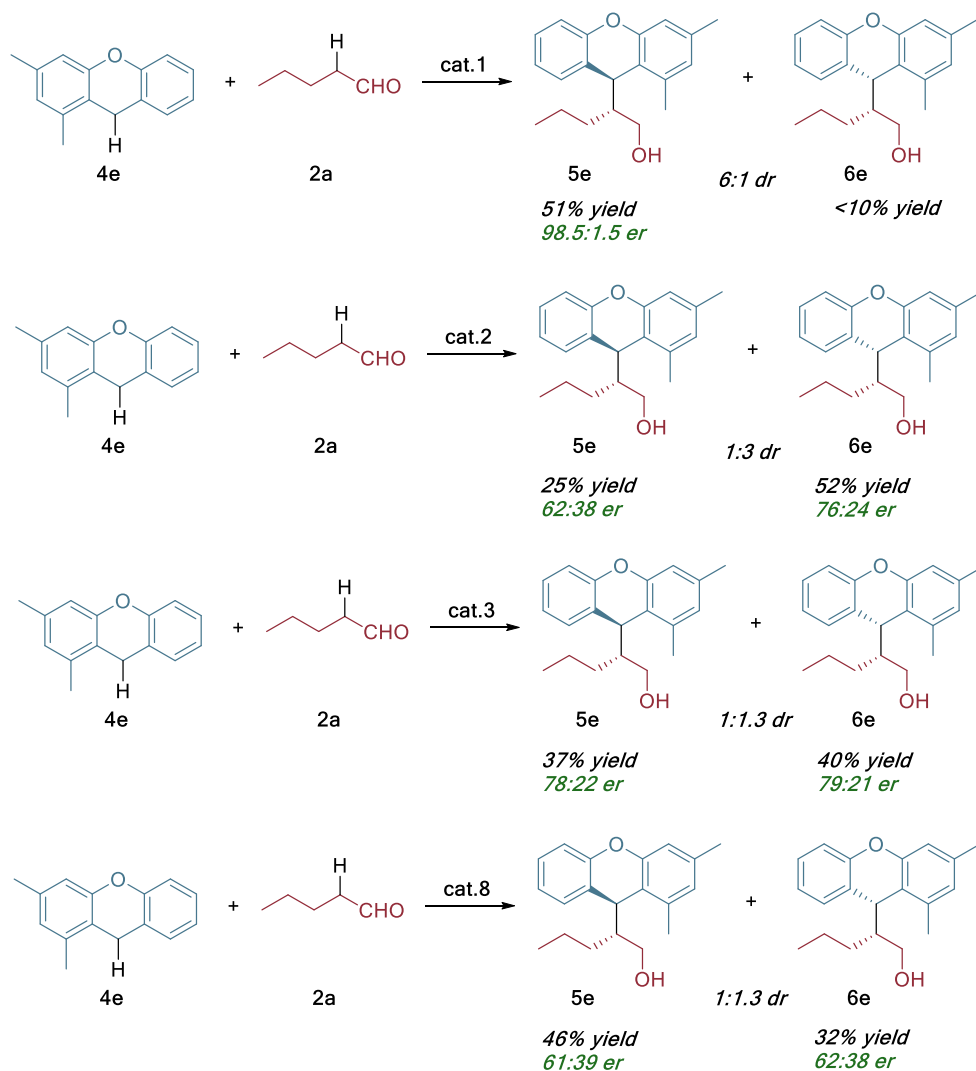
Reactions performed on 0.2 mmol scale. ^[a] Conversion was determined by GC analysis. ^[b] Yield of isolated product. ^[c] Determined by HPLC analysis using a chiral stationary phase. ^[d] With 1.8 equiv Na₃PO₄. *n.d.* not determined.

Table II-5. Final optimization table.

2 mol% of [Ru] was necessary to achieve a reasonable conversion (entry 3). Concentration of 0.1 M of DCE was found to be optimal (entries 4 and 5). Decreasing temperature to 25°C (entry 7), increasing amount of oxidant (entry 8), addition of the phase-transfer catalyst (entry 9) led to lower yields of product, though without considerable change in enantiopurity of the product.

Asymmetric cross-dehydrogenative coupling of aldehydes with xanthenes

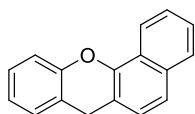
II.4.3.5. Screening of aminocatalysts for the asymmetric CDC of 4e.



Scheme II-15. CDC reaction of 4e with different organocatalysts.

II.4.4. Product characterization

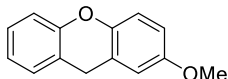
- **Characterization data of xanthenes:**



7H-Benzo[d]xanthene (4a):⁴ Prepared according to modified **GP1** (42 hours refluxing at 155 °C) from 2-hydroxybenzaldehyde (268 mg, 2.2 mmol, 1.1 equiv) and α -tetralone (292 mg, 2 mmol, 1.0 equiv). Purification by column chromatography on silica gel using *n*-pentane:EtOAc (98:2) as eluent afforded the analytically pure product (285 mg, 61%) as a white solid.

¹H NMR (400 MHz, CDCl₃): δ = 8.39 (d, ³J_{H-H} = 8.4 Hz, 1H), 7.81 (d, ³J_{H-H} = 7.6 Hz, 1H), 7.59 - 7.46 (m, 3H), 7.28 - 7.21 (m, 4H), 7.11 - 7.05 (m, 1H), 4.21 (s, 2H).

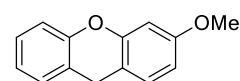
¹³C NMR (100 MHz, CDCl₃): δ = 152.0, 146.6, 133.5, 129.2, 127.8, 127.7, 126.8, 126.1, 126.0, 124.4, 123.4, 122.5, 121.6, 120.6, 116.8, 114.4, 28.3.



2-Methoxy-9H-xanthene (4b):⁴ Prepared according to **GP2** from 2-hydroxy-5-methoxybenzaldehyde (336 mg, 2.2 mmol, 1.1 equiv) and cyclohex-2-en-1-one (192 mg, 2.0 mmol, 1.0 equiv). Purification by column chromatography on silica gel using *n*-pentane:EtOAc (100:0 to 60:1) as eluent afforded the analytically pure product (225 mg, 53%) as an off-white solid.

¹H NMR (400 MHz, CDCl₃): δ = 7.22 - 7.14 (m, 2H), 7.05 - 6.96 (m, 3H), 6.76 (dd, ³J_{H-H} = 8.8 Hz, ⁴J_{H-H} = 3.0 Hz, 1H), 6.73 - 6.67 (m, 1H), 4.04 (s, 2H), 3.79 (s, 3H).

¹³C NMR (100 MHz, CDCl₃): δ = 155.2, 152.2, 146.0, 128.8, 127.6, 122.7, 121.3, 120.0, 117.1, 116.4, 113.4, 113.3, 55.7, 28.3.



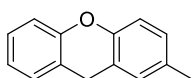
3-Methoxy-9H-xanthene (4c):⁵ Prepared according to modified **GP1** (40 hours refluxing at 155 °C) from 2-hydroxy-4-methoxybenzaldehyde (669 mg, 4.4 mmol, 1.1 equiv) and cyclohex-2-en-1-one (385 mg, 4.0 mmol, 1.0 equiv). Purification by column

Asymmetric cross-dehydrogenative coupling of aldehydes with xanthenes

chromatography on silica gel using *n*-pentane:EtOAc (100:0 to 60:1) as eluent afforded the analytically pure product (154 mg, 18%) as a white solid.

¹H NMR (400 MHz, CDCl₃): δ = 7.23 - 7.14 (m, 2H), 7.09 - 7.00 (m, 3H), 6.66 - 6.60 (m, 2H), 3.99 (s, 2H), 3.81 (s, 3H).

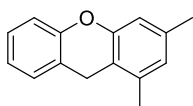
¹³C NMR (100 MHz, CDCl₃): δ = 159.1, 152.3, 151.6, 129.2, 128.8, 127.4, 122.8, 120.6, 116.2, 112.2, 109.5, 101.4, 77.2, 76.8, 76.5, 55.3, 27.0.



2-Methyl-9H-xanthene (4d):⁴ Prepared according to **GP2** from 2-hydroxy-5-methoxybenzaldehyde (450 mg, 3.3 mmol, 1.1 equiv) and cyclohex-2-en-1-one (288 mg, 3.0 mmol, 1.0 equiv). Purification by column chromatography on silica gel using *n*-pentane:EtOAc (100:0 to 60:1) as eluent afforded the analytically pure product (183 mg, 31%) as a white solid.

¹H NMR (500 MHz, CDCl₃): δ = 7.21 - 7.14 (m, 2H), 7.06 - 6.92 (m, 5H), 4.01 (s, 2H), 2.31 (s, 3H).

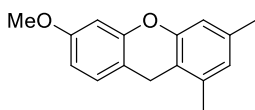
¹³C NMR (100 MHz, CDCl₃): δ = 152.1, 149.8, 132.3, 129.2, 128.9, 128.2, 127.6, 122.7, 120.6, 120.2, 116.4, 116.1, 27.9, 20.7.



1,3-Dimethyl-9H-xanthene (4e):⁴ Prepared according to modified **GP1** (42 hours refluxing at 155 °C) from 2-hydroxybenzaldehyde (403 mg, 3.3 mmol, 1.1 equiv) and 3,5-dimethylcyclohex-2-en-1-one (373 mg, 3.0 mmol, 1.0 equiv). Purification by column chromatography on silica gel using *n*-pentane:EtOAc (100:0 to 60:1) as eluent afforded the analytically pure product (170 mg, 27%) as a white solid.

¹H NMR (400 MHz, CDCl₃): δ = 7.22 - 7.14 (m, 2H), 7.04 - 6.98 (m, 2H), 6.72 (s, 2H), 3.91 (s, 2H), 2.29 (s, 3H), 2.27 (s, 3H).

¹³C NMR (100 MHz, CDCl₃): δ = 150.9, 150.8, 136.9, 136.5, 129.5, 127.7, 125.0, 122.9, 120.1, 115.8, 113.9, 24.5, 20.6, 18.6.



6-Methoxy-1,3-dimethyl-9H-xanthene (4f): Prepared according to **GP1** from 2-hydroxy-4-methoxybenzaldehyde (837 mg, 5.5 mmol, 1.1 equiv) and 3,5-dimethylcyclohex-2-en-1-one (621 mg, 5.0 mmol, 1.0 equiv). Purification by column chromatography on silica gel using *n*-pentane:EtOAc (98:2) as eluent, followed by recrystallization from ethanol afforded the analytically pure product (185 mg, 15%) as an off-white solid.

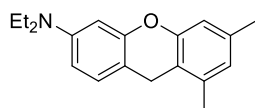
mp: 53 - 55°C.

¹H NMR (400 MHz, CDCl₃): δ = 7.06 (d, ³J_{H-H} = 8.3 Hz, 1H), 6.71 (d, ³J_{H-H} = 5.4 Hz, 2H), 6.62 - 6.56 (m, 2H), 3.84 (s, 2H), 3.80 (s, 3H), 2.29 (s, 3H), 2.26 (s, 3H).

¹³C NMR (100 MHz, CDCl₃): δ = 159.4, 152.4, 151.5, 137.0, 137.0, 129.8, 125.2, 116.3, 114.5, 112.2, 109.6, 101.4, 55.6, 25.0, 21.1, 19.1.

IR (neat): ν 2942, 2915, 2835, 1634, 1616, 1601, 1573, 1508, 1490, 1444, 1411, 1342, 1301, 1277, 1219, 1198, 1161, 1119, 1034, 838 cm⁻¹.

HRMS (ESI+): *m/z* calcd. for C₁₆H₁₅O₂ [M+H]⁺: 239.1067, found: 239.1059.



***N,N*-Diethyl-6,8-dimethyl-9H-xanthen-3-amine (4g):** Prepared according to modified **GP1** (42 hours refluxing at 180 °C) from 4-(diethylamino)2-hydroxybenzaldehyde (850 mg, 4.4 mmol, 1.1 equiv) and 3,5-dimethylcyclohex-2-en-1-one (497 mg, 4.0 mmol, 1.0 equiv). Purification by column chromatography on silica gel using *n*-pentane:EtOAc (98:2) as eluent, followed by recrystallization from ethanol afforded the analytically pure product (282 mg, 25%) as an off-white solid.

mp: 72 - 74°C.

¹H NMR (500 MHz, CDCl₃): δ = 7.00 (d, ³J_{H-H} = 8.4 Hz, 1H), 6.69 (s, 2H), 6.40 (dd, ³J_{H-H} = 8.4 Hz, ⁴J_{H-H} = 2.6 Hz, 1H), 6.33 (d, ⁴J_{H-H} = 2.5 Hz, 1H),

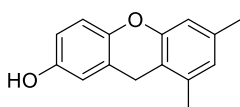
Asymmetric cross-dehydrogenative coupling of aldehydes with xanthenes

3.79 (s, 2H), 3.34 (q, $^3J_{\text{H-H}} = 7.1$ Hz, 4H), 2.28 (s, 3H), 2.25 (s, 3H), 1.17 (t, $^3J_{\text{H-H}} = 7.1$ Hz, 6H).

^{13}C NMR (126 MHz, CDCl_3): $\delta = 152.3, 151.6, 147.7, 136.7, 136.5, 129.5, 124.5, 116.6, 114.3, 107.2, 106.7, 99.2, 44.4, 24.5, 20.9, 18.9, 12.5$.

IR (neat): ν 2666, 2919, 2867, 2831, 1636, 1618, 1558, 1518, 1447, 1340, 1303, 1227, 1204, 1194, 1136, 1111, 1050, 821 cm^{-1} .

HRMS (ESI+): m/z calcd. for $\text{C}_{19}\text{H}_{24}\text{NO}$ $[\text{M}+\text{H}]^+$: 282.1852, found: 282.1851.



6,8-Dimethyl-9H-xanthen-2-ol (4h): Prepared according to GP2 from 2,5-dihydroxybenzaldehyde (456 mg, 3.3 mmol, 1.1 equiv) and 3,5-dimethylcyclohex-2-en-1-one (372 mg, 3.0 mmol, 1.0 equiv). Purification by column chromatography on silica gel using *n*-pentane:EtOAc (5:1) as eluent, followed by recrystallization from ethanol afforded the analytically pure product (96 mg, 14%) as a white solid.

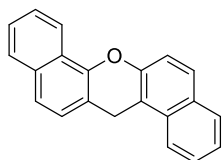
mp: 121 - 123°C.

^1H NMR (400 MHz, CDCl_3): $\delta = 6.91 - 6.86$ (m, 1H), 6.71 - 6.63 (m, 4H), 3.85 (s, 2H), 2.28 (s, 3H), 2.26 (s, 3H), 0.85 (bs, 1H).

^{13}C NMR (100 MHz, CDCl_3): $\delta = 151.8, 150.9, 146.0, 137.1, 136.9, 124.9, 121.3, 117.2, 115.4, 115.2, 114.7, 114.5, 25.9, 21.1, 19.2$.

IR (neat): ν 3372, 3011, 2969, 1632, 1608, 1578, 1488, 1447, 1318, 1292, 1210, 1195, 1154, 1132, 1048, 947, 841 cm^{-1} .

HRMS (ESI+): m/z calcd. for $\text{C}_{15}\text{H}_{15}\text{O}_2$ $[\text{M}+\text{H}]^+$: 227.1067, found: 227.1065.

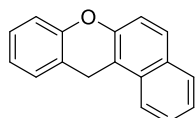


14H-Dibenzo[a,h]xanthene (4i):⁴ Prepared according to GP1 from 2-hydroxy-1-naphthaldehyde (758 mg, 4.4 mmol, 1.1 equiv) and α -tetralone (585 mg, 4.0 mmol, 1.0 equiv). Purification by column chromatography on silica

gel using *n*-pentane:EtOAc (98:2) as eluent, followed by recrystallization from *n*-pentane/CH₂Cl₂ afforded the analytically pure product (592 mg, 52%) as a white solid.

¹H NMR (500 MHz, CDCl₃): δ = 8.44 (d, ³*J*_{H-H} = 8.4 Hz, 1H), 7.91 (d, ³*J*_{H-H} = 8.4 Hz, 1H), 7.87 (d, ³*J*_{H-H} = 8.1 Hz, 1H), 7.83 (d, ³*J*_{H-H} = 8.1 Hz, 1H), 7.80 (d, ³*J*_{H-H} = 8.9 Hz, 1H), 7.63 - 7.56 (m, 3H), 7.54 - 7.43 (m, 3H), 7.38 (d, ³*J*_{H-H} = 8.4 Hz, 1H), 4.51 (s, 2H).

¹³C NMR (126 MHz, CDCl₃): δ = 148.6, 145.6, 133.4, 132.1, 130.3, 128.5, 128.3, 127.6, 127.0, 126.7, 126.1, 126.0, 124.2, 124.2, 122.6, 122.4, 121.4, 118.0, 113.5, 111.7, 25.4.

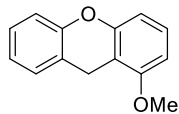


12*H*-Benzo[*a*]xanthene (4j):⁴ Prepared according to GP1 from 2-hydroxybenzaldehyde (268 mg, 2.2 mmol, 1.1 equiv) and β -tetralone (292 mg, 2 mmol, 1.0 equiv). NMR analysis of crude mixture showed 9:1 regioselectivity. Purification by column chromatography on silica gel using *n*-pentane:EtOAc (100:0 to 60:1) as eluent afforded the analytically pure product (203 mg, 44%) as a white solid.

¹H NMR (400 MHz, CDCl₃): δ = 7.88 (d, ³*J*_{H-H} = 9.1 Hz, 1H), 7.84 (d, ³*J*_{H-H} = 8.1 Hz, 1H), 7.74 (d, ³*J*_{H-H} = 8.9 Hz, 1H), 7.59 (ddd, ³*J*_{H-H} = 8.3 Hz, ³*J*_{H-H} = 6.9 Hz, ⁴*J*_{H-H} = 1.3 Hz, 1H), 7.45 (ddd, ³*J*_{H-H} = 8.0 Hz, ³*J*_{H-H} = 6.9 Hz, ⁴*J*_{H-H} = 1.1 Hz, 1H), 7.34 - 7.31 (m, 1H), 7.27 (d, ³*J*_{H-H} = 8.9 Hz, 1H), 7.25 - 7.22 (m, 1H), 7.14 - 7.07 (m, 2H), 4.40 (s, 2H).

¹³C NMR (100 MHz, CDCl₃): δ = 151.2, 148.9, 132.2, 130.3, 129.6, 128.6, 128.4, 127.9, 126.8, 124.3, 123.3, 122.4, 119.7, 118.1, 116.6, 111.7, 25.0.

IR (neat): ν 3038, 2923, 2868, 2827, 1630, 1581, 1490, 1457, 1436, 1400, 1254, 1243, 1180, 1109, 958, 881 cm⁻¹.



1-Methoxy-9*H*-xanthene (4k): Prepared according to GP2 from 2-hydroxy-6-methoxybenzaldehyde (501 mg, 3.3 mmol, 1.1 equiv) and cyclohex-2-en-1-one (288 mg, 3.0

Asymmetric cross-dehydrogenative coupling of aldehydes with xanthenes

mmol, 1.0 equiv). Purification by column chromatography on silica gel using *n*-pentane:EtOAc (98:2) as eluent afforded the analytically pure product (145 mg, 15%) as a white solid.

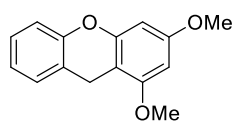
mp: 66 - 68 °C.

¹H NMR (500 MHz, CDCl₃): δ = 7.22 - 7.12 (m, 3H), 7.06 - 7.00 (m, 2H), 6.69 (d, ³*J*_{H-H} = 8.1 Hz, 1H), 6.56 (d, ³*J*_{H-H} = 8.2 Hz, 1H), 3.95 (s, 2H), 3.87 (s, 3H).

¹³C NMR (125 MHz, CDCl₃): δ = 157.7, 152.5, 151.6, 129.5, 127.7, 127.5, 123.0, 120.2, 116.5, 109.5, 109.1, 104.2, 55.8, 22.8.

IR (neat): ν 3010, 2879, 2837, 1624, 1602, 1579, 1468, 1454, 1436, 1346, 1304, 1272, 1245, 1179, 1110, 1080, 878 cm⁻¹.

HRMS (ESI+): *m/z* calcd. for C₁₄H₁₃O₂ [M+H]⁺: 213.0910, found: 213.0908.



1,3-Dimethoxy-9H-xanthene (4I): Prepared according to modified **GP1** (48 hours heating at 200 °C) from 2-hydroxy-4,6-dimethoxybenzaldehyde (1.00 g, 5.5

mmol, 1.1 equiv) and cyclohex-2-en-1-one (481 mg, 5.0 mmol, 1.0 equiv). Purification by column chromatography on silica gel using *n*-pentane:EtOAc (98:2) as eluent, followed by recrystallization from ethanol afforded the analytically pure product (335 mg, 28%) as a white solid.

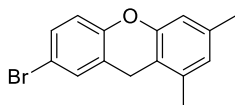
mp: 79 - 81 °C.

¹H NMR (400 MHz, CDCl₃): δ = 7.17 (t, ³*J*_{H-H} = 7.5 Hz, 2H), 7.05 - 6.96 (m, 2H), 6.24 (d, ⁴*J*_{H-H} = 2.3 Hz, 1H), 6.18 (d, ⁴*J*_{H-H} = 2.3 Hz, 1H), 3.87 (s, 2H), 3.83 (s, 3H), 3.80 (s, 3H).

¹³C NMR (100 MHz, CDCl₃): δ = 159.6, 158.2, 152.6, 151.5, 129.4, 127.4, 122.9, 120.3, 116.2, 101.6, 93.2, 93.0, 55.6, 55.4, 22.2.

IR (neat): ν 2995, 2962, 2938, 2836, 1634, 1607, 1578, 1489, 1451, 1426, 1255, 1229, 1216, 1201, 1181, 1142, 1111, 1091, 1048, 799 cm⁻¹.

HRMS (ESI+): *m/z* calcd. for C₁₅H₁₅O₃ [M+H]⁺: 243.1016, found: 243.1016.



7-Bromo-1,3-dimethyl-9H-xanthene (4m): Prepared according to modified **GP1** (42 hours heating at 180 °C) from 5-bromo-2-hydroxybenzaldehyde (884 mg, 4.4 mmol, 1.1 equiv) and 3,5-dimethylcyclohex-2-en-1-one (497 mg, 4.0 mmol, 1.0 equiv). Purification by column chromatography on silica gel using *n*-pentane:EtOAc (98:2) as eluent afforded the analytically pure product (500 mg, 43%) as an off-white solid.

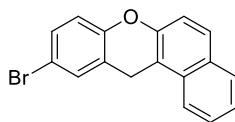
mp: 88 - 89 °C.

¹H NMR (500 MHz, CDCl₃): δ = 7.31 - 7.30 (m, 1H), 7.28 - 7.25 (m, 1H), 6.88 (d, ³*J*_{H-H} = 8.6 Hz, 1H), 6.73 (s, 1H), 6.70 (s, 1H), 3.88 (s, 2H), 2.28 (s, 3H), 2.25 (s, 3H).

¹³C NMR (126 MHz, CDCl₃): δ = 151.2, 150.8, 137.3, 136.8, 131.8, 130.5, 125.3, 122.4, 118.1, 115.1, 114.7, 114.5, 25.4, 21.0, 19.0.

IR (neat): ν 3027, 2967, 2912, 2870, 1631, 1593, 1565, 1475, 1411, 1303, 1238, 1183, 1116, 1045, 955, 845, 815 cm⁻¹.

HRMS (ESI+): *m/z* calcd. for C₁₅H₁₄BrO [M+H]⁺: 289.0223, found: 289.0209.



10-Bromo-12H-benzo[a]xanthene (4n): Prepared according to modified **GP1** (42 hours heating at 180 °C) from 5-bromo-2-hydroxybenzaldehyde (884 mg, 4.4 mmol, 1.1 equiv) and β -tetralone (585 mg, 4.0 mmol, 1.0 equiv). NMR analysis of crude mixture showed 9:1 regioselectivity. Purification by column chromatography on silica gel using *n*-pentane:EtOAc (98:2) as eluent afforded the analytically pure product (338 mg, 27%) as a white solid.

mp: 138-140 °C.

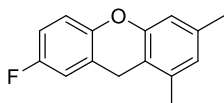
¹H NMR (500 MHz, CDCl₃): δ = 7.84 (dd, ³*J*_{H-H} = 8.1 Hz, ⁴*J*_{H-H} = 3.7 Hz, 2H), 7.74 (d, ³*J*_{H-H} = 8.9 Hz, 1H), 7.59 (ddd, ³*J*_{H-H} = 8.3 Hz, ³*J*_{H-H} = 6.9 Hz, ⁴*J*_{H-H} = 1.2 Hz, 1H), 7.48 - 7.43 (m, 2H), 7.33 (dd, ³*J*_{H-H} = 8.7 Hz, ⁴*J*_{H-H} = 2.4 Hz, 1H), 7.24 (d, ³*J*_{H-H} = 8.9 Hz, 1H), 6.99 (d, ³*J*_{H-H} = 8.6 Hz, 1H), 4.35 (s, 2H).

Asymmetric cross-dehydrogenative coupling of aldehydes with xanthenes

^{13}C NMR (126 MHz, CDCl_3): δ = 150.3, 148.5, 132.2, 132.0, 130.9, 130.4, 128.7, 128.7, 127.0, 124.5, 122.3, 121.9, 118.4, 117.9, 115.4, 111.0, 24.8.

IR (neat): ν 3066, 2922, 2889, 2822, 1630, 1603, 1574, 1515, 1484, 1462, 1430, 1400, 1255, 1240, 1178, 1139, 1117, 1072, 960, 857 cm^{-1} .

HRMS (ESI+): m/z calcd. for $\text{C}_{17}\text{H}_{12}\text{BrO}$ $[\text{M}+\text{H}]^+$: 311.0066, found: 311.0067.



7-Fluoro-1,3-dimethyl-9H-xanthene (4o): Prepared according to modified **GP1** (60 hours heating at 180 °C) from 5-fluoro-2-hydroxybenzaldehyde (616 mg, 4.4 mmol, 1.1 equiv) and 3,5-dimethylcyclohex-2-en-1-one (497 mg, 4.0 mmol, 1.0 equiv). Purification by column chromatography on silica gel using *n*-pentane:EtOAc (98:2) as eluent, followed by recrystallization from ethanol afforded the analytically pure product (259 mg, 28%) as a white solid.

mp: 67 - 68 °C.

mp: 67 - 68 °C.

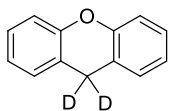
^1H NMR (400 MHz, CDCl_3): δ = 6.99 - 6.91 (m, 1H), 6.91 - 6.83 (m, 2H), 6.73 (s, 1H), 6.70 (s, 1H), 3.89 (s, 2H), 2.29 (s, 3H), 2.26 (s, 3H).

^{13}C NMR (100 MHz, CDCl_3): δ = 158.3 (d, $^1J_{\text{C-F}}$ = 240.1 Hz), 151.6 (C_q), 147.9 (C_q), 137.4 (C_q), 136.8 (C_q), 125.3 (CH), 121.7 (d, $^3J_{\text{C-F}}$ = 7.8 Hz, C_q), 117.4 (d, $^3J_{\text{C-F}}$ = 8.4 Hz, CH), 115.2 (d, $^2J_{\text{C-F}}$ = 23.0 Hz, CH), 115.0 (C_q), 114.6 (CH), 114.5 (d, $^2J_{\text{C-F}}$ = 23.1 Hz, CH), 26.0 (CH_2), 21.1 (CH_3), 19.1 (CH_3).

^{19}F NMR (376 MHz, CDCl_3) δ = -121.6.

IR (neat): ν 3027, 2916, 2826, 1637, 1578, 1500, 1485, 1427, 1330, 1314, 1299, 1227, 1194, 1128, 1041, 951, 854, 832, 816 cm^{-1} .

HRMS (ESI+): m/z calcd. for $\text{C}_{15}\text{H}_{14}\text{FO}$ $[\text{M}+\text{H}]^+$: 229.1023, found: 229.1023.

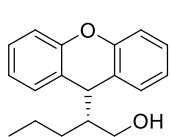


1a-d₂: Prepared according to the literature procedure.⁸

^2H NMR (77 MHz, CDCl_3): δ = 3.98 (s, CD_2).

^{13}C NMR (101 MHz, CDCl_3): δ = 27.2 (quin, $^1J_{\text{C-D}}$ = 20 Hz, CD_2).

• Characterization data of products:



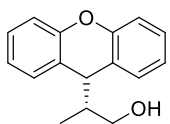
(R)-2-(9H-xanthen-9-yl)pentan-1-ol (3a):⁶ Prepared according to **GP3** from xanthene (36.4 mg, 1.0 equiv) and pentanal (63.8 μ L, 3.0 equiv). Purification by column chromatography on silica gel using *n*-pentane:EtOAc (15:1) as eluent afforded the analytically pure product (33.8 mg, 63%, 97:3 er) as a colorless oil.

¹H NMR (500 MHz, CDCl₃): δ = .7.26 - 7.20 (m, 4H), 7.13 - 7.05 (m, 4H), 4.28 (d, ³J_{H-H} = 4.2 Hz, 1H), 3.53 (m, 2H), 1.89 - 1.79 (m, 1H), 1.36 - 1.15 (m, 4H), 0.77 (t, ³J_{H-H} = 7.1 Hz, 3H).

¹³C NMR (126 MHz, CDCl₃): δ = 153.3, 153.1, 129.5, 128.9, 127.7, 127.5, 124.8, 123.8, 123.2, 123.0, 116.3, 116.2, 62.6, 50.2, 39.4, 29.6, 22.7, 13.9.

[α]_D²⁵: +11.6 (*c* 2.09, CH₂Cl₂), lit.: +8.4 (*c* 3.0, CHCl₃).⁶

HPLC (Daicel Chiralpak AD-H column, *n*-hexane/*i*-PrOH (95:5), flow rate 1.0 mL/min, λ = 210 nm): t_{minor} = 11.4 min; t_{major} = 13.9 min.



(R)-2-(9H-xanthen-9-yl)propan-1-ol (3b):⁶ Prepared according to **GP3** from xanthene (36.4 mg, 1.0 equiv) and propanal (43.2 μ L, 3.0 equiv). Purification by column chromatography on silica gel using *n*-pentane:EtOAc (10:1) as eluent afforded the analytically pure product (30.1 mg, 63%, 96.5:3.5 er) as a white solid.

mp: 60-62 °C.

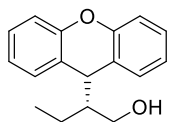
¹H NMR (500 MHz, CDCl₃): δ = 7.25 - 7.21 (m, 4H), 7.12 - 7.06 (m, 4H), 4.23 (d, ²J_{H-H} = 4.3 Hz, 1H, Ar₂CH), 3.54 (dd, ¹J_{H-H} = 10.7 Hz, ²J_{H-H} = 7.9 Hz, 1H, CH₂), 3.45 (dd, ¹J_{H-H} = 10.7 Hz, ²J_{H-H} = 6.0 Hz, 1H, CH₂), 2.06 - 1.93 (m, 1H, CH), 0.65 (d, J = 6.9 Hz, 3H, CH₃).

¹³C NMR (126 MHz, CDCl₃): δ = 153.4, 153.1, 129.7, 128.8, 127.7, 127.5, 125.2, 123.3, 122.9, 122.5, 116.3, 116.2, 64.9, 45.1, 40.3, 12.0.

[α]_D²⁵: +7.2 (*c* 1.52, CH₂Cl₂), lit.: +3.7 (*c* 1.30, CHCl₃).⁶

Asymmetric cross-dehydrogenative coupling of aldehydes with xanthenes

HPLC (Daicel Chiralpak AD-H column, *n*-hexane/*i*-PrOH (95:5), flow rate 1.0 mL/min, $\lambda = 254$ nm): $t_{\text{minor}} = 13.9$ min; $t_{\text{major}} = 15.1$ min.



(*R*)-2-(9*H*-xanthen-9-yl)butan-1-ol (3c):⁶ Prepared according to modified **GP3** (with 2 mol% Ru(bpy)₃Cl₂) from xanthene (36.4 mg, 1.0 equiv) and butanal (53.9 μ L, 3.0 equiv).

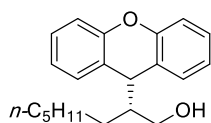
Purification by column chromatography on silica gel using *n*-pentane:EtOAc (15:1) as eluent afforded the analytically pure product (26.1 mg, 51%, 97:3 er) as a colorless oil.

¹H NMR (400 MHz, CDCl₃): $\delta = 7.27 - 7.19$ (m, 4H), 7.12 - 7.04 (m, 4H), 4.28 (d, ³*J*_{H-H} = 4.3 Hz, 1H), 3.66 - 3.46 (m, 2H), 1.82 - 1.71 (m, 1H), 1.42 - 1.30 (m, 1H), 1.15 - 1.02 (m, 1H), 0.82 (t, ³*J*_{H-H} = 7.4 Hz, 3H).

¹³C NMR (100 MHz, CDCl₃): $\delta = 153.3, 153.1, 129.5, 128.9, 127.7, 127.6, 124.9, 123.7, 123.2, 123.0, 116.3, 116.2, 62.1, 52.0, 39.3, 19.7, 12.1$.

[α]_D: +9.8 (*c* 1.23, CH₂Cl₂), lit.: +3.2 (*c* 2.5, CHCl₃).⁶

HPLC (Daicel Chiralpak AD-H column, *n*-hexane/*i*-PrOH (95:5), flow rate 1.0 mL/min, $\lambda = 240$ nm): $t_{\text{minor}} = 12.5$ min; $t_{\text{major}} = 14.9$ min.

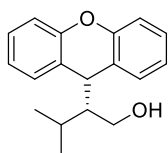


(*R*)-2-(9*H*-xanthen-9-yl)octan-1-ol (3d):⁶ Prepared according to modified **GP3** (with 2 mol% Ru(bpy)₃Cl₂) from xanthene (36.4 mg, 1.0 equiv) and octanal (94.0 μ L, 3.0 equiv).

Purification by column chromatography on silica gel using *n*-pentane:EtOAc (15:1) as eluent afforded an inseparable mixture of *n*-octanol (10.5 mg) and product **3d** (33.0 mg, 53% yield, 98:2 er) as a colorless oil.

¹H NMR (400 MHz, CDCl₃): $\delta = 7.25 - 7.19$ (m, 4H), 7.12 - 7.04 (m, 4H), 4.27 (d, ³*J*_{H-H} = 3.9 Hz, 1H), 3.57 - 3.49 (m, 2H), 1.86 - 1.77 (m, 1H), 1.33 - 1.10 (m, 11H), 0.82 (t, ³*J*_{H-H} = 7.1 Hz, 3H).

HPLC (Daicel Chiralpak AD-H column, *n*-hexane/*i*-PrOH (95:5), flow rate 1.0 mL/min, $\lambda = 240$ nm): $t_{\text{minor}} = 8.3$ min; $t_{\text{major}} = 9.8$ min.



(R)-3-methyl-2-(9H-xanthen-9-yl)butan-1-ol (3e):⁶ Prepared according to modified **GP3** (with 2 mol% Ru(bpy)₃Cl₂) from xanthene (36.4 mg, 1.0 equiv) and 3-methylbutanal (64.0 μL, 3.0 equiv). Purification by column chromatography on silica

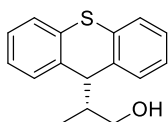
gel using *n*-pentane:EtOAc (15:1) as eluent afforded the analytically pure product (30.6 mg, 57%, 99.5:0.5 er) as a colorless oil.

¹H NMR (400 MHz, CDCl₃): δ = 7.32 - 7.18 (m, 4H), 7.18 - 6.97 (m, 4H), 4.32 (d, ³J_{H-H} = 4.7 Hz, 1H), 3.68 - 3.60 (m, 2H), 1.94 - 1.80 (m, 1H), 1.64 - 1.55 (m, 1H), 1.01 (d, ³J_{H-H} = 6.8 Hz, 3H), 0.72 (d, ³J_{H-H} = 6.8 Hz, 3H).

¹³C NMR (100 MHz, CDCl₃): δ = 153.3, 153.1, 129.3, 128.8, 127.8, 127.6, 125.1, 124.9, 123.4, 123.2, 116.6, 116.4, 60.6, 56.3, 39.0, 26.1, 23.0, 18.7.

[α]_D²⁵: +15.7 (c 1.35, CH₂Cl₂), lit.: +5.5 (c 2.0, CHCl₃).⁶

HPLC (Daicel Chiralpak AD-H column, *n*-hexane/*i*-PrOH (95:5), flow rate 1.0 mL/min, λ = 240 nm): *t*_{minor} = 10.3 min; *t*_{major} = 12.3 min.



(R)-2-(9H-thioxanthen-9-yl)propan-1-ol (3f):⁶ Prepared according to **GP3** from 9H-thioxanthene **1b** (39.7 mg, 1.0 equiv) and propanal (34.8 μL, 3.0 equiv). Purification by

column chromatography on silica gel using *n*-pentane:EtOAc (10:1) as eluent afforded the analytically pure product (16.8 mg, 32%, 97.5:2.5 er) as a colorless oil.

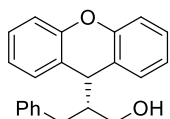
¹H NMR (400 MHz, CDCl₃): δ = 7.47 - 7.40 (m, 2H), 7.37 - 7.30 (m, 1H), 7.32 - 7.18 (m, 5H), 3.97 (d, ³J_{H-H} = 9.9 Hz, 1H), 3.51 - 3.43 (m, 1H), 3.36 - 3.25 (m, 1H), 2.36 - 2.24 (m, 1H), 0.84 (d, ³J_{H-H} = 6.9 Hz, 3H).

¹³C NMR (100 MHz, CDCl₃): δ = 137.4, 137.1, 132.9, 132.8, 130.1, 129.6, 127.2, 127.1, 126.5, 126.4, 126.3, 126.0, 65.7, 51.8, 35.0, 15.7.

[α]_D²⁵: -31.8 (c 1.32, CH₂Cl₂), lit.: -15.6 (c 1.9, CHCl₃).⁷

HPLC (Daicel Chiralpak AD-H column, *n*-hexane/*i*-PrOH (97:3), flow rate 1.0 mL/min, λ = 240 nm): *t*_{minor} = 20.3 min; *t*_{major} = 21.4 min.

Asymmetric cross-dehydrogenative coupling of aldehydes with xanthenes



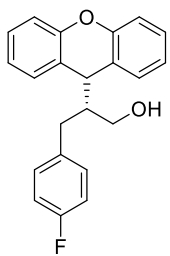
(R)-3-phenyl-2-(9H-xanthen-9-yl)propan-1-ol (3g):⁶ Prepared according to **GP3** from xanthene (36.4 mg, 1.0 equiv) and 3-phenylpropanal (79 μ L, 3.0 equiv). Purification by column chromatography on silica gel using *n*-pentane:EtOAc (10:1) as eluent afforded the analytically pure product (39.0 mg, 61%, 97.5:2.5 er) as a colorless oil.

¹H NMR (400 MHz, CDCl₃): δ = 7.35 (dd, ³J_{H-H} = 7.5 Hz, 1.6, 1H), 7.32 - 7.27 (m, 3H), 7.25 - 7.20 (m, 2H), 7.20 - 7.10 (m, 5H), 7.02 - 6.97 (m, 2H), 4.39 (d, ³J_{H-H} = 3.5 Hz, 1H), 3.56 - 3.42 (m, 2H), 2.73 - 2.64 (m, 1H), 2.29 - 2.17 (m, 2H), 1.23 - 1.14 (m, 1H).

¹³C NMR (100 MHz, CDCl₃): δ = 153.2, 153.2, 140.4, 129.7, 128.9, 128.8, 128.3, 127.8, 127.8, 125.9, 124.7, 123.4, 123.1, 123.1, 116.5, 116.4, 61.8, 52.4, 39.2, 33.3.

[α]_D²⁵: -21.6 (*c* 0.38, CH₂Cl₂), lit.: -13.5 (*c* 4.2, CHCl₃).⁶

HPLC (Daicel Chiralpak AS-H column, *n*-hexane/*i*-PrOH (95:5), flow rate 1.0 mL/min, λ = 254 nm): t_{major} = 11.5 min; t_{minor} = 27.9 min.



(R)-3-(4-fluorophenyl)-2-(9H-xanthen-9-yl)propan-1-ol (3h): Prepared according to modified **GP3** (with 20 mol% **cat.1**) from xanthene (36.4 mg, 1.0 equiv) and 3-(4-fluorophenyl)propanal (91 mg, 3.0 equiv). Purification by column chromatography on silica gel using *n*-pentane:EtOAc (10:1) as eluent afforded the analytically pure product (52.9

mg, 79%, 98:2 er) as a colorless oil.

¹H NMR (400 MHz, CDCl₃): δ = 7.38 - 7.26 (m, 4H), 7.21 - 7.11 (m, 4H), 6.95 - 6.85 (m, 4H), 4.40 (d, ³J_{H-H} = 3.7 Hz, 1H), 3.55 - 3.40 (m, 2H), 2.67 - 2.58 (m, 1H), 2.25 - 2.09 (m, 2H), 1.40 (br s, 1H).

¹³C NMR (100 MHz, CDCl₃): δ = 161.3 (d, ¹J_{C-F} = 243.8 Hz), 153.2, 153.2, 136.0 (d, ⁴J_{C-F} = 3.3 Hz), 130.1 (d, ³J_{C-F} = 7.7 Hz), 129.7, 128.8, 127.9,

127.8, 124.7, 123.3 (d, $^2J_{C-F} = 33.6$ Hz), 122.9, 116.5, 116.4, 115.2, 115.0, 61.6, 52.4, 39.1, 32.4.

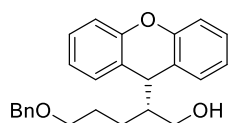
^{19}F NMR (376 MHz, CDCl_3) $\delta = -117.5$.

IR (neat): ν 3389, 3041, 2925, 1601, 1576, 1508, 1477, 1457, 1253, 1220, 1157, 1030, 894, 806 cm^{-1} .

HRMS (ESI+): m/z calcd. for $\text{C}_{22}\text{H}_{19}\text{FNaO}_2$ $[\text{M}+\text{Na}]^+$: 357.1261, found: 357.1266.

$[\alpha]_D^{25}$: -12.6 (c 1.24, CH_2Cl_2).

HPLC (Daicel Chiralpak IC column, *n*-hexane/*i*-PrOH (95:5), flow rate 1.0 mL/min, $\lambda = 240$ nm): $t_{\text{major}} = 11.3$ min; $t_{\text{minor}} = 13.0$ min.



(*R*)-5-(benzyloxy)-2-(9*H*-xanthen-9-yl)pentan-1-ol (3i):

Prepared according to modified **GP3** (with 20 mol% **cat.1**) from xanthene (36.4 mg, 1.0 equiv) and 5-(benzyloxy)pentanal (115 μL , 3.0 equiv). Purification by column chromatography on silica gel using *n*-pentane:EtOAc (5:1) as eluent afforded the mixture of desired product and 5-(benzyloxy)pentan-1-ol. Kugelrohr distillation (at 1.3×10^{-1} mbar) afforded the analytically pure product (59.1 mg, 79%, 98:2 er) as a colorless oil.

^1H NMR (400 MHz, CDCl_3): $\delta = 7.42 - 7.23$ (m, 9H), 7.18 - 7.07 (m, 4H), 4.44 (s, 2H), 4.29 (d, $^3J_{\text{H-H}} = 4.3$ Hz, 1H), 3.55 (d, $^3J_{\text{H-H}} = 6.1$ Hz, 2H), 3.36 (t, $^3J_{\text{H-H}} = 6.4$ Hz, 2H), 1.92 - 1.81 (m, 1H), 1.67 - 1.35 (m, 4H), 1.25 - 1.10 (m, 1H).

^{13}C NMR (100 MHz, CDCl_3): $\delta = 153.2, 153.2, 138.5, 129.5, 129.0, 128.4, 127.7, 127.6, 127.6, 127.5, 124.7, 123.7, 123.3, 123.1, 116.4, 116.3, 72.9, 70.4, 62.4, 50.0, 39.6, 27.6, 23.7$.

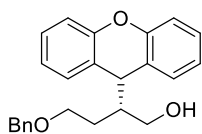
IR (neat): ν 3420, 3031, 2925, 2864, 1600, 1575, 1478, 1457, 1253, 1097, 1032, 894 cm^{-1} .

HRMS (ESI+): m/z calcd. for $\text{C}_{25}\text{H}_{26}\text{NaO}_3$ $[\text{M}+\text{Na}]^+$: 397.1774, found: 397.1784.

Asymmetric cross-dehydrogenative coupling of aldehydes with xanthenes

$[\alpha]_D^{25}$: +2.6 (*c* 1.22, CH₂Cl₂).

HPLC (Daicel Chiralpak AD-H column, *n*-hexane/*i*-PrOH (95:5), flow rate 1.0 mL/min, λ = 240 nm): t_{minor} = 26.0 min; t_{major} = 30.4 min.



(*R*)-4-(benzyloxy)-2-(9*H*-xanthen-9-yl)butan-1-ol (3j):⁶

Prepared according to **GP3** from xanthene (36.4 mg, 1.0 equiv) and 4-(benzyloxy)butanal (107 mg, 3.0 equiv).

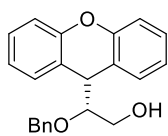
Purification by column chromatography on silica gel using *n*-pentane:EtOAc (5:1) as eluent afforded the analytically pure product (36.2 mg, 50%, 96:4 er) as a colorless oil.

¹H NMR (400 MHz, CDCl₃): δ = 7.37 - 7.16 (m, 9H), 7.11 - 7.02 (m, 4H), 4.38 (s, 2H), 4.19 (d, ³*J*_{H-H} = 4.8 Hz, 1H), 3.70 - 3.59 (m, 1H), 3.57 - 3.41 (m, 2H), 3.38 - 3.29 (m, 1H), 2.02 - 1.88 (m, 1H), 1.77 - 1.61 (m, 1H), 1.48 - 1.34 (m, 1H).

¹³C NMR (100 MHz, CDCl₃): δ = 153.1, 153.0, 137.7, 129.5, 129.1, 128.4, 127.8, 127.7, 127.6, 127.5, 124.8, 123.5, 123.3, 123.0, 116.4, 116.3, 73.0, 69.1, 63.5, 48.7, 41.0, 28.3.

$[\alpha]_D^{25}$: -20.7 (*c* 1.22, CH₂Cl₂), lit.: -7.1 (*c* 3.1, CHCl₃).⁶

HPLC (Daicel Chiralpak AD-H column, *n*-hexane/*i*-PrOH (95:5), flow rate 1.0 mL/min, λ = 240 nm): t_{minor} = 19.1 min; t_{major} = 22.9 min.



2-(Benzyloxy)-2-(9*H*-xanthen-9-yl)ethan-1-ol (3k): Prepared

according to modified **GP3** (with 20 mol% **cat.1**) from xanthene (36.4 mg, 1.0 equiv) and 2-

(benzyloxy)acetaldehyde (84 μ L, 3.0 equiv). Purification by column chromatography on silica gel using *n*-pentane:EtOAc (5:1) as eluent afforded the analytically pure product (55.6 mg, 84%, 50:50 er) as a colorless oil.

¹H NMR (500 MHz, CDCl₃): δ = 7.37 - 7.22 (m, 9H), 7.15 - 7.07 (m, 4H), 4.45 (d, ³*J*_{H-H} = 11.4 Hz, 1H, Ar₂CH), 4.40 (d, ²*J*_{H-H} = 11.4, 1H, PhCH₂O),

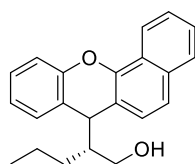
4.28 (d, $^2J_{\text{H-H}} = 5.8$, 1H, PhCH_2O), 3.60 - 3.50 (m, 2H, $\text{CH}_2\text{OH} + \text{CHOBN}$), 3.37 (dd, $^2J_{\text{H-H}} = 11.5$ Hz, $^3J_{\text{H-H}} = 6.1$ Hz, 1H, CH_2OH).

^{13}C NMR (126 MHz, CDCl_3): $\delta = 152.9$ (C_q), 152.9 (C_q), 137.8 (C_q), 129.9 (CH_{Ar}), 129.8 (CH_{Ar}), 128.5 (CH_{Ar}), 128.2 (CH_{Ar}), 128.1 (CH_{Ar}), 128.0 (CH_{Ar}), 127.9 (CH_{Ar}), 123.3 (CH_{Ar}), 123.1 (CH_{Ar}), 122.5 (C_q), 122.0 (C_q), 116.4 (CH_{Ar}), 84.4 (CHOBN), 72.9 (PhCH_2O), 61.4 (CH_2OH), 40.6 (Ar_2CH).

IR (neat): ν 3446, 3064, 3032, 2927, 2876, 1601, 1575, 1478, 1455, 1251, 1207, 1181, 1094, 1028, 898 cm^{-1} .

HRMS (ESI+): m/z calcd. for $\text{C}_{22}\text{H}_{20}\text{NaO}_3$ $[\text{M}+\text{Na}]^+$: 355.1305, found: 355.1299.

HPLC (Daicel Chiralpak AD-H column, *n*-hexane/*i*-PrOH (95:5), flow rate 1.0 mL/min, $\lambda = 240$ nm): $t = 16.7$ min; $t = 37.2$ min.



(2R)-2-(7H-benzo[c]xanthen-7-yl)pentan-1-ol (5a):

Prepared according to GP3 from **4a** (46.4 mg, 1.0 equiv) and pentanal (63.8 μL , 3.0 equiv). Purification by column chromatography on silica gel using *n*-pentane:EtOAc (10:1) as eluent afforded the analytically pure product (40.9 mg, 63%, 1:1 dr) as a colorless oil.

^1H NMR (400 MHz, CDCl_3): $\delta = 8.43$ (d, $^3J_{\text{H-H}} = 8.3$ Hz, 2H), 7.83 (d, $^3J_{\text{H-H}} = 7.8$ Hz, 2H), 7.61 - 7.47 (m, 6H), 7.38 - 7.27 (m, 8H), 7.21 - 7.08 (m, 2H), 4.45 (d, $^3J_{\text{H-H}} = 3.9$ Hz, 1H, Ar_2CH), 4.43 (d, $^3J_{\text{H-H}} = 4.0$ Hz, 1H, Ar_2CH), 3.65 - 3.51 (m, 4H, CH_2OH), 1.98 - 1.88 (m, 2H, CHCH_2OH), 1.34 - 1.17 (m, 8H), 0.78 (t, $^3J_{\text{H-H}} = 7.0$ Hz, 3H, CH_3), 0.73 (t, $^3J_{\text{H-H}} = 7.0$ Hz, 3H, CH_3).

^{13}C NMR (100 MHz, CDCl_3): $\delta = 153.24$ (C_q), 153.16 ($\underline{\text{C}}_q$), 148.01 (C_q), 147.98 (C_q), 133.29 (C_q), 133.25 (C_q), 129.51 (CH_{Ar}), 128.91 (CH_{Ar}), 127.56 (CH_{Ar}), 127.55 (CH_{Ar}), 127.49 (CH_{Ar}), 127.46 (CH_{Ar}), 127.18 (CH_{Ar}), 126.65 (CH_{Ar}), 126.06 (CH_{Ar}), 126.04 (CH_{Ar}), 125.84 (CH_{Ar}), 125.81 (CH_{Ar}), 124.65 (C_q), 124.15 (C_q), 124.11 (C_q), 123.56 (C_q), 123.49 (CH_{Ar}), 123.27 (CH_{Ar}), 122.70 (CH_{Ar}), 122.46 (CH_{Ar}), 121.54 (CH_{Ar}), 121.52 (CH_{Ar}), 118.64 (C_q), 117.71 (C_q), 116.47 (CH_{Ar}), 116.45 (CH_{Ar}), 62.71 (CH_2OH), 62.68 (CH_2OH),

Asymmetric cross-dehydrogenative coupling of aldehydes with xanthenes

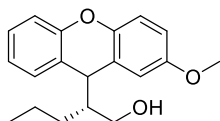
50.14 (CHCH₂OH), 49.84 (CHCH₂OH), 39.56 (Ar₂CH), 39.41 (Ar₂CH), 29.38 (CH₂), 29.05 (CH₂), 20.64 (CH₂), 20.61 (CH₂), 14.21 (CH₃), 14.17 (CH₃).

IR (neat): ν 3379, 3054, 2956, 2927, 2870, 1571, 1487, 1458, 1393, 1263, 1228, 1192, 1079, 1035 cm⁻¹.

HRMS (ESI+): m/z calcd. for C₂₂H₂₂NaO₂ [M+Na]⁺: 341.1512, found: 341.1518.

[α]_D²⁵: +3.4 (*c* 1.54, CH₂Cl₂).

HPLC (Daicel Chiralpak AD-H column, *n*-hexane/*i*-PrOH (96:4), flow rate 1.0 mL/min, λ = 254 nm): t_{major} = 19.3 min; t_{minor} = 27.0 min; t_{minor} = 28.4 min; t_{major} = 46.3 min.

**(2R)-2-(2-methoxy-9H-xanthen-9-yl)pentan-1-ol (5b):**

Prepared according to **GP3** from **4b** (42.4 mg, 1.0 equiv) and pentanal (63.8 μ L, 3.0 equiv). Purification by column chromatography on silica gel using *n*-pentane:EtOAc (10:1) as eluent afforded the analytically pure product (27.0 mg, 45%, 1:1 dr) as a colorless oil.

¹H NMR (400 MHz, CDCl₃): δ = 7.25 - 7.19 (m, 4H), 7.10 - 7.00 (m, 6H), 6.81 - 6.74 (m, 4H), 4.24 (two d, ³ $J_{\text{H-H}}$ = 3.7 Hz, 2H, Ar₂CH), 3.80 (s, 6H, OCH₃), 3.62 - 3.47 (m, 4H, CH₂OH), 1.91 - 1.81 (m, 2H, CHCH₂OH), 1.30 - 1.15 (m, 8H), 1.09 - 0.99 (m, 2H), 0.78 (m, 6H, CH₃).

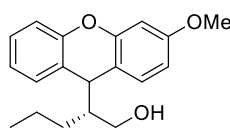
¹³C NMR (100 MHz, CDCl₃): δ = 155.46 (CH₃OC_q), 155.32 (CH₃OC_q), 153.51 (C_q), 153.45 (C_q), 147.40 (C_q), 147.36 (C_q), 129.48 (CH_{Ar}), 128.89 (CH_{Ar}), 127.58 (CH_{Ar}), 127.55 (CH_{Ar}), 125.65 (C_q), 124.63 (C_q), 124.29 (C_q), 123.19 (C_q), 122.98 (CH_{Ar}), 122.78 (CH_{Ar}), 116.88 (CH_{Ar}), 116.85 (CH_{Ar}), 116.24 (CH_{Ar}), 116.22 (CH_{Ar}), 114.15 (CH_{Ar}), 113.39 (CH_{Ar}), 113.27 (CH_{Ar}), 113.13 (CH_{Ar}), 62.65 (CH₂OH), 62.52 (CH₂OH), 55.74 (OCH₃), 49.93 (CHCH₂OH), 49.89 (CHCH₂OH), 39.81 (Ar₂CH), 29.21 (CH₂), 29.12 (CH₂), 20.62 (CH₂), 20.60 (CH₂), 14.23 (CH₃), 14.21 (CH₃).

IR (neat): ν 3398, 2955, 2929, 2871, 1623, 1580, 1479, 1458, 1238, 1203, 1151, 1035 cm^{-1} .

HRMS (ESI+): m/z calcd. for $\text{C}_{19}\text{H}_{22}\text{NaO}_3$ $[\text{M}+\text{Na}]^+$: 321.1461, found: 321.1471.

$[\alpha]_{\text{D}}^{25}$: +3.6 (c 1.4, CH_2Cl_2).

HPLC (Daicel Chiralpak IC column, *n*-hexane/*i*-PrOH (98:2 for 50 min; then 95:5 for 40 min), flow rate 1.0 mL/min, λ = 254 nm): t_{minor} = 39.0 min; t_{major} = 42.0 min; t_{minor} = 70.5 min; t_{minor} = 75.9 min.



(2*R*)-2-(3-methoxy-9*H*-xanthen-9-yl)pentan-1-ol (5c):

Prepared according to **GP3** from **4c** (42.4 mg, 1.0 equiv) and pentanal (63.8 μL , 3.0 equiv). Purification by column chromatography on silica gel using *n*-pentane:EtOAc (15:1) as eluent afforded the analytically pure product (32.0 mg, 54%, 1:1 dr) as a yellow oil.

$^1\text{H NMR}$ (400 MHz, CDCl_3): δ = 7.25 - 7.19 (m, 4H), 7.16 - 7.04 (m, 6H), 6.70 - 6.64 (m, 4H), 4.24 (d, $^3J_{\text{H-H}}$ = 4.0 Hz, 1H, Ar_2CH), 4.22 (d, $^3J_{\text{H-H}}$ = 4.0 Hz, 1H, Ar_2CH), 3.82 (s, 6H, OCH_3), 3.59 - 3.45 (m, 4H, CH_2OH), 1.87 - 1.77 (m, 2H, CHCH_2OH), 1.31 - 1.13 (m, 8H), 1.08 - 0.97 (m, 2H), 0.79 (t, $^3J_{\text{H-H}}$ = 6.2 Hz, 3H, CH_3), 0.76 (t, $^3J_{\text{H-H}}$ = 6.2 Hz, 3H, CH_3).

$^{13}\text{C NMR}$ (100 MHz, CDCl_3): δ = 159.26 (CH_3OC_q), 159.23 (CH_3OC_q), 153.91 (C_q), 153.85 (C_q), 153.10 (C_q), 129.97 (CH_{Ar}), 129.50 (CH_{Ar}), 129.39 (CH_{Ar}), 128.94 (CH_{Ar}), 127.52 (CH_{Ar}), 127.47 (CH_{Ar}), 125.02 (C_q), 124.06 (C_q), 123.21 (CH_{Ar}), 123.04 (CH_{Ar}), 116.52 (C_q), 116.22 (CH_{Ar}), 116.18 (CH_{Ar}), 115.50 (C_q), 109.92 (CH_{Ar}), 109.70 (CH_{Ar}), 101.36 (CH_{Ar}), 62.68 (CH_2OH), 62.64 (CH_2OH), 55.42 (OCH_3), 55.41 (OCH_3), 50.16 (CHCH_2OH), 50.14 (CHCH_2OH), 38.74 (Ar_2CH), 38.65 (Ar_2CH), 29.30 (CH_2), 29.04 (CH_2), 20.62 (CH_2), 20.60 (CH_2), 14.23 (CH_3), 14.21 (CH_3).

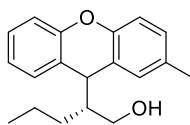
IR (neat): ν 3381, 2956, 2929, 2871, 1629, 1604, 1574, 1505, 1483, 1457, 1441, 1275, 1229, 1154, 1096, 1033 cm^{-1} .

Asymmetric cross-dehydrogenative coupling of aldehydes with xanthenes

HRMS (ESI+): m/z calcd. for $C_{19}H_{22}NaO_3$ $[M+Na]^+$: 321.1461, found: 321.1477.

$[\alpha]_D^{25}$: +0.7 (c 1.38, CH_2Cl_2).

HPLC (Daicel Chiralpak IC column, n -hexane/ i -PrOH (95:5), flow rate 1.0 mL/min, λ = 240 nm): t_{major} = 14.1 min; t_{minor} = 15.6 min; t_{minor} = 31.7 min; t_{major} = 45.7 min.



(2R)-2-(2-methyl-9H-xanthen-9-yl)pentan-1-ol (5d):

Prepared according to modified **GP3** (with 20 mol% **cat.1**) from **4d** (39.2 mg, 1.0 equiv) and pentanal (63.8 μ L, 3.0 equiv). Purification by column chromatography on silica gel using n -pentane:EtOAc (15:1) as eluent afforded the analytically pure product (37.2 mg, 66%, 1:1 dr) as a colorless oil.

1H NMR (400 MHz, $CDCl_3$): δ = 7.25 - 7.19 (m, 4H), 7.09 - 6.97 (m, 10H), 4.23 (two d, $^3J_{H-H}$ = 4.2 Hz, 2H, Ar_2CH), 3.61 - 3.48 (m, 4H, CH_2OH), 2.33 (s, 6H, $ArCH_3$), 1.90 - 1.80 (m, 2H, $CHCH_2OH$), 1.34 - 1.16 (m, 8H), 1.11 - 0.99 (m, 2H), 0.79 (two t, $^3J_{H-H}$ = 6.9 Hz, 6H, CH_3).

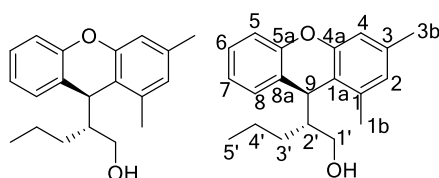
^{13}C NMR (100 MHz, $CDCl_3$): δ = 153.43 (C_q), 153.35 (C_q), 151.12 (C_q), 151.09 (C_q), 132.54 (CH_3C_q), 132.38 (CH_3C_q), 129.70 (CH_{Ar}), 129.51 (CH_{Ar}), 129.20 (CH_{Ar}), 128.97 (CH_{Ar}), 128.22 (CH_{Ar}), 128.18 (CH_{Ar}), 127.53 (CH_{Ar}), 124.66 (C_q), 124.50 (C_q), 123.72 (C_q), 123.51 (C_q), 123.02 (CH_{Ar}), 122.83 (CH_{Ar}), 116.26 (CH_{Ar}), 116.25 (CH_{Ar}), 115.99 (CH_{Ar}), 115.96 (CH_{Ar}), 62.64 (CH_2OH), 62.59 (CH_2OH), 50.20 ($CHCH_2OH$), 50.10 ($CHCH_2OH$), 39.46 (Ar_2CH), 39.42 (Ar_2CH), 29.26 (CH_2), 29.11 (CH_2), 20.82 (CH_2), 20.80 (CH_2), 20.63 ($ArCH_3$), 20.61 ($ArCH_3$), 14.24 (CH_3), 14.23 (CH_3).

IR (neat): ν 3355, 2956, 2926, 2871, 1598, 1579, 1480, 1457, 1256, 1234, 1033, 814 cm^{-1} .

HRMS (ESI+): m/z calcd. for $C_{19}H_{22}NaO_2$ $[M+Na]^+$: 305.1512, found: 305.1524.

$[\alpha]_D^{25}$: +8.3 (c 1.81, CH_2Cl_2).

HPLC (Daicel Chiralpak IC column, *n*-hexane/*i*-PrOH (95:5), flow rate 1.0 mL/min, $\lambda = 240$ nm): $t_{\text{major}} = 9.4$ min; $t_{\text{minor}} = 12.1$ min; $t_{\text{major}} = 21.6$ min; $t_{\text{minor}} = 30.7$ min.



(*R*)-2-((*S*)-1,3-dimethyl-9H-xanthen-9-yl)pentan-1-ol (5e): Prepared according to **GP3** from **4e** (42.0 mg, 1.0 equiv) and pentanal (63.8 μ L, 3.0 equiv).

Purification by column chromatography on silica gel using *n*-pentane:EtOAc (15:1) as eluent afforded the analytically pure product (30.2 mg, 51%, 98.5:1.5 er) as a colorless oil.

R_f: 0.18 (*n*-pentane:EtOAc 10:1).

¹H NMR (500 MHz, CDCl₃): $\delta = 7.26 - 7.23$ (m, 1H, H⁸), 7.23 - 7.20 (m, 1H, H⁷), 7.08 - 7.02 (m, 2H, H⁵+H⁶), 6.79 (s, 2H, H²+H⁴), 4.51 (d, ³J_{H-H} = 3.4 Hz, 1H, H⁹), 3.73 (dd, ²J_{H-H} = 10.8 Hz, ³J_{H-H} = 4.5 Hz, 1H, H^{1'}), 3.51 (dd, ²J_{H-H} = 10.4 Hz, ³J_{H-H} = 10.4 Hz, 1H, H^{1'}), 2.40 (s, 3H, H^{1b}), 2.31 (s, 3H, H^{3b}), 1.90 - 1.78 (m, 1H, H²), 1.39 (br s, 1H, OH), 1.20 - 1.04 (m, 2H, H⁴+H³), 1.00 - 0.85 (m, 1H, H⁴), 0.71 - 0.63 (m, 4H, H⁵+H³).

¹³C NMR (126 MHz, CDCl₃): $\delta = 153.78$ (C^{5a}), 153.66 (C^{4a}), 136.80 (C³), 135.89 (C¹), 129.70 (C⁸H), 127.45 (C⁷H), 126.26 (C²H), 123.18 (C^{8a}), 122.49 (C⁵H), 121.18 (C^{1a}), 116.11 (C⁶H), 114.60 (C⁴H), 62.80 (C^{1'}), 47.25 (C²), 35.91 (C⁹), 27.84 (C³), 21.02 (C^{3b}), 20.69 (C⁴), 18.41 (C^{1b}), 14.24 (C⁵).

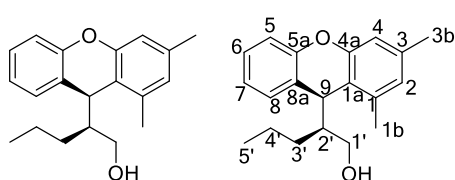
IR (neat): ν 3394, 2956, 2926, 1627, 1605, 1572, 1482, 1458, 1297, 1237, 1135, 1040, 844 cm⁻¹.

HRMS (ESI⁺): *m/z* calcd. for C₂₀H₂₄NaO₂ [M+Na]⁺: 319.1669, found: 319.1677.

[α]_D²⁵: +48.9 (*c* 1.43, CH₂Cl₂).

HPLC (Daicel Chiralpak AD-H column, *n*-hexane/*i*-PrOH (95:5), flow rate 1.0 mL/min, $\lambda = 240$ nm): $t_{\text{major}} = 8.1$ min (2*R*,9*S*); $t_{\text{minor}} = 15.6$ min (2*S*,9*R*).

Asymmetric cross-dehydrogenative coupling of aldehydes with xanthenes



(S)-2-((S)-1,3-dimethyl-9H-xanthene-9-yl)pentan-1-ol (6e): Prepared

according to modified GP3 (with 20 mol% **cat.2**) from **4e** (42.0 mg, 1.0 equiv) and pentanal (63.8 μ L, 3.0 equiv). Purification by column chromatography on silica gel using *n*-pentane:EtOAc (15:1) as eluent afforded the analytically pure product (31.0 mg, 52%, 76:24 er) as a white solid.

mp: 110 - 116 $^{\circ}$ C.

R_f: 0.25 (*n*-pentane:EtOAc 10:1).

¹H NMR (500 MHz, CDCl₃): δ = 7.25 - 7.17 (m, 2H, H⁷+H⁸), 7.11 - 7.03 (m, 2H, H⁵+H⁶), 6.80 (s, 1H, H^{2/4}), 6.79 (s, 1H, H^{2/4}), 4.18 (d, ³J_{H-H} = 3.8 Hz, 1H, H⁹), 3.53 - 3.46 (m, 1H, H^{1'}), 3.21 - 3.14 (m, 1H, H^{1'}), 2.37 (s, 3H, H^{1b}), 2.31 (s, 3H, H^{3b}), 1.82 - 1.73 (m, 1H, H²), 1.64 - 1.54 (m, 2H, H^{4'}+H^{3'}), 1.53 - 1.46 (m, 1H, H^{4'}), 1.45 - 1.38 (m, 1H, H^{3'}), 0.99 (t, ³J_{H-H} = 7.0 Hz, 3H, H⁵), 0.87 (br s, 1H, OH).

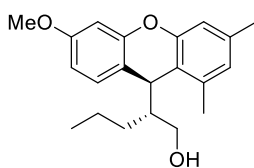
¹³C NMR (126 MHz, CDCl₃): δ = 153.40 (C^{5a}), 153.30 (C^{4a}), 137.06 (C³), 135.88 (C¹), 129.33 (C^{8H}), 127.72 (C^{7H}), 126.46 (C^{2H}), 123.83 (C^{8a}), 122.75 (C^{5H}), 121.59 (C^{1a}), 116.33 (C^{6H}), 114.75 (C^{4H}), 62.55 (C^{1'}), 47.97 (C^{2'}), 37.55 (C⁹), 31.37 (C^{3'}), 20.98 (C^{3b}), 20.68 (C^{4'}), 18.61 (C^{1b}), 14.47 (C^{5'}).

IR (neat): ν 3386, 2955, 2926, 2870, 1627, 1605, 1571, 1480, 1457, 1296, 1234, 1134, 1039, 843 cm⁻¹.

HRMS (ESI+): *m/z* calcd. for C₂₀H₂₄NaO₂ [M+Na]⁺: 319.1669, found: 319.1675.

[α]_D²⁵: -21.9 (*c* 1.5, CH₂Cl₂).

HPLC (Daicel Chiralpak AD-H column, *n*-hexane/*i*-PrOH (95:5), flow rate 1.0 mL/min, λ = 254 nm): *t*_{minor} = 7.3 min (2*R*,9*R*); *t*_{major} = 8.3 min (2*S*,9*S*).



(*R*)-2-((*S*)-6-methoxy-1,3-dimethyl-9*H*-xanthen-9-yl)pentan-1-ol (5f): Prepared according to modified GP3 (with 20 mol% **cat.1**) from **4f** (48.0 mg, 1.0 equiv) and pentanal (63.8 μ L, 3.0 equiv). Purification by column chromatography on silica gel using *n*-pentane:EtOAc (15:1) as eluent afforded the analytically pure product (31.3 mg, 48%, 99:1 er) as a colorless oil.

R_f: 0.14 (*n*-pentane:EtOAc 10:1).

¹H NMR (400 MHz, CDCl₃): δ = 7.14 (d, ³*J*_{H-H} = 8.3 Hz, 1H, CH_{Ar}), 6.78 (s, 1H, CH_{Ar}), 6.77 (s, 1H, CH_{Ar}), 6.65 - 6.61 (m, 2H, CH_{Ar}), 4.46 (d, ³*J*_{H-H} = 3.2 Hz, 1H, Ar₂CH), 3.81 (s, 3H, CH₃O), 3.73 (dd, ²*J*_{H-H} = 10.8 Hz, ³*J*_{H-H} = 4.5 Hz, 1H, CH₂OH), 3.49 (dd, ²*J*_{H-H} = 10.4 Hz, ³*J*_{H-H} = 10.4 Hz, 1H, CH₂OH), 2.39 (s, 3H, ArCH₃), 2.31 (s, 3H, ArCH₃), 1.86 - 1.78 (m, 1H, CHCH₂OH), 1.16 - 1.06 (m, 2H, CH₂), 0.97 - 0.86 (m, 1H, CH₂), 0.69 - 0.59 (m, 4H, CH₂ + CH₂CH₃).

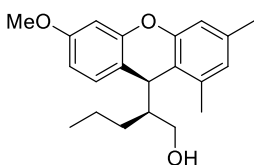
¹³C NMR (100 MHz, CDCl₃): δ = 159.33 (C_q), 154.61 (C_q), 153.72 (C_q), 136.84 (C_q), 136.02 (C_q), 130.25 (CH_{Ar}), 126.41 (CH_{Ar}), 121.53 (C_q), 115.23 (C_q), 114.65 (CH_{Ar}), 109.21 (CH_{Ar}), 101.40 (CH_{Ar}), 63.09 (CH₂OH), 55.52 (CH₃O), 47.34 (CHCH₂OH), 35.38 (Ar₂CH), 27.94 (CH₂), 21.15 (ArCH₃), 20.84 (CH₂), 18.56 (ArCH₃), 14.41 (CH₃).

IR (neat): ν 3422, 2955, 2927, 2871, 1613, 1504, 1441, 1295, 1197, 1159, 1121, 1033, 843 cm⁻¹.

HRMS (ESI+): *m/z* calcd. for C₂₁H₂₆NaO₃ [M+Na]⁺: 349.1774, found: 349.1769.

[α]_D²⁵: -16.5 (*c* 1.58, CH₂Cl₂).

HPLC (Daicel Chiralpak AD-H column, *n*-hexane/*i*-PrOH (95:5), flow rate 1.0 mL/min, λ = 254 nm): *t*_{major} = 14.6 min; *t*_{minor} = 20.0 min.



(*S*)-2-((*S*)-6-methoxy-1,3-dimethyl-9*H*-xanthen-9-yl)pentan-1-ol (6f): Prepared according to modified GP3 (with 20 mol% **cat.2**) from **4f** (48.0 mg, 1.0 equiv) and pentanal (63.8 μ L, 3.0 equiv). Purification by

Asymmetric cross-dehydrogenative coupling of aldehydes with xanthenes

column chromatography on silica gel using *n*-pentane:EtOAc (15:1) as eluent afforded the analytically pure product (21.6 mg, 33%, 73.5:26.5 er) as a colorless oil.

R_f: 0.20 (*n*-pentane:EtOAc 10:1).

¹H NMR (500 MHz, CDCl₃): δ = 7.07 (d, ³J_{H-H} = 7.9 Hz, 1H, CH_{Ar}), 6.78 (s, 2H, CH_{Ar}), 6.67 - 6.60 (m, 2H, CH_{Ar}), 4.12 (d, ³J_{H-H} = 3.5 Hz, 1H, Ar₂CH), 3.80 (s, 3H, CH₃O), 3.46 (dd, ²J_{H-H} = 11.3 Hz, ³J_{H-H} = 4.5 Hz, 1H, CH₂OH), 3.18 (dd, ²J_{H-H} = 11.2 Hz, ³J_{H-H} = 5.9 Hz, 1H, CH₂OH), 2.35 (s, 3H, ArCH₃), 2.30 (s, 3H, ArCH₃), 1.79 - 1.69 (m, 1H, CHCH₂OH), 1.65 - 1.37 (m, 4H, CH₂ + OH), 0.99 (t, ³J_{H-H} = 7.0 Hz, 3H, CH₂CH₃).

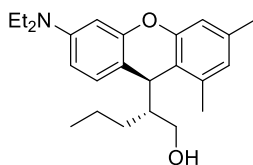
¹³C NMR (126 MHz, CDCl₃): δ = 159.54 (C_q), 154.23 (C_q), 153.32 (C_q), 137.11 (C_q), 136.00 (C_q), 129.88 (CH_{Ar}), 126.62 (CH_{Ar}), 121.94 (C_q), 115.75 (C_q), 114.80 (CH_{Ar}), 109.51 (CH_{Ar}), 101.63 (CH_{Ar}), 62.84 (CH₂OH), 55.55 (CH₃O), 48.10 (CHCH₂OH), 37.07 (Ar₂CH), 31.71 (CH₂), 21.11 (ArCH₃), 20.81 (CH₂), 18.73 (ArCH₃), 14.63 (CH₃).

IR (neat): ν 2955, 2927, 2870, 1632, 1614, 1572, 1504, 1442, 1296, 1273, 1198, 1160, 1122, 1036 cm⁻¹.

HRMS (ESI⁺): *m/z* calcd. for C₂₁H₂₆NaO₃ [M+Na]⁺: 349.1774, found: 349.1775.

[α]_D²⁵: +11.6 (*c* 0.83, CH₂Cl₂).

HPLC (Daicel Chiralpak IC column, *n*-hexane/*i*-PrOH (95:5), flow rate 1.0 mL/min, λ = 254 nm): *t*_{minor} = 10.3 min; *t*_{major} = 11.8 min.



(*R*)-2-((*S*)-6-(diethylamino)-1,3-dimethyl-9*H*-xanthen-9-yl)pentan-1-ol (5g): Prepared according to modified GP3 (with 20 mol% cat.1) from **4g** (56.2 mg, 1.0 equiv) and pentanal (63.8 μL, 3.0 equiv). Purification

by column chromatography on silica gel using *n*-pentane:EtOAc (15:1) as eluent afforded the analytically pure product (17.5 mg, 24%, 79.5:20.5 er) as a red oil.

R_f: 0.25 (*n*-pentane:EtOAc 10:1).

¹H NMR (400 MHz, CDCl₃): δ = 7.05 (d, ³J_{H-H} = 8.7 Hz, 1H), 6.75 (s, 2H), 6.45 - 6.37 (m, 2H), 4.38 (d, ³J_{H-H} = 3.1 Hz, 1H, Ar₂CH), 3.74 (dd, ²J_{H-H} = 10.8 Hz, ³J_{H-H} = 4.5 Hz, 1H, CH₂OH), 3.55 (dd, ²J_{H-H} = 10.8 Hz, ³J_{H-H} = 9.8 Hz, 1H, CH₂OH), 3.34 (q, ³J_{H-H} = 7.1 Hz, 4H, CH₂N), 2.38 (s, 3H, ArCH₃), 2.30 (s, 3H, ArCH₃), 1.87 - 1.77 (m, 1H, CHCH₂OH), 1.21 - 1.07 (m, 8H, CH₃CH₂N + CH₂CH₂), 0.98 - 0.82 (m, 1H, CH₂CH₂), 0.80 - 0.69 (m, 1H, CH₂CH₂), 0.66 (t, ³J_{H-H} = 7.1 Hz, 3H, CH₂CH₂CH₃).

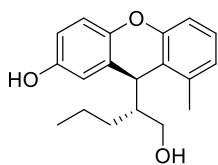
¹³C NMR (101 MHz, CDCl₃): δ = 154.72 (C_q), 153.95 (C_q), 147.80 (Et₂NC_q), 136.39 (C_q), 135.74 (C_q), 129.97 (CH_{Ar}), 125.87 (CH_{Ar}), 121.89 (C_q), 114.50 (CH_{Ar}), 109.95 (C_q), 106.95 (CH_{Ar}), 99.27 (CH_{Ar}), 63.29 (CH₂OH), 47.34 (CHCH₂OH), 44.41 (CH₂N), 35.28 (Ar₂CH), 27.79 (CH₂), 21.02 (ArCH₃), 20.74 (CH₂), 18.48 (ArCH₃), 14.29 (NCH₂CH₃), 12.63 (CH₃).

IR (neat): ν 3393, 2961, 2927, 2871, 1634, 1615, 1558, 1514, 1456, 1375, 1356, 1297, 1279, 1218, 1138, 1115, 1045 cm⁻¹.

HRMS (ESI+): *m/z* calcd. for C₂₄H₃₄NO₂ [M+H]⁺: 368.2584, found: 368.2579.

[α]_D²⁵: -28.8 (*c* 0.49, CH₂Cl₂).

HPLC (Daicel Chiralpak AD-H column, *n*-hexane/*i*-PrOH (95:5), flow rate 1.0 mL/min, λ = 240 nm): *t*_{minor} = 11.4 min; *t*_{major} = 13.3 min.



(S)-9-((R)-1-hydroxypentan-2-yl)-6,8-dimethyl-9H-

xanthen-2-ol (5h): Prepared according to modified GP3 (with 20 mol% **cat.1**) from **4h** (45.2 mg, 1.0 equiv) and pentanal (63.8 μL, 3.0 equiv). Purification by column

chromatography on silica gel using *n*-pentane:EtOAc (5:1) as eluent afforded the analytically pure product (28.3 mg, 45%, 98:2 er) as a white solid.

mp: 60 - 65 °C.

R_f: 0.36 (*n*-pentane:EtOAc 2:1).

Asymmetric cross-dehydrogenative coupling of aldehydes with xanthenes

¹H NMR (400 MHz, CDCl₃): δ = 6.94 (d, ³J_{H-H} = 8.6 Hz, 1H), 6.83 (s, 1H), 6.76 - 6.71 (m, 3H), 4.45 (d, ³J_{H-H} = 2.7 Hz, 1H, Ar₂CH), 3.78 (dd, ²J_{H-H} = 11.0 Hz, ³J_{H-H} = 4.3, 1H, CH₂OH), 3.56 (dd, ²J_{H-H} = 10.7 Hz, ³J_{H-H} = 10.7 Hz, 1H, CH₂OH), 2.34 (s, 3H, ArCH₃), 2.29 (s, 3H, ArCH₃), 1.92 - 1.81 (m, 1H, CHCH₂OH), 1.19 - 1.05 (m, 2H, CH₂), 0.97 - 0.84 (m, 1H, CH₂), 0.71 - 0.60 (m, 4H, CH₂ + CH₂CH₃).

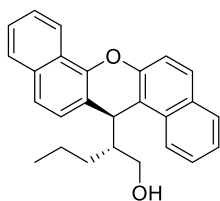
¹³C NMR (100 MHz, CDCl₃): δ = 153.93 (C_q), 150.91 (C_q), 147.83 (C_q), 136.83 (C_q), 135.73 (C_q), 126.06 (CH_{Ar}), 123.78 (C_q), 120.49 (C_q), 116.88 (CH_{Ar}), 115.73 (CH_{Ar}), 114.53 (CH_{Ar}), 62.96 (CH₂OH), 47.01 (CHCH₂OH), 36.01 (Ar₂CH), 27.66 (CH₂), 21.01 (ArCH₃), 20.71 (CH₂), 18.39 (ArCH₃), 14.21 (CH₃).

IR (neat): ν 3309, 2956, 2926, 2871, 1629, 1577, 1486, 1456, 1377, 1292, 1227, 1134, 1032 cm⁻¹.

HRMS (ESI+): *m/z* calcd. for C₂₀H₂₄NaO₃ [M+Na]⁺: 335.1618, found: 335.1620.

[α]_D²⁵: +48.1 (*c* 1.15, CH₂Cl₂).

HPLC (Daicel Chiralpak AD-H column, *n*-hexane/*i*-PrOH (92:8), flow rate 1.0 mL/min, λ = 254 nm): *t*_{major} = 15.5 min; *t*_{minor} = 23.2 min.

**(*R*)-2-((*S*)-14*H*-dibenzo[*a,h*]xanthen-14-yl)pentan-1-ol**

(5i): Prepared according to modified GP3 (with 20 mol% cat.1) from 4i (56.5 mg, 1.0 equiv) and pentanal (63.8 μ L, 3.0 equiv). Purification by column chromatography on silica gel using *n*-pentane:EtOAc (10:1) as eluent

afforded the analytically pure product (49.3 mg, 67%, 97:3 er) as a colorless oil.

R_f: 0.15 (*n*-pentane:EtOAc 10:1).

¹H NMR (500 MHz, CDCl₃): δ = 8.50 (d, ³J_{H-H} = 8.3 Hz, 1H), 8.26 (d, ³J_{H-H} = 8.4 Hz, 1H), 7.87 (t, ³J_{H-H} = 8.2 Hz, 2H), 7.80 (d, ³J_{H-H} = 8.8 Hz, 1H), 7.63 - 7.57 (m, 3H), 7.52 (m, 3H), 7.48 - 7.43 (m, 1H), 5.37 (d, ³J_{H-H} = 2.9 Hz, 1H,

Ar_2CH), 3.82 (dd, $^2J_{\text{H-H}} = 10.7$ Hz, $^3J_{\text{H-H}} = 4.7$ Hz, 1H, CH_2OH), 3.68 (dd, $^2J_{\text{H-H}} = 10.6$ Hz, $^3J_{\text{H-H}} = 10.6$ Hz, 1H, CH_2OH), 2.29 - 2.20 (m, 1H, CHCH_2OH), 1.21 - 1.14 (m, 1H, CH_2), 1.10 - 0.99 (m, 1H, CH_2), 0.92 - 0.79 (m, 2H, $\text{CH}_2 + \text{OH}$), 0.74 - 0.64 (m, 1H, CH_2), 0.52 (t, $^3J_{\text{H-H}} = 7.3$ Hz, 3H, CH_3).

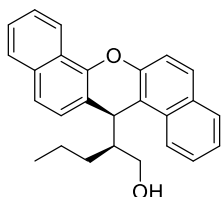
^{13}C NMR (126 MHz, CDCl_3): $\delta = 151.16$ (C_q), 148.25 (C_q), 133.44 (C_q), 131.52 (C_q), 131.28 (C_q), 128.86 (CH_{Ar}), 128.29 (CH_{Ar}), 127.85 (CH_{Ar}), 127.62 (CH_{Ar}), 126.81 (CH_{Ar}), 126.17 (CH_{Ar}), 125.93 (CH_{Ar}), 124.28 (CH_{Ar}), 124.21 (C_q), 122.87 (CH_{Ar}), 122.55 (CH_{Ar}), 121.71 (CH_{Ar}), 117.85 (CH_{Ar}), 117.53 (C_q), 116.36 (C_q), 63.21 (CH_2OH), 47.33 (CHCH_2OH), 35.12 (Ar_2CH), 28.36 (CH_2), 20.79 (CH_2), 14.32 (CH_3).

IR (neat): ν 3393, 3056, 2956, 2928, 2871, 1625, 1598, 1574, 1463, 1436, 1398, 1259, 1236, 1082 cm^{-1} .

HRMS (ESI+): m/z calcd. for $\text{C}_{26}\text{H}_{24}\text{NaO}_2$ $[\text{M}+\text{Na}]^+$: 391.1669, found: 391.1661.

$[\alpha]_{\text{D}}^{25}$: -164.9 (c 2.48, CH_2Cl_2).

HPLC (Daicel Chiralpak IB column, *n*-hexane/*i*-PrOH (98:2), flow rate 1.0 mL/min, $\lambda = 240$ nm): $t_{\text{minor}} = 17.9$ min; $t_{\text{major}} = 33.3$ min.



(S)-2-((S)-14H-dibenzo[*a,h*]xanthen-14-yl)pentan-1-ol

(6i): Prepared according to modified GP3 (with 20 mol% cat.2) from 4i (56.5 mg, 1.0 equiv) and pentanal (63.8 μL , 3.0 equiv). Purification by column chromatography on silica gel using *n*-pentane:EtOAc (10:1) as eluent

afforded the analytically pure product (27.5 mg, 37%, 69.5:30.5 er, 1:1 dr) as a colorless oil.

R_f : 0.25 (*n*-pentane:EtOAc 10:1).

^1H NMR (500 MHz, CDCl_3): $\delta = 8.48$ (d, $^3J_{\text{H-H}} = 8.1$ Hz, 1H), 8.13 (d, $^3J_{\text{H-H}} = 8.5$ Hz, 1H), 7.87 (t, $^3J_{\text{H-H}} = 8.5$ Hz, 2H), 7.80 (d, $^3J_{\text{H-H}} = 8.9$ Hz, 1H), 7.65 - 7.57 (m, 3H), 7.56 - 7.49 (m, 2H), 7.46 (ddd, $^3J_{\text{H-H}} = 7.9$ Hz, $^3J_{\text{H-H}} = 6.9$ Hz, $^4J_{\text{H-H}} = 1.0$ Hz, 1H), 7.42 (d, $^3J_{\text{H-H}} = 8.4$ Hz, 1H), 5.01 (d, $^3J_{\text{H-H}} = 3.2$ Hz, 1H, Ar_2CH), 3.50 (dd, $^3J_{\text{H-H}} = 11.1$ Hz, $^3J_{\text{H-H}} = 5.1$ Hz, 1H, CH_2OH), 3.27 (dd, $^2J_{\text{H-H}}$

Asymmetric cross-dehydrogenative coupling of aldehydes with xanthenes

= 11.1 Hz, $^3J_{\text{H-H}} = 5.9$ Hz, 1H, CH_2OH), 2.12 - 2.07 (m, 1H, CHCH_2OH), 1.70 - 1.63 (m, 1H, CH_2), 1.58 (m, 5H, $\text{CH}_2 + \text{OH}$), 1.00 (t, $^3J_{\text{H-H}} = 6.9$ Hz, 3H, CH_3).

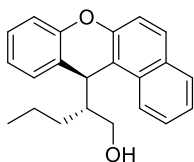
^{13}C NMR (126 MHz, CDCl_3): $\delta = 150.96$ (C_q), 147.85 (C_q), 133.44 (C_q), 131.68 (C_q), 131.29 (C_q), 128.97 (CH_{Ar}), 128.52 (CH_{Ar}), 127.67 (CH_{Ar}), 127.25 (CH_{Ar}), 126.84 (CH_{Ar}), 126.35 (CH_{Ar}), 126.14 (CH_{Ar}), 124.38 (CH_{Ar}), 124.16 (C_q), 122.91 (CH_{Ar}), 122.57 (CH_{Ar}), 121.64 (CH_{Ar}), 117.86 (CH_{Ar}), 117.59 (C_q), 117.33 (C_q), 63.15 (CH_2OH), 48.56 (CHCH_2OH), 36.77 (Ar_2CH), 31.68 (CH_2), 21.02 (CH_2), 14.62 (CH_3).

IR (neat): ν 3388, 3056, 2955, 2926, 2870, 1625, 1599, 1574, 1463, 1435, 1397, 1258, 1235, 1081 cm^{-1} .

HRMS (ESI+): m/z calcd. for $\text{C}_{26}\text{H}_{24}\text{NaO}_2$ $[\text{M}+\text{Na}]^+$: 391.1669, found: 391.1662.

$[\alpha]_{\text{D}}^{25}$: +68.6 (c 1.04, CH_2Cl_2).

HPLC (Daicel Chiralpak AD-H column, n -hexane/ i -PrOH (95:5), flow rate 1.0 mL/min, $\lambda = 240$ nm): $t_{\text{minor}} = 20.8$ min; $t_{\text{major}} = 22.5$ min.

**(R)-2-((S)-12H-benzo[a]xanthen-12-yl)pentan-1-ol (5j):**

Prepared according to modified GP3 (with 20 mol% cat.1) from **4j** (46.5 mg, 1.0 equiv) and pentanal (63.8 μL , 3.0 equiv). Purification by column chromatography on silica gel using n -pentane:EtOAc (15:1) as eluent afforded the analytically pure product (31.9 mg, 50%, 99:1 er) as a colorless oil.

R_f : 0.20 (n -pentane:EtOAc 10:1).

^1H NMR (500 MHz, CDCl_3): $\delta = 8.20$ (d, $^3J_{\text{H-H}} = 8.4$ Hz, 1H), 7.85 (d, $^3J_{\text{H-H}} = 8.1$ Hz, 1H), 7.75 (d, $^3J_{\text{H-H}} = 8.8$ Hz, 1H), 7.57 (ddd, $^3J_{\text{H-H}} = 8.4$ Hz, $^3J_{\text{H-H}} = 6.8$ Hz, $^4J_{\text{H-H}} = 1.4$ Hz, 1H), 7.43 (ddd, $^3J_{\text{H-H}} = 8.1$ Hz, $^3J_{\text{H-H}} = 6.8$ Hz, $^4J_{\text{H-H}} = 1.1$ Hz, 1H), 7.39 (dd, $^3J_{\text{H-H}} = 7.5$ Hz, $^4J_{\text{H-H}} = 1.7$ Hz, 1H), 7.32 (d, $^3J_{\text{H-H}} = 8.9$ Hz, 1H), 7.29 - 7.25 (m, 1H), 7.17 (dd, $^3J_{\text{H-H}} = 8.1$ Hz, $^4J_{\text{H-H}} = 1.3$ Hz, 1H), 7.13 (ddd, $^3J_{\text{H-H}} = 7.4$ Hz, $^3J_{\text{H-H}} = 7.4$ Hz, $^4J_{\text{H-H}} = 1.3$ Hz, 1H), 5.21 (d, $^3J_{\text{H-H}} = 3.0$

Hz, 1H, Ar₂CH), 3.80 (dd, ²J_{H-H} = 10.7 Hz, ³J_{H-H} = 4.5 Hz, 1H, CH₂OH), 3.62 (dd, ²J_{H-H} = 10.5 Hz, ³J_{H-H} = 10.5 Hz, 1H, CH₂OH), 2.14 (dddd, ³J_{H-H} = 10.5 Hz, ³J_{H-H} = 10.5 Hz, ³J_{H-H} = 4.6 Hz, ³J_{H-H} = 3.2 Hz, ³J_{H-H} = 3.2 Hz, 1H, CHCH₂OH), 1.57 (br s, 1H, OH), 1.20 - 1.09 (m, 1H, CH₂), 1.12 - 1.00 (m, 1H, CH₂), 0.89 - 0.77 (m, 1H, CH₂), 0.72 - 0.65 (m, 1H, CH₂), 0.55 (t, ³J_{H-H} = 7.2 Hz, 3H, CH₃).

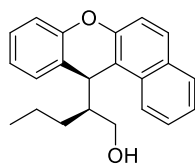
¹³C NMR (126 MHz, CDCl₃): δ = 153.20 (C_q), 150.93 (C_q), 131.37 (C_q), 130.94 (C_q), 129.88 (CH_{Ar}), 128.70 (CH_{Ar}), 128.18 (CH_{Ar}), 127.56 (CH_{Ar}), 126.64 (CH_{Ar}), 124.03 (CH_{Ar}), 123.05 (CH_{Ar}), 122.58 (CH_{Ar}), 122.07 (C_q), 117.65 (CH_{Ar}), 117.29 (C_q), 116.13 (CH_{Ar}), 62.86 (CH₂OH), 46.97 (CHCH₂OH), 34.60 (Ar₂CH), 28.10 (CH₂), 20.62 (CH₂), 14.20 (CH₃).

IR (neat): ν 3394, 3060, 2956, 2928, 2871, 1626, 1579, 1516, 1487, 1457, 1436, 1397, 1238, 1028, 960, 813 cm⁻¹.

HRMS (ESI⁺): *m/z* calcd. for C₂₂H₂₂NaO₂ [M+Na]⁺: 341.1512, found: 341.1505.

[α]_D²⁵: -28.2 (c 1.61, CH₂Cl₂).

HPLC (Daicel Chiralpak AD-H column, *n*-hexane/*i*-PrOH (96:4), flow rate 0.8 mL/min, λ = 254 nm): *t*_{minor} = 17.4 min; *t*_{major} = 31.2 min.



(S)-2-((S)-12H-benzo[a]xanthen-12-yl)pentan-1-ol (6j):

Prepared according to modified GP3 (with 20 mol% cat.2) from 4j (46.5 mg, 1.0 equiv) and pentanal (63.8 μL, 3.0 equiv). Purification by column chromatography on silica

gel using *n*-pentane:EtOAc (15:1) as eluent afforded the analytically pure product (28.4 mg, 45%, 73:27 er) as a colorless oil.

*R*_f: 0.25 (*n*-pentane:EtOAc 10:1).

¹H NMR (400 MHz, CDCl₃): δ = 8.06 (d, ³J_{H-H} = 8.5 Hz, 1H), 7.85 (dd, ³J_{H-H} = 8.1 Hz, ⁴J_{H-H} = 1.3 Hz, 1H), 7.75 (d, ³J_{H-H} = 8.8 Hz, 1H), 7.57 (ddd, ³J_{H-H} = 8.5 Hz, ³J_{H-H} = 6.8 Hz, ⁴J_{H-H} = 1.4 Hz, 1H), 7.43 (ddd, ³J_{H-H} = 8.1 Hz, ³J_{H-H} = 6.8 Hz, ⁴J_{H-H} = 1.1 Hz, 1H), 7.35 - 7.25 (m, 3H), 7.20 - 7.09 (m, 2H), 4.86 (d, ³J_{H-H} = 3.3 Hz, 1H, Ar₂CH), 3.46 (dd, ²J_{H-H} = 11.2 Hz, ³J_{H-H} = 4.9 Hz, 1H,

Asymmetric cross-dehydrogenative coupling of aldehydes with xanthenes

CH_2OH), 3.25 (dd, $^2J_{\text{H-H}} = 11.2$ Hz, $^3J_{\text{H-H}} = 5.9$ Hz, 1H, CH_2OH), 2.07 - 1.95 (m, 1H, CHCH_2OH), 1.74 - 1.48 (m, 4H, 2CH_2), 1.00 (t, $^3J_{\text{H-H}} = 6.7$ Hz, 3H, CH_3).

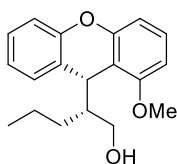
^{13}C NMR (100 MHz, CDCl_3): $\delta = 152.92$ (C_q), 150.90 (C_q), 131.63 (C_q), 131.11 (C_q), 129.58 (CH_{Ar}), 128.97 (CH_{Ar}), 128.57 (CH_{Ar}), 127.96 (CH_{Ar}), 126.83 (CH_{Ar}), 124.28 (CH_{Ar}), 123.47 (CH_{Ar}), 123.13 (C_q), 122.38 (CH_{Ar}), 117.82 (CH_{Ar}), 117.50 (C_q), 116.47 (CH_{Ar}), 62.93 (CH_2OH), 48.24 (CHCH_2OH), 36.50 (Ar_2CH), 31.53 (CH_2), 20.93 (CH_2), 14.61 (CH_3).

IR (neat): ν 3387, 3057, 2955, 2926, 2869, 1626, 1579, 1515, 1487, 1456, 1436, 1396, 1236, 1031, 958, 812 cm^{-1} .

HRMS (ESI+): m/z calcd. for $\text{C}_{22}\text{H}_{22}\text{NaO}_2$ $[\text{M}+\text{Ma}]^+$: 341.1512, found: 341.1509.

$[\alpha]_{\text{D}}^{25}$: +20.8 (c 1.24, CH_2Cl_2).

HPLC (Daicel Chiralpak AD-H column, *n*-hexane/*i*-PrOH (96:4), flow rate 0.8 mL/min, $\lambda = 254$ nm): $t_{\text{minor}} = 21.3$ min; $t_{\text{major}} = 23.1$ min.

**(*R*)-2-((*R*)-1-methoxy-9H-xanthen-9-yl)pentan-1-ol (6k):**

Prepared according to modified GP3 (with 20 mol% **cat.1**) from **4k** (42.4 mg, 1.0 equiv) and pentanal (63.8 μL , 3.0 equiv). According to ^1H NMR analysis, the crude mixture

contained **5k** and **6k** in ratio 1.25:1, which were then separated into individual diastereomers by column chromatography on silica gel using mixtures of *n*-pentane and EtOAc as eluent.

Elution with *n*-pentane:EtOAc (20:1) afforded the minor diastereomer **6k** (14.9 mg, 25%, 95.5:4.5 er) as a colorless oil.

R_f : 0.25 (*n*-pentane:EtOAc 15:1).

^1H NMR (400 MHz, CDCl_3): $\delta = 7.25 - 7.17$ (m, 3H), 7.12 - 7.05 (m, 2H), 6.78 (dd, $^3J_{\text{H-H}} = 8.2$ Hz, $^4J_{\text{H-H}} = 1.0$ Hz, 1H), 6.65 (dd, $^3J_{\text{H-H}} = 8.3$ Hz, $^4J_{\text{H-H}} = 1.0$ Hz, 1H), 4.49 (d, $^3J_{\text{H-H}} = 3.3$ Hz, 1H, Ar_2CH), 3.90 (s, 3H, CH_3O), 3.47 - 3.37 (m, 1H, CH_2OH), 3.38 - 3.28 (m, 1H, CH_2OH), 2.42 - 2.35 (m, 1H, OH),

1.97 - 1.88 (m, 1H, $CHCH_2OH$), 1.39 - 1.20 (m, 2H, CH_2), 1.24 - 1.11 (m, 1H, CH_2), 1.07 - 0.99 (m, 1H, CH_2), 0.78 (t, $^3J_{H-H} = 7.0$ Hz, 3H, CH_2CH_3).

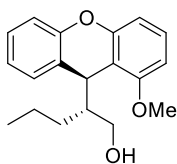
^{13}C NMR (100 MHz, $CDCl_3$): $\delta = 157.17$ (C_q), 154.77 (C_q), 153.35 (C_q), 129.06 (CH_{Ar}), 127.86 (CH_{Ar}), 127.65 (CH_{Ar}), 125.07 (C_q), 123.55 (CH_{Ar}), 116.25 (CH_{Ar}), 112.70 (C_q), 109.94 (CH_{Ar}), 105.09 (CH_{Ar}), 63.49 (CH_2OH), 56.06 (CH_3O), 49.88 ($CHCH_2OH$), 34.16 (Ar_2CH), 29.08 (CH_2), 20.64 (CH_2), 14.34 (CH_2CH_3).

IR (neat): ν 3444, 2956, 2930, 2871, 1601, 1577, 1456, 1272, 1243, 1080 cm^{-1} .

HRMS (ESI+): m/z calcd. for $C_{19}H_{22}NaO_3$ $[M+Na]^+$: 321.1461, found: 321.1457.

$[\alpha]_D^{25}$: +7.3 (c 0.62, CH_2Cl_2).

HPLC (Daicel Chiralpak AD-H column, *n*-hexane/*i*-PrOH (93:7), flow rate 1.0 mL/min, $\lambda = 254$ nm): $t_{minor} = 9.6$ min; $t_m = 10.4$ min.



(*R*)-2-((*S*)-1-methoxy-9H-xanthen-9-yl)pentan-1-ol (5k):

Further elution with *n*-pentane:EtOAc (15:1) gave the major diastereomer **5k** (21.5 mg, 36%, 96.5:3.5 er) as a colorless oil.

R_f: 0.20 (*n*-pentane:EtOAc 15:1).

1H NMR (400 MHz, $CDCl_3$): $\delta = 7.28 - 7.21$ (m, 2H), 7.21 - 7.16 (m, 1H), 7.12 - 7.03 (m, 2H), 6.79 (dd, $^3J_{H-H} = 8.1$ Hz, $^4J_{H-H} = 1.0$ Hz, 1H), 6.66 (dd, $^3J_{H-H} = 8.2$ Hz, $^4J_{H-H} = 1.0$ Hz, 1H), 4.42 (d, $^3J_{H-H} = 6.2$ Hz, 1H, Ar_2CH), 3.90 (s, 3H, OCH_3), 3.57 - 2.48 (m, 2H, CH_2OH), 2.03 (br s, 1H, OH), 1.77 - 1.64 (m, 1H, $CHCH_2OH$), 1.31 - 1.21 (m, 1H, CH_2), 1.23 - 1.11 (m, 1H, CH_2), 1.13 - 1.03 (m, 1H, CH_2), 1.07 - 0.94 (m, 1H, CH_2), 0.70 (t, $^3J_{H-H} = 7.1$ Hz, 3H, CH_3).

^{13}C NMR (100 MHz, $CDCl_3$): $\delta = 156.95$ (C_q), 154.60 (C_q), 153.62 (C_q), 129.87 (CH_{Ar}), 127.61 (CH_{Ar}), 127.54 (CH_{Ar}), 124.67 (C_q), 123.00 (CH_{Ar}), 116.45 (CH_{Ar}), 115.14 (C_q), 109.89 (CH_{Ar}), 105.18 (CH_{Ar}), 62.56 (CH_2OH),

Asymmetric cross-dehydrogenative coupling of aldehydes with xanthenes

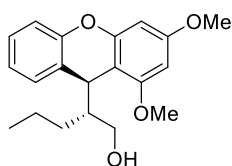
56.09 (CH₃O), 47.11 (CHCH₂OH), 34.60 (Ar₂CH), 29.41 (CH₂), 20.76 (CH₂), 14.34 (CH₂CH₃).

IR (neat): ν 3420, 2956, 2930, 2871, 1601, 1577, 1456, 1272, 1243, 1081 cm⁻¹.

HRMS (ESI+): m/z calcd. for C₁₉H₂₂NaO₃ [M+Ma]⁺: 321.1461, found: 321.1458.

[α]_D²⁵: +22.8 (*c* 0.85, CH₂Cl₂).

HPLC (Daicel Chiralpak AD-H column, *n*-hexane/*i*-PrOH (95:5), flow rate 1.0 mL/min, λ = 254 nm): t_{major} = 15.2 min; t_{minor} = 21.1 min.



(R)-2-((S)-1,3-dimethoxy-9H-xanthen-9-yl)pentan-1-ol

(5I): Prepared according to modified GP3 (with 20 mol% cat.1) from 4I (48.5 mg, 1.0 equiv) and pentanal (63.8 μ L, 3.0 equiv). Purification by column chromatography

on silica gel using *n*-pentane:EtOAc (10:1) as eluent afforded the analytically pure product (38.2 mg, 58%, 94:6 er) as a colorless oil.

R_f: 0.25 (*n*-pentane:EtOAc 5:1).

¹H NMR (400 MHz, CDCl₃): δ = 7.29 - 7.20 (m, 2H), 7.15 - 7.05 (m, 2H), 6.37 (d, ⁴J_{H-H} = 2.4, 1H), 6.29 (d, ⁴J_{H-H} = 2.4 Hz, 1H), 4.37 (d, ³J_{H-H} = 5.9 Hz, 1H, Ar₂CH), 3.88 (s, 3H, OCH₃), 3.84 (s, 3H, OCH₃), 3.58 (dd, ²J_{H-H} = 11.4 Hz, ³J_{H-H} = 4.1 Hz, 1H, CH₂OH), 3.51 (dd, ²J_{H-H} = 11.5 Hz, ³J_{H-H} = 6.7 Hz, 1H, CH₂OH), 2.00 (br s, 1H, OH), 1.75 - 1.67 (m, 1H, CHCH₂OH), 1.33 - 1.14 (m, 2H, CH₂), 1.12 - 0.98 (m, 2H, CH₂), 0.73 (t, ³J_{H-H} = 6.9 Hz, 3H, CH₂CH₃).

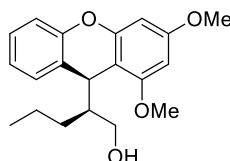
¹³C NMR (100 MHz, CDCl₃): δ = 159.55 (CH₃OC_q), 157.40 (CH₃OC_q), 154.88 (C_q), 153.49 (C_q), 129.74 (CH_{Ar}), 127.30 (CH_{Ar}), 124.65 (C_q), 122.86 (CH_{Ar}), 116.18 (CH_{Ar}), 107.14 (C_q), 93.99 (CH_{Ar}), 93.79 (CH_{Ar}), 62.53 (CH₂OH), 55.87 (CH₃O), 55.46 (CH₃O), 47.22 (CHCH₂OH), 34.02 (Ar₂CH), 29.25 (CH₂), 20.67 (CH₂), 14.26 (CH₂CH₃).

IR (neat): ν 3422, 2956, 2931, 2871, 2840, 1627, 1603, 1576, 1485, 1456, 1438, 1425, 1230, 1202, 1143, 1091, 1051 cm⁻¹.

HRMS (ESI+): m/z calcd. for $C_{20}H_{24}NaO_4$ $[M+Na]^+$: 351.1567, found: 351.1563.

$[\alpha]_D^{25}$: +55.8 (c 1.97, CH_2Cl_2).

HPLC (Daicel Chiralpak IB column, n -hexane/ i -PrOH (98:2), flow rate 1.0 mL/min, λ = 240 nm): t_{minor} = 16.0 min; t_{major} = 24.4 min.



(S)-2-((S)-1,3-dimethoxy-9H-xanthen-9-yl)pentan-1-ol

(6I): Prepared according to modified **GP3** (with 20 mol% **cat.2**) from **4I** (48.5 mg, 1.0 equiv) and pentanal (63.8 μ L, 3.0 equiv). Purification by column chromatography

on silica gel using n -pentane:EtOAc (10:1) as eluent afforded the analytically pure product (22.2 mg, 34%, 66.5:33.5 er) as a colorless oil.

R_f: 0.30 (n -pentane:EtOAc 5:1).

¹H NMR (400 MHz, $CDCl_3$): δ = 7.25 - 7.18 (m, 2H), 7.10 - 7.04 (m, 2H), 6.33 (d, $^4J_{H-H}$ = 2.3 Hz, 1H), 6.26 (d, $^4J_{H-H}$ = 2.4 Hz, 1H), 4.40 (d, $^3J_{H-H}$ = 3.2 Hz, 1H, Ar_2CH), 3.86 (s, 3H, OCH_3), 3.81 (s, 3H, OCH_3), 3.47 - 3.40 (m, 1H, CH_2OH), 3.31 (dd, $^2J_{H-H}$ = 10.0 Hz, $^3J_{H-H}$ = 10.0 Hz, 1H, CH_2OH), 2.44 - 2.35 (m, 1H, OH), 1.95 - 1.83 (m, 1H, $CHCH_2OH$), 1.31 - 1.10 (m, 3H, CH_2), 1.06 - 0.93 (m, 1H, CH_2), 0.76 (t, $^3J_{H-H}$ = 7.0 Hz, 3H, CH_2CH_3).

¹³C NMR (100 MHz, $CDCl_3$): δ = 159.66 (C_q), 157.60 (C_q), 155.07 (C_q), 153.23 (C_q), 128.89 (CH_{Ar}), 127.37 (CH_{Ar}), 125.18 (C_q), 123.39 (CH_{Ar}), 115.95 (CH_{Ar}), 104.64 (C_q), 93.94 (CH_{Ar}), 93.82 (CH_{Ar}), 63.40 (CH_2OH), 55.84 (CH_3O), 55.46 (CH_3O), 49.84 ($CHCH_2OH$), 33.62 (Ar_2CH), 28.82 (CH_2), 20.48 (CH_2), 14.18 (CH_2CH_3).

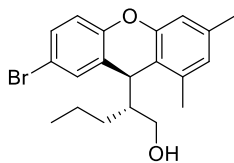
IR (*neat*): ν 3372, 2959, 2930, 1627, 1602, 1576, 1484, 1455, 1438, 1228, 1202, 1142, 1113, 1088, 1049, 950 cm^{-1} .

HRMS (ESI+): m/z calcd. for $C_{20}H_{24}NaO_4$ $[M+Na]^+$: 351.1567, found: 351.1578.

$[\alpha]_D^{25}$: -47.6 (c 1.11, CH_2Cl_2).

Asymmetric cross-dehydrogenative coupling of aldehydes with xanthenes

HPLC (Daicel Chiralpak AD-H column, *n*-hexane/*i*-PrOH (95:5), flow rate 1.0 mL/min, $\lambda = 254$ nm): $t_{\text{minor}} = 17.7$ min; $t_{\text{m}} = 45.5$ min.



(R)-2-((S)-7-bromo-1,3-dimethyl-9H-xanthen-9-

yl)pentan-1-ol (5m): Prepared according to modified **GP3** (with 20 mol% **cat.1**) from **4m** (57.8 mg, 1.0 equiv) and pentanal (63.8 μ L, 3.0 equiv). Purification by

column chromatography on silica gel using *n*-pentane:EtOAc (15:1) as eluent afforded the product (66.8 mg, 89%, 5:1 dr) as a colorless oil. According to ^1H NMR analysis, the product contains 10% of inseparable impurity (presumably **cat.1** decomposition product).

^1H NMR (400 MHz, CDCl_3): $\delta = 7.40$ (d, $^4J_{\text{H-H}} = 2.4$ Hz, 1H-major), 7.34 - 7.29 (m, 1H-major + 2H-minor), 6.99 - 6.93 (m, 1H-major + 1H-minor), 6.82 - 6.75 (m, 2H-major + 2H-minor), 4.51 (d, $^3J_{\text{H-H}} = 3.2$ Hz, 1H-major, Ar_2CH), 4.15 (d, $^3J_{\text{H-H}} = 4.0$ Hz, 1H-minor, Ar_2CH), 3.75 (dd, $^2J_{\text{H-H}} = 10.8$ Hz, $^3J_{\text{H-H}} = 4.6$ Hz, 1H-major, CH_2OH), 3.56 - 3.42 (m, 1H-major + 1H-minor, CH_2OH), 3.18 (dd, $^2J_{\text{H-H}} = 11.1$ Hz, $^3J_{\text{H-H}} = 6.1$ Hz, 1H-minor, CH_2OH), 2.41 - 2.33 (m, 3H-major + 3H-minor, ArCH_3), 2.34 - 2.27 (m, 3H-major + 3H-minor, ArCH_3), 1.92 - 1.81 (m, 1H-major, CHCH_2OH), 1.67 - 1.61 (m, 1H-minor, CHCH_2OH), 1.61 - 1.46 (m, 1H-major + 1H-minor, OH), 1.18 - 1.06 (m, 2H-major + 2H-minor, CH_2), 1.05 - 0.87 (m, 2H-major + 2H-minor, CH_2), 0.85 (t, $^3J_{\text{H-H}} = 7.3$ Hz, 3H-minor, CH_2CH_3), 0.66 (t, $^3J_{\text{H-H}} = 7.1$ Hz, 3H-major, CH_2CH_3).

^{13}C NMR (100 MHz, CDCl_3): $\delta = 153.31$ (C_q -major), 153.06 (C_q -minor), 152.90 (C_q -major), 152.60 (C_q -minor), 137.32 (C_q -minor), 137.06 (C_q -major), 135.97 (C_q -major+minor), 132.19 (CH_{Ar} -major), 131.82 (CH_{Ar} -minor), 130.53 (CH_{Ar} -minor), 130.33 (CH_{Ar} -major), 126.75 (CH_{Ar} -minor), 126.58 (CH_{Ar} -major), 126.37 (C_q -minor), 125.38 (C_q -major), 120.84 (C_q -minor), 120.43 (C_q -major), 118.02 (CH_{Ar} -minor), 117.83 (CH_{Ar} -major), 114.95 (C_q -minor), 114.76 (CH_{Ar} -minor), 114.73 (C_q -major), 114.56 (CH_{Ar} -

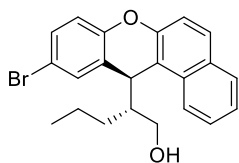
major), 62.39 (CH_2OH -major), 62.28 (CH_2OH -minor), 47.87 (CHCH_2OH -minor), 46.99 (CHCH_2OH -major), 37.41 (Ar_2CH), 35.57 (Ar_2CH -major), 31.04 (CH_2 -minor), 27.75 (CH_2 -major), 21.01 (ArCH_3 -major), 20.98 (ArCH_3 -minor), 20.65 (CH_2 -major), 20.61 (CH_2 -minor), 18.61 (ArCH_3 -minor), 18.35 (ArCH_3 -major), 14.41 (CH_2CH_3 -minor), 14.21 (CH_2CH_3 -major).

IR (neat): ν 3395, 2957, 2927, 2872, 1627, 1592, 1568, 1477, 1416, 1296, 1278, 1241, 1180, 1136, 1038, 845, 815 cm^{-1} .

HRMS (ESI+): m/z calcd. for $\text{C}_{20}\text{H}_{23}\text{BrNaO}_2$ $[\text{M}+\text{Na}]^+$: 397.0774, found: 397.0766.

$[\alpha]_{\text{D}}^{25}$: +4.6 (c 1.51, CH_2Cl_2).

HPLC (Daicel Chiralpak AD-H column, *n*-hexane/*i*-PrOH (97:3), flow rate 1.0 mL/min, λ = 254 nm): **5m**: t_{major} = 9.9 min; t_{minor} = 26.6 min; **6m**: t_{minor} = 11.9 min; t_{major} = 13.2 min.



(*R*)-2-((*S*)-10-bromo-12*H*-benzo[*a*]xantho-12-yl)pentan-1-ol (5n): Prepared according to modified **GP3** (with 20 mol% **cat.1**) from **4n** (62.2 mg, 1.0 equiv) and pentanal (63.8 μL , 3.0 equiv). According to ^1H

NMR analysis, the crude mixture contained **5n** and **6n** in ratio 1.9:1, which were then separated into individual diastereomers by column chromatography on silica gel using mixtures of *n*-pentane and EtOAc as eluent.

Elution with *n*-pentane:EtOAc (20:1) afforded the major diastereomer **5n** (39 mg, 49%, 98.5:1.5 er) as a colorless oil. According to ^1H NMR analysis, the product contains 20% of inseparable impurity (presumably **cat.1** decomposition product).

R_f: 0.30 (*n*-pentane:EtOAc 15:1).

^1H NMR (400 MHz, CDCl_3): δ = 8.17 (d, $^3J_{\text{H-H}}$ = 8.5 Hz, 1H), 7.85 (d, $^3J_{\text{H-H}}$ = 8.1 Hz, 1H), 7.75 (d, $^3J_{\text{H-H}}$ = 8.8 Hz, 1H), 7.58 (ddd, $^3J_{\text{H-H}}$ = 8.4 Hz, $^3J_{\text{H-H}}$ = 6.8 Hz, $^4J_{\text{H-H}}$ = 1.4 Hz, 1H), 7.53 (d, $^4J_{\text{H-H}}$ = 2.4 Hz, 1H), 7.44 (ddd, $^3J_{\text{H-H}}$ = 7.9 Hz, $^3J_{\text{H-H}}$ = 6.8 Hz, $^4J_{\text{H-H}}$ = 1.1 Hz, 1H), 7.37 (dd, $^3J_{\text{H-H}}$ = 8.6 Hz, $^4J_{\text{H-H}}$ = 2.4 Hz,

Asymmetric cross-dehydrogenative coupling of aldehydes with xanthenes

1H), 7.30 (d, $^3J_{\text{H-H}} = 8.9$ Hz, 1H), 7.04 (d, $^3J_{\text{H-H}} = 8.6$ Hz, 1H), 5.20 (d, $^3J_{\text{H-H}} = 2.9$ Hz, 1H, Ar_2CH), 3.82 (dd, $^2J_{\text{H-H}} = 10.7$ Hz, $^3J_{\text{H-H}} = 4.6$ Hz, 1H, CH_2OH), 3.59 (t, $^2J_{\text{H-H}} = 10.7$ Hz, $^3J_{\text{H-H}} = 10.7$ Hz, 1H, CH_2OH), 2.21 - 2.11 (m, 1H, CHCH_2OH), 1.16 - 1.01 (m, 2H, CH_2), 0.91 - 0.76 (m, 2H, CH_2+OH), 0.74 - 0.61 (m, 1H, CH_2), 0.55 (t, $^3J_{\text{H-H}} = 7.0$ Hz, 3H, CH_3).

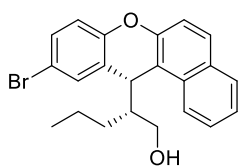
^{13}C NMR (100 MHz, CDCl_3): $\delta = 152.32$ (C_q), 150.60 (C_q), 132.34 (CH_Ar), 131.18 (C_q), 131.04 (C_q), 130.48 (CH_Ar), 128.74 (CH_Ar), 128.43 (CH_Ar), 126.85 (CH_Ar), 124.29 (C_q), 124.26 (CH_Ar), 122.56 (CH_Ar), 117.87 (CH_Ar), 117.45 (CH_Ar), 116.65 (C_q), 115.32 (C_q), 62.47 (CH_2OH), 46.67 (CHCH_2OH), 34.35 (Ar_2CH), 28.05 (CH_2), 20.58 (CH_2), 14.19 (CH_3).

IR (neat): ν 3392, 2958, 2929, 2872, 1627, 1574, 1482, 1461, 1437, 1373, 1278, 1252, 1177, 1139, 1074, 961 cm^{-1} .

HRMS (ESI+): m/z calcd. for $\text{C}_{22}\text{H}_{22}\text{BrO}_2$ $[\text{M}+\text{H}]^+$: 397.0798, found: 397.0799.

$[\alpha]_D^{25}$: -40.8 (c 1.18, CH_2Cl_2).

HPLC (Daicel Chiralpak AD-H column, n -hexane/ i -PrOH (95:5), flow rate 1.0 mL/min, $\lambda = 254$ nm): $t_{\text{minor}} = 10.5$ min; $t_{\text{major}} = 13.4$ min.



(*R*)-2-((*R*)-10-bromo-12*H*-benzo[*a*]xanthen-12-yl)pentan-1-ol (6n): Further elution with n -pentane:EtOAc (15:1) gave the minor diastereomer **6n** (11.5 mg, 15%, 98:2 er) as a colorless oil.

R_f : 0.25 (n -pentane:EtOAc 15:1).

^1H NMR (400 MHz, CDCl_3): $\delta = 8.05$ (d, $^3J_{\text{H-H}} = 8.5$ Hz, 1H), 7.85 (dd, $^3J_{\text{H-H}} = 8.1$ Hz, $^4J_{\text{H-H}} = 1.3$ Hz, 1H), 7.76 (d, $^3J_{\text{H-H}} = 8.9$ Hz, 1H), 7.58 (ddd, $^3J_{\text{H-H}} = 8.4$ Hz, $^3J_{\text{H-H}} = 6.8$ Hz, $^4J_{\text{H-H}} = 1.4$ Hz, 1H), 7.49 - 7.40 (m, 2H), 7.37 (dd, $^3J_{\text{H-H}} = 8.6$, $^4J_{\text{H-H}} = 2.4$ Hz, 1H), 7.30 (d, $^3J_{\text{H-H}} = 8.9$ Hz, 1H), 7.05 (d, $^3J_{\text{H-H}} = 8.6$ Hz, 1H), 4.83 (d, $^3J_{\text{H-H}} = 3.4$ Hz, 1H, Ar_2CH), 3.45 (dd, $^2J_{\text{H-H}} = 11.1$ Hz, $^3J_{\text{H-H}} = 5.2$ Hz, 1H, CH_2OH), 3.26 (dd, $^2J_{\text{H-H}} = 11.1$ Hz, $^3J_{\text{H-H}} = 5.9$ Hz, 1H, CH_2OH), 2.05

- 1.93 (m, 1H, $CHCH_2OH$), 1.68 - 1.41 (m, 5H, $2CH_2 + OH$), 0.97 (t, $^3J_{H-H} = 6.9$ Hz, 3H, CH_3).

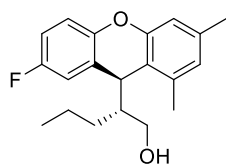
^{13}C NMR (100 MHz, $CDCl_3$): $\delta = 152.00$ (C_q), 150.58 (C_q), 131.91 (CH_{Ar}), 131.44 (C_q), 131.03 (C_q), 130.65 (CH_{Ar}), 128.85 (CH_{Ar}), 128.67 (CH_{Ar}), 126.85 (CH_{Ar}), 125.65 (C_q), 124.36 (CH_{Ar}), 122.23 (CH_{Ar}), 118.01 (CH_{Ar}), 117.52 (CH_{Ar}), 116.69 (C_q), 115.52 (C_q), 62.59 (CH_2OH), 48.22 ($CHCH_2OH$), 36.21 (Ar_2CH), 31.00 (CH_2), 20.74 (CH_2), 14.40 (CH_3).

IR (neat): ν 3396, 3059, 2956, 2925, 2870, 1626, 1573, 1516, 1480, 1459, 1396, 1250, 1181, 1072, 1026, 813 cm^{-1} .

HRMS (ESI+): m/z calcd. for $C_{22}H_{21}BrNaO_2$ $[M+Na]^+$: 419.0617, found: 419.0627.

$[\alpha]_D^{25}$: +83.8 (c 0.49, CH_2Cl_2).

HPLC (Daicel Chiralpak AD-H column, *n*-hexane/*i*-PrOH (98:2), flow rate 0.8 mL/min, $\lambda = 254$ nm): $t_{major} = 46.0$ min; $t_{minor} = 48.4$ min.



(*R*)-2-((*S*)-7-fluoro-1,3-dimethyl-9H-xanthen-9-yl)pentan-1-ol (5o): Prepared according to modified GP3 (with 20 mol% **cat.1**) from **4o** (45.6 mg, 1.0 equiv) and pentanal (63.8 μ L, 3.0 equiv). Purification by column

chromatography on silica gel using *n*-pentane:EtOAc (15:1) as eluent afforded the analytically pure product (26.6 mg, 42%, 4.7:1 dr) as a colorless oil.

R_f : 0.20 (*n*-pentane:EtOAc 15:1).

1H NMR (400 MHz, $CDCl_3$): $\delta = 7.06 - 6.98$ (m, 2H-major + 1H-minor), 6.95 - 6.88 (m, 1H-major + 2H-minor), 6.81 - 6.76 (m, 2H-major + 2H-minor), 4.52 (d, $^3J_{H-H} = 3.4$ Hz, 1H-major, Ar_2CH), 4.15 (d, $^3J_{H-H} = 3.7$ Hz, 1H-minor, Ar_2CH), 3.76 (dd, $^2J_{H-H} = 10.7$ Hz, $^3J_{H-H} = 4.6$ Hz, 1H-major, CH_2OH), 3.54 - 3.43 (m, 1H-minor + 1H-major, CH_2OH), 3.19 (dd, $^2J_{H-H} = 11.1$ Hz, $^3J_{H-H} = 6.0$ Hz, 1H-minor, CH_2OH), 2.39 (s, 3H-major, $ArCH_3$), 2.36 (s, 3H-minor, $ArCH_3$), 2.31 (s, 3H-major, $ArCH_3$), 2.30 (s, 3H-minor, $ArCH_3$), 1.94 - 1.81 (m, 1H-major, $CHCH_2OH$), 1.82 - 1.72 (m, 1H-minor, $CHCH_2OH$), 1.59 -

Asymmetric cross-dehydrogenative coupling of aldehydes with xanthenes

1.49 (m, 3H-minor, CH_2), 1.45 - 1.35 (m, 1H-minor, CH_2), 1.20 - 1.06 (m, 2H-major, CH_2), 1.03 - 0.95 (m, 3H-minor, CH_3), 0.97 - 0.86 (m, 1H-major, CH_2), 0.70 - 0.62 (m, 4H-major, $CH_2 + CH_2CH_3$).

^{13}C NMR (100 MHz, $CDCl_3$): δ = 158.23 (d, $^1J_{C-F}$ = 239.8 Hz, C_q -major+minor), 153.64 (C_q -major), 153.34 (C_q -minor), 149.88 (d, $^4J_{C-F}$ = 2.2 Hz, C_q -major), 149.57 (d, $^4J_{C-F}$ = 2.3 Hz, C_q -minor), 137.29 (C_q -minor), 137.02 (C_q -major), 135.90 (C_q -major), 135.88 (C_q -minor), 126.61 (CH_{Ar} -minor), 126.40 (CH_{Ar} -major), 125.56 (d, $^3J_{C-F}$ = 7.5 Hz, C_q -minor), 124.66 (d, $^3J_{C-F}$ = 7.6 Hz, C_q -major), 120.76 (C_q -minor), 120.32 (C_q -major), 117.24 (d, $^3J_{C-F}$ = 8.5 Hz, CH -minor), 116.95 (d, $^3J_{C-F}$ = 8.4 Hz, CH -major), 115.75 (d, $^2J_{C-F}$ = 23.0 Hz, CH -major), 115.40 (d, $^2J_{C-F}$ = 23.1 Hz, CH -minor), 114.73 (CH_{Ar} -minor), 114.55 (CH_{Ar} -major), 114.30 (d, $^2J_{C-F}$ = 23.5 Hz, CH -minor), 114.05 (d, $^2J_{C-F}$ = 23.4 Hz, CH -major), 62.56 (CH_2OH -major), 62.37 (CH_2OH -minor), 47.85 ($CHCH_2OH$ -minor), 46.92 ($CHCH_2OH$ -major), 37.76 (Ar_2CH -minor), 35.95 (Ar_2CH -major), 31.26 (CH_2 -minor), 27.85 (CH_2 -major), 21.01 ($ArCH_3$ -major), 20.98 ($ArCH_3$ -minor), 20.68 (CH_2 -minor), 20.66 (CH_2 -major), 18.61 ($ArCH_3$ -minor), 18.37 ($ArCH_3$ -major), 14.42 (CH_2CH_3 -minor), 14.22 (CH_2CH_3 -major).

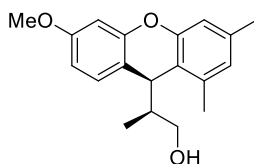
^{19}F NMR (376 MHz, $CDCl_3$) δ = -121.63 (major), -121.04 (minor).

IR (neat): ν 3391, 2957, 2928, 2872, 1633, 1577, 1486, 1458, 1435, 1297, 1228, 1193, 1132, 1039 cm^{-1} .

HRMS (ESI+): m/z calcd. for $C_{20}H_{23}FNaO_2$ $[M+Na]^+$: 337.1574, found: 337.1581.

$[\alpha]_D^{25}$: +44.7 (c 1.31, CH_2Cl_2).

SFC-UPC2 (Chiralpak ID column, $CO_2/EtOH$ 97:3, 3 ml/min, 1500 psi): major diastereomer: t_{major} = 2.19 min; t_{minor} = 2.45 min; minor diastereomer: t_{minor} = 2.77 min; t_{major} = 3.71 min.



(*S*)-2-((*S*)-6-methoxy-1,3-dimethyl-9*H*-xanthen-9-yl)propan-1-ol (**6p**): Prepared according to modified

GP3 (with 20 mol% **cat.2**) from **4f** (48.0 mg, 1.0 equiv) and propanal (43.3 μL , 3.0 equiv). Purification by column chromatography on silica gel using *n*-pentane:EtOAc (10:1) as eluent afforded the analytically pure product (15.6 mg, 26%, 74.5:25.5 er) as a colorless oil.

R_f: 0.20 (*n*-pentane:EtOAc 10:1).

¹H NMR (500 MHz, CDCl₃): δ = 7.10 (d, ³*J*_{H-H} = 8.2 Hz, 1H), 6.79 (s, 1H), 6.78 (s, 1H), 6.68 - 6.61 (m, 2H), 3.98 (d, ³*J*_{H-H} = 4.3 Hz, 1H, Ar₂CH), 3.81 (s, 3H, OCH₃), 3.45 (dd, ²*J*_{H-H} = 10.8 Hz, ³*J*_{H-H} = 4.8 Hz, 1H, CH₂OH), 3.12 (dd, ²*J*_{H-H} = 10.8 Hz, ³*J*_{H-H} = 7.1 Hz, 1H, CH₂OH), 2.36 (s, 3H, ArCH₃), 2.30 (s, 3H, ArCH₃), 1.96 - 1.86 (m, 1H, CHCH₂OH), 1.05 (d, ³*J*_{H-H} = 7.0 Hz, 3H, CHCH₃).

¹³C NMR (126 MHz, CDCl₃): δ = 159.50 (C_q), 154.21 (C_q), 153.30 (C_q), 137.07 (C_q), 136.16 (C_q), 129.91 (CH_{Ar}), 126.52 (CH_{Ar}), 121.77 (C_q), 116.20 (C_q), 114.78 (CH_{Ar}), 109.41 (CH_{Ar}), 101.59 (CH_{Ar}), 64.75 (CH₂OH), 55.56 (OCH₃), 43.32 (CHCH₂OH), 39.31 (Ar₂CH), 21.12 (ArCH₃), 18.81 (ArCH₃), 15.73 (CHCH₃).

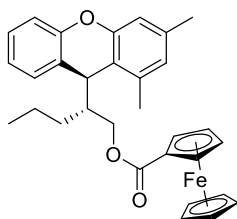
IR (neat): ν 3411, 2958, 2933, 2877, 1631, 1613, 1572, 1504, 1442, 1295, 1282, 1273, 1196, 1160, 1122, 1033, 845 cm⁻¹.

HRMS (ESI+): *m/z* calcd. for C₁₉H₂₂NaO₃ [M+Na]⁺: 321.1461, found: 321.1467.

[α]_D²⁰: +17.5 (*c* 0.59, CH₂Cl₂).

HPLC (Daicel Chiralpak IC column, *n*-hexane/*i*-PrOH (95:5), flow rate 1.0 mL/min, λ = 254 nm): *t*_{minor} = 12.1 min; *t*_{major} = 14.7 min.

Characterization Data of Ferrocenyl Derivative 5e-Fe



(*R*)-2-((*S*)-1,3-dimethyl-9*H*-xanthen-9-yl)pentyl ferrocenylcarboxylate (5e-Fe): **5e** (9.1 mg, 0.031 mmol, 1.0 equiv), 4-dimethylaminopyridine (4.1 mg, 0.034

Asymmetric cross-dehydrogenative coupling of aldehydes with xanthenes

mmol, 1.1 equiv) and ferrocenecarboxylic acid (7.8 mg, 0.034 mmol, 1.1 equiv) were dissolved in dry DCM (600 μ l). EDC (6.9 mg, 0.034 mmol, 1.1 equiv) was added and the mixture was stirred for 40 h at room temperature. After completion of the reaction as indicated by TLC, the reaction mixture was quenched with water, extracted with DCM, washed with brine and concentrated. Purification by column chromatography on silica gel using *n*-pentane:EtOAc (20:1) as eluent afforded the analytically pure product (14.3 mg, 92%) as a yellow solid.

mp: 70-72°C.

R_f: 0.50 (*n*-pentane:EtOAc 20:1).

¹H NMR (500 MHz, CDCl₃): δ = 7.25 - 7.22 (m, 1H), 7.21 - 7.15 (m, 1H), 7.11 - 7.04 (m, 2H), 6.81 (s, 2H), 4.93 - 4.87 (m, 2H, C₅H₄COO), 4.49 - 4.43 (m, 3H, Ar₂CH + C₅H₄COO), 4.31 - 4.25 (m, 6H, CH₂OH + C₅H₅), 4.12 (dd, ²J_{H-H} = 11.3 Hz, ³J_{H-H} = 10.4 Hz, 1H, CH₂OH), 2.45 (s, 3H, ArCH₃), 2.32 (s, 3H, ArCH₃), 2.14 - 2.05 (m, 1H, CHCH₂OH), 1.27 - 1.19 (m, 3H, CH₂), 1.07 - 0.96 (m, 1H, CH₂), 0.69 (t, ³J_{H-H} = 7.1 Hz, 3H, CH₃).

¹³C NMR (126 MHz, CDCl₃): δ = 171.95 (C=O), 153.85 (C_q), 153.61 (C_q), 137.26 (C_q), 135.85 (C_q), 129.54 (CH_{Ar}), 127.92 (CH_{Ar}), 126.51 (CH_{Ar}), 122.85 (CH_{Ar}), 122.46 (C_q), 120.73 (C_q), 116.48 (CH_{Ar}), 114.89 (CH_{Ar}), 71.56 (C₅H₄COO), 71.53 (C₅H₄COO), 71.50 (C_q^{Cp}), 70.33 (C₅H₄COO), 70.20 (C₅H₄COO), 69.89 (C₅H₅), 64.78 (CH₂OH), 44.33 (CHCH₂OH), 36.83 (Ar₂CH), 27.95 (CH₂), 21.19 (ArCH₃), 20.71 (CH₂), 18.60 (ArCH₃), 14.32 (CH₃).

IR (neat): ν 3100, 2957, 2869, 1712, 1572, 1483, 1458, 1298, 1271, 1238, 1135, 965, 844 cm⁻¹.

HRMS (ESI+): *m/z* calcd. for C₃₁H₃₂FeNaO₃ [M+Na]⁺: 531.1593, found: 531.1595.

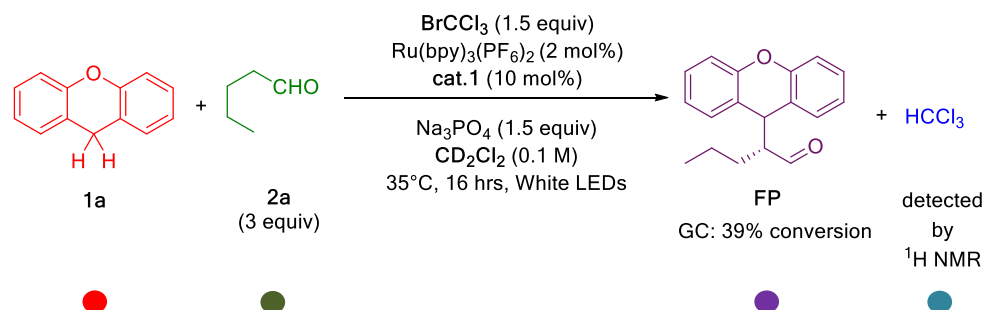
[α]_D²⁵: +75.8 (*c* 0.53, CH₂Cl₂).

Single crystals suitable for X-ray analysis were grown by slow diffusion of *n*-hexane into the diethyl ether solution of **5e-Fe**.

II.4.5. Detection of CHCl_3 in the reaction mixture

Reaction in CD_2Cl_2

Catalytic reaction was carried out with xanthene (**1a**) according to **GP3** in CD_2Cl_2 as solvent. Conversion to FP determined by GC analysis was 39%. Direct analysis of the crude reaction mixture by ^1H NMR showed presence of CHCl_3 (chemical shift 7.37 ppm).



Asymmetric cross-dehydrogenative coupling of aldehydes with xanthenes

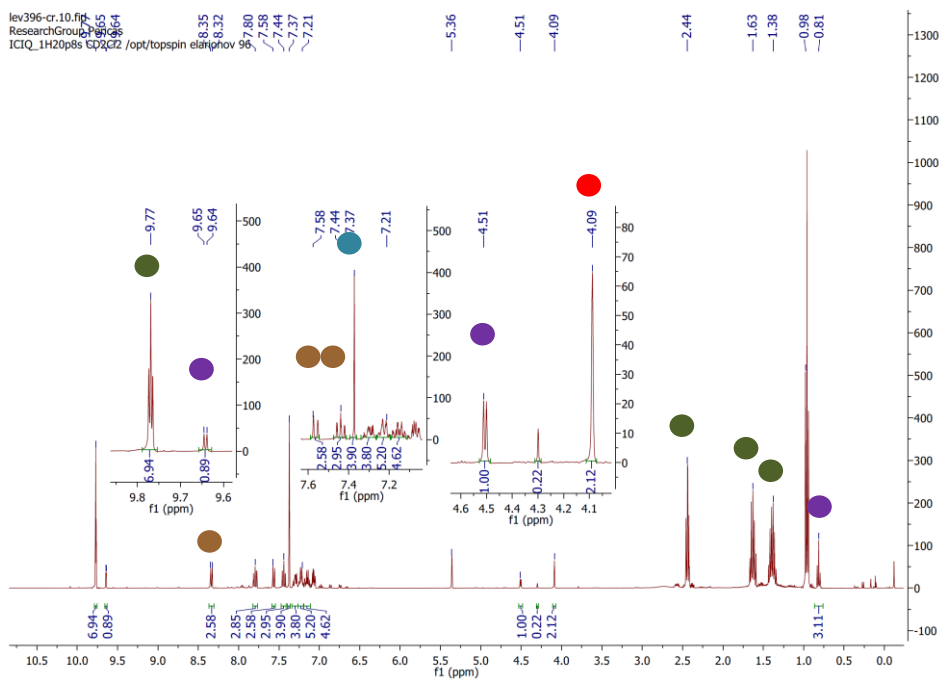
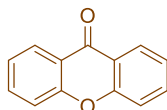


Figure II-19. ^1H NMR spectrum of the reaction mixture.

Impurity formed during the reaction:



Reaction with $1a-d_2$

Catalytic reaction was carried out with deuterated xanthene $1a-d_2$ according to **GP3**. Conversion to FP determined by GC analysis was 28%. Direct analysis of the crude reaction mixture by ^2H NMR showed presence of CDCl_3 (chemical shift 7.38 ppm).

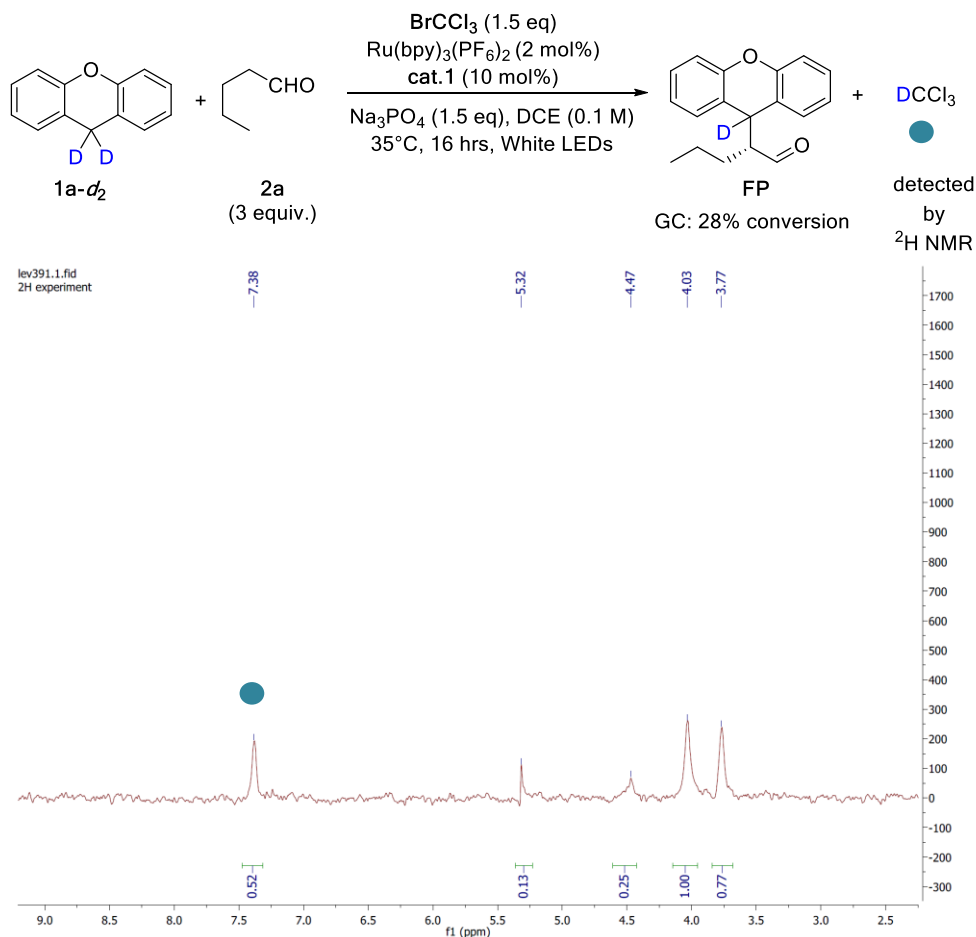
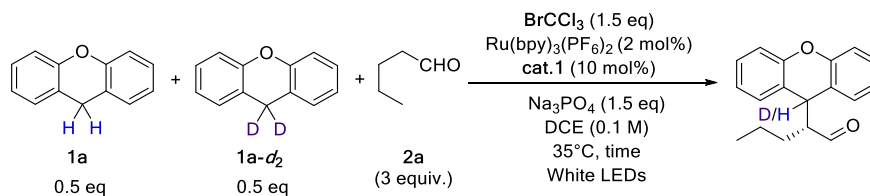


Figure II-20. ^2H NMR spectrum of the reaction mixture.

II.4.6. KIE measurement



After 4 hrs: 40.5% conversion, 60.0% SM recovered - 69.4% D \Rightarrow KIE = 3.8
 After 2 hrs: 31.5% conversion, 68.5% SM recovered - 64.1% D \Rightarrow KIE = 4.2
 After 2 hrs: 31.5% conversion, 68.5% SM recovered - 64.1% D \Rightarrow KIE = 4.2

Scheme II-16. Competitive KIE measurements.

Asymmetric cross-dehydrogenative coupling of aldehydes with xanthenes

Catalytic reaction was carried out with **1a-d₂** (18.4 mg, 0.1 mmol) and **1a** (18.2 mg, 0.1 mmol) according to **GP3**. After a given time, conversion of SM was determined by GC analysis. After quenching, the crude reaction mixture was subjected to column chromatography to separate any unreacted xanthene. The deuterium content at the C9 position of the unreacted xanthene was determined by ¹H NMR analysis.

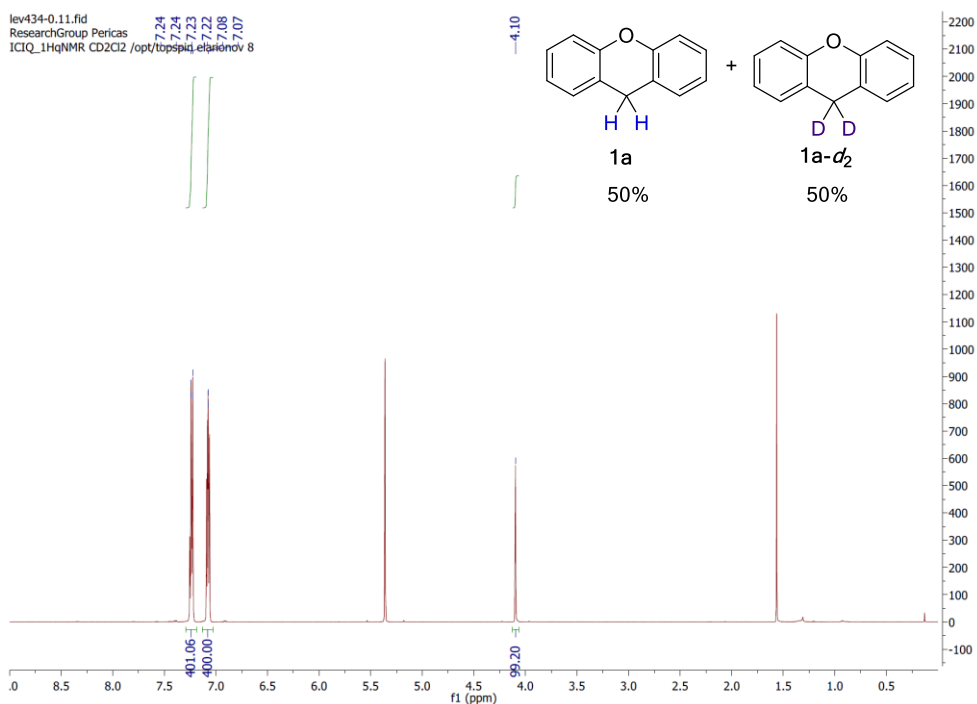
For the calculation of the KIE it was assumed that the reaction is first order in substrate **1a**.

If *x* - overall conversion of SM and *y* - deuterium content in recovered SM, then (1-*x*)(1-*y*) is amount of **1a** and (1-*x*)*y* is the amount of **1a-d₂** in the recovered mixture.

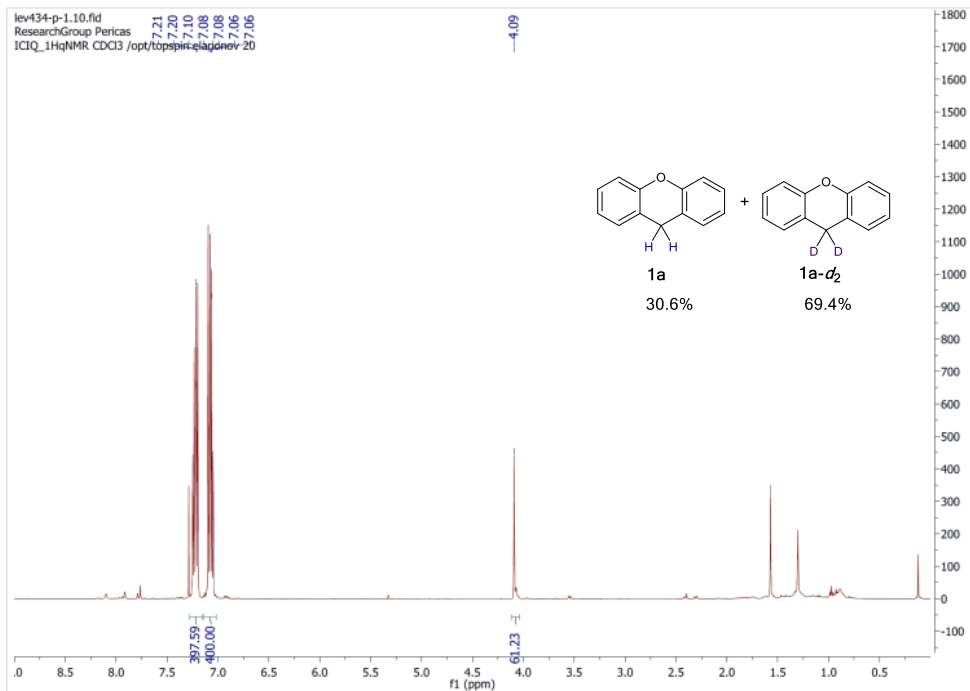
$$KIE = \frac{0.5 - (1 - x)(1 - y)}{0.5 - (1 - x)y}$$

Application of this formula gives: **KIE = 4.0 ± 0.2**.

Before the reaction:



Recovered xanthene after the reaction:



Asymmetric cross-dehydrogenative coupling of aldehydes with xanthenes

Compound	G ₂₉₈ (H)	G ₂₉₈ (D)
CCl ₃ [•]	-1418.648243	-1418.648243
1a	-576.476516	-576.479917
TS1	-1995.101817	-1995.103848
ΔG [‡] , kcal/mol	14.4	15.3
ΔΔG [‡] = 0.9 kcal/mol		
KIE = 4.3		

Table II-6. Kinetic isotope effect calculations: $KIE = \exp(\Delta\Delta G^\ddagger/RT)$, where $\Delta\Delta G^\ddagger = \Delta G^\ddagger(D) - \Delta G^\ddagger(H)$

II.4.7. Quenching studies

General procedure: 130 mL of DCE was degassed through 3 freeze-pump-thaw cycles and used to prepare a 2.01×10^{-5} M solution of [Ru(bpy)₃](PF₆)₂ (100 mL), a 5.03×10^{-3} M solution of Xanthene (10 mL) and a 5.03×10^{-3} M solution of CBrCl₃ (10 mL). In order to prepare each solution for the quenching experiment 1 mL of the Ru standard solution was added to the appropriate volume of quencher solution and the total volume was increased to 3 mL using degassed DCE. [Ru(bpy)₃](PF₆)₂ was excited at 454 nm and emission intensity collected at 591 nm.

Rates of quenching (k_q) were determined using Stern-Volmer kinetics:

$$I_0/I = 1 + k_q \times \tau_0 \times [\text{quencher}]$$

where I_0 is the luminescence intensity without the quencher, I is the intensity with the quencher, and τ_0 is the lifetime of the photocatalyst.

The lifetime of Ru(bpy)₃Cl₂ measured in CH₂Cl₂ ($\tau_0 = 488$ ns)⁹ was used for the calculations of quenching rates k_q .

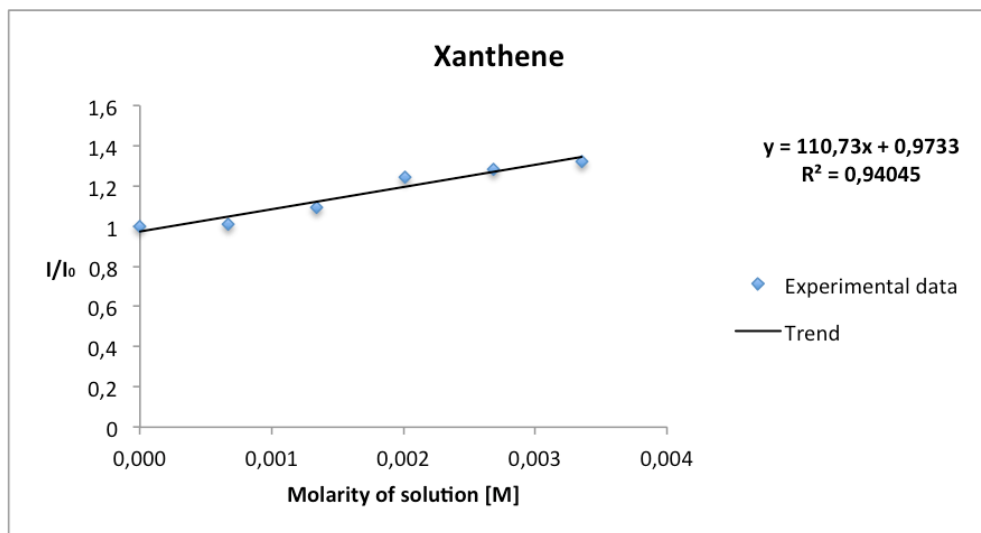
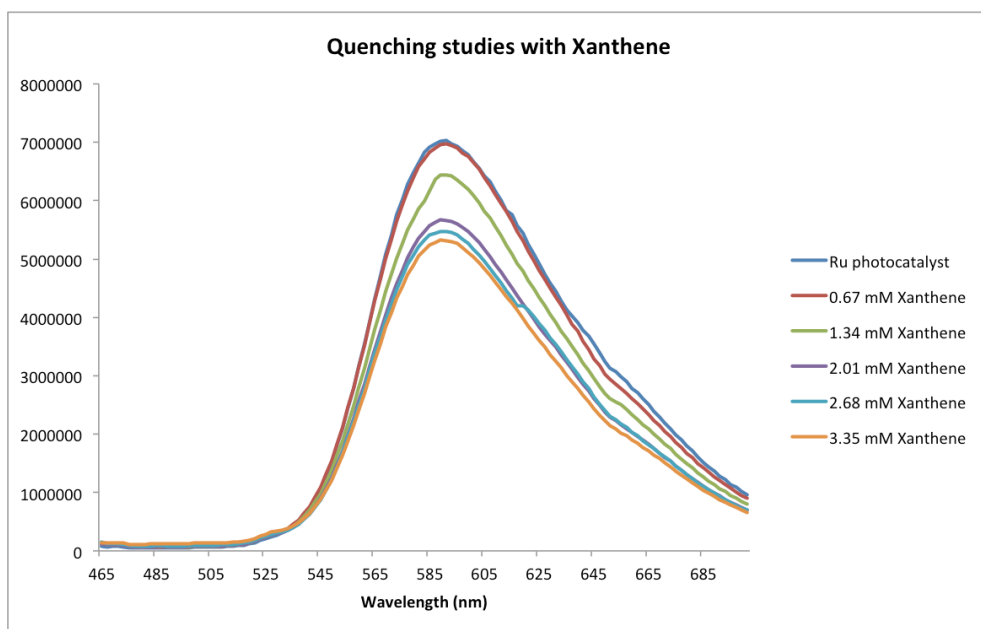


Figure II-21. Quenching by xanthene.

Quenching rate by xanthene: $k_q = 2.3 \times 10^8 \text{ M}^{-1} \text{ s}^{-1}$.

Asymmetric cross-dehydrogenative coupling of aldehydes with xanthenes

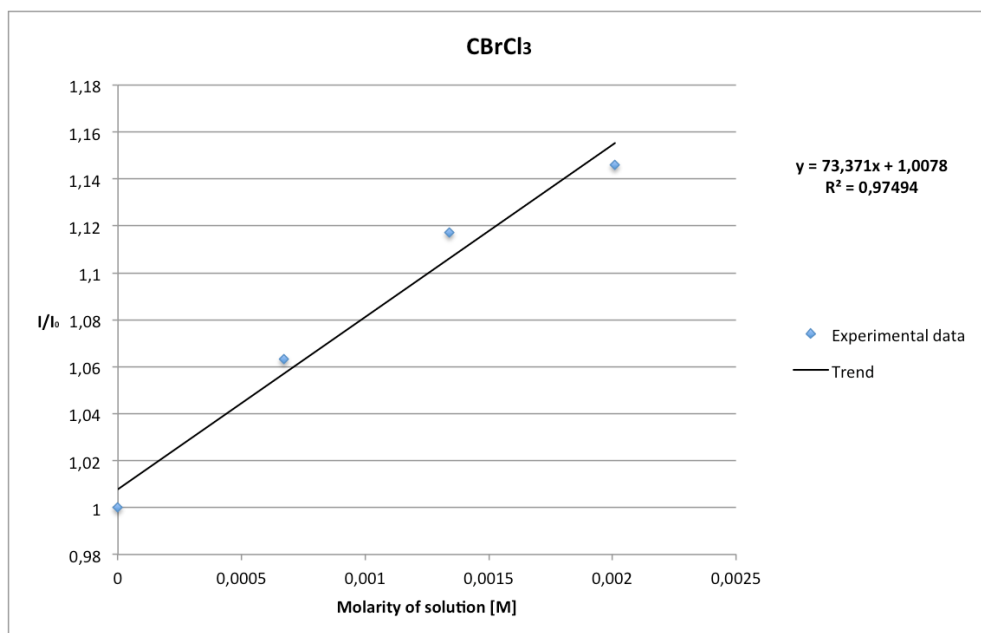
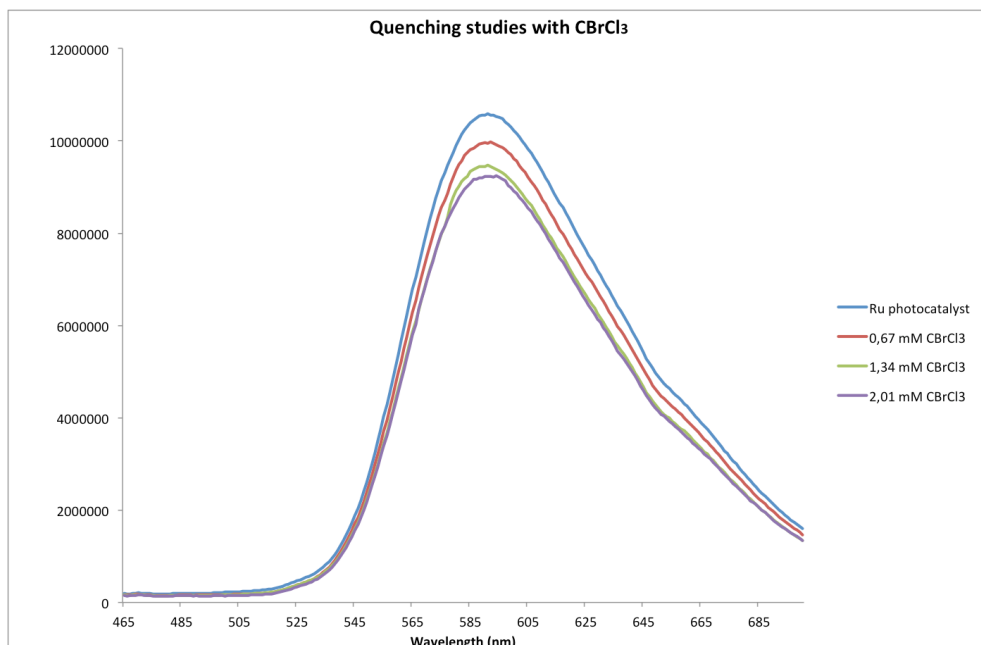


Figure II-22. Quenching by BrCCl₃.

Quenching rate by BrCCl₃: $k_q = 1.5 \times 10^8 \text{ M}^{-1} \text{ s}^{-1}$.

II.4.8. Computational details

Density functional calculations were used to examine important segments of the potential energy surface. The geometry optimizations have been carried out at B3LYP/6-31G(d) level. Single point SMD-PCM calculations in DCE at B2PLYP-D3 level with 6-311+G(d,p) basis set were carried out for all the gas phase optimized structures, yielding the solvent corrected energy E_{solv} . Thermochemical corrections to free energies (G_{298}) and enthalpies at 298.15 K (H_{298}) have been calculated at the same level as that used for geometry optimization. Due to the large number of low frequencies, hindered rotor approximation was used for the calculation of thermochemical corrections.¹⁰ Gas phase Gibbs free energy corrections G_{corr} were considered for each species and the total Gibbs free energy G of each optimized structure was taken as $G = E_{\text{solv}} + G_{\text{corr}}$. A frequency calculation was performed on all intermediates and transition states to verify minima and first order saddle points, respectively. Intrinsic reaction coordinate (irc) calculations were used to connect transition states with the corresponding intermediates. The calculations were performed with the Gaussian09 package.

Asymmetric cross-dehydrogenative coupling of aldehydes with xanthenes

II.4.8.1. Photoredox cycle

- Oxidative quenching mechanism

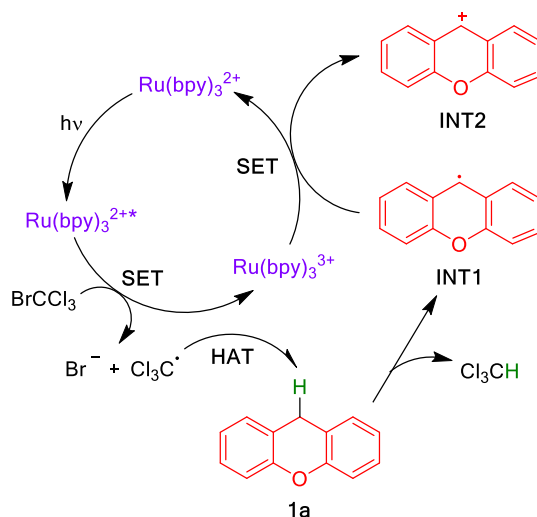


Figure II-22. Oxidative quenching cycle with BrCCl_3 as oxidant.

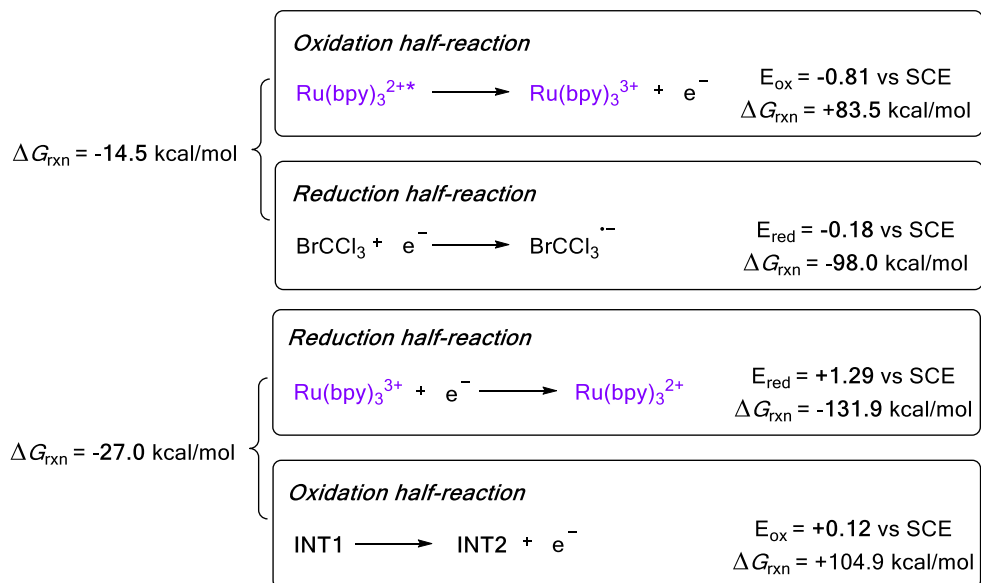


Figure II-23. Redox half-reactions for the cycle depicted in Figure II-22.

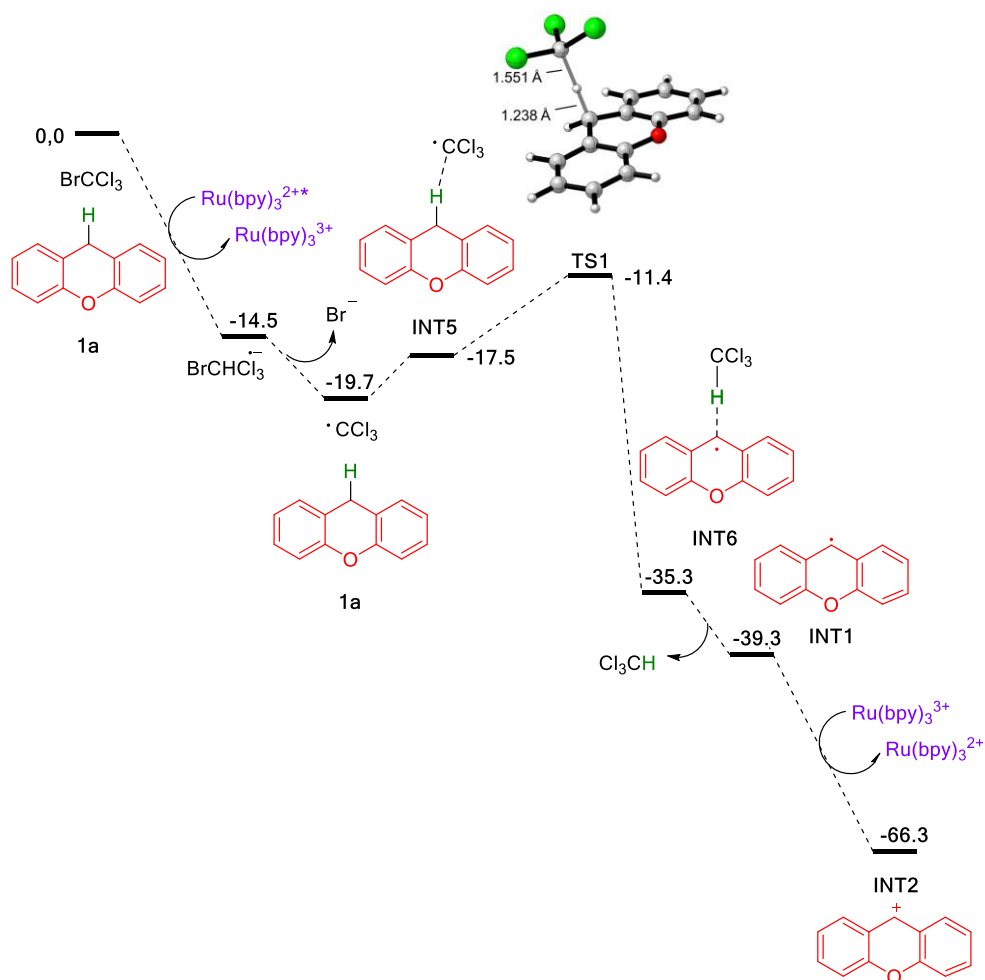


Figure II-24. Calculated reaction profile (ΔG, kcal/mol).

Asymmetric cross-dehydrogenative coupling of aldehydes with xanthenes

- Oxidative quenching mechanism and direct oxidation of **1a** to the corresponding radical-cation INT7.

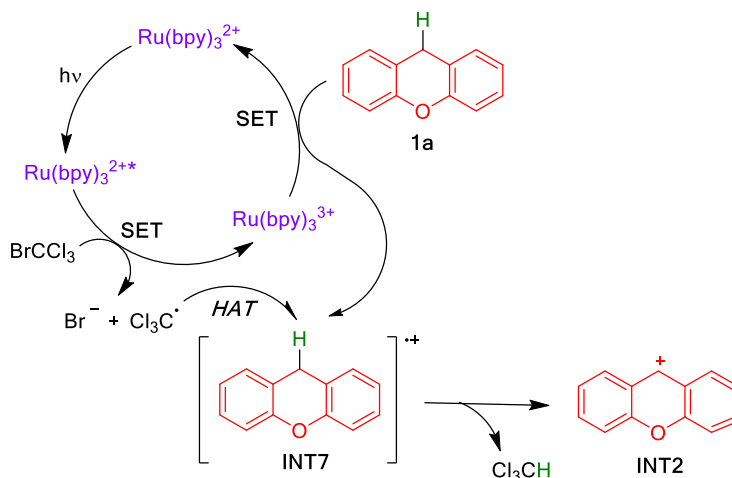


Figure II-25. Oxidative quenching cycle with direct oxidation of **1a**.

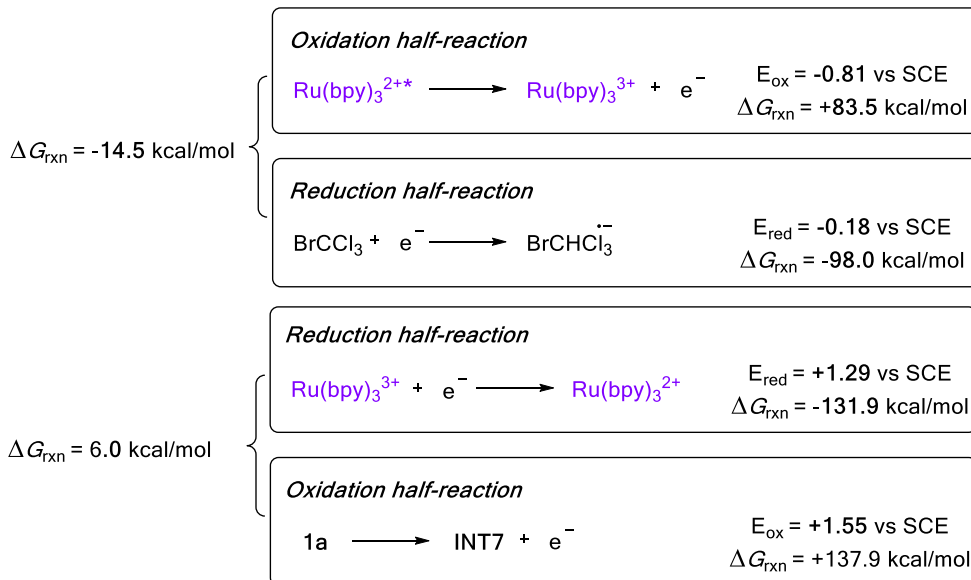


Figure II-26. Redox half-reactions for the cycle depicted in Figure II-25.

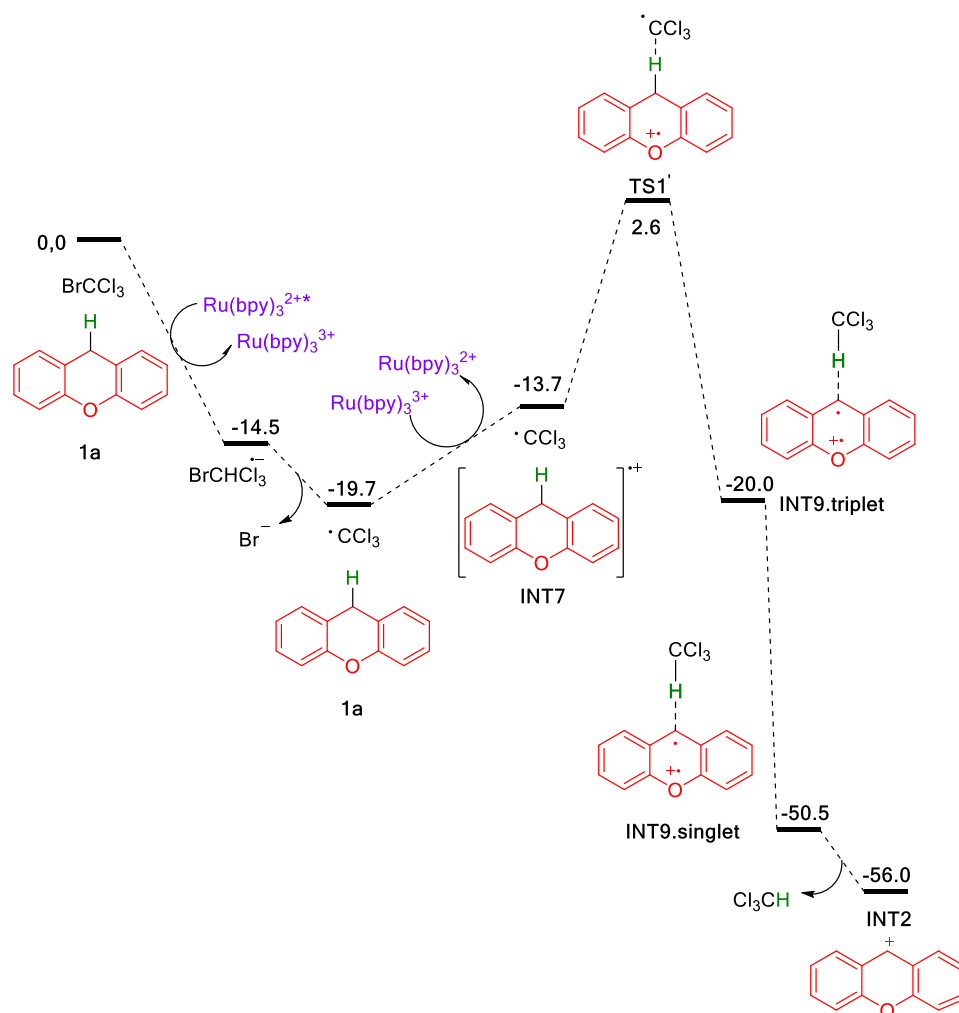


Figure II-27. Calculated reaction profile (ΔG , kcal/mol).

Comparison of reaction profiles (Figures II-23 and II-26) shows that oxidative quenching followed by hydrogen abstraction from **1a** by CCl₃ radical is more energetically favorable ($\Delta G^\ddagger = 8.3$ kcal/mol) than oxidative quenching followed by hydrogen atom abstraction from INT7 ($\Delta G^\ddagger = 18.8$ kcal/mol).

Asymmetric cross-dehydrogenative coupling of aldehydes with xanthenes

- Reductive quenching mechanism with **1a** as the quencher.

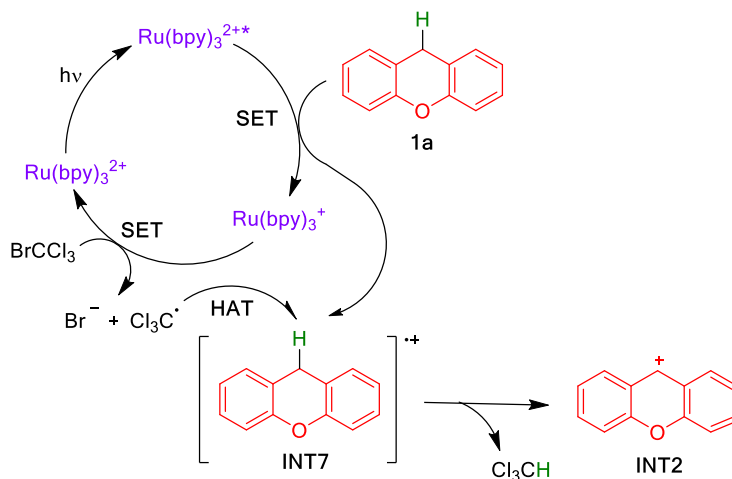


Figure II-28. Reductive quenching cycle with **1a** as the quencher.

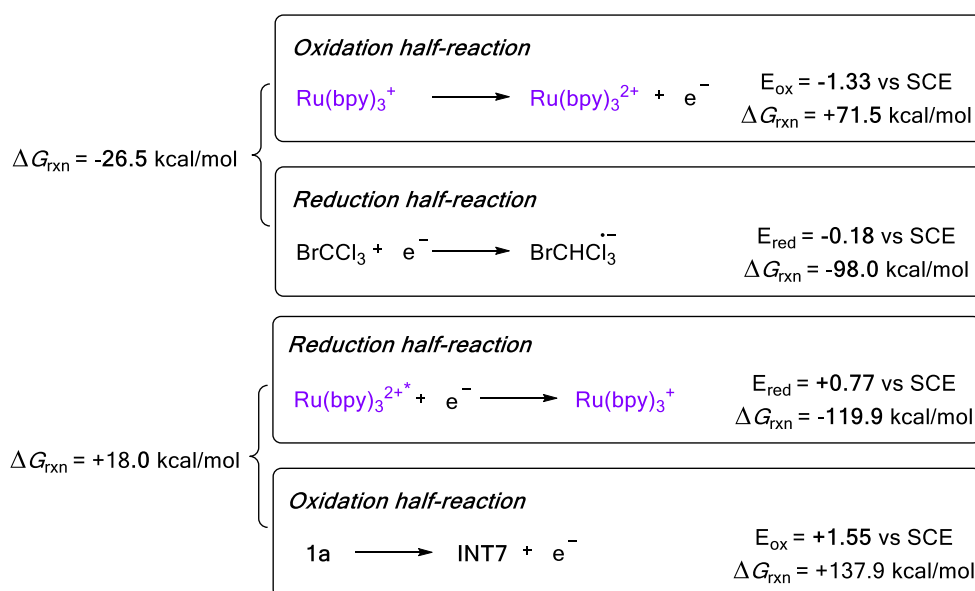


Figure II-29. Redox half-reactions for the cycle depicted in Figure II-28.

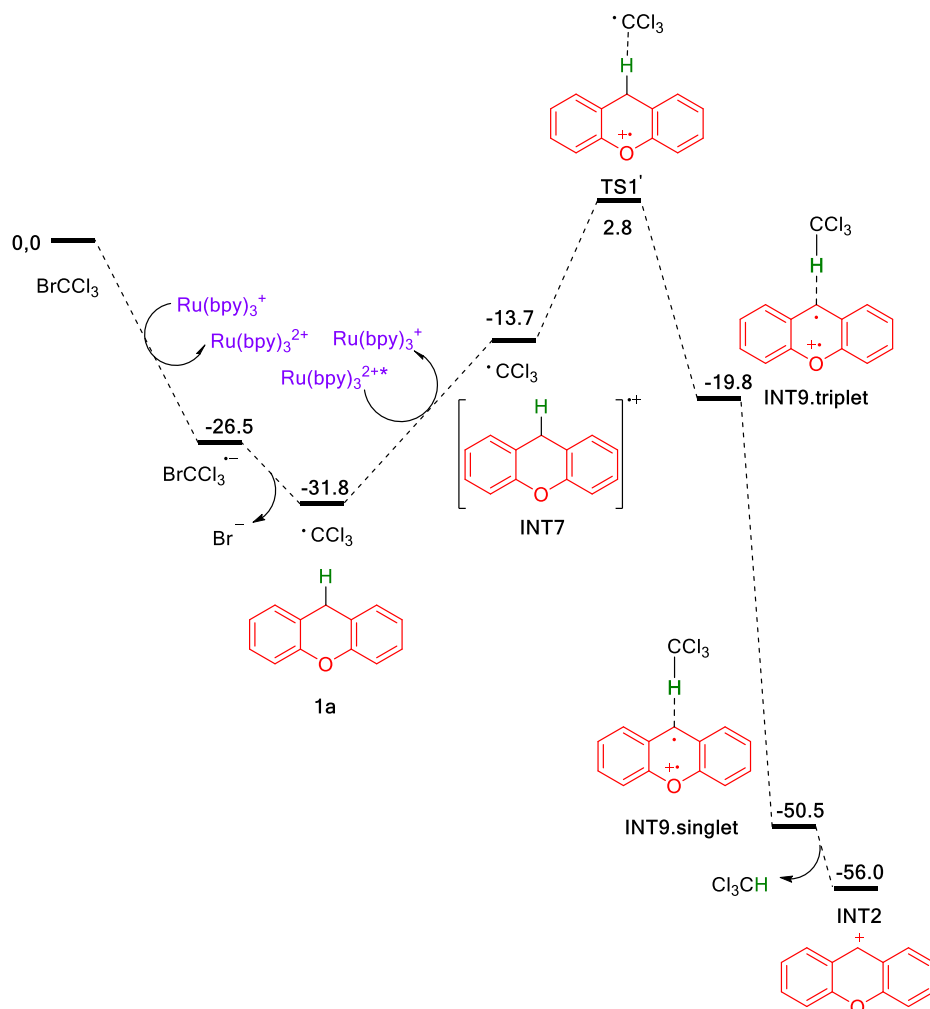


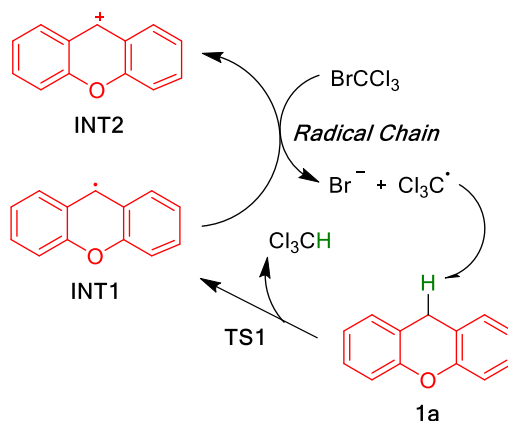
Figure II-30. Calculated reaction profile (ΔG , kcal/mol).

Direct quenching of Ru(II)* by xanthene is unfavorable due to two factors:
a) high reduction potential INT7/1a; b) high activation barrier for the hydrogen abstraction from INT7.

Asymmetric cross-dehydrogenative coupling of aldehydes with xanthenes

II.4.8.2. Radical chain mechanism

a) Radical chain



b) Redox half reactions

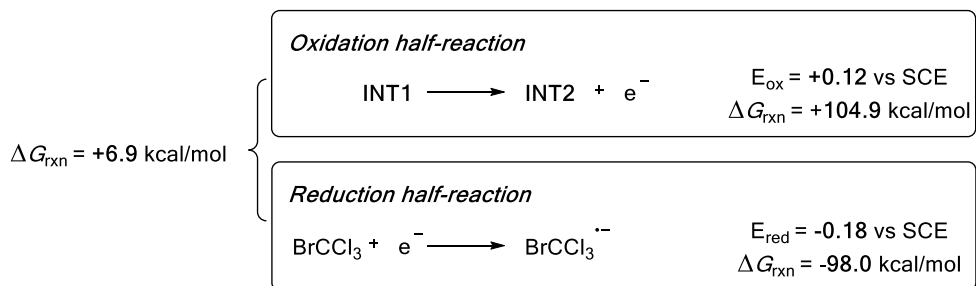
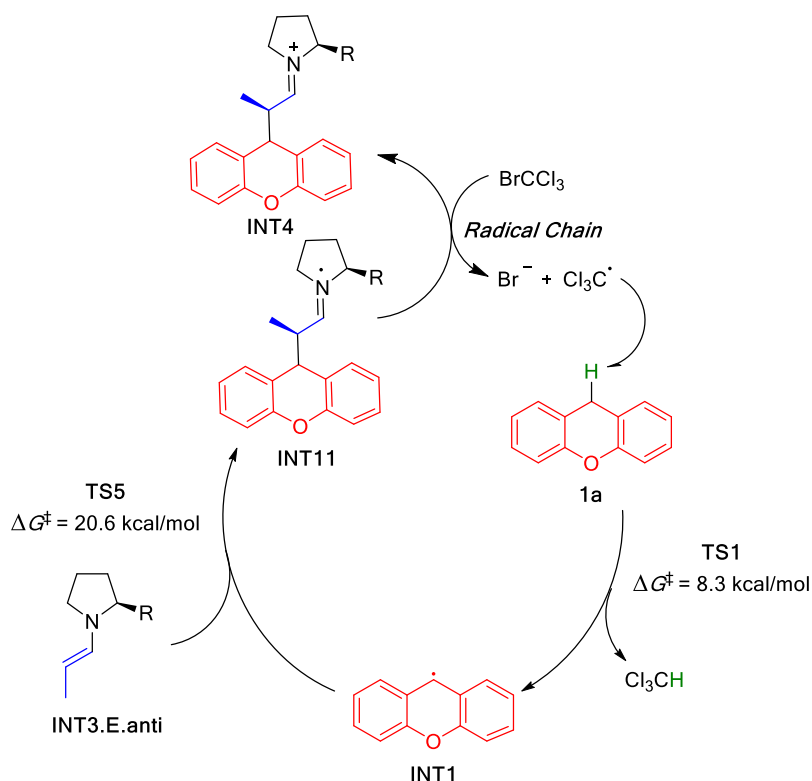


Figure II-31. Radical chain pathway.

a) Catalytic cycle



b) Redox half reactions

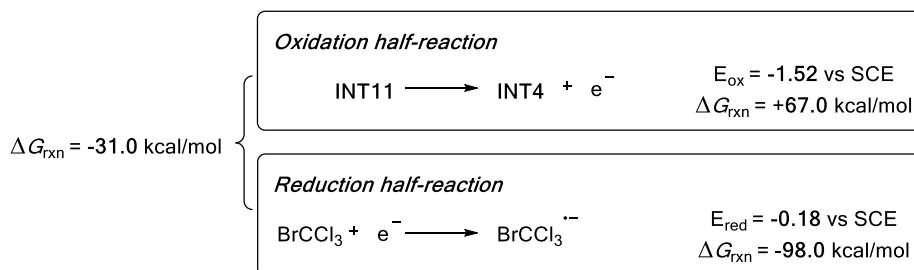


Figure II-32. Alternative radical chain pathway.

Even though a reduction potential of **INT4** is more negative than of BrCCl_3 , the C–C bond formation step has a higher activation barrier of 20.6 kcal/mol. That makes this pathway much less favorable.

Asymmetric cross-dehydrogenative coupling of aldehydes with xanthenes

II.4.8.3. C–C bond formation

- Enamine formation

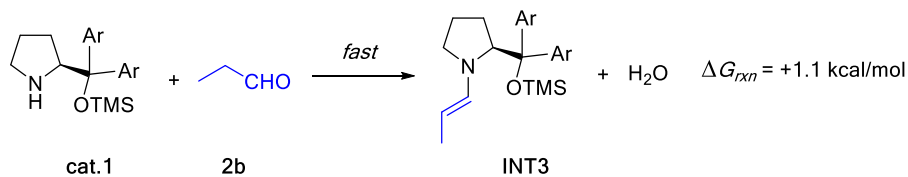


Figure II-33. Reaction free energy for the enamine formation.

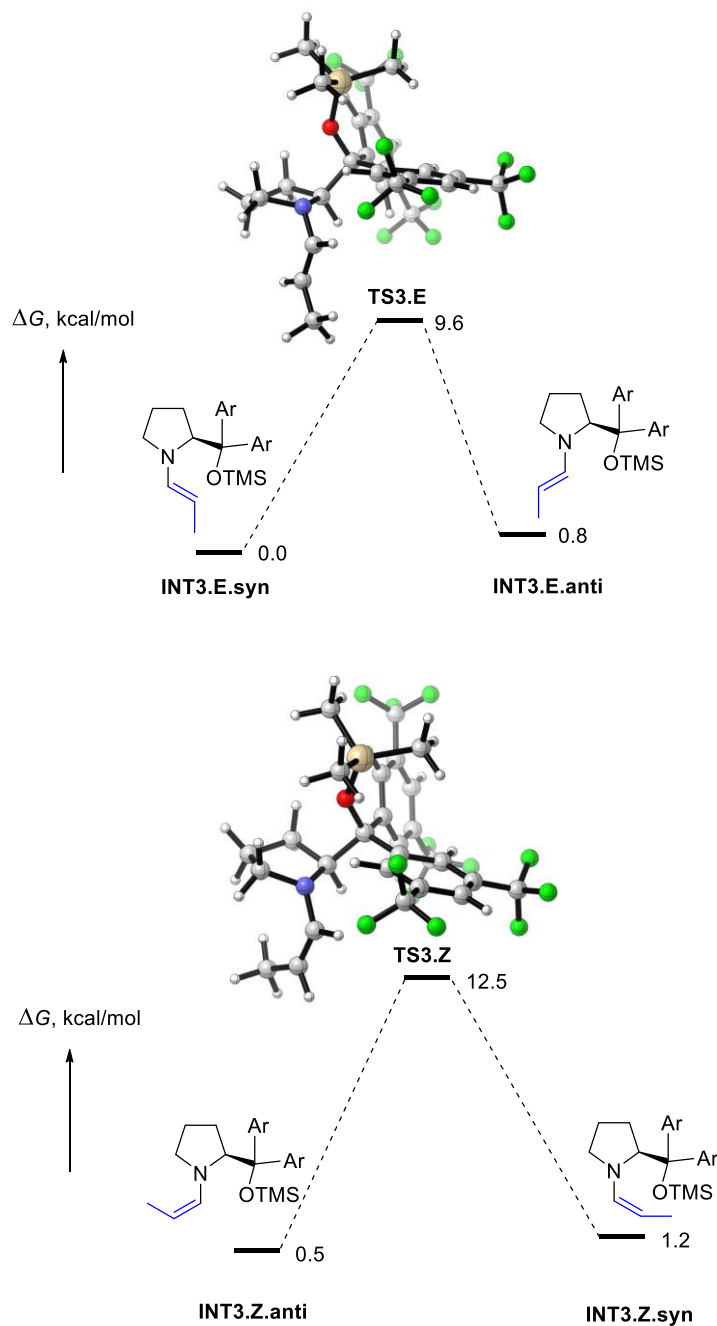


Figure II-34. Enamine stereoisomers and transition states for the rotation around C-N bond.

Asymmetric cross-dehydrogenative coupling of aldehydes with xanthenes

• Second Oxidation and C-C Bond Formation

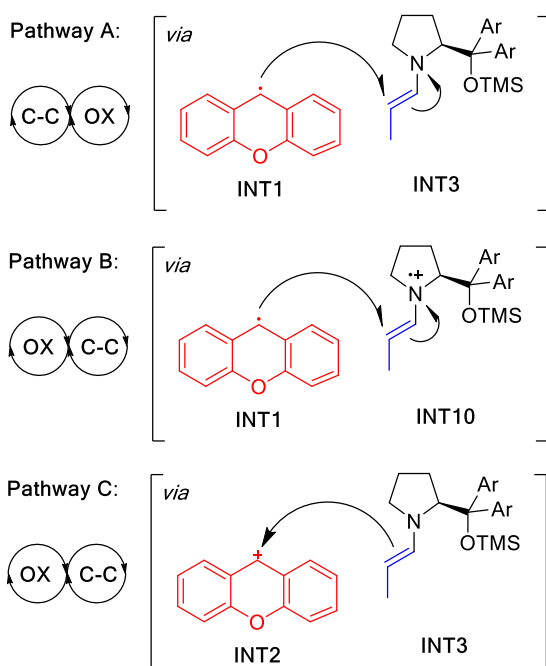
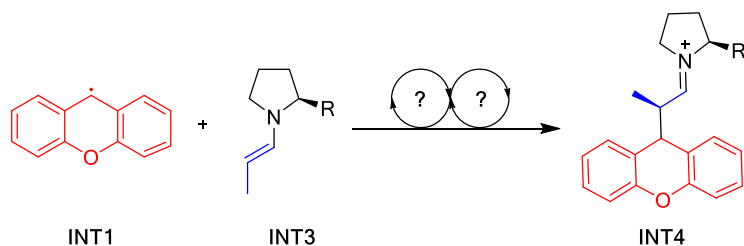
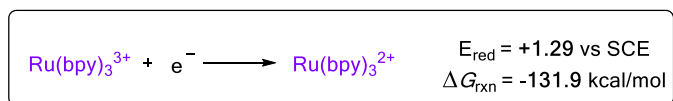


Figure II-35. Three possible mechanisms were considered, that differ in the order of oxidation/C-C bond formation steps.

Reduction half-reaction:



Oxidation half-reactions:

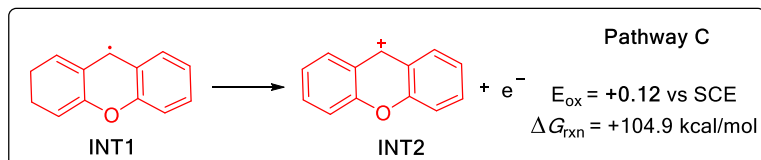
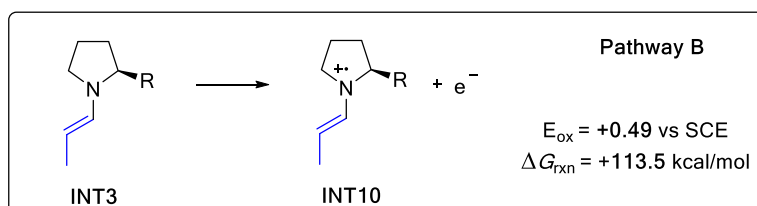
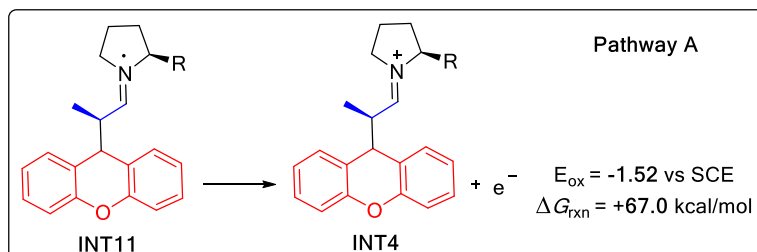


Figure II-36. Redox half-reactions for pathways A, B and C.

Asymmetric cross-dehydrogenative coupling of aldehydes with xanthenes

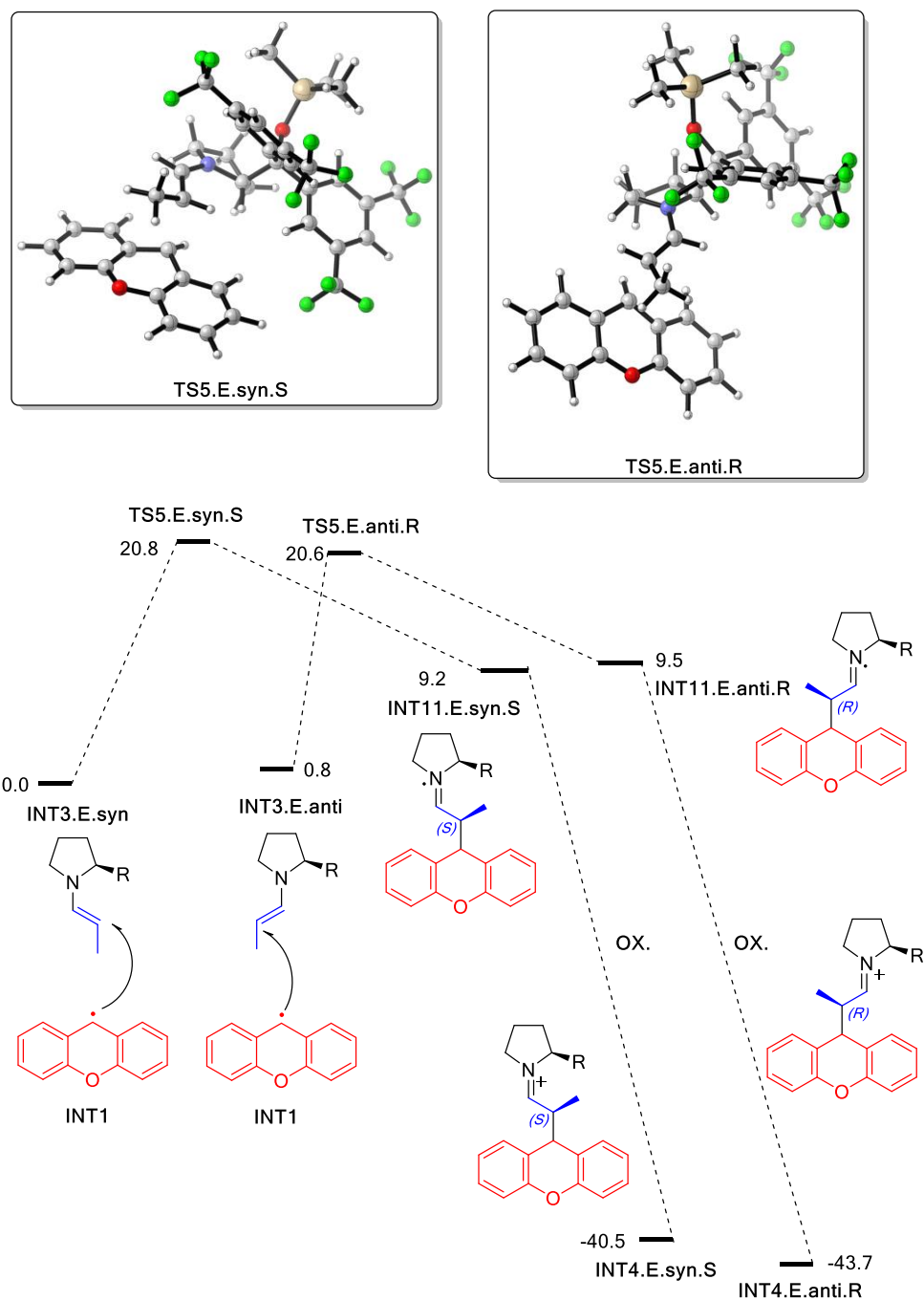


Figure II-37. Pathway A: direct attack of enamine by the xanthyl radical followed by oxidation of the formed iminium radical.

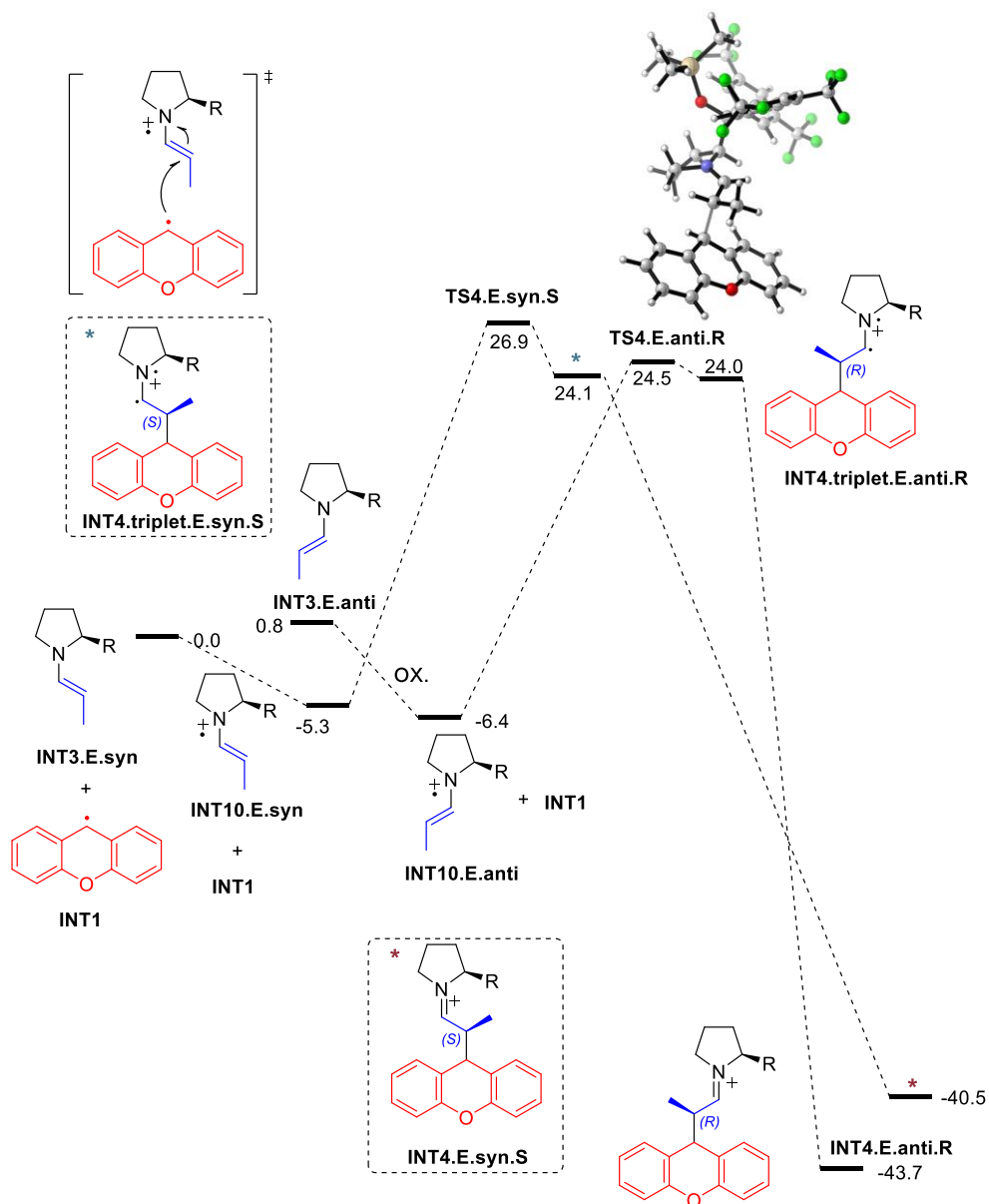


Figure II-38. Pathway B: oxidation of enamine to radical-cation followed by the radical-radical coupling.

Asymmetric cross-dehydrogenative coupling of aldehydes with xanthenes

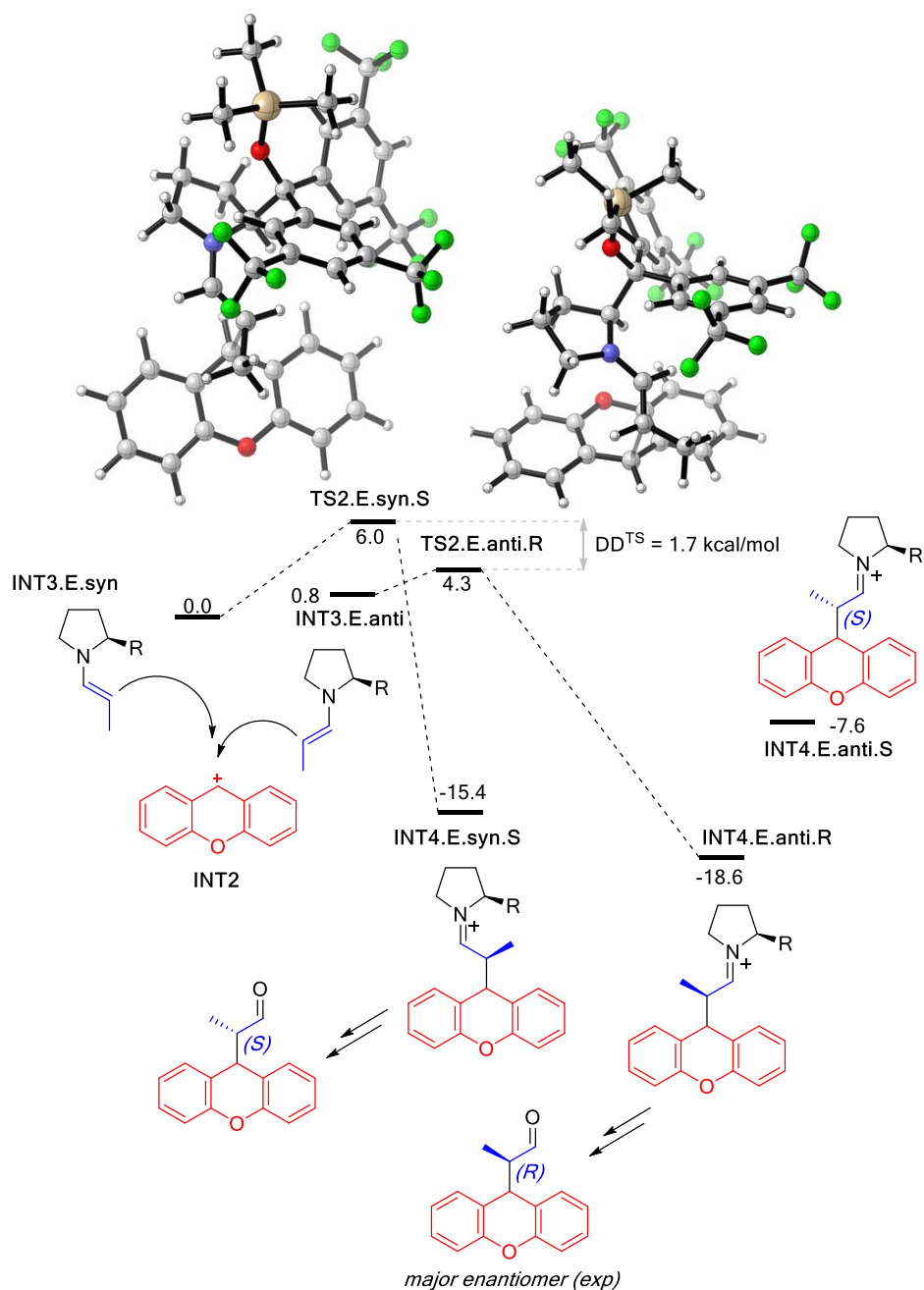


Figure II-39. Pathway C: oxidation of xanthyl radical to cation followed by the enamine attack.

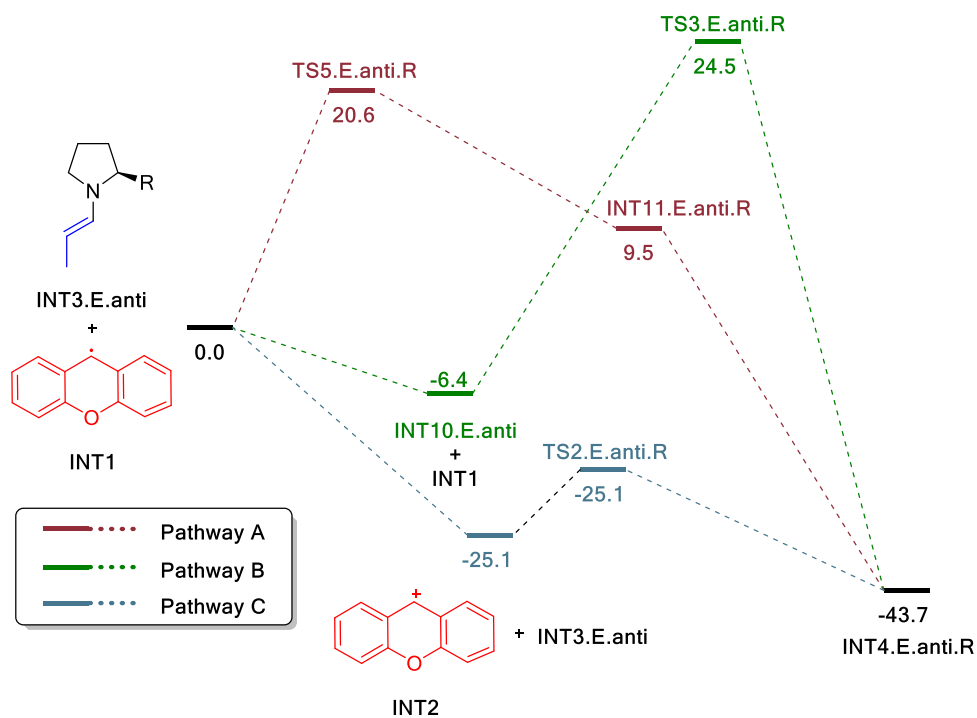


Figure II-40. Comparison of three mechanisms for the **E.anti.R** pathway.

Pathway C clearly has a much lower activation barrier compared with the other two mechanisms.

Asymmetric cross-dehydrogenative coupling of aldehydes with xanthenes

- Alternative pathway via reductive quenching by enamine INT3.

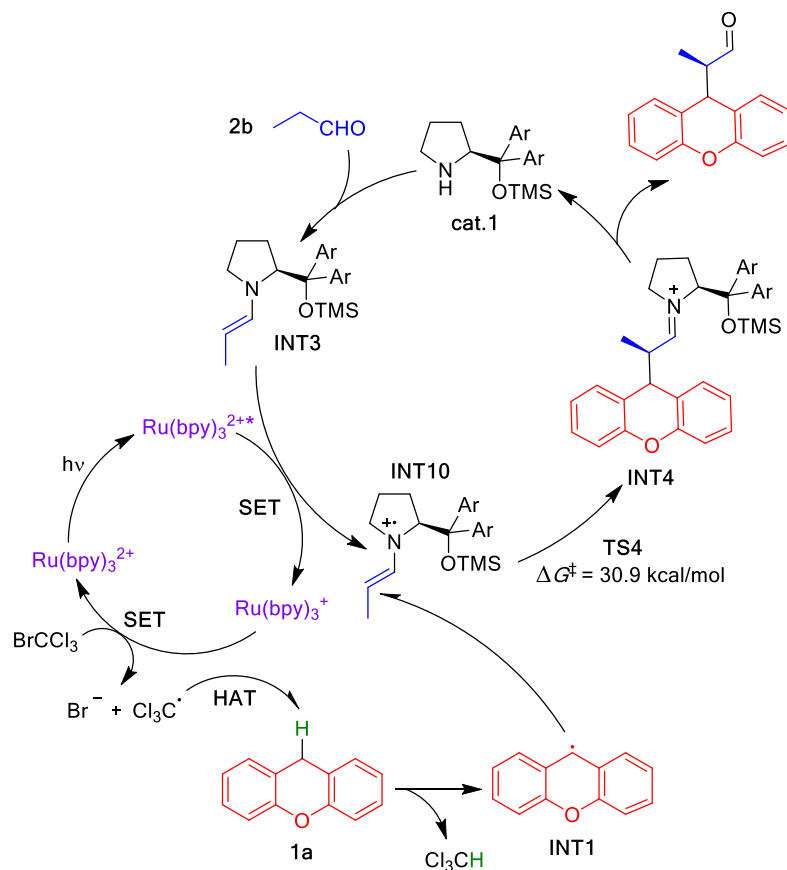


Figure II-41. Alternative mechanism based on enamine oxidation.

II.4.9. References

¹ Boros, E. E.; Edwards, C. E.; Foster, S. A.; Fujii, M.; Fujiwara, T.; Garvey, E. P.; Golden, P. L.; Hazen, R. J.; Jeffrey, J. L.; Johns, B. A.; Kawasuji, T.; Kiyama, R.; Koble, C. S.; Kurose, N.; Miller, W. H.; Mote, A. L.; Murai, H.; Sato, A.; Thompson, J. B.; Woodward, M. C.; Yoshinaga, T. *J. Med. Chem.* **2009**, *52*, 2754-2761.

- ² Shinde, D. B.; Kanth, B. S.; Srilatha, M.; Das, B. *Synthesis* **2012**, 469-473.
- ³ Heuser, S. *Synlett* **2007**, *3*, 497-499.
- ⁴ Böb, E.; Hillringhaus, T.; Nitsch, J.; Klussmann, M. *Org. Biomol. Chem.* **2011**, *9*, 1744-1748.
- ⁵ Stopka, T.; Marzo, L.; Zurro, M.; Janich, S.; Würthwein, E.-U.; Daniliuc, C. G.; Alemán, J.; Mancheño, O. G. *Angew. Chem. Int. Ed.* **2015**, *54*, 5049-5053.
- ⁶ Xiao, J. *Org. Lett.* **2012**, *14*, 1716-1719.
- ⁷ Xiao, J.; Zaho, K.; Loh, T. P. *Chem. Comm.* **2012**, *48*, 3548-3549.
- ⁸ Lewandowska-Andralojc, A.; Grills, D. C.; Zhang, J.; Bullock, R. M.; Miyazawa, A.; Kawanishi, Y.; Fujita, E. *J. Am. Chem. Soc.* **2014**, *136*, 3572-3578.
- ⁹ Caspar, J. V.; Meyer, T. J. *J. Am. Chem. Soc.* **1983**, *105*, 5583-5590.
- ¹⁰ McClurg, R. B.; Flagan, R. C.; Goddard III, W. A. *J. Chem. Phys.* **1997**, *106*, 6675 - 6680.

UNIVERSITAT ROVIRA I VIRGILI

Harnessing Visible Light for the Development of Novel Synthetic Strategies

Marco Michele Mastandrea

CHAPTER III

Decarboxylative hydroalkylation of alkynes

III.1. Introduction	155
III.1.1. Addition of C-centered radicals to alkynes	155
III.1.2. Double bond photoisomerization	157
III.1.3. Copper in visible-light photocatalysis	161
III.2. Objective	166
III.3. Dual Cu-photoredox catalyzed hydroalkylation of alkynes	168
III.3.1. HTE screening and control experiments	168
III.3.2. Reaction scope	170
III.3.3. Mechanistic investigation	174
III.3.4. Conclusions	178
III.4. Supporting Information	180

UNIVERSITAT ROVIRA I VIRGILI

Harnessing Visible Light for the Development of Novel Synthetic Strategies

Marco Michele Mastandrea

CHAPTER III

Decarboxylative hydroalkylation of alkynes

III.1. Introduction

III.1.1. Addition of carbon-centered radicals to alkynes

Over the last decade, the resurgence of visible-light photoredox catalysis has disclosed unprecedented opportunities in the generation of radical intermediates by selective activation of small organic molecules under mild reaction conditions.

In this context, radical additions to simple alkenes, styrenes, and α,β -unsaturated carbonyl compounds have been widely explored.¹ In contrast and despite its attractiveness, the reaction of radicals with alkynes has been less exploited.^{2, 3} In fact, alkynes are ubiquitous structural motifs and the ability of a photocatalyst to perform selective energy transfer to them may lay the foundations for unprecedented stereoselective processes.

From a mechanistic perspective, the reasons for the limited development of radical addition to alkynes can be probably ascribed to the slow rate of C–C bond formation. Despite a higher exothermicity, reactions of radicals with alkynes are generally slower than with the corresponding alkenes. This seemingly contradictory behavior arises from the smaller electron affinities

¹ a) Silva-Costa, D. C. *Arabian J. Chem.* **2020**, *13*, 799-834; b) Zard, S. S. Z. *Acc. Chem. Res.* **2018**, *51*, 1722-1733.

² Herein we will limit the discussion to the addition of nucleophilic alkyl radicals to electronically unbiased alkynes.

³ a) Wille, U. *Chem. Rev.* **2013**, *113*, 813-853; b) Huang, M.-H. Hao, W.-J. Li, G.; Tu, S.-J.; Jiang, B. *Chem. Commun.* **2018**, *54*, 10791-10811.

Decarboxylative hydroalkylation of alkynes

and larger ionization energies in alkynes compared with alkenes, which results in diminished polar effects. As a consequence, decreased selectivity and increase in activation barriers result. Another possible explanation is that the singlet-triplet gap is higher for alkynes than for alkenes. This barrier-raising effect outweighs the barrier-lowering effect of the reaction exothermicity.⁴ Another factor that explains the underdevelopment of such radical additions is the generation of high-energy vinyl radical intermediates that can readily participate in various undesirable open-shell pathways.

Besides Tang report, dealing with the preparation of *Z*-alkenes by photocatalyzed decarboxylative coupling between terminal aryl alkynes and alkyl *N*-hydroxyphthalimide (NHPI) esters,⁵ the aforementioned lack of reactivity has been circumvented by adopting a multicatalytic approach. In particular, nickel metallaphotoredox catalysis enabled to achieve alkynes hydroalkylation. Thus, MacMillan⁶ and Rueping⁷ independently developed an Ir/Ni photocatalytic decarboxylative hydroalkylation of alkynes that takes advantage of a migratory insertion step to afford terminal and internal alkenes (Scheme III-I, a and b). The latter extended the developed methodology also to the arylalkylation of C–C triple bonds with carboxylic acids and aryl bromides. Instead, Wu proposed a Ni–H catalyzed hydroalkylation of internal phenylacetylenes and enynes **8** with photocatalytically generated α -heteroatom radicals (Scheme III-I, c).⁸ Besides the intrinsic mechanistic differences, it's noteworthy that in all these reports the alkyl radicals are thought to be trapped by nickel rather than by the alkyne.

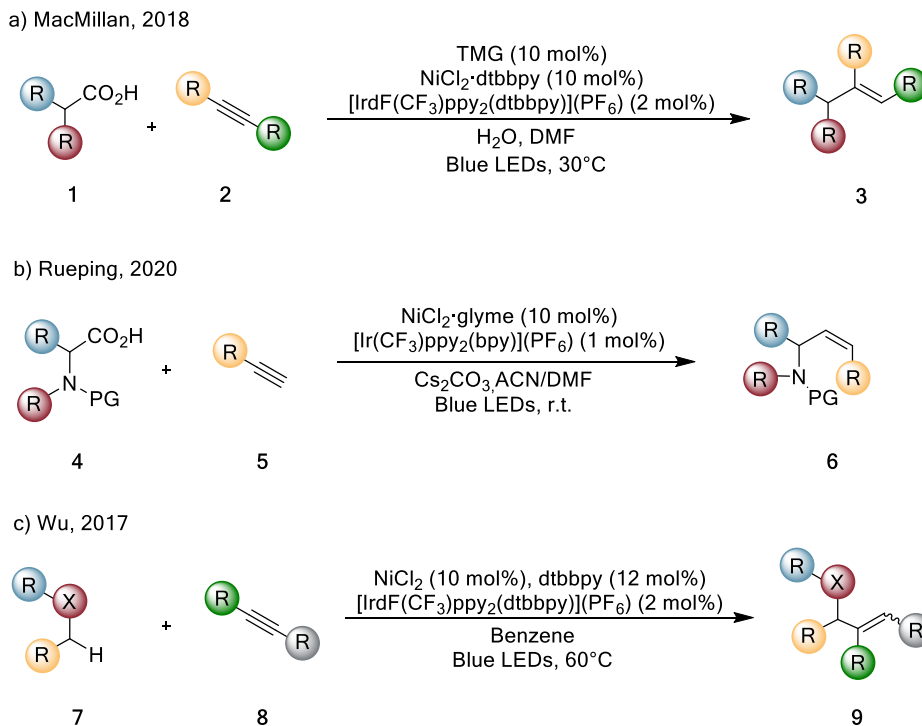
⁴ a) Fischer, H.; Radom, L. *Angew. Chem., Int. Ed.* **2001**, *40*, 1340-1371. (b) Gómez-Balderas, R.; Coote, M. L.; Henry, D. J.; Fischer, H.; Radom, L. *J. Phys. Chem. A* **2003**, *107*, 6082-6090; (c) Giese, B.; Lachhein, S. *Angew. Chem., Int. Ed. Engl.* **1982**, *21*, 768-775.

⁵ Dai, G.-L.; Lai, S.-Z.; Luo, Z.; Tang, Z.-Y. *Org. Lett.* **2019**, *21*, 2269-2272.

⁶ Till, N. A.; Smith, R. T.; MacMillan, D. W. C. *J. Am. Chem. Soc.* **2018**, *140*, 5701-5705.

⁷ Yue, H.; Zhu, C.; Kancherla, R.; Liu, F.; Rueping, M. *Angew. Chem. Int. Ed.* **2020**, *59*, 5738-5746.

⁸ Deng, H.-P.; Fan, X.-Z.; Chen, Z.-H.; Xu, Q.-H.; Wu, J. *J. Am. Chem. Soc.* **2017**, *139*, 13579-13584.



Scheme III-1. a) Dual-catalytic alkyne hydroalkylation. TMG = 1,1,3,3-tetramethylguanidine; b) photoredox/nickel dual-catalyzed hydroalkylation of alkynes; c) hydroalkylation of internal alkynes with ether and amide α -hetero C(sp³)-H bonds.

III.1.2. Double bond photoisomerization

In the framework of classical radical chemistry, the stereoselectivity of intermolecular addition of radicals to alkynes has been widely investigated.⁹ The structure of vinyl radicals, generated upon radical addition to the triple bond, is a key factor in controlling the stereochemical outcome of their reactions (Figure III-1). The nature of the substituents in the alkyne

⁹ a) Goumans, T. P. M.; van Alem, K.; Lodder, G. *Eur. J. Org. Chem.* **2008**, 435-443; b) Giese, B.; González-Gómez, J. A.; Lachhein, S.; Metzger, J. O. *Angew. Chem., Int. Ed. Engl.* **1987**, *26*, 479-480.

Decarboxylative hydroalkylation of alkynes

precursor dictates the configuration of vinyl radicals. When the substituent is not able to stabilize the unpaired electron by resonance, the reaction of terminal alkynes leads to the formation of *Z* and *E* configured σ -type vinyl radicals. *E/Z* isomerizations in these radicals are usually very fast and the geometry of the final product is determined by the relative population of the two isomeric radicals, the rate by which each one is trapped and steric effects. Instead, the presence of a resonance-stabilizing substituent leads to a linearized geometry in the vinyl radical (π -radical). In this case, the stereochemical outcome of the overall reactions depends on the steric hindrance of the attacking radical and on the degree of reactivity of the hydrogen atom donor. From this description emerges how several concurring and hard-to-control factors affect the stereoselectivity of radical additions to alkynes.

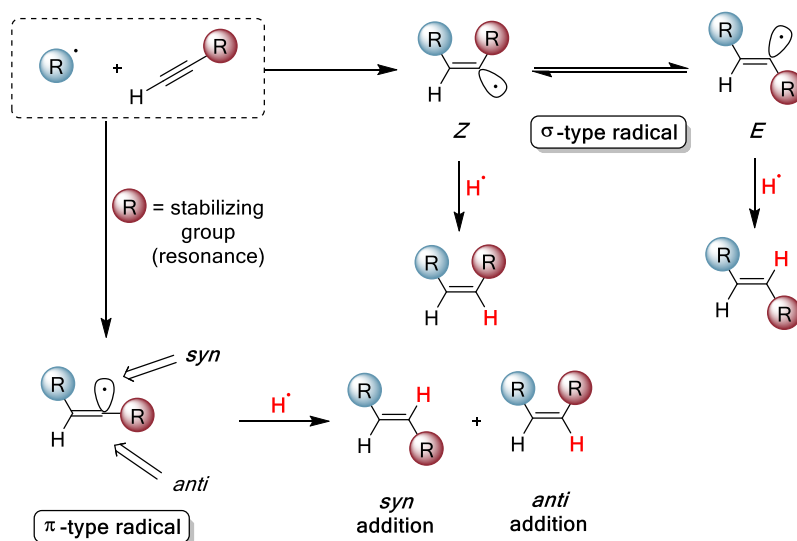


Figure III-1. Stereochemistry of radical additions to alkynes.

In this context, a great advantage is offered by photoredox catalysis. In fact, some of the commonly employed photocatalysts are able to isomerize alkenes *via* energy transfer processes in a highly predictable manner.¹⁰

The configurational isomerization of alkenes to generate the *Z*-isomer is perhaps one of the most important processes enabled by an energy transfer activation strategy. Seminal *E* → *Z* photoisomerization protocols typically require the use of (over)stoichiometric amounts of photosensitizers in combination with strong UV-irradiation.¹¹ Thus, as photoredox catalysis in radical generation strategies, mild visible-light mediated photoisomerizations of alkenes have also been developed.

Triplet sensitization of an alkene by a suitable photosensitizer allows the excitation of an electron from a π - to a π^* -orbital resulting in a decrease in bond order and, in turn, permitting rotation around σ -axis (Figure III-2). The stability of the excited state is strictly related with geometry, so that twisting around the central axis leads to an energy minimum (corresponding to the perpendicular arrangement). This point is a funnel for transitions to the twisted energy maximum on the ground-state energy hypersurface, subsequently allowing relaxation to the *E*- or *Z*-configured alkene. In this scenario, direct excitation of an alkene yields statistical *E/Z* mixtures unless one of the isomers can be selectively excited at a specific wavelength. In the case of conjugated olefins, instead, the triplet energies of the *E*- and *Z*-isomers can differ significantly: since excitation is a vertical process (*i.e.* the triplet structure reflects the ground state geometry), very often the *Z*-isomer triplet state is therefore disfavored due to nonbonding interactions and steric effects disrupting conjugation. Therefore, in order to achieve high selective *E* → *Z* isomerizations, a photosensitizer with $E_T < E_T$ (*Z*-alkene) should be employed since it selectively sensitizes the *E*-isomer, leading to gradual

¹⁰ Metternich, J. B.; Gilmour, R. *Synlett*, **2016**, *27*, 2541-2552 and references therein.

¹¹ Hammond, G. S.; Turro, N. J.; Leermakers, P. A. *J. Phys. Chem.* **1962**, *66*, 1144

Decarboxylative hydroalkylation of alkynes

accumulation of the *Z*-isomer. In this context, triplet sensitizers are particularly valuable due to their extended lifetimes.

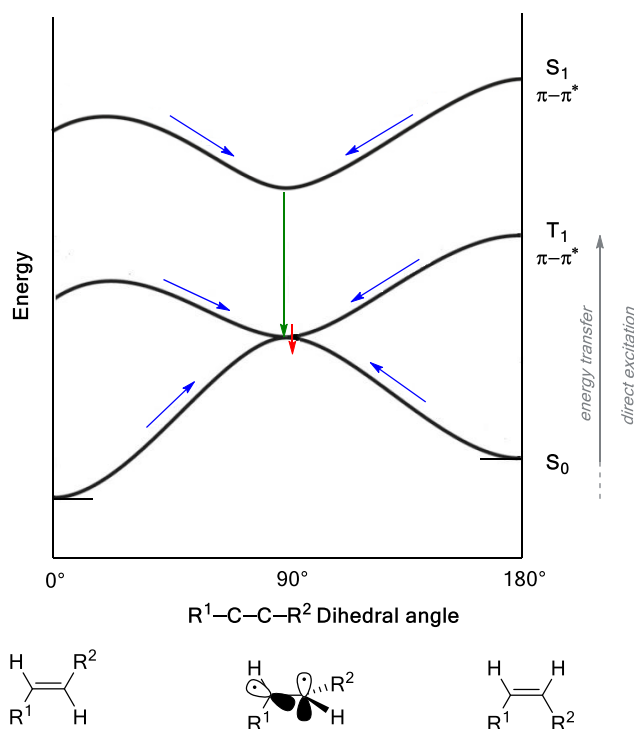


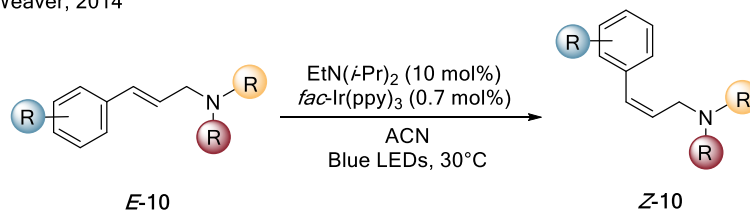
Figure III-2. Simplified energy hypersurface diagram explaining the effect of the RCCR dihedral angle during excitation-induced or sensitized isomerization of olefins. S_0 singlet ground state; S_1 first singlet excited state; T_1 first triplet excited state; blue arrows correspond to movement along the respective potential energy surface; green arrow corresponds to surface crossings without change of multiplicity; red arrow corresponds to surface crossing with change of multiplicity (inter-system crossing or ISC).

This strategy has been exploited by Weaver in 2014, who reported the triplet-sensitized, highly selective isomerization of allylic amines **10** using *fac*-Ir(ppy)₃ as the photocatalyst (Scheme III-2, a).¹² In 2015, Gilmour achieved the *E* → *Z* photoisomerization of activated olefins **11** employing (-)-riboflavin as an energy transfer catalyst (Scheme III-2, b).¹³

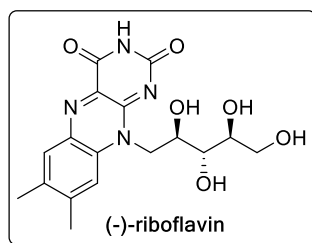
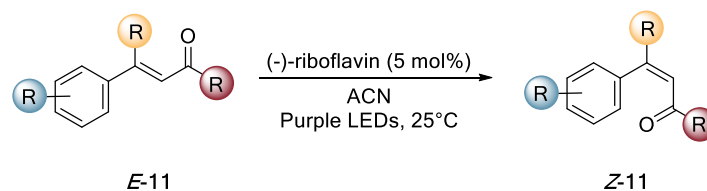
¹² Singh, K.; Staig, S. J.; Weaver, J. D. *J. Am. Chem. Soc.* **2014**, *136*, 5275-5278.

¹³ Metternich, J. B.; Gilmour, R. *J. Am. Chem. Soc.* **2015**, *137*, 11254-11257.

a) Weaver, 2014



b) Gilmour, 2014



Scheme III-2. a) Energy transfer catalysis allows the selective $E \rightarrow Z$ isomerization of styrenyl alkenes; b) bio-inspired $E \rightarrow Z$ photoisomerization of diverse α,β -unsaturated styrenyl motifs by triplet sensitization.

III.1.3. Copper in visible-light photocatalysis

In the 2000s renaissance of photocatalysis, Ru(II)- or Ir(III)-polypyridyl complexes and organic dyes have been widely employed due to their long excited state lifetimes, strong absorption in the visible region and high reduction or oxidation potentials of the corresponding excited states. However, there are common drawbacks in the use of such catalysts. Organic dyes often suffer from low photostability while heavy transition metal-based complexes are expensive and environmentally unfriendly. Moreover, the restrictive conformational constraints and coordinative

Decarboxylative hydroalkylation of alkynes

saturation of Ir- and Ru-based catalyst limit inner-sphere substrate interactions and chiral ligand design for asymmetric transformation. In this regard, even if stereoselective transformations have been developed,¹⁴ the synthesis of appropriate chiral octahedral complexes with labile ligands remains a substantial challenge. In this scenario, first row transition-metal complexes are promising alternatives in terms of enabling inner sphere photoredox processes and, hence, reaction control through their ligand environment.¹⁵ In particular, copper-based photocatalysis is an appealing alternative due to: i) highly tunable excited state redox properties; ii) flexibility in ligand architecture, allowing stereoinduction; iii) access to multiple oxidation states resulting in rapid radical capture or facile reductive elimination; iv) control over the photoredox processes occurring in inner coordination sphere. In this transformations, Cu(I) and Cu(II) species can act as standalone photocatalysts, cocatalyze photoredox processes or form a photoactive complex with a substrate. The latter class of reaction manifolds is pertinent with the topic of the chapter and will be treated in detail, while for the others we suggest excellent reviews on the topic.¹⁶

- **Photoexcitation of in situ-generated Cu(I) substrate complexes**

Recently, a copper specific class of reaction manifolds has emerged in which suitable substrates can elicit visible light absorbing complexes by coordination with Cu(I). The excited Cu(I)-substrate complex acts as single electron reductant towards an electron acceptor, and the resulting Cu(II) species then participates in a diverse range of cross couplings and functional group modifications (Figure III-3).

¹⁴ Huo, H.; Shen, X.; Wang, C.; Zhang, L.; Rose, P.; Chen, L.-A.; Harms, K.; Marsch, M.; Hilt, G.; Meggers, E. *Nature* **2014**, *515*, 100-103

¹⁵ Larsen, B. C.; Wenger O. S. *Chem. Eur. J.* **2018**, *24*, 2039-2058.

¹⁶ a) Paria, S.; Reiser, O. *ChemCatChem* **2014**, *6*, 2477 - 2483; b) O. Reiser *Acc. Chem. Res.* **2016**, *49*, 1990–1996. c) McLean, E. B.; Lee A.-L. *Tetrahedron* **2018**, *74*, 4881-4902; d) Hossain, A.; Bhattacharyya, A.; Reiser, O. *Science* **2019**, *364*, eaav9713.

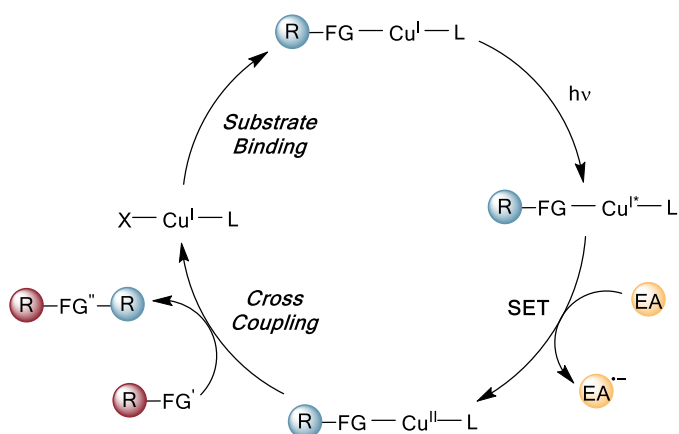


Figure III-3. Cross-coupling reaction by means of photoexcitation of in situ-generated Cu(I)-substrate complexes. FG = functional group; X = counter anion; EA = electron acceptor.

By capitalizing on this concept, Liu reported the synthesis of 2-aminothiazoles (**13**) from vinyl azides (**12**) exploiting the double role of in situ-generated $\text{Cu}(\text{NCS})_2^-$ as photocatalyst and Lewis acid (Scheme III-3, a).¹⁷ Wu, instead, developed a C–H functionalization of 2-arylaminoacetates (**14**) affording indolo[3,2-*d*]quinoline (**16**) (Scheme III-3, b).¹⁸ Key intermediate is the Cu(I) complex formed with **14** that, upon photoexcitation, promotes the alkylation of enolates.

However, the substrates that undoubtedly were more successfully employed in this mechanistic paradigm are terminal alkynes. Several studies were focused on photophysics of monomeric or high-nuclearity Cu(I) alkynide complexes.¹⁹ Cu(I) acetylide complexes, indeed, exhibit long-lived intense phosphorescence both in the solid state and solution. The origin of the emission has been proposed to involve substantial ligand-to-metal charge

¹⁷ Lei, W.-L.; Wang, T.; Feng, K.-W.; Wu, L.-Z.; Liu, Q. *ACS Catal.* **2017**, *7*, 7941-7945.

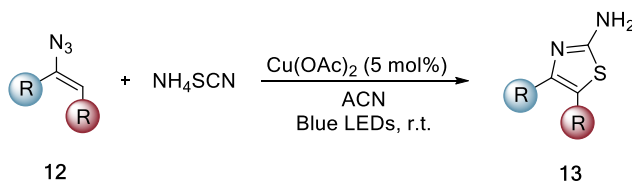
¹⁸ Meng, Q.-Y.; Gao, X.-W.; Lei, T.; Liu, Z.; Zhan, F.; Li, Z.-J.; Zhong, J.-J.; Xiao, H.; Feng, K.; Chen, B.; Tao, Y.; Tung, C.-H.; Wu, L.-Z. *Sci. Adv.* **2017**, *3*, e1700666.

¹⁹ a) Yam, V. W. -W.; Lee, W. K.; Lai, T. F. *Organometallics* **1993**, *12*, 2383-2387; (b) Yam, V. W.-W.; Lee, W.-K.; Cheung, K. K.; Lee, H.-K.; Leung, W.-P. *J. Chem. Soc. Dalton Trans.* **1996**, 2889-2891; c) Yam, V. W.-W.; Lo, K. K.-W.; Wong, K. M.-C. *J. Organomet. Chem.* **1999**, *578*, 3-30.

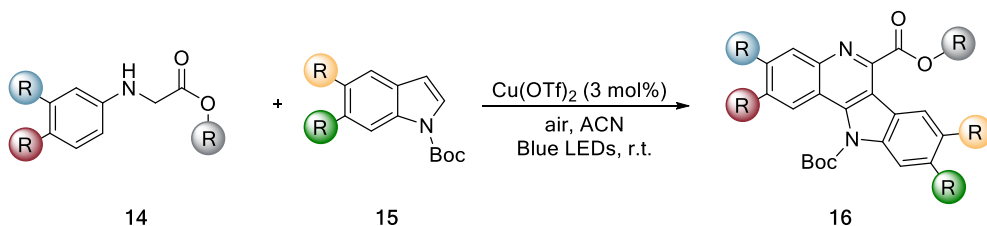
Decarboxylative hydroalkylation of alkynes

transfer (LMCT) [acetylide \rightarrow Cu_n] character. These π d states arise from the transfer of electronic charge from the ligand π system to a metal centered orbital. However, in view of the short Cu–Cu distances in polynuclear complexes, it is likely that the lowest-lying emissive state is mixed with some metal-centered 3d⁹4s¹ state.

a) Liu, 2017



b) Wu, 2017



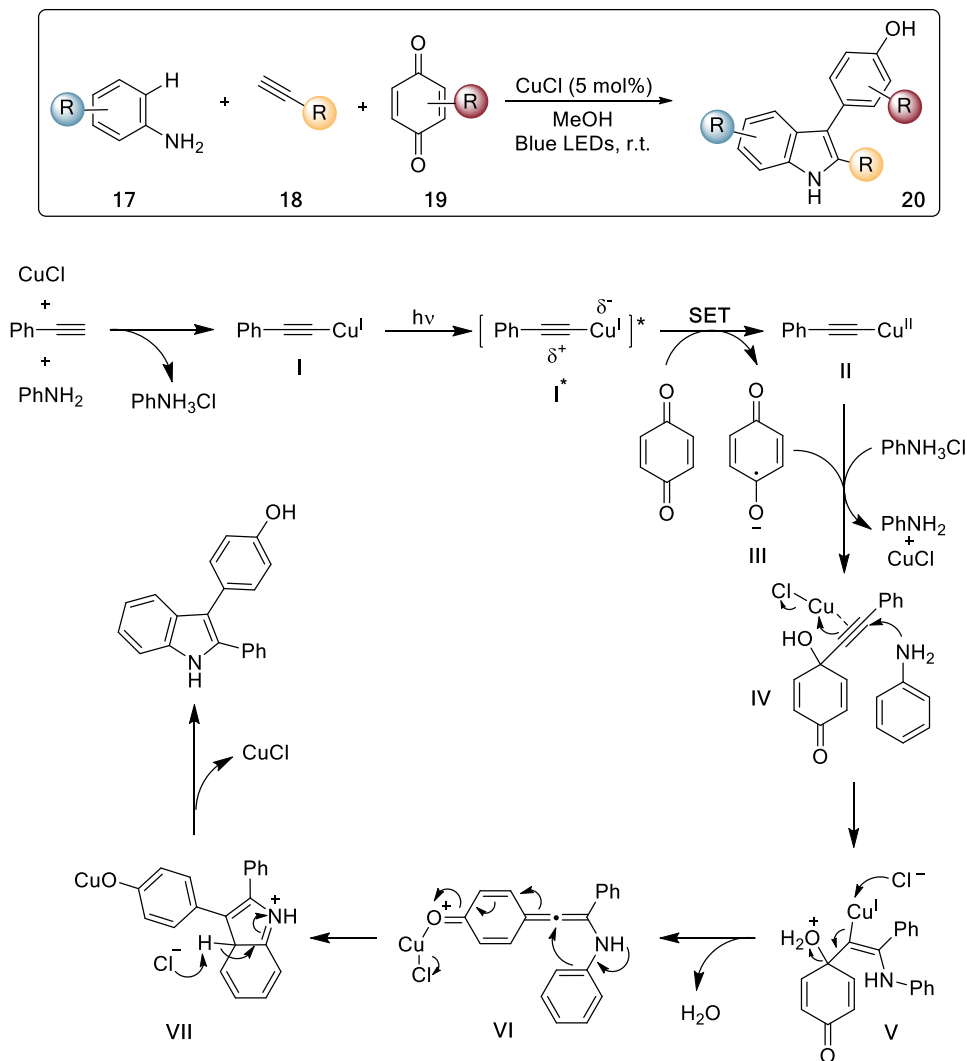
Scheme III-3. a) Visible-light driven synthesis of 4-alkyl/aryl-2-aminothiazoles promoted by *in situ* generated copper photocatalyst; b) Cu(II) salt-catalyzed C-H activation of secondary aromatic amines under visible light irradiation.

Moreover, Cu(I) acetylide complexes have been found to exhibit rich photoredox properties, as exemplified by the quenching of the low-energy phosphorescence of Cu(I) alkynyls by pyridinium ions.²⁰ This process happens through an outer-sphere oxidative electron transfer mechanism and has been widely exploited by the Hwang group.²¹

²⁰ a) V.W.-W. Yam, *Acc. Chem. Res.* **2002**, *35*, 555-563; b) Yam, V.W.-W.; Lee, W.-K.; Cheung, K.-K.; Crystall, B.; Phillips, *J. Chem. Soc. Dalton Trans.* **1996**, 3283-3287.

²¹ a) Sagadevan, A.; Hwang, K. C. *Adv. Synth. Catal.* **2012**, *354*, 3421-3427; b) Sagadevan, A.; Ragupathi, A.; Lin, C.-C.; Hwu, J. R.; Hwang, K. C. *Green Chem.* **2015**, *17*, 1113-1119; c) Sagadevan, A.; Charpe, V. P.; Ragupathi, A.; Hwang, K. C. *J. Am. Chem. Soc.* **2017**, *139*, 2896-2899; d) Charpe, V. P.; Hande, A. A.; Sagadevan, A.; Hwang, K. C. *Green Chem.* **2018**, *20*, 4859-4864; e) Das, D. K.; Pampana, V. K. K.; Hwang, K. C. *Chem. Sci.* **2018**, *9*,

An example of application of the ability of Cu(I) acetylides to act as excited-state single-electron reductants has been reported in 2015 and is depicted in Scheme III-4.²²



Scheme III-4. Photoinduced copper-catalyzed regioselective synthesis of indoles.

7318-7326; f) Sagadevan, A.; Pampana, V. K. K.; Hwang, K. C. *Copper* *Angew. Chem. Int. Ed.* **2019**, *58*, 3838-3842; g) Pampana, V. K. K.; Sagadevan, A.; Ragupathiand, A.; Hwang, K. C. *Green Chem.* **2020**, *22*, 1164-1170.

²² Sagadevan, A.; Ragupathi, A.; Hwang, K. C. *Angew. Chem. Int. Ed.* **2015**, *54*, 13896-13901.

Decarboxylative hydroalkylation of alkynes

Under blue LEDs irradiation, a three-component coupling of anilines (**17**), terminal alkynes (**18**) and benzoquinones (**19**), affording functionalized indoles (**20**), was accomplished. Irradiation of the *in situ* generated complex I produces the long-lived triplet photoexcited I^* ($\tau = 15.95 \mu\text{s}$) by LMCT. Subsequent reduction of benzoquinone to III produces Cu(II) phenylacetylide (II). Then, radical anion III attacks II regenerating Cu(I) catalyst and Cu(I)-coordinated alkyne complex IV. This species then undergoes nucleophilic attack by aniline providing complex V and sequentially VI. Friedel-Crafts-type cyclization of VI delivers intermediate VII that, upon re-aromatization, evolves into the desired product.

III.2. Objective

Despite the tremendous progress in the field of visible-light photoredox catalysis, direct addition of electron-rich alkyl radical to alkynes has been underexploited due to unfavorable kinetics and lack of control on the fate of the so generated vinyl radical. State of the art synthetic methodologies rely upon the use of prefunctionalized sources of alkyl radicals or expensive Ir-based photocatalysts. Moreover, in all of these reports the stereochemical outcome of the reaction (double bond configuration) is unidirectionally determined by the relative ability of the photocatalyst to perform *E/Z* isomerization, *i.e.* alkyl-substituted olefins are obtained as *E* enriched mixture while aryl-substituted ones are obtained mainly in *Z* enriched form.

The first challenge associated with the development of radical hydroalkylation of terminal alkynes stands in the low kinetic constants intrinsically associated with the addition of nucleophilic radicals to C–C triple bonds. However, it has been observed that for alkynes bearing an electron-

withdrawing group rate constant are generally higher, due to an increase of polar effects contribution (Figure III-4).²³

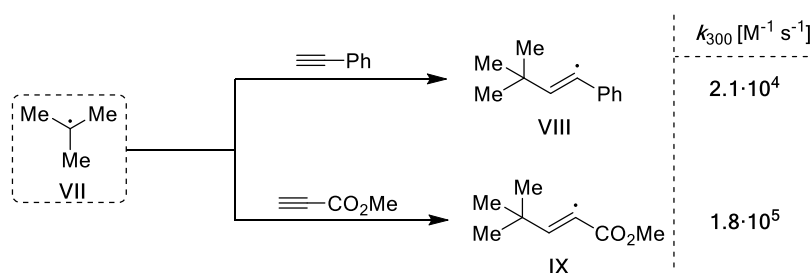


Figure III-4. Rate constants (at 300 K) for the addition of Me_3C radical to alkynes in 1,2-epoxypropane.

We wondered if electron-rich alkynes could be activated towards radical addition enhancing polar effects but in a catalytic and traceless fashion. Our strategy to address this synthetic challenge is based on the perturbation of the ground-state electronic properties of terminal alkynes through the formation and photoexcitation of the corresponding copper acetylides. The irradiation of copper acetylides with visible light, in fact, results in a ligand-to-metal charge transfer (LMCT) increasing the electrophilicity on the alkyne moiety.

Next, we turned our attention to more practical aspects of the transformation. Since the first stages of reaction planning, we chose to develop an economical advantageous and green process. In order to do so, cheap and abundant carboxylic acids were chosen as alkyl radical precursors²⁴ in the framework of organic photocatalysis.

Therefore, the final aim of the project is to develop a dual copper and photoredox catalyzed decarboxylative hydroalkylation of terminal alkynes from carboxylic acid as radical sources and an organic photocatalyst.

²³ Rubin, H.; Fischer, H. *Helv. Chim. Acta* **1996**, *79*, 1670-1682.

²⁴ a) Xuan, J.; Zhang, Z.-G.; Xiao, W.-J. *Angew. Chem. Int. Ed.* **2015**, *54*, 15632-15641; b) Jin Y.; Fu, H. *Asian J. Org. Chem.* **2017**, *6*, 368-385.

Decarboxylative hydroalkylation of alkynes

III.3. Dual Cu-photoredox catalyzed hydroalkylation of alkynes

III.3.1. HTE screening and control experiments

Considering all the variables involved in the designed process, we considered a multivariate high-throughput experimentation (HTE) approach to screen the ligand, base, copper source and solvent in a rapid and cost-effective manner (Figure III-5).²⁵ We chose *N*-Boc proline (**1a**) and phenylacetylene (**2a**) as model substrates, and 4CzIPN²⁶ as a photocatalyst. It emerged that the best results in terms of yield and *Z:E* ratio were achieved employing either CuOAc or Cu(OAc)₂, (1*R*,2*R*)-*trans*-1,2-diaminocyclohexane (**L1**) as ligand²⁷ and CsOAc as base under blue LEDs irradiation for 18 hours (wells A9 and E9, Figure III-5). Translation of the optimal conditions to synthetically relevant scale allowed us to isolate the desired product (**3a**) in 82% yield with a *Z:E* ratio of 78:22. Moreover, the HTE screening also revealed that the reaction can be performed in a diastereodivergent manner just by switching the ligand and the base to oleylamine (**L4**) and CsHCO₃ (wells A8 and E8, Figure 1). The *E* isomer is preferentially obtained under these conditions with minimal erosion of the yield (Entry 2, Table III-1). The choice of the ligand turned out to be key for the stereoselectivity switch, since the combination of **L4** and CsOAc also provided **3a** as an *E*-enriched product (wells A12 and E12, Figure 1).

²⁵ The project discussed in this Chapter has been conducted in collaboration with Dr. Santiago Cañellas and Dr. Xisco Caldentey.

²⁶ a) Luo, J.; Zhang, J. *ACS Catal.* **2016**, *6*, 873-877; b) Speckmeier, E.; Fischer, T.G.; Zeitler, K. *J. Am. Chem. Soc.* **2018**, *140*, 15353-15365; c) Shang, T.-Y.; Lu, L.-H.; Cao, Z.; Liu, Y.; He, W.-M.; Yu, B. *Chem. Commun.* **2019**, *55*, 5408-5419. d) Note: this reaction also works with metal-based photocatalysts such as [IrdF(CF₃)ppy₂(dtbpy)]PF₆.

²⁷ The reaction works identically with racemic *trans*-1,2-diaminocyclohexane. The reaction product (**3a**) is obtained in racemic form, as it is the case for all products in Figure III-5 derived from carboxylic acids containing a single stereocenter α to the carboxy group.

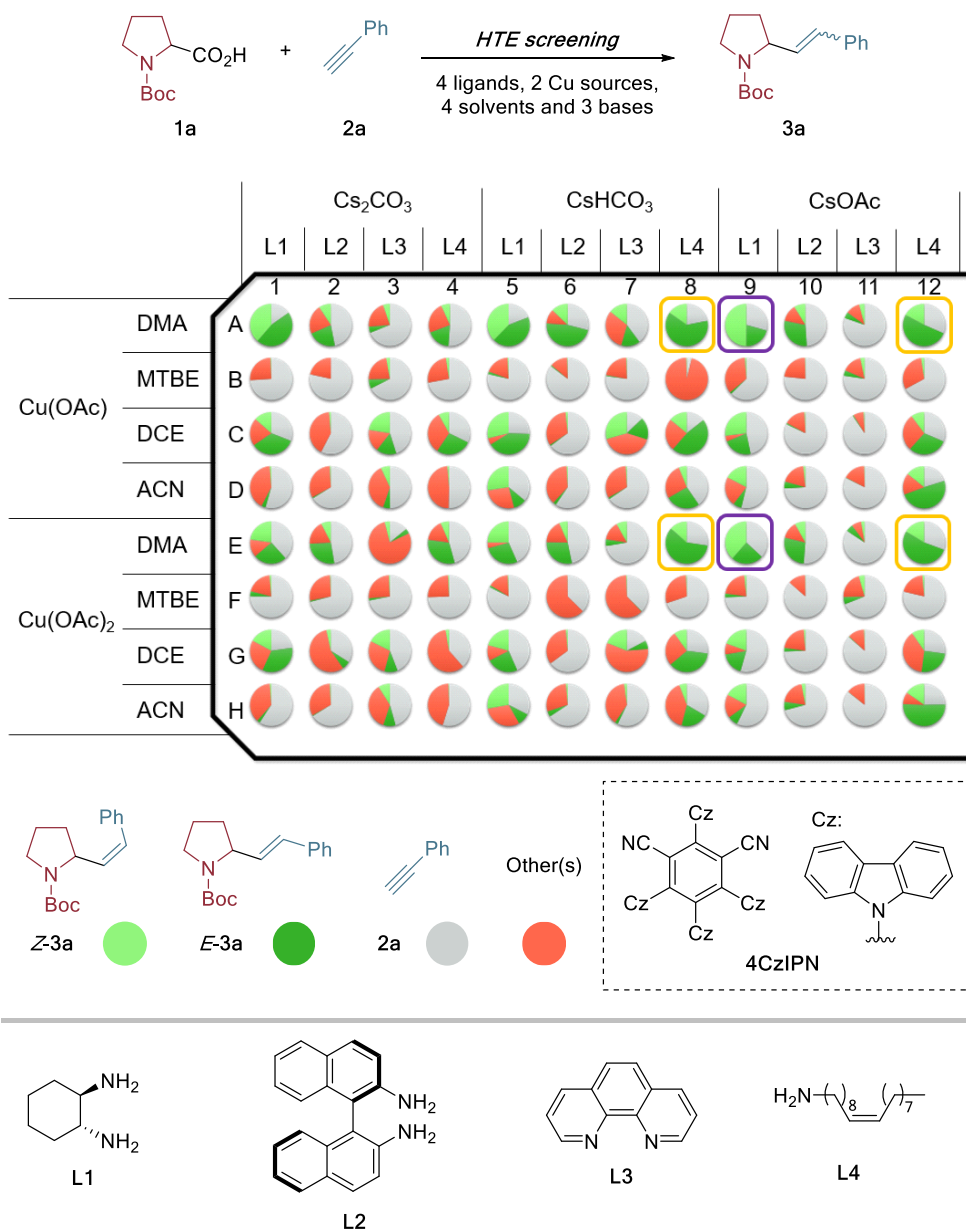


Figure III-5. Multivariate-HTE screening of solvents, bases, ligands and copper sources for the hydroalkylation of **2a** under standard conditions [**1a** (15 μ mol), **2a** (10 μ mol), Base (20 μ mol), Copper Source (2 μ mol), Ligand (4 μ mol if monodentate, 2 μ mol if bidentate), 4CzIPN (0.25 μ mol), solvent (0.1 mL), blue LEDs irradiation, room temperature, 18 hours]. Yields (%) and (*Z*:*E*) ratios [GC-FID analysis on the reaction crude using 1,1'-biphenyl as internal standard] for selected entries: **A8**: 79% (20:80), **A9**: 71% (71:29), **A12**: 69% (25:75), **E8**: 73% (19:81), **E9**: 71% (63:39), **E12**: 71% (23:77).

Decarboxylative hydroalkylation of alkynes

Control experiments showed that copper, photocatalyst and light are fundamental for the reaction efficiency (entries 3, 4, 6 and 7, Table III-1) and the nature of the ligand²⁸ is important for the selectivity of the transformation (entries 2 and 5, Table III-1). Interestingly, work at 3 mmol scale (entry 8) is well tolerated.



Entry	Deviation from standard conditions ^[a]	Yield (%) ^[b]	Z:E ^[c]
1	None	82	78:22
2	L4 (40 mol%) instead of L1 . CsHCO ₃ instead of CsOAc ^[d]	72	23:77
3	No Cu(OAc) ₂	19	78:22
4	CuCl instead of Cu(OAc) ₂	78	77:23
5	No L1	58	69:31
6	No photocatalyst	0	n.d.
7	Dark	0	n.d.
8	3 mmol scale	76	67:33

Table III-1. ^[a]Standard conditions: **1a** (0.3 mmol), **2a** (0.2 mmol), CsOAc (0.4 mmol), DMA (2.0 mL), blue LEDs (4.5 W, Irradiation Setup 1 - See Section III.4.2).

^[b]Isolated yield. ^[c]Determined by GC-FID analysis on the reaction crude. ^[d]36 hours, Irradiation Setup 2 (see Section III.4.2).

III.3.2. Reaction scope

The scope of this transformation was next investigated under the optimal reaction conditions (Figure III-6,7).

²⁸ Hazra, A.; Lee, M. T.; Chiu, J. F.; Lalic G. *Angew. Chem. Int. Ed.* **2018**, *57*, 5492-5496.

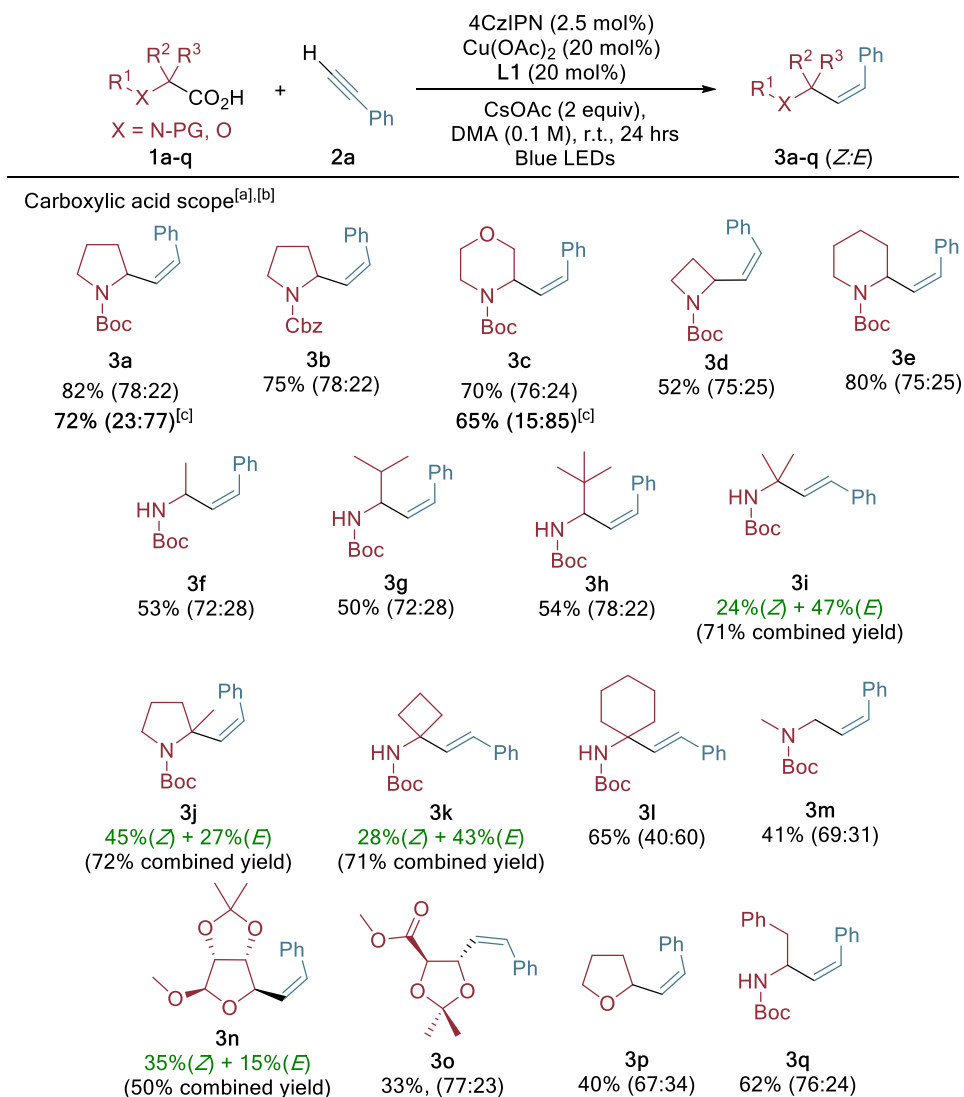


Figure III-6. Carboxylic acid scope in the copper/photoredox catalyzed hydroalkylation of alkynes. All yields shown refer to isolated products. ^[a]Reactions performed with carboxylic acid (0.3 mmol), alkyne (0.2 mmol), CsOAc (0.4 mmol), DMA (2.0 mL), blue LEDs (4.5 W). ^[b]Z:E ratios determined by GC-FID on the reaction crude. Compounds isolated as pure stereoisomers contained <1% of the alternative geometrical isomer. ^[c]Results in boldface refer to reaction conditions favoring *E* selectivity: **L4** (40 mol%) instead of **L1**, CsHCO₃ instead of CsOAc.

Sources of primary, secondary, tertiary α -amino radicals as well as secondary α -oxy radicals were tested in the *Z*-selective coupling. In all

Decarboxylative hydroalkylation of alkynes

cases the desired products were isolated in synthetically useful yields ranging from moderate to good. It is worth mentioning that the standard purification procedure by flash chromatography affords in some instances completely separated *Z/E* stereoisomers. These results have been highlighted in green in Figure III-6 and III-7. For comparison purposes, the combined yield is also given in these cases. As a general trend, a clear selectivity towards the *Z* isomer is recorded except for the reactions in which a quaternary carbon is formed: in these circumstances (with the notable exception of **3j**) the selectivity is reversed in favor of the *E* isomer likely because of steric factors. In the two cases where stereocenters with defined configuration were already present in the carboxylic acids, the corresponding products (**3n** and **3o**) were isolated with very high diastereoselectivity (**3n** >20:1; **3o** >12:1). In the exploration of the scope of the alkyne partner we first examined terminal phenylacetylenes bearing electron withdrawing and electron donating groups in *ortho* or *para* position. In the case of electron-rich aromatic rings, a reverse stoichiometry of both coupling partners was needed in order to achieve good yields. Besides this, all products were obtained in good yields regardless of the nature and position of the substituents (Figure III-7). Also, more challenging heteroaromatic alkynes could be employed in the reaction (**4j-l**) as well as an enyne (**4m**), albeit the reaction took place in this case with moderate yield and *E* selectivity. Other non-conjugated alkynes (1-hexyne and *tert*-butyldimethylsilylacetylene) turned out to be unsuitable substrates for this transformation and failed to afford the corresponding decarboxylative hydroalkylation products. We then tested on selected substrates (**3a**, **3c**, **4b** and **4i**) the applicability of the stereo-complementary approach. Notably, all of them were obtained in good yields and *E*-selectivities.

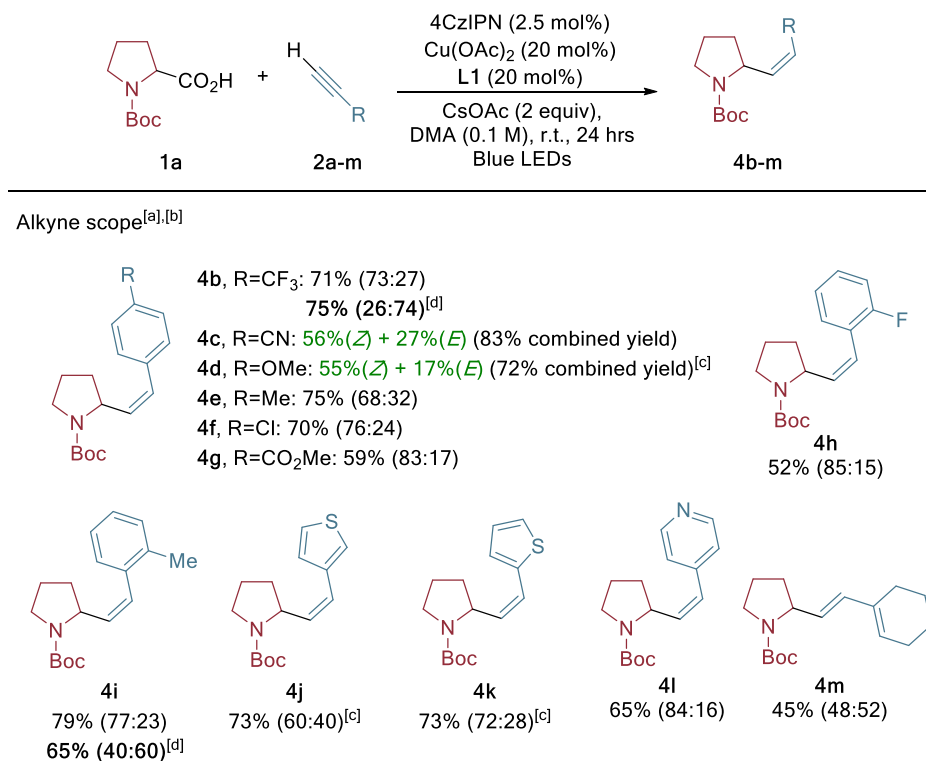


Figure III-7. Alkyne scope in the copper/photoredox catalyzed hydroalkylation of alkynes. All yields shown refer to isolated products. ^[a]Reactions performed with carboxylic acid (0.3 mmol), alkyne (0.2 mmol), CsOAc (0.4 mmol), DMA (2.0 mL), blue LEDs (4.5 W). ^[b]*Z*:*E* ratios determined by GC-FID on the reaction crude.

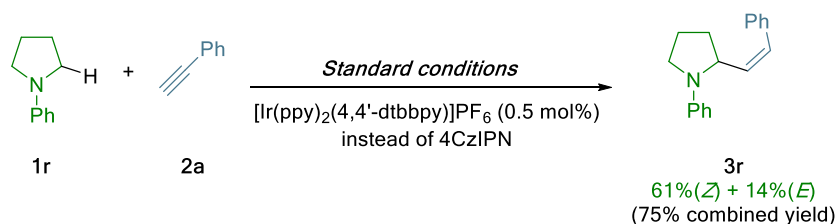
Compounds isolated as pure stereoisomers contained <1% of the alternative geometrical isomer. ^[c]Reactions performed with carboxylic acid (0.2 mmol), alkyne (0.7 mmol). ^[d]Results in boldface refer to reaction conditions favoring *E* selectivity: **L4** (40 mol%) instead of **L1**, CsHCO₃ instead of CsOAc.

Then, we tested the developed methodology in the direct vinylation of inactivated C–H bonds. Upon single-electron oxidation and deprotonation, aromatic amines generate the corresponding α -amino radicals,²⁹ that could be trapped by the excited copper acetylide complex thus forging a new C–C bond. However, when we tested the feasibility of the transformation using the optimized conditions to the cross dehydrogenative coupling between **1r** and **2a**, we were unable to achieve satisfactory results. Fortunately, a

²⁹ Hu, J.; Wang, J.; Nguyen, T. H.; Zheng, N. *Beilstein J. Org. Chem.* **2013**, *9*, 1977-2001.

Decarboxylative hydroalkylation of alkynes

second HTE screening of photocatalysts and bases (See Section III.4.4 for further details) revealed that switching from 4CzIPN to $[\text{Ir}(\text{ppy})_2(4,4'\text{-dtbbpy})]\text{PF}_6$, the formation of **3r** could be achieved in good yield (75%) and high *Z*-selectivity (82:18) (Scheme III-5)



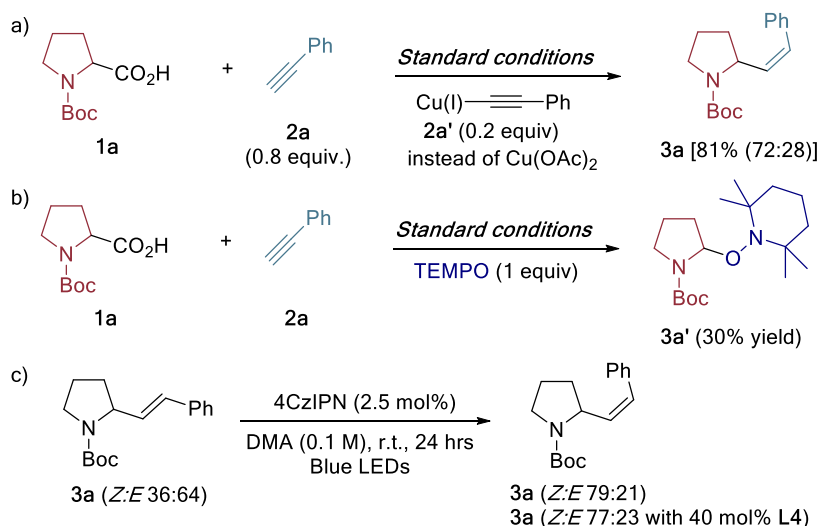
Scheme III-5. Cross dehydrogenative coupling between **1r** and **2a** allowing the vinylation of inactivated C-H bonds.

From a synthetic perspective, it is important to note that simple stereoconvergent transformations of **3-4**, such as the selective hydrogenation of the double bond would result in products formally arising from a very general decarboxylative hydroxyalkylation of alkenes, a process being actively developed these days.³⁰

III.3.3. Mechanistic investigation

Next, we performed a series of experiments aimed at shedding light on key mechanistic aspects of this transformation. First, we questioned whether Cu(I) phenylacetylide (**2a'**) is an active intermediate in the reaction. To examine this hypothesis, we conducted the reaction under the standard conditions replacing $\text{Cu}(\text{OAc})_2$ with 0.2 equiv. of **2a'** and reducing the amount of phenylacetylene to 0.8 equiv. (Scheme III-6, a).

³⁰ a) Green, S. A.; Huffman, T. R.; McCourt, R. O.; van der Puyl, V.; Shenvi, R. A. *J. Am. Chem. Soc.* **2019**, *141*, 7709-7714; b) He, S.-J.; Wang, J.-W.; Li, Y.; Xu, Z.-Y.; Wang, X.-X.; Lu, X.; Fu, Y. *J. Am. Chem. Soc.* **2020**, *142*, 214-221.



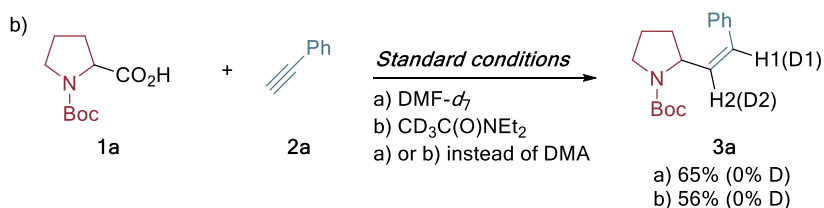
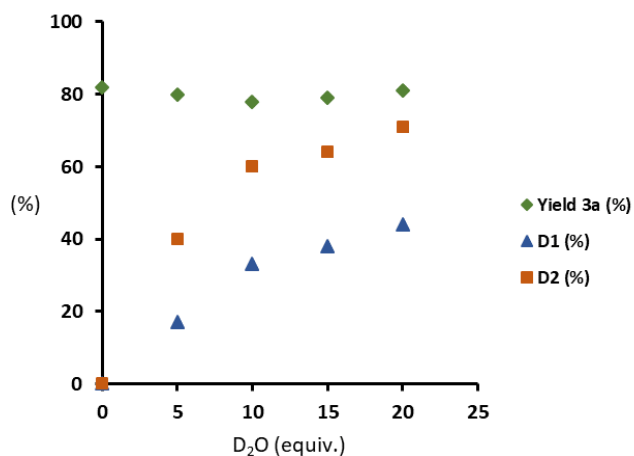
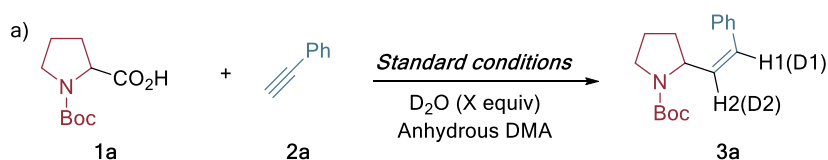
Scheme III-6. Mechanistic experiments.

The corresponding product **3a** was obtained in similar yield and *Z*-selectivity, supporting the intermediacy of Cu(I)-phenylacetylide. On the other hand, the addition of TEMPO (1 equiv.) completely quenches the reaction (Scheme III-6, b) and yields **3a'** indicating the involvement of α -amino/oxy radical intermediates in the transformation. Then, an *E*-enriched mixture of **3a** (0.1 M in DMA) was irradiated for 24 hours in the presence of 4CzIPN (2.5 mol%) being isomerized to the same *Z*:*E* value of the model reaction. This experiment suggests that the *E*/*Z* selectivity of the reaction arises from an energy transfer process mediated by the photocatalyst (Scheme III-6, c). The same result was obtained adding **L4** (40 mol%) to the mixture, excluding that the *E* selectivity arises from quenching of the excited state of 4CzIPN exerted by the double bond present in the ligand.

Finally, we investigated the source of vinylic hydrogens in the final product and consequently the process involved in their incorporation. To do so, we designed experiments choosing deuterated compounds able to exchange deuterium *via* a polar or a radical process (deuterium atom abstraction). We selected deuterium oxide as deuterons exchanger and performed the model

Decarboxylative hydroalkylation of alkynes

reaction adding increasingly larger amounts of D₂O. These experiments showed that there is a correlation between the amount of D₂O and the incorporation of deuterium in both positions of the double bond (Scheme III-7, a). On the other hand, experiments using other deuterated solvents such as DMF-*d*₇ and *N,N*-diethylacetamide-*d*₃ (chosen as deuterium atoms donors) furnished the desired product with no significant deuterium incorporation (Scheme III-7, b).



Scheme III-7. Deuterium labeling experiments.

Taking all these results into account, the tentative mechanistic proposal shown in Scheme III-8 was formulated. Upon irradiation, the photocatalyst 4CzIPN can reach its excited state PC^* ($E_{1/2} \text{PC}^*/\text{PC}^* = -1.04 \text{ V vs SCE}$ and $E_{1/2} \text{PC}^*/\text{PC}^- = +1.35 \text{ V vs SCE}$)²⁵ and it is able to reduce the Cu(II) complexes present in solution (e.g., $E_{1/2} \text{Cu(II)/Cu(I)} = -0.363 \text{ V vs SCE}$ for $[\text{Cu(L1)}_2](\text{ClO}_4)_2$)³¹ as well as to oxidize α -amino and α -oxy carboxylates (e.g., Boc-Pro-OCs, $E_{1/2}^{\text{ox}} = +0.95 \text{ V vs SCE}$).³² Stern-Volmer studies indicate that the reductive quenching of the catalyst exerted by the Boc-Pro-OCs is faster ($K_{\text{SV}} = 2.9 \cdot 10^{-2} \text{ M}^{-1}$) than the one exerted by $[\text{Cu(L1)}_2](\text{OAc})_2$ ($K_{\text{SV}} = 1.4 \cdot 10^{-2} \text{ M}^{-1}$).³³ The Cu(I) complex generated either by disproportionation of the Cu(II) source or SET by PC^* (or PC^- [$\text{PC}/\text{PC}^- = -1.21 \text{ V vs SCE}$]) can form complex I (the structure of I might be either a monomeric or a polymeric form or both) with the assistance of a base (CsOAc).³⁴ Direct photoexcitation of I ($\lambda_{\text{abs}} = 476 \text{ nm}$ for Cu(I) phenylacetylide)³³ to I^* could determine a depletion of charge on the alkyne moiety through ligand-to-metal charge transfer (LMCT), accelerating the attack of the radical IV (formed upon deprotonation and single electron oxidation of **1a** either by PC^* or PC^+ [$\text{PC}^+/\text{PC} = +1.52 \text{ V vs SCE}$]). This addition results in the formation of the vinyl radical II which forms the corresponding vinyl anion III oxidizing PC^- . Anion protonation and proto-demetalation of the Cu–C bond afford the desired product **3a**, regenerating the Cu(I) species. Taking into account the outcome of the *E*-selective methodology, and the control experiment previously shown, it is reasonable to assume that the product is formed as an *E*-enriched mixture and then is

³¹ Sureshbabu, P.; Tjakraatmadja, A. A. J. S.; Hanmandlu, C.; Elavarasan, K.; Kulak, N.; Sabiah, S. *RSC Adv.* **2015**, *5*, 22405-22418. A correction of -0.045 has been applied to the potential given in this manuscript, referred to Ag/AgCl. Excited Cu(I)-acetylides, albeit present in low concentration, could also play a role as reductants in the catalytic cycle due to its long lifetime and high reducing potential ($E_{1/2} = -1.77 \text{ V vs SCE}$). See ref. 18.

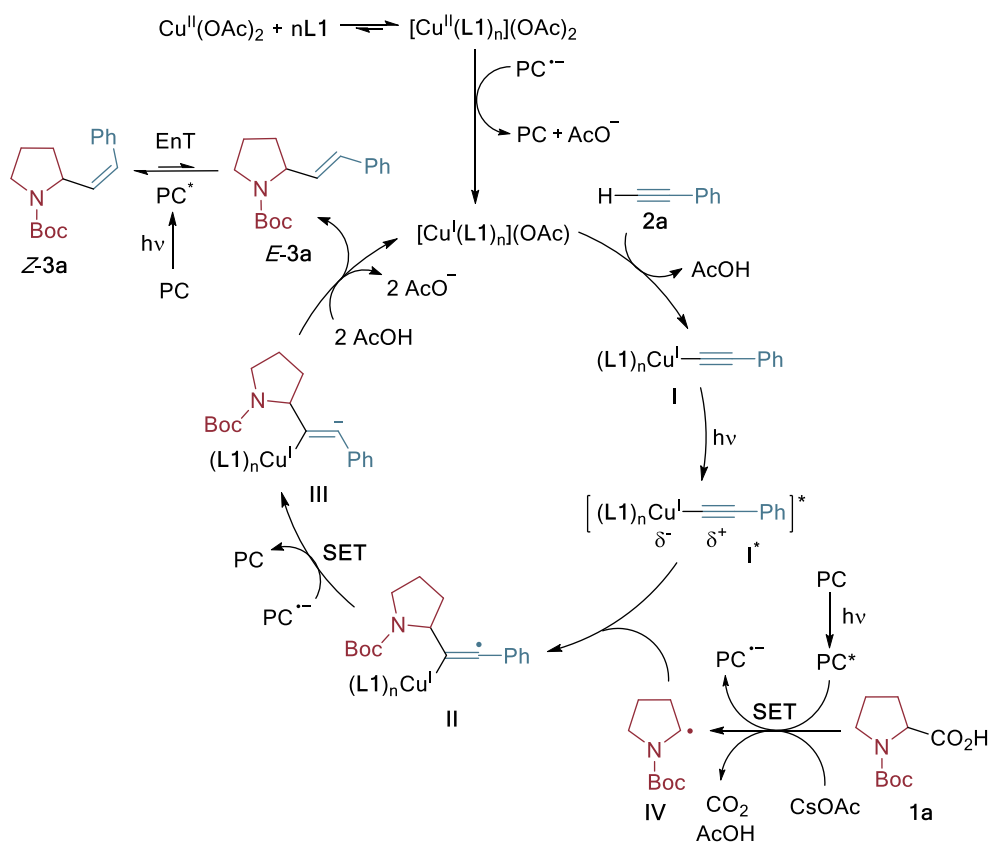
³² Zuo, Z.; MacMillan, D. W. C. *J. Am. Chem. Soc.* **2014**, *136*, 5257-5260.

³³ See Section III.4.3.5.

³⁴ I can also be formed in presence of Cu(I) species under visible light irradiation without the assistance of a base, see: Sagadevan, A.; Charpe, V. P.; Hwang, K. C. *Catal. Sci. Technol.* **2016**, *6*, 7688-7692.

Decarboxylative hydroalkylation of alkynes

isomerized *via* energy transfer (E_T (4CzIPN) = 60 kcal·mol⁻¹)²⁵ mediated by the photocatalyst.



Scheme III-8. Proposed reaction mechanism.

III.3.4. Conclusions

In summary, we have developed a catalytic method for intermolecular hydroalkylation of terminal alkynes with carboxylic acids. The use of a widely available and stable copper-based catalyst allows the overcoming of the intrinsic kinetic barrier associated with the addition of radicals to triple bonds. At the same time, this transformation exploits the ability of an organic photocatalyst to generate alkyl radicals from *in situ* generated carboxylates

and isomerize the formed alkene to the less stable *Z* isomer. In this work, HTE screening of reaction conditions revealed that the proper choice of copper ligand and base makes possible the selective shutdown of the latter process without compromising the efficiency of the former one, thereby paving the way to the stereodivergency of the reaction. These aspects, along with the low cost and abundance of the starting materials as well as catalysts, suggest that this synthetic methodology can complement other photoredox hydroalkylation reactions of alkynes relying upon the use of iridium catalysts and prefunctionalized substrates.

Decarboxylative hydroalkylation of alkynes

III.4. Supporting Information

III.4.1. Table of contents

III.4.2. General information	181
III.4.3. Mechanistic investigation	184
III.4.3.1. Copper-acetylide intermediacy test	184
III.4.3.2. Radical trapping experiment	184
III.4.3.3. Alkene isomerization experiments	186
III.4.3.4. Deuterium labeling experiment	188
III.4.3.5. Stern-Volmer fluorescence quenching studies	191
III.4.4. High-Throughput experimentation	196
III.4.5. Experimental procedures	199
III.4.6. Product characterization	203
III.4.7. References	222

III.4.2. General information

If not specified, all reagents were purchased and used without any further purification. The reaction progress was checked by thin layer chromatography (TLC). Therefore aluminium-foil backed silica TLC plates with a fluorescent indicator (TLC Silica gel 60 F254) from Merck were used. Compounds were detected either with a UV lamp ($\lambda = 254$ nm) or by employing a p-anisaldehyde stain in sulfuric acid, acetic acid and ethanol. For column chromatography, Aldrich flash grade silica gel (230-400 mesh) was used as a stationary phase. UV-Vis measurements were carried out on a Shimadzu UV-2401PC spectrophotometer equipped with a photomultiplier detector, double beam optics and D2 and W light sources.

Fluorescence measurements were carried out on a Fluorolog Horiba Jobin Yvon spectrofluorimeter equipped with photomultiplier detector, double monochromator and Xenon light source.

High-resolution mass spectra (HRMS) was carried out using High Resolution Mass Spectrometry on Waters GCT gas chromatograph coupled time-of-flight mass spectrometer (GC/MS-TOF) with electron ionization (EI).

GC/FID analysis was conducted on an Agilent GC (model 7890N) equipped with an Agilent GC injector 80. (Column used: Zebron ZB-5MS-plus column (30.0 m x 250.0 μm x 0.25 μm)).

NMR spectra were recorded at 25 °C on a Bruker Avance 400 or Bruker Avance 500 Ultrashield for ^1H NMR, 101 or 126 MHz for ^{13}C NMR in CDCl_3 , having the solvent resonance as internal standard. The chemical shifts (δ) were given in ppm and the coupling constants (J) are reported in Hz. Multiplicities were abbreviated by s (singlet), bs (broad singlet), d (doublet), t (triplet), m (multiplet), bm (broad multiplet). All products that are known were characterized by comparison of their physical and spectroscopic properties with those described in the literature.

Decarboxylative hydroalkylation of alkynes

4CzIPN¹ and [Cu(L1)₂](OAc)₂² have been prepared following reported procedures. The characterization data are matching with those reported.

Irradiation setup 1: *Z*-selective reactions: a five single blue LEDs photoreactor has been used (Figure III-8). The overall setup allows for the simultaneous irradiation of five 10 mL reaction vessels under magnetic stirring at constant temperature (internal measured temperature of 25°C). The measured emission intensity of the blue LEDs at 700 mA is 75 mW/cm². The typical relative spectral power vs. wavelength graph is depicted in Chart 1. LEDs were purchased from Digi-Key. (https://www.digikey.com/products/en?WT.z_cid=sp_1537_buynow&site=us&mpart=LZ4-40B208-0000)

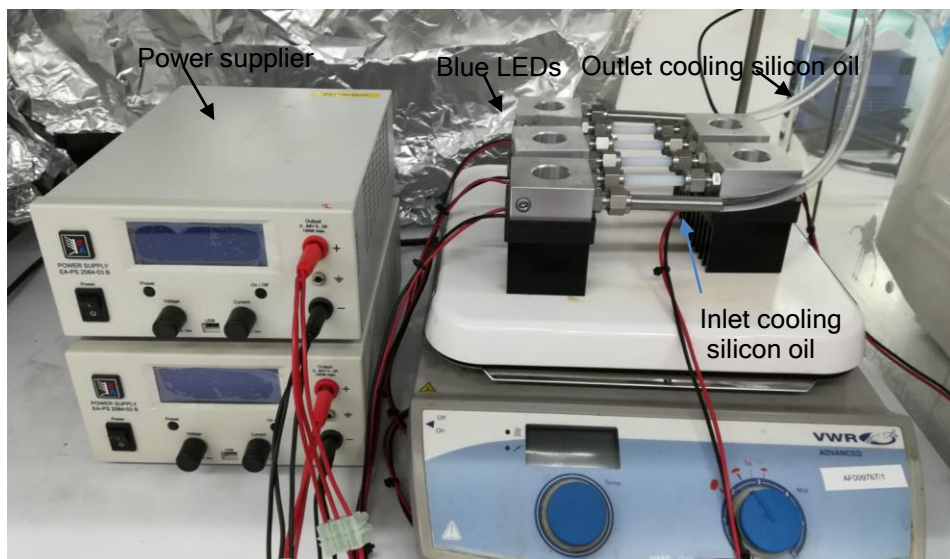


Figure III-8. Irradiation setup 1 used in the *Z*-selective decarboxylative hydroalkylation of Alkynes

Irradiation setup 2: *E*-selective reactions: a 96 single LEDs plate photoreactor has been used (Figure III-9). Reaction tubes are placed at 1 cm of distance from the light source and kept under magnetic stirring. A fan

ensures the cooling of the reaction mixture at room temperature (internal measured temperature of 27°C). The measured emission intensity (at the external wall of the reaction tube) of the blue LEDs at 250 mA is 15 mW/cm². LEDs were purchased from Farnell ([https://es.farnell.com/multicomp/mcl053sb1c/led-5-mm-azul-2-5cd-472nm/dp/1581185?scope=partnumberlookahead&ost=1581185&searchref=searchlookahead&exaMfpn=true&ddkey=https%3Aes-ES%2FElement14 Spain%2Fw%2Fsearch](https://es.farnell.com/multicomp/mcl053sb1c/led-5-mm-azul-2-5cd-472nm/dp/1581185?scope=partnumberlookahead&ost=1581185&searchref=searchlookahead&exaMfpn=true&ddkey=https%3Aes-ES%2FElement14%20Spain%2Fw%2Fsearch))

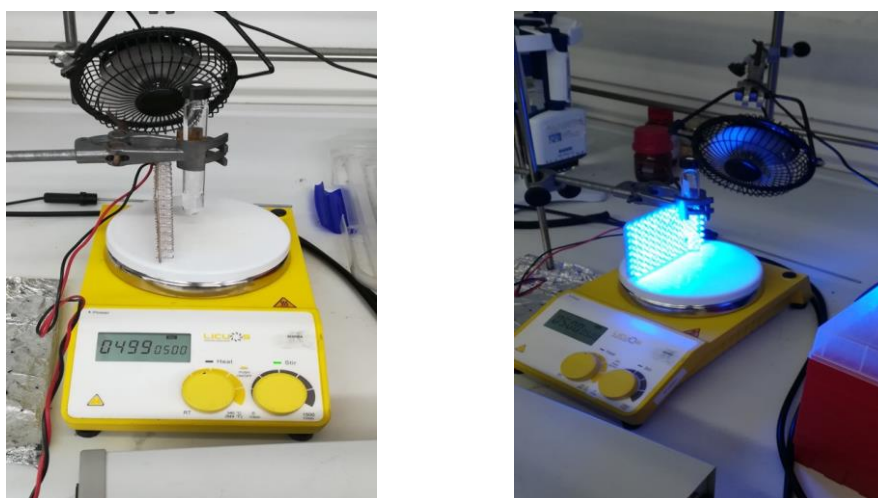
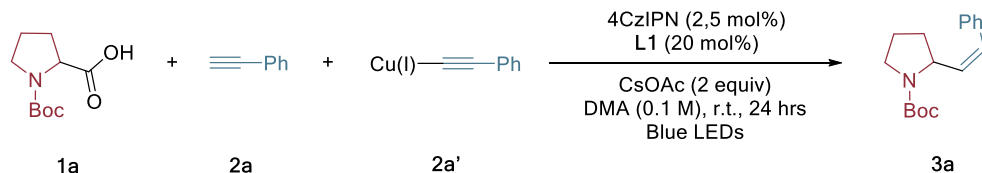


Figure III-9. Irradiation Setup 2 used in the *E*-selective Decarboxylative Hydroalkylation of Alkynes

Decarboxylative hydroalkylation of alkynes

III.4.3. Mechanistic investigation

III.4.3.1. Copper-acetylide intermediacy test



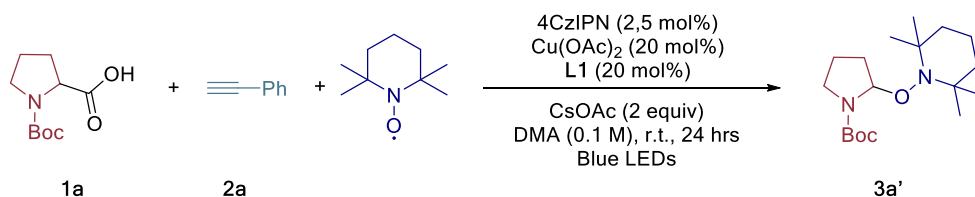
Scheme III-9. Cu(I) phenylacetylide intermediacy tests

In a N₂-filled glovebox, **1a** (0.3 mmol, 65 mg) was mixed in a 10 mL vial with CsOAc (0.4 mmol, 77 mg), (1*R*,2*R*)-cyclohexane-1,2-diamine (**L1**) (0.04 mmol, 4.6 mg), 4CzIPN (0.005 mmol, 3.9 mg), **2a'** (0.04 mmol, 6.6 mg) and **2a** (0.16 mmol, 16.0 mg, 17 μL). Then the vial was sealed and taken out the glovebox. After adding degassed DMA (2.0 mL), the mixture was stirred under blue LEDs irradiation for 24 hours (setup depicted in Figure III-8) at room temperature. Afterwards, the vial was opened (three drops of the reaction mixture were taken and used for the GC-FID *Z:E* ratio determination: *Z:E* 72:28), 15.0 mL of EtOAc were added and the mixture was washed with water three times (3 x 10 mL) and brine (10 mL). The separated organic phase was then dried over MgSO₄, filtered and concentrated under vacuum. The desired product was purified by silica gel (previously neutralized with NEt₃ 2.5% w/w) column chromatography (DCM/Petroleum ether 0% to 100%) and isolated in 81% yield.

III.4.3.2. Radical trapping experiment

In a N₂-filled glovebox, **1a** (0.3 mmol, 65 mg) was mixed in a 10 mL vial with CsOAc (0.4 mmol, 77 mg), (1*R*,2*R*)-cyclohexane-1,2-diamine **L1** (0.04 mmol, 4.6 mg), 4CzIPN (0.005 mmol, 3.9 mg), TEMPO (0.2 mmol, 31 mg) and **2a** (0.2 mmol, 20.0 mg, 22 μL). Then the vial was sealed and taken

glovebox. After adding degassed DMA (2.0 mL), the mixture was stirred under blue LEDs irradiation for 24 hours (setup depicted in Figure III-8) at room temperature.

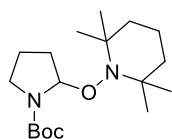


Scheme III-10. Radical trapping experiment

The initial reaction mixture is not completely homogeneous (insoluble inorganic base), and more precipitate forms (likely the corresponding copper acetylide) after few minutes of irradiation. Afterwards, the vial was open, 15 mL of EtOAc were added and the mixture was washed with water three times (3 x 10 mL) and brine (10 mL). The separated organic phase was then dried over MgSO₄, filtered and concentrated under vacuum. Product **3a'** was purified by silica gel (previously neutralized with NEt₃ 2.5% w/w) column chromatography (DCM/Petroleum ether 0% to 100%) and isolated in 30% yield as a colourless oil.

***tert*-butyl 2-((2,2,6,6-tetramethylpiperidin-1-yl)oxy)pyrrolidine-1-carboxylate (**3a'**)**

This compound exists as an approximately 2:1 mixture of rotamers A and B (A+B)



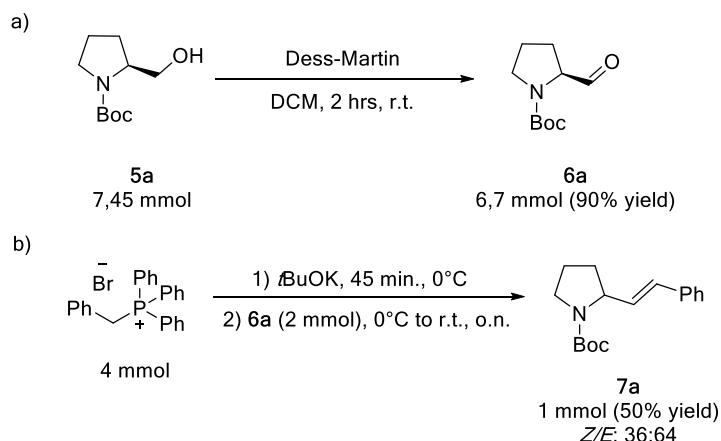
¹H NMR (500 MHz, CDCl₃) (mixture of rotamers A and B) δ
 5.70 (d, *J* = 5.0 Hz, 0.35H, B), 5.61 (d, *J* = 5.0 Hz, 0.65H, A),
 3.43 (td, *J* = 10.3, 8.0 Hz, 0.7H, B), 3.34 (td, *J* = 8.9, 4.8 Hz,
 1.3H, A), 2.12 - 2.01 (m, 1H, A+B), 1.96 (dd, *J* = 12.2, 6.7 Hz, 1H, A+B),
 1.92 - 1.86 (m, 1H, A+B), 1.75 - 1.66 (m, 1H, A+B), 1.53 (s, 7H, A+B), 1.47
 (s, 6H, A+B), 1.38 - 1.27 (m, 2H, A+B), 1.24 - 1.20 (m, 3H, A+B), 1.09 (d, *J*
 = 5.4 Hz, 4H, A+B), 1.02 (d, *J* = 6.7 Hz, 5H, A+B).

Decarboxylative hydroalkylation of alkynes

^{13}C NMR (126 MHz, CDCl_3) (mixture of rotamers A and B) δ 154.2, 90.8, 89.7, 78.9, 78.4, 59.7, 58.2, 45.0, 44.9, 39.7, 39.4, 39.0, 36.1, 32.8, 32.4, 32.0, 31.1, 31.0, 29.1, 28.2, 27.9, 27.9, 24.14, 22.9, 22.3, 21.5, 19.6, 19.5, 16.8, 16.7.

HRMS (ESI) m/z calculated for $(\text{C}_{18}\text{H}_{35}\text{N}_2\text{O}_3)$ 327.2642 $[\text{M}+\text{H}]^+$; found 327.2636

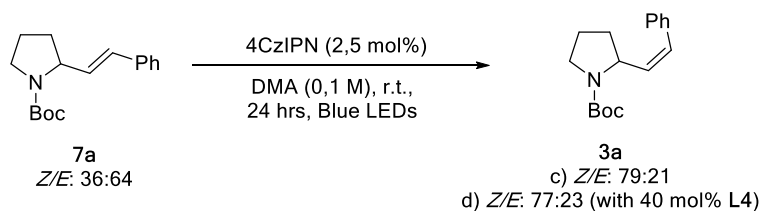
III.4.3.3. Alkene isomerization experiments

Scheme III-11. **7a** Preparation from **5a**

a) Following a reported procedure,¹⁴ **6a** has been prepared in 90% yield (6.7 mmol, 1.335 g) from **5a** (7.45 mmol, 1.5 g) and used in the next step without further purification.

b) In an oven-dried flask benzyl triphenylphosphonium bromide (2.0 equiv, 4.0 mmol, 1.733 g) was dissolved in dry THF (6.4 mL). After cooling the solution to 0°C , $t\text{BuOK}$ (2.0 equiv, 4.0 mmol, 453.0 mg) was added, and the resulting yellow suspension was stirred at 0°C for 45 min. To this suspension a solution of **6a** (1.0 equiv, 2 mmol, 398.5 mg) in dry THF (1.4 mL) was added dropwise. The resulting mixture was warmed gradually to

room temperature and stirred for 16 hours. The suspension was then filtered through a pad of Celite. The filter cake was washed with CH_2Cl_2 . The filtrate was concentrated under reduced pressure to yield a yellow oil. The desired product was purified by silica gel (previously neutralized with NEt_3 2.5% w/w) column chromatography (DCM/Petroleum ether 0% to 100%) and isolated in 50% yield (273.4 mg) ($Z:E$ ratio = 36:64 determined on the isolated product by GC-FID analysis),



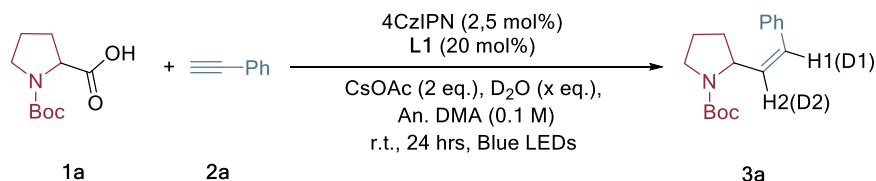
Scheme III-12. Alkene isomerization experiments

c) In a N_2 -filled glovebox, **7a** (0.2 mmol, 55 mg) was mixed in a 10 mL vial with 4CzIPN (0,005 mmol, 3.9 mg). Then the vial was sealed and taken out the glovebox. After adding degassed DMA (2.0 mL), the mixture was stirred under blue LEDs irradiation for 24 hours (setup depicted in Figure III-8) at room temperature. Afterwards, the vial was opened, and three drops of the reaction mixture were taken and used for the GC-FID $Z:E$ ratio determination. The analysis revealed a 79:21 $Z:E$ ratio.

d) In a N_2 -filled glovebox **7a** (0.2 mmol, 55 mg) was mixed in a 10 mL vial with **L4** (0.08 mmol, 21 mg, 26 μL) and 4CzIPN (0,005 mmol, 3.9 mg). Then the vial was sealed and taken out the glovebox. After adding degassed DMA (2.0 mL), the mixture was stirred under blue LEDs irradiation for 24 hours (setup depicted in Figure III-8) at room temperature. Afterwards, the vial was opened, and three drops of the reaction mixture were taken and used for the GC-FID $Z:E$ ratio determination. The analysis revealed a 77:23 $Z:E$ ratio.

Decarboxylative hydroalkylation of alkynes

III.4.3.4. Deuterium labeling experiment



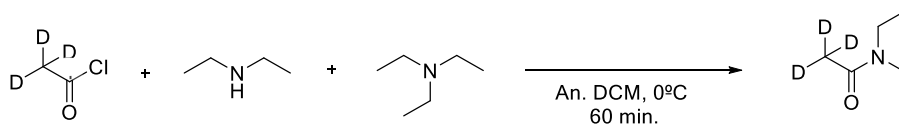
Scheme III-13. Deuterium incorporation experiments.

In a N₂-filled glovebox **1a** (0.3 mmol, 65 mg) was mixed in a 10 mL vial with CsOAc (0.4 mmol, 77 mg), (1*R*,2*R*)-cyclohexane-1,2-diamine **L1** (0.04 mmol, 4.6 mg), 4CzIPN (0.005 mmol, 3.9 mg), D₂O (x eq.) and **2a** (0.2 mmol, 20.0 mg, 22 μ L). Then the vial was sealed and taken out the glovebox. After adding degassed anhydrous DMA (2.0 mL), the mixture was stirred under blue LEDs irradiation for 24 hours (setup depicted in Figure III-8) at room temperature. The initial reaction mixture is not completely homogeneous (insoluble inorganic base), and more precipitate forms (likely the corresponding copper acetylide) after few minutes of irradiation. Afterwards, the vial was open (three drops of the reaction mixture were taken and used for the GC-FID *Z:E* ratio determination), 15.0 mL of EtOAc were added and the mixture was washed with water three times (3 x 10 mL) and brine (10.0 mL). The separated organic phase was then dried over MgSO₄, filtered and concentrated under vacuum. Product **3a** was purified by silica gel (previously neutralized with NEt₃ 2.5% w/w) column chromatography (DCM/Petroleum ether 0% to 100%) and isolated as a colourless oil. Determination of the relative deuterium incorporations has been performed by ¹H-NMR spectroscopy on the isolated products and the results are reported in Table 1.

D ₂ O (equiv)	%D (D1)	%D (D2)	Yield (%)	Z:E
0	0%	0%	82%	78:22
5	17%	40%	80%	73:27
10	33%	60%	78%	71:29
15	38%	64%	79%	75:25
20	44%	71%	81%	74:26

Table III-2. Relative deuterium incorporation.

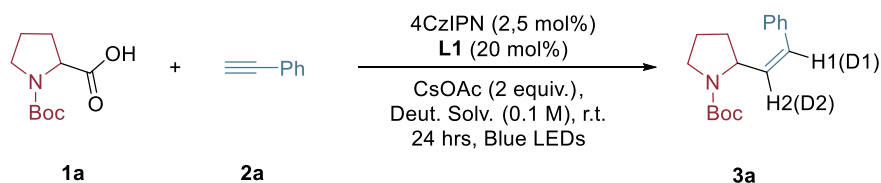
N,N-Diethylacetamide-*d*₃



Scheme III-14. Preparation of *N,N*-Diethylacetamide-*d*₃.

To a stirred solution of diethylamine (29 mmol, 2.121 g, 3 mL) in anhydrous DCM (70 mL) at 0°C was added triethylamine (29 mmol, 2.930 g, 4.04 mL). Acetyl-*d*₃ chloride (29 mmol, 2.364 g, 2.149 mL) was then added dropwise to the solution. The solution was then allowed to warm to room temperature and stirred for one hour before quenching the reaction with saturated aqueous NaHCO₃ solution (45 mL). The two layers were separated and the organic phase was washed with 1M HCl (15 mL) and brine (15 mL) and dried over Na₂SO₄ before being carefully concentrated in vacuo. The ¹H-NMR analysis performed on the synthesized *N,N*-Diethylacetamide-*d*₃ revealed deuterium labelling higher than 95%. ¹H NMR (400 MHz, CDCl₃) δ 3.39 - 3.13 (m, 2H), 1.24 - 0.95 (m, 3H).

Decarboxylative hydroalkylation of alkynes



Scheme III-15. Deuterium incorporation from solvents.

In a N₂-filled glovebox **1a** (0.3 mmol, 65 mg) was mixed in a 10 mL vial with CsOAc (0.4 mmol, 77 mg), (1*R*,2*R*)-cyclohexane-1,2-diamine L1 (0.04 mmol, 4.6 mg), 4CzIPN (0.005 mmol, 3.9 mg) and **2a** (0.2 mmol, 20.0 mg, 22 μ L). Then the vial was sealed and taken out the glovebox. After adding degassed deuterated solvent (2.0 mL), the mixture was stirred under blue LEDs irradiation for 24 hours (setup depicted in Figure III-8) at room temperature. The initial reaction mixture is not completely homogeneous (insoluble inorganic base), and more precipitate forms (likely the corresponding copper acetylide) after few minutes of irradiation. Afterwards, the vial was open (three drops of the reaction mixture were taken and used for the GC-FID *Z:E* ratio determination), 15 mL of EtOAc were added and the mixture was washed with water three times (3 x 10 mL) and brine (10 mL). The separated organic phase was then dried over MgSO₄, filtered and concentrated under vacuum. Product **3a** was purified by silica gel (previously neutralized with NEt₃ 2.5% w/w) column chromatography (DCM/Petroleum ether 0% to 100%) and isolated as a colorless oil. Determination of the relative deuterium incorporations has been performed by ¹H-NMR spectroscopy on the isolated products and the results are reported in Table 2.

Solvent	%D (D1)	%D (D2)	Yield (%)	<i>Z:E</i>
<i>N,N</i> -Dimethylformamide- <i>d</i> ₇	0%	0%	65%	71:29
Acetonitrile- <i>d</i> ₃	0%	0%	57%	81:19
<i>N,N</i> -Diethylacetamide- <i>d</i> ₃	0%	0%	56%	80:20

Table III-3. Relative deuterium incorporation from solvents.

III.4.3.5. Stern-Volmer fluorescence quenching studies

Preliminary studies have been conducted in order to choose the proper excitation wavelength for 4CzIPN as well as to check possible absorbance at the maximum emission wavelength of 4CzIPN by the complex $[\text{Cu}(\text{L1})_2](\text{OAc})_2$. In order to do so, a 1.1 mM DMA solution of $[\text{Cu}(\text{L1})_2](\text{OAc})_2$ has been prepared and an UV-VIS absorption spectrum acquired. It has been evaluated that at 367 nm and 531 nm the absorbance of $[\text{Cu}(\text{L1})_2](\text{OAc})_2$ is neglectable.

The emission spectra were recorded in a Fluorolog Horiba Jobin Yvon spectrofluorimeter equipped with a photomultiplier detector, a double monochromator, and a 350W xenon light source. 2.5 mL of a 4.71 μM solution of 4CzIPN in degassed DMA were placed in a 10x10 mm light path quartz fluorescence cuvette equipped with Silicone/PTFE 3.2 mm septum under an argon atmosphere. The excitation wavelength was fixed at 367 nm (incident light slit regulated to 5 mm), while the emission light was acquired from 400 nm to 720 nm (emission light slit regulated to 8 mm). A solvent blank was subtracted from the measurements.

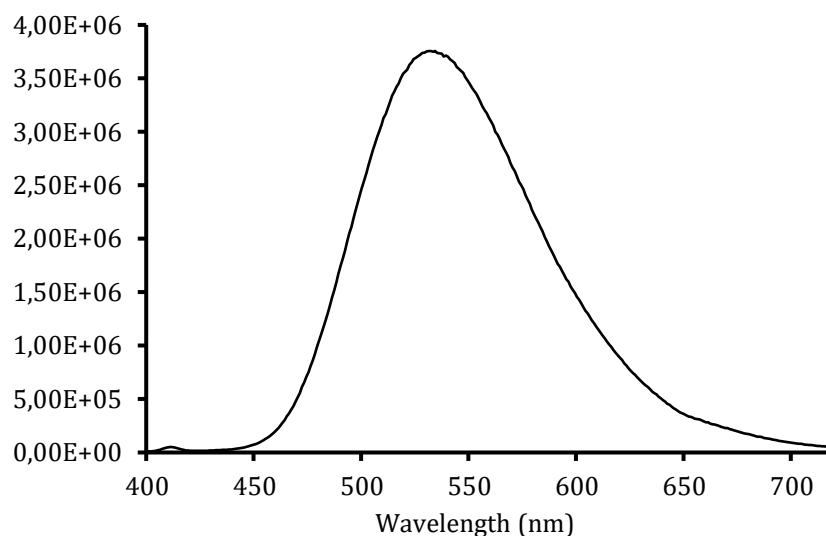


Figure III-10. Emission spectrum of 4CzIPN (excitation wavelength at 367 nm).

Decarboxylative hydroalkylation of alkynes

Stern-Volmer Quenching Studies with $[\text{Cu}(\text{L1})_2](\text{OAc})_2$

25 μL of a 23.55 mM solution of $[\text{Cu}(\text{L1})_2](\text{OAc})_2$ in DMA were added to the solution of 4CzIPN (2.5 mL, 4.71 μM). The addition was repeated four consecutive times. After each addition, an absorption spectrum and an emission spectrum of the solution were recorded. The excitation wavelength was fixed at 367 nm (incident light slit regulated to 5 mm), the emission light was acquired from 400 nm to 720 nm (emission light slit regulated to 8 mm). A solvent blank was subtracted from all the measurements. The results shown in Figure III-11 indicate that $[\text{Cu}(\text{L1})_2](\text{OAc})_2$ quenches the excited state of 4CzIPN and its emission.

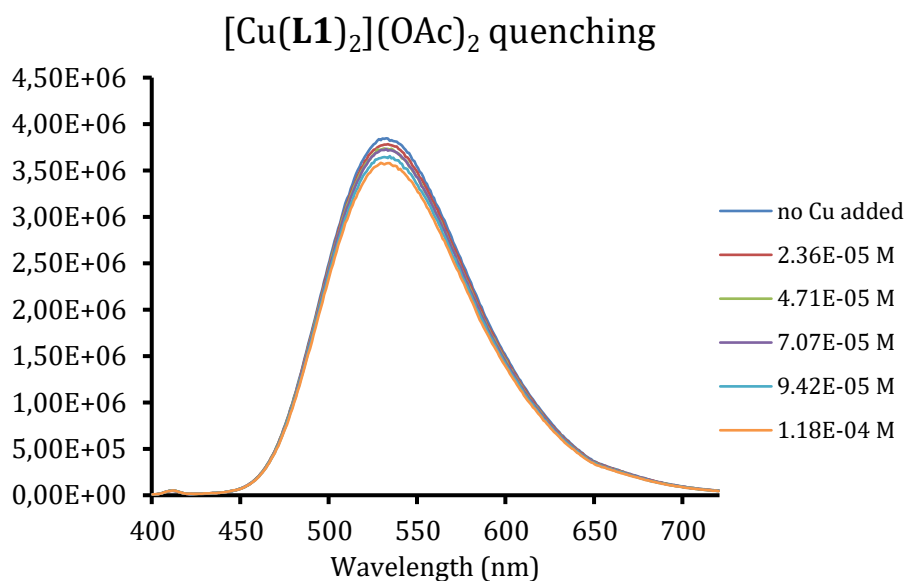


Figure III-11. Quenching of 4CzIPN emission in the presence of increasing amounts of $[\text{Cu}(\text{L1})_2](\text{OAc})_2$.

The Stern-Volmer plot, reported in Figure III-12, shows a linear correlation between the amounts of $[\text{Cu}(\text{L1})_2](\text{OAc})_2$ and the ratio I_0/I . On the basis of the following Equation 1, it is possible to calculate the Stern-Volmer constant K_{SV} .³

$$I_0/I = 1 + K_{SV}[Q] \quad \text{Eq. 1}$$

The calculated Stern-Volmer quenching constant is 0.0144 M^{-1} .

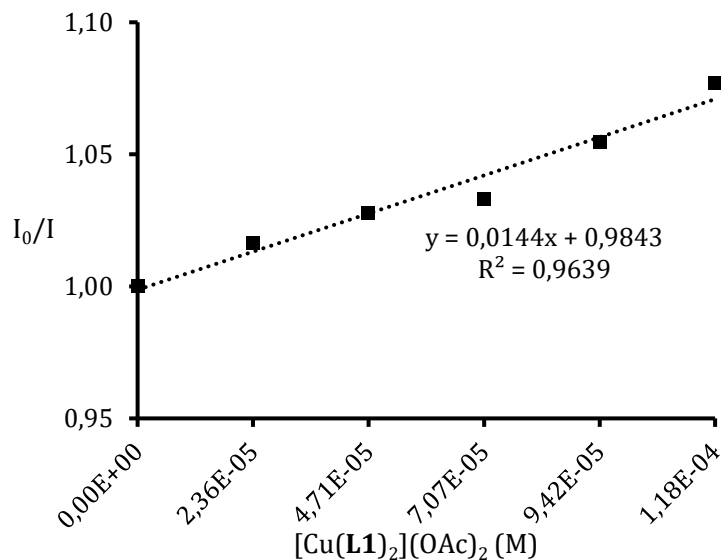


Figure III-12. Stern-Volmer quenching plot for $[\text{Cu}(\mathbf{L1})_2](\text{OAc})_2$.

Stern-Volmer Quenching Studies with **2a**

25 μL of a 23.55 mM solution of **2a** in DMA were added to the solution of 4CzIPN (2.5 mL, 4.71 μM). The addition was repeated four consecutive times. After each addition, an absorption spectrum and an emission spectrum of the solution were recorded. The excitation wavelength was fixed at 367 nm (incident light slit regulated to 5 mm), the emission light was acquired from 400 nm to 720 nm (emission light slit regulated to 8 mm). A solvent blank was subtracted from all the measurements. The results shown in Figure III-13 indicate that **2a** do not significantly quenches the excited state of 4CzIPN and its emission.

Decarboxylative hydroalkylation of alkynes

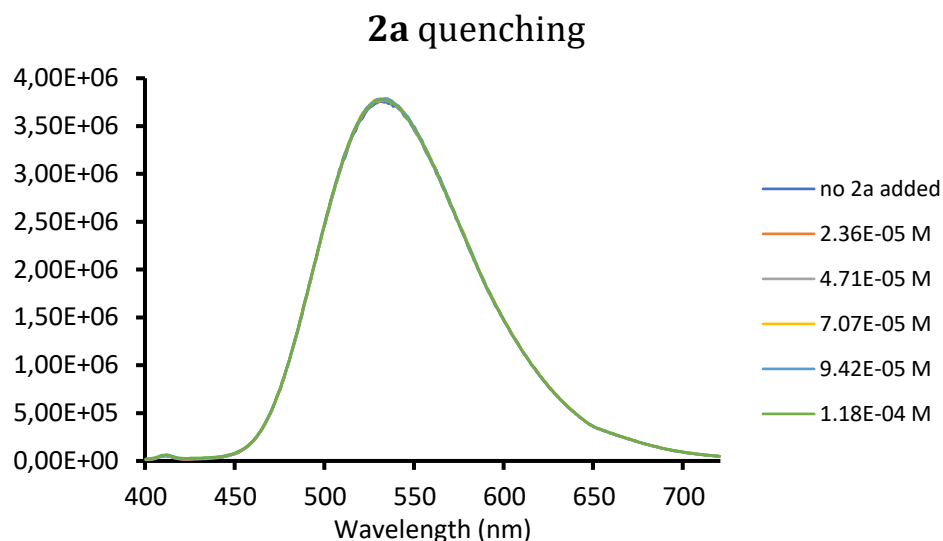


Figure III-13. Quenching of 4CzIPN emission in the presence of increasing amounts of **2a**.

Stern-Volmer Quenching Studies with Boc-Pro-OCs

25 μ L of a 23.55 mM solution of Boc-Pro-OCs (Caesium (*tert*-butoxycarbonyl)-*L*-prolinate) in DMA were added to the solution of 4CzIPN (2.5 mL, 4.71 μ M). The addition was repeated four consecutive times. After each addition, an absorption spectrum and an emission spectrum of the solution were recorded. The excitation wavelength was fixed at 367 nm (incident light slit regulated to 5 mm), the emission light was acquired from 400 nm to 720 nm (emission light slit regulated to 8 mm). A solvent blank was subtracted from all the measurements. The results shown in Figure III-14 indicate that Boc-Pro-OCs quenches the excited state of 4CzIPN and its emission.

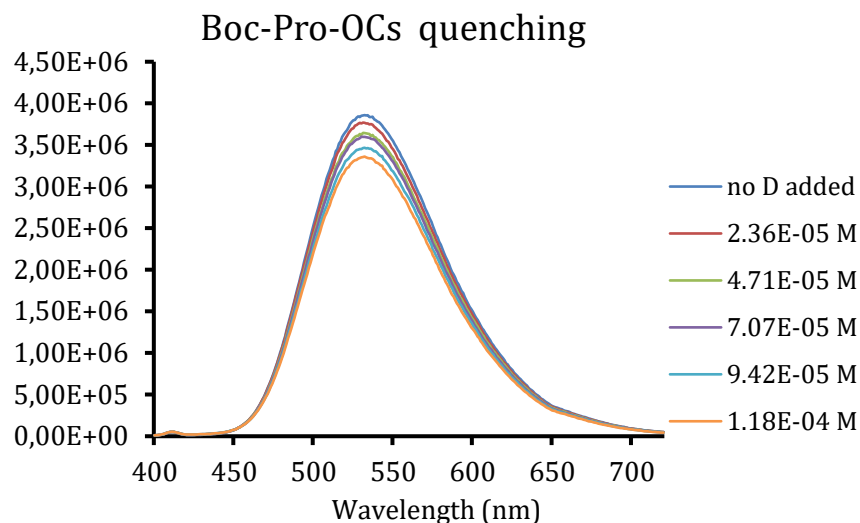


Figure III-14. Quenching of 4CzIPN emission in the presence of increasing amounts of Boc-Pro-OCs.

The Stern-Volmer plot, reported in Figure III-15, shows a linear correlation between the amounts of Boc-Pro-OCs and the ratio I_0/I . On the basis of the Equation 1, it is possible to calculate the Stern-Volmer constant K_{SV} . The calculated Stern-Volmer quenching constant is 0.0295 M^{-1} .

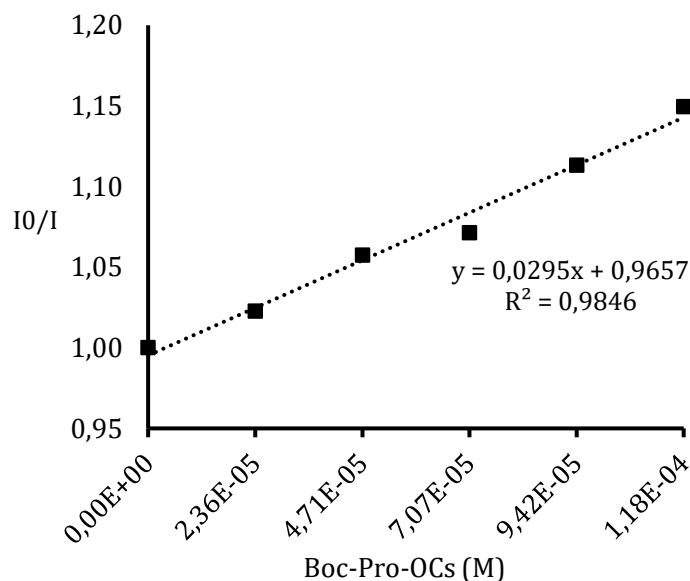


Figure III-15. Stern-Volmer quenching plot for Boc-Pro-OCs.

Decarboxylative hydroalkylation of alkynes

III.4.4. High-Throughput experimentation

Experiments were set inside a glovebox under a nitrogen atmosphere. Screening experiment was carried out in 0.75 mL glass vials (8x30mm) in a photoredox 96-well block assembly (equipment available from Analytical Sales and Services, #96973) adapted with a 96-blue (InGaN, 20 mA, 3.4 V, 472 nm) LED array and stirred with a tumble stirrer (V&P Scientific, VP710C3HMCE-P). Chemicals were dosed as solutions using pipettors or weighted directly into the reaction vials.

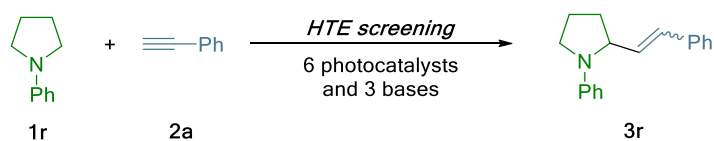
Procedure

20 μmol of the corresponding inorganic base were added as a slurry in THF. However, a good slurry for accurate dosing of CsOAc in THF was not obtained and therefore CsOAc (20 μmol , 3.85 mg) was directly weighted into the reaction vials. After base dosing, THF was removed with a GeneVac Evaporator placed inside the Glovebox. After evaporation Cu sources (2 μmol), ligands (2 μmol for bidentate and 4 μmol for monodentate ligands) and the photocatalyst (0.25 μmol) were added in THF to the corresponding positions of the 96-well plate. Solvent was removed again in the GeneVac leaving the reagents dosed in the reaction vials and a Teflon coated micro stir bar (5x2mm) was then added to each reaction vial. Then the substrates solutions containing 10 μmol of Phenylacetylene and 15 μmol of Boc-Proline in 100 μL of the corresponding reaction solvent were added to the reaction vials. The plate was sealed and stirred under blue light irradiation overnight. The temperature of the plate slightly raised during irradiation and was stabilized at 27°C after 10 minutes. After 18 hours, 500 μL of a solution of biphenyl (used as internal standard) in acetonitrile (0.005 M) was added into each vial. The plate was covered again and the vials stirred to ensure good mixing. After stirring, the plate was centrifuged for 20 min in order that all the insoluble settle to the bottom of the vial. Into a separate 96-well LC block was added 500 μL of acetonitrile, followed by 40

μL of the supernatant diluted reaction mixtures. The LC block was then sealed with a silicon-rubber storage mat and mounted on an automated UPLC instrument for analysis. Best reactions were further analyzed by GC/FID in order to determine *E:Z* ratios and yields.

Results are depicted in Figure III-5.

Base/Photocatalyst screening for the cross-dehydrogenative coupling



Scheme III-16. HTE screening of photocatalysts and bases for the cross dehydrogenative coupling between **1r** and **2a**.

Following the previously described set-up and using a 24-well block assembly (equipment available from Analytical Sales and Services, #24253), 6 different photocatalysts and 3 different bases were tested.

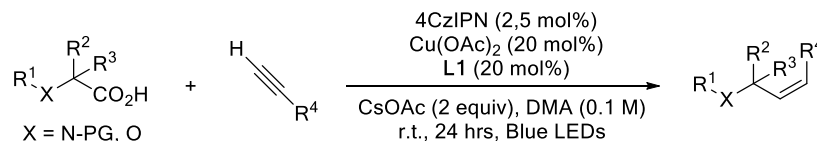
Decarboxylative hydroalkylation of alkynes

Position	Photocatalyst	Base	Ratio Absorbance Areas 3q/IS	Conv. 1q %	Conv. 2a %
A01	[Ir(dtbbpy)(ppy) ₂] ₂ PF ₆	CsOAc	3.5	79	79
A02	Ir(ppy) ₃	CsOAc	0.3	11	15
A03	Ir(Fppy) ₃	CsOAc	0.1	6	12
A04	[Ir{dF(CF ₃)ppy} ₂ (dtbpy)]PF ₆	CsOAc	3.1	62	59
A05	Ru(bpy) ₃ Cl ₂ .6H ₂ O	CsOAc	0.5	18	18
A06	Eosin Y	CsOAc	0	7	11
B01	[Ir(dtbbpy)(ppy) ₂] ₂ PF ₆	Cs ₂ CO ₃	0.6	53	50
B02	Ir(ppy) ₃	Cs ₂ CO ₃	0	3	20
B03	Ir(Fppy) ₃	Cs ₂ CO ₃	0	1	21
B04	[Ir{dF(CF ₃)ppy} ₂ (dtbpy)]PF ₆	Cs ₂ CO ₃	0.1	9	20
B05	Ru(bpy) ₃ Cl ₂ .6H ₂ O	Cs ₂ CO ₃	0.1	8	17
B06	Eosin Y	Cs ₂ CO ₃	0	3	21
C01	[Ir(dtbbpy)(ppy) ₂] ₂ PF ₆	NaOAc	2.5	57	56
C02	Ir(ppy) ₃	NaOAc	0.2	7	14
C03	Ir(Fppy) ₃	NaOAc	0	0	17
C04	[Ir{dF(CF ₃)ppy} ₂ (dtbpy)]PF ₆	NaOAc	1.7	37	38
C05	Ru(bpy) ₃ Cl ₂ .6H ₂ O	NaOAc	0.3	15	15
C06	Eosin Y	NaOAc	0	0	20
D01	[Ir(dtbbpy)(ppy) ₂] ₂ PF ₆	No base	2.2	49	47
D02	Ir(ppy) ₃	No base	0.1	7	14
D03	Ir(Fppy) ₃	No base	0	1	19
D04	[Ir{dF(CF ₃)ppy} ₂ (dtbpy)]PF ₆	No base	1.1	27	30
D05	Ru(bpy) ₃ Cl ₂ .6H ₂ O	No base	0.2	17	15
D06	Eosin Y	No base	0	0	22

Scheme III-4. Results of the HTE screening of bases and photocatalysts for the cross dehydrogenative coupling.

III.4.5. Experimental procedures

General procedure for the Decarboxylative Hydroalkylation of Alkynes (GP1)

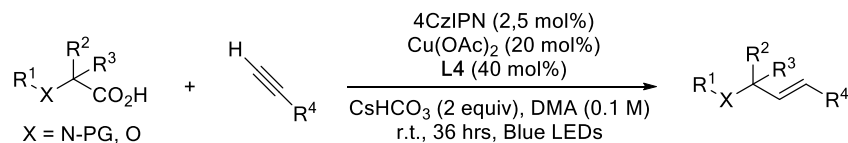


Scheme III-17. Decarboxylative Hydroalkylation of Alkynes.

In a N₂-filled glovebox, the corresponding carboxylic acid (0.3 mmol) was mixed in a 10 mL vial with CsOAc (0.4 mmol, 77 mg), Cu(OAc)₂ (0.04 mmol, 7.3 mg), (*1R,2R*)-cyclohexane-1,2-diamine **L1** (0.04 mmol, 4.6 mg) (the reaction works equally well with the racemic **L1**, the enantiopure ligand has been used just for practical reasons), 4CzIPN (0.005 mmol, 3.9 mg) and the alkyne (0.2 mmol). Then the vial was sealed and taken out the glovebox. After adding degassed DMA (2.0 mL), the mixture was stirred under blue LEDs irradiation (setup depicted in Figure III-8) for 24 hours at room temperature. The initial reaction mixture is not completely homogeneous (insoluble inorganic base), and more precipitate forms (likely the corresponding copper acetylide) after few minutes of irradiation. Afterwards, the vial was open (three drops of the reaction mixture were taken and used for the GC-FID *Z:E* ratio determination), 15.0 mL of EtOAc were added and the mixture was washed with water three times (3 x 10 mL) and brine (10.0 mL). The separated organic phase was then dried over MgSO₄, filtered and concentrated under vacuum. The desired product was purified by silica gel (previously neutralized with NEt₃ 2.5% w/w) column chromatography (DCM/Petroleum ether 0% to 100%).

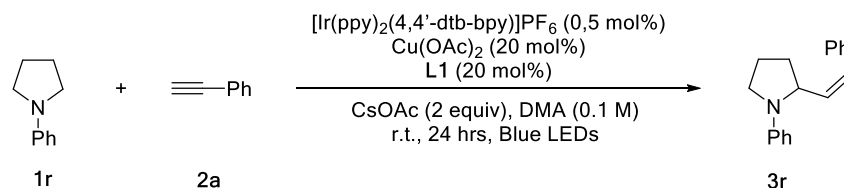
When alkynes **2d**, **2j**, **2k**, **2m** were used in the synthesis of the corresponding products the same procedure has been using but modifying the alkyne/carboxylic acid stoichiometric ratio from 1/1.5 (**GP1**) to 3/1.

Decarboxylative hydroalkylation of alkynes

General procedure for the *E*-selective Decarboxylative Hydroalkylation of Alkynes (GP2)**Scheme III-18.** *E*-selective Decarboxylative Hydroalkylation of Alkynes.

In a N_2 -filled glovebox the corresponding carboxylic acid (0.3 mmol) was mixed in a 16 mL reaction tube with CsHCO_3 (0.4 mmol, 78 mg), $\text{Cu}(\text{OAc})_2$ (0.04 mmol, 7.3 mg), **L4** (0.08 mmol, 21 mg, 26 μL), 4CzIPN (0.005 mmol, 3.9 mg) and the alkyne (0.2 mmol). Then the vial was closed with a screw cap and taken out the glovebox. After adding degassed DMA (2.0 mL), the tube was wrapped with Parafilm® and the mixture was stirred under blue LEDs irradiation (setup depicted in Figure III-9) for 36 hours at room temperature. The initial reaction mixture is not completely homogeneous (insoluble inorganic base), and more precipitate forms (likely the corresponding copper acetylide) after few minutes of irradiation. Afterwards, the vial was open (three drops of the reaction mixture were taken and used for the GC-FID *Z:E* ratio determination), 15.0 mL of EtOAc were added and the mixture was washed with water three times (3 x 10 mL) and brine (10.0 mL). The separated organic phase was then dried over MgSO_4 , filtered and concentrated under vacuum. The desired product was purified by silica gel (previously neutralized with NEt_3 2.5% w/w) column chromatography (DCM/Petroleum ether 0% to 100%).

Procedure for the *Z*-selective Cross dehydrogenative coupling between 1-phenylpyrrolidine (**1r**) and ethynylbenzene (**1a**) (GP3)

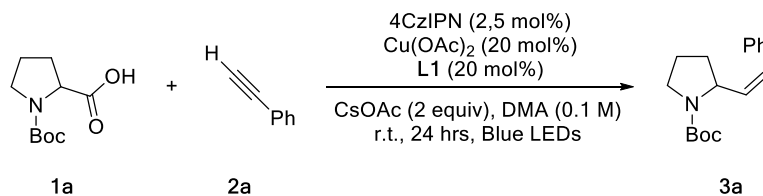


Scheme III-19. *Z*-selective cross dehydrogenative coupling.

In a N_2 -filled glovebox 1-phenylpyrrolidine (**1r**) (0.3 mmol, 44 mg, 43 μl) was mixed in a 10 mL vial with CsOAc (0.4 mmol, 77 mg), $\text{Cu}(\text{OAc})_2$ (0.04 mmol, 7.3 mg), **L1** (0.04 mmol, 4.6 mg) (the reaction works equally well with the racemic **L1**, the enantiopure ligand has been used just for practical reasons), $[\text{Ir}(\text{ppy})_2(4,4'\text{-dtb-bpy})]\text{PF}_6$ (0.5 mol%, 0.9 mg) ethynylbenzene (**1a**) (0.2 mmol, 20 mg, 22 μl). Then the vial was sealed and taken out the glovebox. After adding degassed DMA (2.0 mL), the mixture was stirred under blue LEDs irradiation (setup depicted in Figure III-8) for 24 hours at room temperature. The initial reaction mixture is not completely homogeneous (insoluble inorganic base), and more precipitate forms (likely the corresponding copper acetylide) after few minutes of irradiation. Afterwards, the vial was open (three drops of the reaction mixture were taken and used for the GC-FID *Z*:*E* ratio determination), 15.0 mL of EtOAc were added and the mixture was washed with water three times (3 x 10 mL) and brine (10.0 mL). The separated organic phase was then dried over MgSO_4 , filtered and concentrated under vacuum. The desired product was purified by silica gel column chromatography (DCM/Petroleum ether 0% to 100%).

Decarboxylative hydroalkylation of alkynes

Procedure for the 3 mmol-scale decarboxylative hydroalkylation of ethynylbenzene (**2a**) with (*tert*-butoxycarbonyl)-*L*-proline (**1a**) (GP4)



Scheme III-20. 3 mmol-scale decarboxylative hydroalkylation of ethynylbenzene (**2a**).

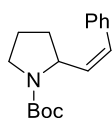
In a N₂-filled glovebox (*tert*-butoxycarbonyl)-proline (**1a**) (4.5 mmol, 975 mg) was mixed in a 20 mL vial with CsOAc (6 mmol, 1.155 g), Cu(OAc)₂ (0.6 mmol, 109.5 mg), (*1R,2R*)-cyclohexane-1,2-diamine **L1** (0.6 mmol, 69 mg) (the reaction works equally well with the racemic **L1**, the enantiopure ligand has been used just for practical reasons), 4CzIPN (0.075 mmol, 58.5 mg) and ethynylbenzene (**2a**) (3 mmol, 300 mg, 330 μL). Then the vial was sealed and taken out the glovebox. After adding degassed DMA (15.0 mL), the mixture was stirred under blue LEDs irradiation (setup depicted in Figure III-16) for 24 hours at room temperature. The initial reaction mixture is not completely homogeneous (insoluble inorganic base), and more precipitate forms (likely the corresponding copper acetylide) after few minutes of irradiation. Afterwards, the vial was open (three drops of the reaction mixture were taken and used for the GC-FID *Z:E* ratio determination), 150.0 mL of EtOAc were added and the mixture was washed with water three times (3 x 100 mL) and brine (100.0 mL). The separated organic phase was then dried over MgSO₄, filtered and concentrated under vacuum. The desired product was purified by silica gel (previously neutralized with NEt₃ 2.5% w/w) column chromatography (DCM/Petroleum ether 0% to 100%).



Figure III-16. Irradiation setup used in the 3 mmol-scale decarboxylative hydroalkylation of alkynes

III.4.6. Product characterization

tert-butyl (*Z*)-2-styrylpyrrolidine-1-carboxylate (**3a**)⁴



Following GP1, **3a** was prepared starting from (*tert*-butoxycarbonyl)-*L*-proline (**1a**) (0.3 mmol, 65 mg) and ethynylbenzene (**2a**) (0.2 mmol, 20 mg, 22 μ L) and it was obtained as a *Z/E* mixture with a *Z:E* ratio of 78:22 and isolated as a colorless oil (45 mg, 82% yield).

¹H NMR (400 MHz, CDCl₃) (*Z/E* mixture) δ 7.37 - 7.29 (m, 3H, *Z+E*), 7.25 - 7.19 (m, 2H, *Z+E*), 6.40 (d, *J* = 11.8 Hz, 1H, *Z+E*), 6.09 (bs, 0.3H, *E*), 5.61 (t, *J* = 10.1 Hz, 0.7H, *Z*), 4.73 (bs, 0.7H, *Z*), 4.59 - 4.33 (m, 0.3H, *E*), 3.54 -

Decarboxylative hydroalkylation of alkynes

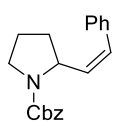
3.39 (m, 2H, *Z+E*), 2.30 - 2.03 (m, 1H, *Z+E*), 1.98 - 1.74 (m, 3H, *Z+E*), 1.49 - 1.25 (m, 9H, *Z+E*).

¹³C NMR (101 MHz, CDCl₃) (*Z/E* mixture) δ 154.8, 137.2, 137.1, 135.0, 130.8, 129.5, 128.9, 128.6, 128.2, 128.0, 127.4, 126.8, 126.4, 79.3, 79.3, 59.1, 55.1, 46.6, 34.0, 32.7, 28.6, 28.5, 24.0, 23.2.

Following GP2, **3a** was prepared starting from (*tert*-butoxycarbonyl)-*L*-proline (**1a**) (0.3 mmol, 65 mg) and ethynylbenzene (**2a**) (0.2 mmol, 20 mg, 22 μL) and it was obtained as a *Z/E* mixture with a *Z:E* ratio of 23:77 and isolated as a colorless oil (39 mg, 72% yield).

Following GP4, **3a** was prepared starting from (*tert*-butoxycarbonyl)-*L*-proline (**1a**) (4.5 mmol, 969 mg) and ethynylbenzene (**2a**) (3 mmol, 300 mg, 330 μL) and it was obtained as a *Z/E* mixture with a *Z:E* ratio of 67:33 and isolated as a colorless oil (620 mg, 76% yield).

benzyl (*Z*)-2-styrylpyrrolidine-1-carboxylate (**3b**)⁵

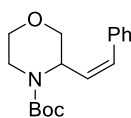


Following GP1, **3b** was prepared starting from (benzyloxycarbonyl)-*L*-proline (**1b**) (0.3 mmol, 75 mg) and ethynylbenzene (**2a**) (0.2 mmol, 20 mg, 22 μL) and it was obtained as a *Z/E* mixture with a *Z:E* ratio of 78:22 and isolated as a colorless oil (46 mg, 75% yield).

¹H NMR (400 MHz, CDCl₃) (*Z/E* mixture) δ 7.48 - 7.27 (m, 6H, *Z+E*), 7.25 - 7.13 (m, 4H, *Z+E*), 6.57 - 6.32 (m, 1H, *Z+E*), 6.11 (d, *J* = 18.4 Hz, 0.25H, *E*), 5.64 (dd, *J* = 11.6, 9.2 Hz, 0.75H, *Z*), 5.22 - 4.99 (m, 2H, *Z+E*), 4.92 - 4.78 (m, 0.75H, *Z*), 4.66 - 4.47 (m, 0.25H, *E*), 3.61 - 3.38 (m, 2H, *Z+E*), 2.29 - 2.06 (m, 1H, *Z+E*), 1.97 (ddd, *J* = 15.2, 10.0, 6.3 Hz, 1H, *Z+E*), 1.91 - 1.80 (m, 2H, *Z+E*).

^{13}C NMR (126 MHz, CDCl_3) (*Z/E* mixture) δ 155.2, 155.0, 137.0, 134.1, 133.8, 130.3, 123.0, 129.4, 129.0, 128.8, 128.6, 128.5, 128.3, 128.0, 127.8, 127.7, 127.5, 127.0, 126.5, 66.9, 66.7, 59.0, 55.7, 55.0, 47.1, 46.9, 46.8, 46.5, 34.1, 33.4, 32.8, 31.8, 29.8, 24.5, 23.9, 23.1, 22.8.

tert-butyl (*Z*)-3-styrylmorpholine-4-carboxylate (**3c**)⁶

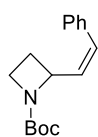


Following GP1, **3c** was prepared starting from 4-(*tert*-butoxycarbonyl)morpholine-3-carboxylic acid (**1c**) (0.3 mmol, 69 mg) and ethynylbenzene (**2a**) (0.2 mmol, 20 mg, 22 μL) and it was obtained as a *Z/E* mixture with a *Z:E* ratio of 76:24 and isolated as a white solid (41 mg, 70% yield).

^1H NMR (400 MHz, CDCl_3) (*Z/E* mixture) δ 7.40 - 7.37 (m, 0.60H, *E*), 7.36 - 7.29 (m, 1.4H, *Z*), 7.27 - 7.21 (m, 3H, *Z+E*), 6.62 - 6.54 (m, 1H, *Z+E*), 6.39 (dd, $J = 16.0, 6.4$ Hz, 0.3H, *E*), 6.09 (dd, $J = 11.8, 9.7$ Hz, 0.7H, *Z*), 5.07 - 4.95 (m, 0.7H, *Z*), 4.59 (bs, 0.3H, *E*), 4.00 - 3.83 (m, 2H, *Z+E*), 3.80 - 3.68 (m, 2H, *Z+E*), 3.52 (ddt, $J = 12.2, 11.3, 2.7$ Hz, 1H, *Z+E*), 3.36 - 3.20 (m, 1H, *Z+E*), 1.48 (s, 2.7H, *E*), 1.24 (s, 6.3H, *Z*).

^{13}C NMR (101 MHz, CDCl_3) (*Z/E* mixture) δ 155.0, 154.9, 136.8, 136.8, 132.5, 130.8, 128.7, 128.7, 128.5, 127.8, 127.7, 127.2, 126.5, 126.0, 80.3, 80.1, 71.3, 70.1, 67.2, 67.1, 49.4, 40.0, 39.5, 28.5, 28.2.

tert-butyl (*Z*)-2-styrylazetidine-1-carboxylate (**3d**)⁴



Following GP1, **3d** was prepared starting from 1-(*tert*-butoxycarbonyl)azetidine-2-carboxylic acid **1d** (0.3 mmol, 60 mg) and ethynylbenzene (**2a**) (0.2 mmol, 20 mg, 22 μL) and it was obtained as a *Z/E* mixture with a *Z:E* ratio of 75:25 and isolated as a colorless oil (27 mg, 52% yield).

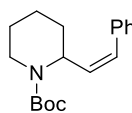
^1H NMR (500 MHz, CDCl_3) (*Z/E* mixture) δ 7.41 - 7.37 (m, 0.5H, *E*), 7.35 - 7.29 (m, 2H, *Z*), 7.27 - 7.21 (m, 3H, *Z+E*), 6.58 - 6.49 (m, 1H, *Z+E*), 6.34

Decarboxylative hydroalkylation of alkynes

(dd, $J = 15.8, 7.0$ Hz, 0.25H, *E*), 5.94 (dd, $J = 11.6, 8.5$ Hz, 0.75H, *Z*), 5.15 (tdd, $J = 8.2, 6.2, 1.3$ Hz, 0.75H, *Z*), 4.80 (q, $J = 7.2$ Hz, 0.25H, *E*), 3.94 - 3.77 (m, 2H, *Z+E*), 2.48 - 2.40 (m, 1H, *Z+E*), 2.11 - 1.98 (m, 1H, *Z+E*), 1.42 (s, 2.25H, *E*), 1.40 (s, 6.75H, *Z*).

^{13}C NMR (126 MHz, CDCl_3) (*Z/E* mixture) δ 156.8, 156.40, 136.9, 136.8, 133.6, 131.0, 130.1, 130.0, 128.8, 128.6, 128.3, 127.7, 127.2, 126.6, 79.5, 79.5, 59.1, 46.4, 28.6, 24.0, 23.4.

HRMS (ESI) m/z calculated for $\text{C}_{16}\text{H}_{21}\text{NNaO}_2$ 282.1464 [$\text{M}+\text{Na}$] $^+$; found 282.1458

***tert*-butyl (*Z*)-2-styrylpiperidine-1-carboxylate (**3e**)⁵**

Following GP1, **3e** was prepared starting from 1-(*tert*-butoxycarbonyl)piperidine-2-carboxylic acid (**1e**) (0.3 mmol, 69 mg) and ethynylbenzene (**2a**) (0.2 mmol, 20 mg, 22 μL) and it was obtained as a *Z/E* mixture with a *Z:E* ratio of 75:25 and isolated as a colorless oil (46 mg, 80% yield)

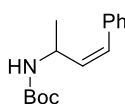
^1H NMR (500 MHz CDCl_3) (*Z/E* mixture) δ 7.45 - 7.26 (m, 4H, *Z+E*), 7.25 - 7.19 (m, 1H, *Z+E*), 6.48 (dd, $J = 11.9, 1.3$ Hz, 0.8H, *Z*), 6.39 (dd, $J = 16.2, 2.0$ Hz, 0.2H, *E*), 6.18 (dd, $J = 16.1, 4.8$ Hz, 0.2H, *E*), 5.97 (dd, $J = 11.9, 9.4$ Hz, 0.8H, *Z*), 5.33 - 5.26 (m, 0.8H, *Z*), 4.96 (bs, 0.2H, *E*), 4.04 - 3.92 (m, 1H, *Z+E*), 2.97 (td, $J = 13.1, 3.0$ Hz, 0.8H, *Z*), 2.93 - 2.87 (m, 0.2H, *E*), 1.78 - 1.73 (m, 2H, *Z+E*), 1.71 - 1.57 (m, 3H, *Z+E*), 1.48 (s, 1.8H, *E*), 1.46 - 1.41 (m, 1H, *Z+E*), 1.24 (s, 7.2H, *Z*).

^{13}C NMR (126 MHz, CDCl_3) (*Z/E* mixture) δ 155.5, 155.3, 137.2, 137.1, 130.9, 129.7, 129.5, 128.9, 128.8, 128.7, 128.4, 127.5, 127.1, 126.4, 79.6, 79.4, 48.9, 39.9, 30.6, 29.7, 28.6, 28.3, 25.7, 25.6, 20.0, 19.8.

Following GP2, **3a** was prepared starting from 1-(*tert*-butoxycarbonyl)piperidine-2-carboxylic acid (**1e**) (0.3 mmol, 69 mg) and

ethynylbenzene (**2a**) (0.2 mmol, 20 mg, 22 μ L) and it was obtained as a *Z/E* mixture with a *Z:E* ratio of 30:70 and isolated as a colorless oil (43 mg, 74% yield).

***tert*-butyl (*Z*)-(4-phenylbut-3-en-2-yl)carbamate (**3f**)⁷**

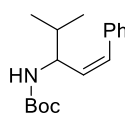


Following GP1, **3f** was prepared starting from (*tert*-butoxycarbonyl)-*L*-alanine (**1f**) (0.3 mmol, 57 mg) and ethynylbenzene (**2a**) (0.2 mmol, 20 mg, 22 μ L) and it was obtained as a *Z/E* mixture with a *Z:E* ratio of 72:28 and isolated as a white solid (26 mg, 53% yield)

¹H NMR (500 MHz, CDCl₃) (*Z/E* mixture) δ 7.38 - 7.28 (m, 4H, *Z+E*), 7.25 - 7.20 (m, 1H, *Z+E*), 6.50 (d, *J* = 15.8 Hz, 0.4H, *E*), 6.43 (dd, *J* = 11.7, 1.1 Hz, 0.6H, *Z*), 6.16 (dd, *J* = 15.9, 5.7 Hz, 0.4H, *E*), 5.50 (dd, *J* = 11.7, 9.2 Hz, 0.6H, *Z*), 4.70 (bs, 0.6H, *Z*), 4.52 (s, 1H, *Z+E*), 4.40 (s, 0.4H, *E*), 1.46 (s, 3.6H, *E*), 1.41 (bs, 5.4H, *Z*), 1.31 (d, *J* = 6.8 Hz, 1.2H, *E*), 1.27 (d, *J* = 6.6 Hz, 1.8H, *Z*).

¹³C NMR (126 MHz, CDCl₃) (*Z/E* mixture) δ 155.28, 155.1, 137.0, 136.7, 134.0, 131.9, 129.8, 129.3, 128.9, 128.7, 128.5, 127.6, 127.3, 126.5, 79.5, 48.0, 44.9, 28.6, 28.5, 22.3, 21.3.

***tert*-butyl (*Z*)-(4-methyl-1-phenylpent-1-en-3-yl)carbamate (**3g**)⁵**



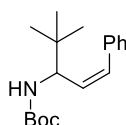
Following GP1, **3g** was prepared starting from (*tert*-butoxycarbonyl)-*L*-valine (**1g**) (0.3 mmol, 65 mg) and ethynylbenzene (**2a**) (0.2 mmol, 20 mg, 22 μ L) and it was obtained as a *Z/E* mixture with a *Z/E* ratio of 72:28 and isolated as a white solid (28 mg, 50% yield)

¹H NMR (500 MHz, CDCl₃) (*Z/E* mixture) δ 7.39 - 7.28 (m, 4H, *Z+E*), 7.25 - 7.20 (m, 1H, *Z+E*), 6.59 - 6.45 (m, 1H, *Z+E*), 6.09 (dd, *J* = 15.9, 6.6 Hz, 0.3H, *E*), 5.49 (dd, *J* = 11.8, 9.5 Hz, 0.7H, *Z*), 4.62 (d, *J* = 9.9 Hz, 0.7H, *Z*),

Decarboxylative hydroalkylation of alkynes

4.51 (bs, 1H, *Z+E*), 4.14 (bs, 0.3H, *E*), 1.86 (q, $J = 6.5$ Hz, 0.3H, *E*), 1.77 (bs, 0.7H, *Z*), 1.46 (s, 2.7H, *E*), 1.44 (s, 6.3H, *Z*), 0.95 (dd, $J = 6.8, 5.1$ Hz, 2H, *Z+E*), 0.88 (d, $J = 6.7$ Hz, 4H, *Z+E*).

^{13}C NMR (126 MHz, CDCl_3) (*Z/E* mixture) δ 155.6, 155.4, 137.1, 136.9, 131.3, 131.0, 130.8, 129.2, 128.9, 128.6, 128.4, 127.5, 127.26, 126.5, 79.5, 79.2, 57.9, 53.5, 33.6, 33.0, 28.6, 28.5, 18.9, 18.6, 18.5, 18.3.

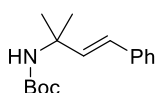
***tert*-butyl (*Z*)-(4,4-dimethyl-1-phenylpent-1-en-3-yl)carbamate (**3h**)**

Following GP1, **3h** was prepared starting from (*S*)-2-((*tert*-butoxycarbonyl)amino)-3,3-dimethylbutanoic acid (**1h**) (0.3 mmol, 69 mg) and ethynylbenzene (**2a**) (0.2 mmol, 20 mg, 22 μL) and it was obtained as a *Z/E* mixture with a *Z:E* ratio of 78:22 and isolated as a white amorphous solid (31 mg, 54% yield).

^1H NMR (500 MHz, CDCl_3) (*Z/E* mixture) δ 7.43 - 7.27 (m, 4H, *Z+E*), 7.24 - 7.18 (m, 1H, *Z+E*), 6.54 (d, $J = 11.8$ Hz, 0.75H, *Z*), 6.50 (d, $J = 15.9$ Hz, 0.25H, *E*), 6.14 (dd, $J = 15.9, 7.1$ Hz, 0.25H, *E*), 5.56 - 5.45 (m, 0.75H, *Z*), 4.63 (bs, 0.75H, *Z*), 4.53 (bs, 1H, *Z+E*), 4.07 (s, 0.25H, *E*), 1.55 - 1.31 (m, 9H, *Z+E*), 0.95 (s, 2.25H, *E*), 0.83 (s, 6.75H, *Z*).

^{13}C NMR (126 MHz, CDCl_3) (*Z/E* mixture) δ 155.8, 155.4, 137.2, 136.9, 131.7, 131.5, 129.6, 128.9, 128.6, 128.4, 127.9, 127.5, 127.1, 126.5, 79.4, 79.1, 61.2, 55.9, 35.6, 35.0, 28.6, 28.5, 26.6, 26.0.

HRMS (ESI) m/z calculated for $(\text{C}_{18}\text{H}_{27}\text{NNaO}_2)$ 312.1934 $[\text{M}+\text{Na}]^+$; found 312.1932

***tert*-butyl (*E*)-(2-methyl-4-phenylbut-3-en-2-yl)carbamate (**3i**)**

Following GP1, **3i** was prepared starting from 2-((*tert*-butoxycarbonyl)amino)-2-methylpropanoic acid (**1i**) (0.3 mmol, 61 mg) and ethynylbenzene (**2a**) (0.2 mmol, 20 mg, 22

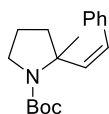
μL) and it was obtained as a *Z/E* mixture with a *Z:E* ratio of 34:66 and isolated as single isomers, both as white amorphous solids (37 mg, 71 % yield).

^1H NMR (400 MHz, CDCl_3) (*E* isomer) δ 7.39 - 7.35 (m, 2H), 7.33 - 7.27 (m, 2H), 7.24 - 7.18 (m, 1H), 6.45 (d, $J = 16.2$ Hz, 1H), 6.36 (d, $J = 16.3$ Hz, 1H), 4.67 (bs, 1H), 1.48 (s, 6H), 1.44 (s, 9H). (*Z* isomer) δ 7.32 - 7.27 (m, 2H), 7.26 - 7.18 (m, 3H), 6.49 (d, $J = 12.6$ Hz, 1H), 5.76 (d, $J = 12.6$ Hz, 1H), 4.50 (bs, 1H), 1.38 (s, 6H), 1.32 (s, 9H).

^{13}C NMR (101 MHz, CDCl_3) (*E* isomer) δ 154.8, 137.3, 136.3, 128.6, 127.4, 126.9, 126.5, 79.4, 53.4, 28.6, 28.0. (*Z* isomer) δ 154.0, 138.2, 138.0, 129.0, 128.4, 127.9, 126.7, 78.9, 53.2, 29.6, 28.5.

HRMS (ESI) m/z calculated for $(\text{C}_{16}\text{H}_{23}\text{NNaO}_2)$ 284.1621 $[\text{M}+\text{Na}]^+$; found 284.1624.

***tert*-butyl (*Z*)-2-methyl-2-styrylpyrrolidine-1-carboxylate (**3j**)⁸**



Following GP1, **3j** was prepared starting from (*S*)-1-(*tert*-butoxycarbonyl)-2-methylpyrrolidine-2-carboxylic acid (**1j**) (0.3 mmol, 69 mg) and ethynylbenzene (**2a**) (0.2 mmol, 20 mg, 22 μL)

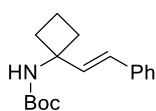
and it was obtained as a *Z/E* mixture with a *Z:E* ratio of 62:38 and isolated as single isomers, both as colourless oils (41 mg, 72 % yield).

The *Z* isomer exists as an approximately 1:1.2 mixture of rotamers A and B

^1H NMR (400 MHz, CDCl_3) (*Z* isomer, A/B mixture) δ 7.35 - 7.29 (m, 2H, A+B), 7.26 - 7.14 (m, 3H, A+B), 6.50 (d, $J = 12.9$ Hz, 0.5H, A), 6.44 (d, $J = 12.9$ Hz, 0.5H, B), 6.02 (d, $J = 12.7$ Hz, 0.5H, A), 5.88 (d, $J = 12.8$ Hz, 0.5H, B), 3.49 (dt, $J = 11.4, 6.6$ Hz, 0.5H, B), 3.41 - 3.34 (m, 0.5H, A), 3.27 (dt, $J = 10.7, 7.6$ Hz, 0.5H, B), 3.10 (q, $J = 9.0, 8.5$ Hz, 0.5H, B), 2.16 - 2.03 (m, 1H, A+B), 1.85 - 1.63 (m, 3H, A+B), 1.50 (s, 4.5H, A), 1.43 (s, 4.5H, A), 1.36 - 1.25 (m, 3H, A+B). (*E* isomer) δ 7.39 - 7.27 (m, 4H), 7.25 - 7.17 (m, 1H), 6.36 - 6.18 (m, 2H), 3.64 - 3.43 (bm, 2H), 2.00 (dt, $J = 12.5, 6.4$ Hz, 1H), 1.93 - 1.76 (m, 3H), 1.66 - 1.52 (m, 3H), 1.51 - 1.36 (m, 9H).

Decarboxylative hydroalkylation of alkynes

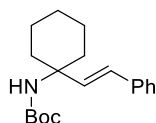
^{13}C NMR (101 MHz, CDCl_3) (*Z* isomer, *A/B* mixture) δ 154.2, 153.3, 140.0, 138.9, 138.6, 138.4, 128.7, 128.7, 128.0, 127.8, 127.8, 127.3, 126.7, 126.4, 79.5, 78.8, 63.2, 63.0, 47.5, 47.4, 41.9, 41.4, 28.7, 27.0, 26.1, 22.9, 22.3. (*E* isomer) δ 154.7, 137.5, 136.2, 128.7, 127.2, 126.8, 126.3, 79.4, 63.1, 48.2, 42.4, 28.6, 25.0, 21.8.

***tert*-butyl (*E*)-(1-styrylcyclobutyl)carbamate (**3k**)⁴**

Following GP1, **3k** was prepared starting from 1-((*tert*-butoxycarbonyl)amino)cyclobutane-1-carboxylic acid (**1k**) (0.3 mmol, 65 mg) and ethynylbenzene (**2a**) (0.2 mmol, 20 mg, 22 μL) and it was obtained as a *Z/E* mixture with a *Z:E* ratio of 39:61 and isolated as single isomers, both as white amorphous solids (39 mg, 71 % yield)

^1H NMR (500 MHz, CDCl_3) (*E* isomer) δ 7.41 - 7.37 (m, 2H), 7.31 (dd, J = 8.4, 6.9 Hz, 2H), 7.25 - 7.20 (m, 1H), 6.53 - 6.42 (m, 2H), 4.83 (bs, 1H), 2.41 - 2.25 (m, 4H), 2.04 - 1.93 (m, 1H), 1.93 - 1.85 (m, 1H), 1.44 (s, 9H). (*Z* isomer) δ 7.32 - 7.27 (m, 2H), 7.24 - 7.20 (m, 3H), 6.48 (d, J = 12.1 Hz, 1H), 6.07 (d, J = 12.1 Hz, 1H), 4.74 (bs, 1H), 2.37 (bs, 2H), 2.27 - 2.14 (m, 2H), 2.00 - 1.84 (m, 1H), 1.75 (p, J = 8.8 Hz, 1H), 1.36 (s, 9H).

^{13}C NMR (126 MHz, CDCl_3) (*E* isomer) δ 154.6, 137.3, 133.8, 128.7, 127.4, 126.9, 126.6, 79.4, 57.3, 34.6, 28.6, 15.0. (*Z* isomer) δ 154.3, 137.6, 137.5, 129.8, 129.0, 128.1, 127.0, 79.2, 56.2, 35.6, 28.5, 15.2.

***tert*-butyl (*E*)-(1-styrylcyclohexyl)carbamate (**3l**)**

Following GP1, **3l** was prepared starting from 1-((*tert*-butoxycarbonyl)amino)cyclohexane-1-carboxylic acid (**1l**) (0.3 mmol, 73 mg) and ethynylbenzene (**2a**) (0.2 mmol, 20 mg, 22

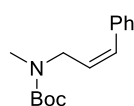
μL) and it was obtained as a *Z/E* mixture with a *Z:E* ratio of 40:60 and isolated as a slightly yellow oil (39 mg, 65% yield).

^1H NMR (400 MHz, CDCl_3) (*Z/E* mixture) δ 7.41 - 7.34 (m, 1H, *Z+E*), 7.32 - 7.26 (m, 2H, *Z+E*), 7.25 - 7.16 (m, 2H, *Z+E*), 6.53 (d, $J = 12.6$ Hz, 0.35H, *Z*), 6.46 (d, $J = 16.2$ Hz, 0.65H, *E*), 6.31 (d, $J = 16.4$ Hz, 0.65H, *E*), 5.75 (d, $J = 12.6$ Hz, 0.35H, *Z*), 4.53 (bs, 0.65H, *E*), 4.33 (bs, 0.35H, *Z*), 2.13 - 2.01 (bm, 1.3H, *E*), 1.91 (s, 0.7H, *Z*), 1.70 - 1.51 (m, 8H, *Z+E*), 1.43 (s, 5.85H, *E*), 1.31 (bs, 3.15H, *Z*).

^{13}C NMR (101 MHz, CDCl_3) (*Z/E* mixture) δ 154.3, 138.5, 137.5, 136.0, 129.2, 128.8, 128.6, 127.9, 127.4, 127.3, 126.5, 79.0, 78.6, 55.5, 54.9, 36.9, 35.8, 28.6, 28.5, 25.7, 25.5, 21.9, 21.9.

HRMS (ESI) m/z calculated for $(\text{C}_{19}\text{H}_{27}\text{NNaO}_2)$ 324.1934 $[\text{M}+\text{Na}]^+$; found 324.1934.

***tert*-butyl (*Z*)-methyl(3-phenylallyl)carbamate (**3m**)⁹**



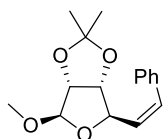
Following GP1, **3m** was prepared starting from *N*-(*tert*-butoxycarbonyl)-*N*-methylglycine (**1m**) (0.3 mmol, 57 mg) and ethynylbenzene (**2a**) (0.2 mmol, 20 mg, 22 μL) and it was

obtained as a *Z/E* mixture with a *Z:E* ratio of 69:31 and isolated as a colorless oil (21 mg, 41% yield).

^1H NMR (500 MHz, CDCl_3) (*Z/E* mixture) δ 7.40 - 7.29 (m, 3H, *Z+E*), 7.25 - 7.18 (m, 2H, *Z+E*), 6.59 (dt, $J = 11.7, 2.1$ Hz, 0.7H, *Z*), 6.46 (d, $J = 15.8$ Hz, 0.3H, *E*), 6.14 (d, $J = 16.1$ Hz, 0.3H, *E*), 5.63 (dt, $J = 11.7, 6.4$ Hz, 0.7H, *Z*), 4.12 (bs, 1.4H, *Z*), 3.98 (bs, 0.6H, *E*), 2.86 (bs, 0.9H, *E*), 2.78 (bs, 2.1H, *Z*), 1.48 (s, 2.7H, *E*), 1.43 (bs, 6.3H, *Z*).

^{13}C NMR (126 MHz, CDCl_3) (*Z/E* mixture) δ 155.9, 136.9, 136.8, 131.3, 128.9, 128.7, 128.4, 127.7, 127.2, 126.5, 125.4, 79.7, 79.7, 46.3, 33.9, 28.6, 28.5.

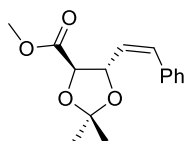
Decarboxylative hydroalkylation of alkynes

(3aR,4R,6R,6aR)-4-methoxy-2,2-dimethyl-6-((*Z*)-styryl)tetrahydrofuro[3,4-*d*][1,3]dioxole (3n)¹⁰

Following GP1, **3n** was prepared starting from (3a*S*,4*S*,6*R*,6a*R*)-6-methoxy-2,2-dimethyltetrahydrofuro[3,4-*d*][1,3]dioxole-4-carboxylic acid (**1n**) (0.3 mmol, 65 mg) and ethynylbenzene (**2a**) (0.2 mmol, 20 mg, 22 μ L) and it was obtained as a *Z/E* mixture with a *Z:E* ratio of 70:30 and d.r. >20:1. They were isolated as single isomers, both as colorless oils (28 mg, 50% yield)

¹H NMR (400 MHz, CDCl₃) (*E* isomer) δ 7.39 - 7.35 (m, 2H), 7.34 - 7.29 (m, 2H), 7.28 - 7.25 (m, 1H), 6.59 (d, *J* = 15.7 Hz, 1H), 6.22 (dd, *J* = 15.9, 8.8 Hz, 1H), 5.03 (s, 1H), 4.80 (dt, *J* = 8.9, 1.2 Hz, 1H), 4.71 (dd, *J* = 6.0, 1.0 Hz, 1H), 4.68 (d, *J* = 5.9 - 7.25 (m, 1H), 6.59 (dd, *J* = 11.7, 1.3 Hz, 1H), 5.74 (dd, *J* = 11.7, 9.8 Hz, 1H), 5.07 - 5.03 (m, 2H), 4.72 - 4.67 (m, 2H), 3.37 (s, 3H), 1.49 (d, *J* = 0.7 Hz, 3H), 1.33 (d, *J* = 0.7 Hz, 3H).

¹³C NMR (101 MHz, CDCl₃) (*E* isomer) δ 136.6, 133.0, 128.9, 128.7, 128.1, 126.8, 112.6, 109.4, 88.4, 85.8, 84.9, 54.8, 26.7, 25.2. (*Z* isomer) δ 136.0, 132.3, 130.7, 129.3, 128.5, 127.6, 112.5, 109.2, 86.0, 85.3, 83.2, 54.6, 26.6, 25.2.

methyl (4*R*,5*R*)-2,2-dimethyl-5-((*Z*)-styryl)-1,3-dioxolane-4-carboxylate (3o)

Following GP1, **3o** was prepared starting from (4*R*,5*R*)-5-(methoxycarbonyl)-2,2-dimethyl-1,3-dioxolane-4-carboxylic acid (**1o**) (0.3 mmol, 61 mg, 51 μ L) and ethynylbenzene (**2a**) (0.2 mmol, 20 mg, 22 μ L) and it was obtained as a 12:1 anti/syn mixture (*Z:E* ratio of the anti diastereomer 77:33, *Z:E* ratio of the syn diastereomer 64:36) and isolated as a colorless oil (18 mg, 33% yield)

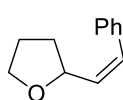
¹H NMR (400 MHz, CDCl₃) (anti diastereomer as *Z/E* mixture) δ 7.45 - 7.27 (m, 5H, *Z+E*), 6.85 (d, *J* = 11.5 Hz, 0.8H, *Z*), 6.75 (d, *J* = 15.8 Hz, 0.2H, *E*),

6.24 (dd, $J = 15.9, 7.0$ Hz, 0.2H, E), 5.75 (dd, $J = 11.5, 9.2$ Hz, 0.8H, Z), 4.96 (ddd, $J = 9.2, 7.5, 1.0$ Hz, 0.8H, Z), 4.75 (ddd, $J = 8.0, 6.0, 1.1$ Hz, 0.2H, E), 4.32 (dd, $J = 7.7, 1.3$ Hz, 1H, $Z+E$), 3.80 (s, 0.6H, E), 3.69 (s, 2.4H, Z), 1.54 - 1.52 (m, 4.8H, Z), 1.49 (d, $J = 0.8$ Hz, 1.2H, E).

^{13}C NMR (101 MHz, CDCl_3) (anti diastereomer as Z/E mixture) δ 170.7, 170.6, 136.4, 135.9, 134.3, 128.8, 128.7, 128.5, 128.4, 127.9, 127.1, 126.9, 125.2, 111.6, 111.5, 80.0, 79.6, 79.4, 75.2, 52.6, 52.5, 30.5, 29.8, 27.4, 27.1, 26.1, 26.1.

HRMS (ESI) m/z calculated for $\text{C}_{15}\text{H}_{18}\text{NaO}_4$ 285.1097 $[\text{M}+\text{Na}]^+$; found 285.1101

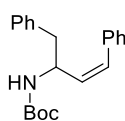
(Z)-2-styryltetrahydrofuran (**3p**)¹¹



Following GP1, **3p** was prepared starting from tetrahydrofuran-2-carboxylic acid (**1p**) (0.3 mmol, 35 mg, 29 μL) and ethynylbenzene (**2a**) (0.2 mmol, 20 mg, 22 μL) and it was obtained as a Z/E mixture with a $Z:E$ ratio of 67:34 and isolated as a colorless oil (14 mg, 40% yield).

^1H NMR (500 MHz, CDCl_3) (Z/E mixture) δ 7.40 - 7.37 (m, 1H, $Z+E$), 7.36 - 7.29 (m, 3H, $Z+E$), 7.28 - 7.21 (m, 1H, $Z+E$), 6.61 - 6.57 (m, 1H, $Z+E$), 6.21 (dd, $J = 15.9, 6.6$ Hz, 0.35H, E), 5.71 (dd, $J = 11.6, 8.9$ Hz, 0.65H, Z), 4.67 (dddd, $J = 9.0, 7.7, 6.6, 1.1$ Hz, 0.65H, Z), 4.48 (td, $J = 7.9, 7.3, 6.1$ Hz, 0.35H, E), 3.97 (dq, $J = 8.2, 6.6$ Hz, 1H), 3.85 (td, $J = 7.9, 6.2$ Hz, 0.35H, E), 3.79 (td, $J = 8.0, 6.0$ Hz, 0.65H, Z), 2.20 - 2.08 (m, 1H, $Z+E$), 2.07 - 1.88 (m, 2H, $Z+E$), 1.76 - 1.65 (m, 1H, $Z+E$). ^{13}C NMR (126 MHz, CDCl_3) (Z/E mixture) δ 137.0, 136.9, 133.0, 131.6, 130.7, 130.6, 129.0, 128.6, 128.3, 127.6, 127.2, 126.6, 79.8, 75.2, 68.3, 68.2, 33.1, 32.5, 26.5, 26.1.

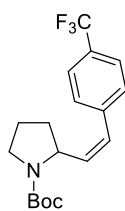
Decarboxylative hydroalkylation of alkynes

***tert*-butyl (*Z*)-(1,4-diphenylbut-3-en-2-yl)carbamate (**3q**)¹³**

Following GP1, **3q** was prepared starting from (*tert*-butoxycarbonyl)-*L*-phenylalanine (**1q**) (0.3 mmol, 79 mg) and ethynylbenzene (**2a**) (0.2 mmol, 20 mg, 22 μ L) and it was obtained as a *Z/E* mixture with a *Z:E* ratio of 76:24 and isolated as a colorless oil (40 mg, 62% yield).

¹H NMR (400 MHz, CDCl₃) (*Z/E* mixture) δ 7.34 - 7.27 (m, 4H, *Z+E*), 7.24 - 7.11 (m, 6H, *Z+E*), 6.47 (m, 1H, *Z+E*), 6.14 (dd, *J* = 15.9, 5.8 Hz, 0.25H, *E*), 5.52 (dd, *J* = 11.7, 9.4 Hz, 0.75H, *Z*), 4.86 (bs, 0.75H, *Z*), 4.64 - 4.46 (bm, 1.25H, *Z+E*), 2.99 - 2.80 (m, 2H, *Z+E*), 1.43 (bm, 9H, *Z+E*).

¹³C NMR (101 MHz, CDCl₃) (*Z/E* mixture) δ 155.5, 155.2, 137.7, 137.7, 137.1, 136.8, 131.7, 131.2, 130.5, 130.0, 129.9, 129.4, 128.9, 128.8, 128.7, 128.6, 127.8, 127.5, 126.8, 126.8, 126.7, 125.6, 79.7, 50.0, 49.9, 42.3, 42.1, 28.7, 28.4.

***tert*-butyl (*Z*)-2-(4-(trifluoromethyl)styryl)pyrrolidine-1-carboxylate (**4b**)⁴**

Following GP1, **4b** was prepared starting from (*tert*-butoxycarbonyl)-*L*-proline (**1a**) (0.3 mmol, 65 mg) and 1-ethynyl-4-(trifluoromethyl)benzene (**2b**) (0.2 mmol, 34 mg, 33 μ L) and it was obtained as a *Z/E* mixture with a *Z:E* ratio of 73:27 and isolated as a colorless oil (48 mg, 71% yield).

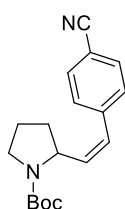
¹H NMR (400 MHz, CDCl₃) (*Z/E* mixture) δ 7.63 - 7.51 (m, 2H, *Z+E*), 7.46 - 7.34 (m, 2H, *Z+E*), 6.42 (d, *J* = 11.9 Hz, 1H, *Z+E*), 6.20 (bs, 0.3H, *E*), 5.72 (t, *J* = 10.5 Hz, 0.7H, *Z*), 4.68 (bs, 0.7H, *Z*), 4.57 - 4.26 (bm, 0.3H, *Z*), 3.45 (bs, 2H, *Z+E*), 2.18 (bs, 1H), 2.03 - 1.72 (m, 3H, *Z+E*), 1.53 - 1.15 (m, 9H, *Z+E*).

¹⁹F NMR (376 MHz, CDCl₃) (*Z/E* mixture) δ -62.18 (*E*), -62.20(*Z*).

^{13}C NMR (101 MHz, CDCl_3) (*Z* isomer reported only) δ 154.7, 140.7, 137.2, 129.1, 126.6, 125.7, 125.2 (q, $J = 3.8$ Hz), 123.0, 79.5, 55.0, 46.7, 33.9, 28.6, 24.0.

Following GP2, **4b** was prepared starting from (*tert*-butoxycarbonyl)-*L*-proline (**1a**) (0.3 mmol, 65 mg) and 1-ethynyl-4-(trifluoromethyl)benzene (**2b**) (0.2 mmol, 34 mg, 33 μL) and it was obtained as a *Z/E* mixture with a *Z/E* ratio of 26:74 and isolated as a colorless oil (53 mg, 78% yield).

tert-butyl (*Z*)-2-(4-cyanostyryl)pyrrolidine-1-carboxylate (**4c**)¹²

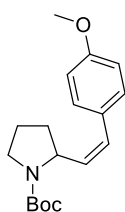


Following GP1, **4c** was prepared starting from (*tert*-butoxycarbonyl)-*L*-proline (**1a**) (0.3 mmol, 65 mg) and 4-ethynylbenzonitrile (**2c**) (0.2 mmol, 25 mg) and it was obtained as a *Z/E* mixture with a *Z/E* ratio of 67:33 and isolated as single isomers, both as colorless oils (50 mg, 83% yield).

^1H NMR (400 MHz, CDCl_3) (*Z* isomer) δ 7.62 (d, $J = 8.0$ Hz, 2H), 7.57 - 7.33 (m, 2H), 6.40 (d, $J = 11.8$ Hz, 1H), 5.76 (dd, $J = 11.8, 9.3$ Hz, 1H), 4.65 (bs, 1H), 3.44 (bs, 2H), 2.21 - 2.12 (bm, 1H), 2.02 - 1.69 (m, 3H), 1.51 - 1.18 (m, 9H). (*E* isomer) δ 7.57 (bs, 2H), 7.42 (d, $J = 8.2$ Hz, 2H), 6.41 (bs, 1H), 6.24 (bs, 1H), 4.61 - 4.36 (bm, 1H), 3.47 (bs, 2H), 2.14 (bs, 1H), 1.95 - 1.84 (m, 2H), 1.84 - 1.77 (m, 1H), 1.40 (bs, 9H).

^{13}C NMR (126 MHz, CDCl_3) (*Z* isomer reported only) δ 154.6, 141.8, 138.2, 132.2, 129.6, 126.4, 119.1, 110.3, 79.6, 54.9, 46.7, 33.9, 28.6, 24.0.

tert-butyl (*Z*)-2-(4-methoxystyryl)pyrrolidine-1-carboxylate (**4d**)⁴



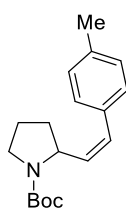
Following GP1, **4d** was prepared starting from (*tert*-butoxycarbonyl)-*L*-proline (**1a**) (0.2 mmol, 43 mg) and 1-ethynyl-4-methoxybenzene (**2d**) (0.6 mmol, 25 mg, 78 μL) and it was

Decarboxylative hydroalkylation of alkynes

obtained as a *Z/E* mixture with a *Z:E* ratio of 77:23 and isolated as single isomers both as slightly yellow oils (44 mg, 72% yield).

^1H NMR (500 MHz, CDCl_3) (*Z* isomer) δ 7.20 (s, 2H), 6.91 - 6.82 (m, 2H), 6.33 (d, $J = 11.7$ Hz, 1H), 5.52 (bs, 1H), 4.72 (bs, 1H), 3.81 (s, 3H), 3.53 - 3.39 (bm, 2H), 2.28 - 2.12 (bm, 1H), 2.01 - 1.88 (m, 1H), 1.87 - 1.76 (m, 2H), 1.55 - 1.23 (bm, 9H). (*E* isomer) δ 7.30 - 7.26 (m, 2H), 6.84 (d, $J = 8.2$ Hz, 2H), 6.34 (d, $J = 15.5$ Hz, 1H), 5.94 (bs, 1H), 4.55 - 4.31 (bm, 1H), 3.80 (s, 3H), 3.45 (bs, 2H), 2.06 (bs, 1H), 1.97 - 1.89 (m, 1H), 1.87 - 1.82 (m, 1H), 1.81 - 1.73 (m, 1H), 1.42 (s, 9H).

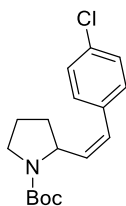
^{13}C NMR (126 MHz, CDCl_3) (*Z* isomer reported only) δ 158.6, 154.8, 133.7, 130.2, 129.9, 127.5, 113.7, 79.2, 55.4, 55.2, 46.6, 34.0, 28.6, 24.0.

***tert*-butyl (*Z*)-2-(4-methylstyryl)pyrrolidine-1-carboxylate (**4e**)⁴**

Following GP1, **4e** was prepared starting from (*tert*-butoxycarbonyl)-*L*-proline (**1a**) (0.3 mmol, 65 mg) and 1-ethynyl-4-methylbenzene (**2e**) (0.2 mmol, 23 mg, 25 μL) and it was obtained as a *Z/E* mixture with a *Z:E* ratio of 68:32 and isolated as colorless oil (43 mg, 75% yield).

^1H NMR (500 MHz, CDCl_3) (*Z/E* mixture) δ 7.24 (d, $J = 8.0$ Hz, 1H, *Z+E*), 7.13 (d, $J = 7.9$ Hz, 3H, *Z+E*), 6.36 (d, $J = 11.9$ Hz, 1H, *Z+E*), 6.03 (bs, 0.3H, *E*), 5.67 - 5.50 (bm, 0.7H, *Z*), 4.72 (bs, 0.7H, *Z*), 4.56 - 4.31 (bm, 0.3H, *E*), 3.60 - 3.28 (bm, 2H, *Z+E*), 2.34 (s, 2.1H, *Z*), 2.33 (s, 0.9H, *E*), 2.26 - 2.03 (bm, 1H, *Z+E*), 1.96 - 1.88 (m, 1H, *Z+E*), 1.87 - 1.75 (m, 2H, *Z+E*), 1.49 - 1.21 (m, 9H, *Z+E*).

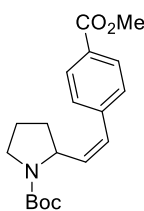
^{13}C NMR (126 MHz, CDCl_3) (*Z/E* mixture) δ 154.8, 137.2, 136.5, 134.5, 134.4, 134.3, 129.3, 128.9, 128.8, 127.9, 126.3, 79.2, 59.2, 55.2, 46.6, 46.2, 34.1, 32.7, 28.6, 28.6, 24.0, 23.2, 21.3.

***tert*-butyl (*Z*)-2-(4-chlorostyryl)pyrrolidine-1-carboxylate (**4f**)⁴**

Following GP1, **4f** was prepared starting from (*tert*-butoxycarbonyl)-*L*-proline (**1a**) (0.3 mmol, 65 mg) and 1-chloro-4-ethynylbenzene (**2f**) (0.2 mmol, 27 mg) and it was obtained as a *Z/E* mixture with a *Z:E* ratio of 76:24 and isolated as colorless oil (43 mg, 70% yield).

¹H NMR (400 MHz, CDCl₃) (*Z/E* mixture) δ 7.36 - 7.27 (m, 2H, *Z+E*), 7.26 - 7.14 (m, 2H, *Z+E*), 6.43 - 6.29 (m, 1H, *Z+E*), 6.07 (bs, 0.25H, *E*), 5.62 (dd, *J* = 11.5, 9.5 Hz, 0.75H, 1H, *Z+E*), 1.97 - 1.70 (m, 3H, *Z+E*), 1.42 (s, 2.25H, *E*), 1.30 (s, 6.75H, *Z*).

¹³C NMR (101 MHz, CDCl₃) (*Z/E* mixture) δ 154.7, 137.1, 135.8, 135.6, 135.1, 132.7, 130.2, 128.9, 128.8, 128.4, 128.2, 127.6, 126.8, 79.4, 59.0, 55.0, 46.6, 33.9, 32.6, 28.6, 28.6, 24.0, 23.2.

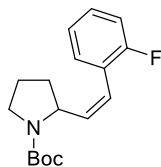
***tert*-butyl (*Z*)-2-(4-(methoxycarbonyl)styryl)pyrrolidine-1-carboxylate (**4g**)⁴**

Following GP1, **4g** was prepared starting from (*tert*-butoxycarbonyl)-*L*-proline (**1a**) (0.3 mmol, 65 mg) and methyl 4-ethynylbenzoate (**2g**) (0.2 mmol, 32 mg) and it was obtained as a *Z/E* mixture with a *Z:E* ratio of 83:17 and isolated as colorless oil (39 mg, 59% yield).

¹H NMR (500 MHz, CDCl₃) (*Z/E* mixture) δ 7.98 (d, *J* = 8.3 Hz, 2H, *Z+E*), 7.53 - 7.28 (bm, 2H, *Z+E*), 6.41 (d, *J* = 11.8 Hz, 1H, *Z+E*), 6.21 (bs, 0.1H, *E*), 5.70 (bs, 0.9H, *Z*), 4.68 (bs, 0.9H, *Z*), 4.56 - 4.34 (bm, 0.1H, *E*), 3.89 (s, 3H, *Z+E*), 3.52 - 3.38 (bm, 2H, *Z+E*), 2.32 - 2.07 (bm, 1H, *Z+E*), 1.96 - 1.77 (m, 3H, *Z+E*), 1.40 (s, 0.9H, *E*), 1.26 (s, 8.1H, *Z*).

Decarboxylative hydroalkylation of alkynes

^{13}C NMR (126 MHz, CDCl_3) (*Z/E* mixture) δ 167.0, 154.7, 141.8, 137.1, 130.0, 129.6, 128.9, 128.5, 127.1, 126.2, 79.4, 79.4, 55.0, 53.5, 52.2, 52.11, 46.7, 33.9, 28.7, 28.6, 24.0.

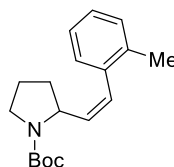
***tert*-butyl (*Z*)-2-(2-fluorostyryl)pyrrolidine-1-carboxylate (**4h**)⁴**

Following GP1, **4h** was prepared starting from (*tert*-butoxycarbonyl)-*L*-proline (**1a**) (0.3 mmol, 65 mg) and methyl 1-ethynyl-2-fluorobenzene (**2h**) (0.2 mmol, 24 mg, 23 μL) and it was obtained as a *Z/E* mixture with a *Z:E* ratio of 85:15 and isolated as colorless oil (30 mg, 52% yield).

^1H NMR (400 MHz, CDCl_3) (*Z:E* mixture) δ 7.41 (t, $J = 7.7$ Hz, 0.15H, *E*), 7.26 (s, 0.85H, *Z*), 7.25 - 7.18 (m, 1H, *Z+E*), 7.10 (t, $J = 7.2$ Hz, 1H, *Z+E*), 7.03 (dd, $J = 10.2, 8.1$ Hz, 1H, *Z+E*), 6.55 (d, $J = 15.9$ Hz, 0.15H, *E*), 6.43 (d, $J = 11.7$ Hz, 0.85H, *Z*), 6.17 (bs, 0.15H, *E*), 5.80 - 5.54 (m, 0.85H, *Z*), 4.59 (bs, 0.85H, *Z*), 4.39 (bs, 0.15H, *E*), 3.57 - 3.36 (bm, 2H, *Z+E*), 2.19 (bs, 1H, *Z+E*), 1.99 - 1.76 (m, 3H, *Z+E*), 1.43 (s, 1.35H, *E*), 1.30 (s, 7.65H, *Z*).

^{19}F NMR (376 MHz, CDCl_3) (*Z/E* mixture) δ -114.43 (*Z*), -114.86 (*Z*), -117.86 (*E*).

^{13}C NMR (101 MHz, CDCl_3) (*Z* isomer reported only) δ 160.2 (d, $J = 247.2$ Hz), 154.8, 136.6, 130.8, 128.8 (d, $J = 8.0$ Hz), 124.7 (d, $J = 14.6$ Hz), 123.7, 120.7, 115.5 (d, $J = 22.0$ Hz), 79.4, 55.2, 46.7, 33.8, 28.5, 24.0.

***tert*-butyl (*Z*)-2-(2-methylstyryl)pyrrolidine-1-carboxylate (**4i**)**

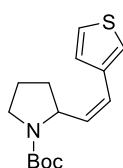
Following GP1, **4i** was prepared starting from (*tert*-butoxycarbonyl)-*L*-proline (**1a**) (0.3 mmol, 65 mg) and methyl 1-ethynyl-2-methylbenzene (**2i**) (0.2 mmol, 23 mg, 25 μL) and it was obtained as a *Z/E* mixture with a *Z:E* ratio of 76:24 and isolated as colorless oil (45 mg, 79% yield).

^1H NMR (400 MHz, CDCl_3) (Z/E mixture) δ 7.43 - 7.37 (m, 1H, $Z+E$), 7.20 - 7.11 (m, 3H, $Z+E$), 6.61 (d, $J = 15.5$ Hz, 0.2H, E), 6.42 (d, $J = 11.6$ Hz, 0.8H, Z), 5.97 (dd, $J = 15.6, 6.3$ Hz, 0.2H, E), 5.68 (dd, $J = 11.6, 8.8$ Hz, 0.8H, Z), 4.68 - 4.57 (m, 0.8H, Z), 4.43 (bs, 0.2H, E), 3.43 (bs, 2H, $Z+E$), 2.32 (s, 0.6H, E), 2.28 (s, 2.4H, Z), 2.16 - 2.03 (bm, 1H, $Z+E$), 1.97 - 1.85 (m, 1H, $Z+E$), 1.83 - 1.72 (m, 2H, $Z+E$), 1.45 (s, 1.8H, E), 1.35 (s, 7.2H, Z).

^{13}C NMR (101 MHz, CDCl_3) (Z isomer reported only) δ 154.8, 136.3, 134.6, 130.0, 129.1, 127.2, 127.1, 125.8, 125.5, 79.2, 55.0, 46.6, 34.1, 28.6, 23.8, 20.1. HRMS (ESI) m/z calculated for ($\text{C}_{18}\text{H}_{25}\text{NNaO}_2$) 310.1777 [$\text{M}+\text{Na}$] $^+$; found 310.1777

Following GP2, **4i** was prepared starting from (*tert*-butoxycarbonyl)-*L*-proline (**1a**) (0.3 mmol, 65 mg) and 1-ethynyl-4-(trifluoromethyl)benzene (**2b**) (0.2 mmol, 23 mg, 25 μL) and it was obtained as a Z/E mixture with a $Z:E$ ratio of 40:60 and isolated as a colorless oil (35 mg, 61% yield).

tert-butyl (Z)-2-(2-(thiophen-3-yl)vinyl)pyrrolidine-1-carboxylate (**4j**)



Following GP1, **4j** was prepared starting from (*tert*-butoxycarbonyl)-*L*-proline (**1a**) (0.2 mmol, 43 mg) and methyl 3-ethynylthiophene (**2j**) (0.6 mmol, 65 mg, 60 μL) and it was obtained as a Z/E mixture with a $Z:E$ ratio of 60:40 and isolated as yellow amorphous solid (31 mg, 55% yield).

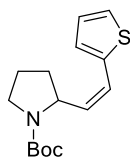
^1H NMR (500 MHz, CDCl_3) (Z/E mixture) δ 7.30 - 7.22 (m, 1H, $Z+E$), 7.20 - 7.06 (m, 2H, $Z+E$), 6.48 - 6.29 (bm, 1H, $Z+E$), 5.94 (bs, 0.4H, E), 5.55 (bs, 0.6H, Z), 4.79 (bs, 0.6H, Z), 4.54 - 4.28 (bm, 0.4H, E), 3.53 - 3.40 (bm, 2H, $Z+E$), 2.19 (bs, 0.6H, Z), 2.07 (bs, 0.4H, E), 1.99 - 1.72 (m, 3H, $Z+E$), 1.43 (bs, 5.4H, Z), 1.31 (bs, 3.6H, E).

^{13}C NMR (126 MHz, CDCl_3) (Z isomer reported only) δ 154.8, 138.1, 134.4, 130.7, 128.7, 125.2, 123.8, 79.3, 55.6, 46.5, 33.7, 28.6, 24.0.

Decarboxylative hydroalkylation of alkynes

HRMS (ESI) m/z calculated for (C₁₅H₂₁NNaO₂S) 302.1185 [M+Na]⁺; found 302.1186

tert-butyl (*Z*)-2-(2-(thiophen-3-yl)vinyl)pyrrolidine-1-carboxylate (**4k**)



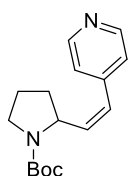
Following GP1, **4k** was prepared starting from (*tert*-butoxycarbonyl)-*L*-proline (**1a**) (0.2 mmol, 43 mg) and methyl 2-ethynylthiophene (**2k**) (0.6 mmol, 65 mg, 57 μ L) and it was obtained as a *Z/E* mixture with a *Z:E* ratio of 72:28 and isolated as yellow amorphous solid (41 mg, 73% yield).

¹H NMR (400 MHz, CDCl₃) (*Z/E* mixture) δ 7.24 (d, J = 5.7 Hz, 0.55H, *Z*), 7.11 (d, J = 5.1 Hz, 0.45H, *E*), 7.02 - 6.87 (m, 2H, *Z+E*), 6.60 - 6.39 (bm, 1H, *Z+E*), 5.92 (dd, J = 15.7, 6.6 Hz, 0.45H, *E*), 5.52 (bs, 0.55H, *Z*), 4.93 (td, J = 8.3, 4.4 Hz, 0.55H, *Z*), 4.56 - 4.24 (bm, 0.45H, *E*), 3.54 - 3.38 (bm, 2H, *Z+E*), 2.27 (dq, J = 12.3, 7.6 Hz, 0.55H, *Z*), 2.06 (bs, 0.45H, *E*), 1.96 - 1.81 (m, 2H, *Z+E*), 1.81 - 1.71 (m, 1H, *Z+E*), 1.42 (s, 4.95H, *Z*), 1.30 (s, 4.05H, *E*).

¹³C NMR (101 MHz, CDCl₃) (*Z/E* mixture) δ 154.8, 142.3, 139.8, 133.7, 130.7, 127.8, 127.4, 126.9, 125.5, 125.3, 123.9, 122.9, 120.5, 79.4, 79.3, 58.8, 55.8, 46.5, 46.3, 33.3, 32.6, 28.6, 28.5, 24.1, 23.2.

HRMS (ESI) m/z calculated for (C₁₅H₂₁NNaO₂S) 302.1185 [M+Na]⁺; found 302.1189

tert-butyl (*Z*)-2-(2-(pyridin-4-yl)vinyl)pyrrolidine-1-carboxylate (**4l**)⁵



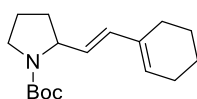
Following GP1, **4l** was prepared starting from (*tert*-butoxycarbonyl)-*L*-proline (**1a**) (0.3 mmol, 65 mg) and methyl 4-ethynylpyridine (**2l**) (0.2 mmol, 21 mg) and it was obtained as a

Z/E mixture with a *Z:E* ratio of 84:16 and isolated as a pale yellow solid (36 mg, 65% yield).

^1H NMR (500 MHz, CDCl_3) (*Z* isomer) δ 8.55 (s, 2H), 7.42 - 7.03 (m, 2H), 6.31 (d, $J = 11.8$ Hz, 1H), 5.78 (dd, $J = 11.8, 9.2$ Hz, 1H), 4.67 (bs, 2H), 3.63 - 3.23 (bm, 2H), 2.34 - 2.03 (bm, 1H), 1.94 - 1.73 (m, 3H), 1.42 - 1.21 (m, 9H).

^{13}C NMR (126 MHz, CDCl_3) (*Z* isomer) δ 154.6, 149.9, 144.6, 139.0, 125.5, 123.6, 79.5, 54.9, 46.7, 33.9, 28.5, 24.0.

***tert*-butyl (*E*)- 2-(2-(cyclohex-1-en-1-yl)vinyl)pyrrolidine-1-carboxylate (**4m**)**



Following GP1, **4m** was prepared starting from (*tert*-butoxycarbonyl)-*L*-proline (**1a**) (0.2 mmol, 43 mg) and methyl 1-ethynylcyclohex-1-ene (**2m**) (0.6 mmol, 64 mg,

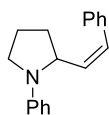
71 μL) and it was obtained as a *Z/E* mixture with a *Z:E* ratio of 48:52 and isolated as colorless oil (25 mg, 45% yield).

^1H NMR (500 MHz, C_6D_6 , 343 K) (*Z/E* mixture) δ 6.39 (d, $J = 15.7$ Hz, 0.5H, *E*), 5.95 (d, $J = 11.7$ Hz, 0.5H, *Z*), 5.89 - 5.83 (m, 1H, *Z+E*), 5.67 (dd, $J = 15.7, 6.1$ Hz, 0.5H, *E*), 5.44 (dd, $J = 11.7, 9.2$ Hz, 0.5H, *Z*), 5.02 (bs, 0.5H, *Z*), 4.55 (bs, 0.5H, *E*), 3.65 - 3.47 (bm, 2H, *Z+E*), 2.49 - 2.33 (m, 1H, *Z+E*), 2.27 - 2.16 (m, 3H, *Z+E*), 2.00 - 1.83 (m, 1H, *Z+E*), 1.81 - 1.75 (m, 3H, *Z+E*), 1.70 - 1.68 (m, 9H, *Z+E*), 1.68 - 1.62 (m, 3H, *Z+E*), 1.61 - 1.54 (m, 1H, *Z+E*).

^{13}C NMR (126 MHz, C_6D_6 , 343 K) (*Z/E* mixture) δ 154.5, 154.4, 135.8, 135.7, 133.7, 132.4, 128.4, 128.3, 127.4, 78.6, 78.5, 59.2, 55.7, 46.8, 46.7, 34.4, 32.8, 29.3, 28.8, 28.8, 26.2, 26.0, 25.2, 24.0, 23.6, 23.3, 23.0, 23.0, 22.5.

HRMS (ESI) m/z calculated for ($\text{C}_{17}\text{H}_{27}\text{NNaO}_2$) 300.1934 [$\text{M}+\text{Na}$] $^+$; found 300.1929

Decarboxylative hydroalkylation of alkynes

(Z)-1-phenyl-2-styrylpyrrolidine (3r)⁵

3r was prepared following GP3, obtained as a *Z/E* mixture with a *Z:E* ratio of 82:18 and isolated as single isomers, both as colourless oils (37.4 mg, 75% yield).

¹H NMR (500 MHz, CDCl₃) (*E* isomer) δ 7.36 - 7.33 (m, 2H), 7.31 - 7.26 (m, 2H), 7.24 - 7.18 (m, 3H), 6.72 - 6.61 (m, 3H), 6.46 (dd, *J* = 15.8, 1.4 Hz, 1H), 6.23 (dd, *J* = 15.8, 5.4 Hz, 1H), 4.32 (ddt, *J* = 7.4, 5.4, 2.0 Hz, 1H), 3.57 (ddd, *J* = 9.7, 7.5, 2.5 Hz, 1H), 3.30 (td, *J* = 9.1, 6.7 Hz, 1H), 2.22 - 2.13 (m, 1H), 2.11 - 2.04 (m, 1H), 2.03 - 1.96 (m, 1H), 1.93 (ddd, *J* = 11.6, 5.9, 2.8 Hz, 1H). (*Z* isomer) δ 7.46 - 7.40 (m, 2H), 7.37 (dd, *J* = 6.7, 1.8 Hz, 2H), 7.35 - 7.31 (m, 1H), 7.16 - 7.10 (m, 2H), 6.64 (tt, *J* = 8.9, 1.4 Hz, 1H), 6.57 (dd, *J* = 11.7, 1.2 Hz, 1H), 6.43 (d, *J* = 8.1 Hz, 2H), 5.69 (dd, *J* = 11.7, 9.2 Hz, 1H), 4.64 (tdd, *J* = 9.6, 3.4, 1.3 Hz, 1H), 3.58 (ddd, *J* = 8.9, 6.2, 3.0 Hz, 1H), 3.41 - 3.23 (m, 2H), 2.43 - 2.34 (m, 1H), 2.23 - 2.12 (m, 1H), 2.05 - 2.01 (m, 1H).

¹³C NMR (126 MHz, CDCl₃) (*E* isomer) δ 147.7, 137.2, 131.8, 129.6, 128.6, 127.4, 126.5, 115.9, 112.4, 60.9, 48.9, 33.2, 23.5. (*Z* isomer) δ 147.5, 136.2, 129.5, 129.2, 129.1, 129.0, 128.4, 127.2, 115.9, 112.4, 56.5, 48.8, 33.9, 24.5.

III.4.7. References

¹ Luo, J.; Zhang, J. *ACS Catal.*, **2016**, *6*, 873-877.

² Sureshbabu, P.; Tjakraatmadja, A. A. J. S.; Hanmandlu, C.; Elavarasan, K.; Kulak, N.; Sabiah, S. *RSC Adv.*, **2015**, *5*, 22405-22418.

³ Lakowicz, J. R. Ed. *Principles of Fluorescence Spectroscopy*, chap. 3, pp. 52-93 (Plenum Press, New York, 1983).

⁴ Dai, G.-L.; Lai, S.-Z.; Luo, Z.; Tang, Z.-Y. *Org. Lett.*, **2019**, *21*, 2269-2272.

- ⁵ Noble, A.; MacMillan, D. W. C. *J. Am. Chem. Soc.*, **2014**, *136*, 11602-11605.
- ⁶ Ketcham, J. M.; Cardoso, F. S. P.; Biannic, B.; Piras, H.; Aponick, A. *Isr. J. Chem.*, **2013**, *53*, 923-931.
- ⁷ Kano, T.; Kobayashi, R.; Maruoka, K. *Org. Lett.*, **2016**, *18*, 276-279.
- ⁸ Ma, X.; Hazelden, I. R.; Langer, T.; Munday, R. H.; Bower, J. F. *J. Am. Chem. Soc.*, **2019**, *141*, 3356-3360.
- ⁹ Lei, Y.; Qiu, R.; Zhang, L.; Xu, C.; Pan, Y.; Qin, X.; Li, H.; Xu, L.; Deng, Y. *ChemCatChem*, **2015**, *7*, 1275-1279.
- ¹⁰ Pal, T. K.; Pathak, T. *Carbohydr. Res.*, **2008**, *343*, 2826-2829.
- ¹¹ Li, J.; Zhang, J.; Tan, H.; Wang, D. Z. *Org. Lett.*, **2015**, *17*, 2522-2525.
- ¹² Heitz, D.R.; Rizwan, K.; Molander G. A. *J. Org. Chem.*, **2016**, *81*, 7308-7313.
- ¹³ Koy, M.; Sandfort, F.; Tlahuext-Aca, A.; Quach, L.; Daniliuc, C. G.; Glorius, F. *Chem. Eur. J.*, **2018**, *24*, 4552-4555
- ¹⁴ Wang, X.; Dong, S.; Feng, D.; Chen, Y.; Ma, M.; Hu W. *Tetrahedron*, **2017**, *73*, 2255-2266.

UNIVERSITAT ROVIRA I VIRGILI

Harnessing Visible Light for the Development of Novel Synthetic Strategies

Marco Michele Mastandrea

CHAPTER IV

Anion- π interactions in light-induced reactions

IV.1. Introduction	227
IV.1.1. Anion-π interactions	227
IV.1.2. Anion-π catalysis	229
IV.1.3. Nitrogen-centered radicals	230
IV.1.4. Amidyl radicals	233
IV.2. Objective	241
IV.3. Anion-π interactions driven amidation of aromatic systems	244
IV.3.1. Preliminary studies and optimization	244
IV.3.2. Reaction scope	246
IV.3.3. Mechanistic investigation	249
IV.3.4. Conclusions	256
IV.4. Supporting information	257

UNIVERSITAT ROVIRA I VIRGILI

Harnessing Visible Light for the Development of Novel Synthetic Strategies

Marco Michele Mastandrea

CHAPTER IV

Anion- π interactions in light-induced reactions

IV.1. Introduction

IV.1.1. Anion- π interactions

In sharp contrast to the well-studied cation binding to aromatic systems, anion- π interactions have been largely overlooked, primarily due to their counterintuitive nature (anions are not expected to show attractive interactions with aromatic π -system). After the first reports,¹ mainly focused on anion receptors, in the early 1990s Schneider described a distinct attractive interaction between negative charges and polarizable aromatic regions of host-guest systems.² Only in 2002, three theoretical studies by Alkorta,³ Deyà,⁴ and Mascal⁵ confirmed the presence of favorable interactions between electron deficient aromatic rings and anions, with binding energies similar to hydrogen bonds (20-50 kJ mol⁻¹). The term “anion- π interactions” was coined by Deyà to define energetically privileged non-covalent forces between a π -acidic aromatic system and an anion.

¹ a) Park, C. H.; Simmons, H. E. *J. Am. Chem. Soc.* **1968**, *90*, 2431-2432; b) Beer, P. D.; Gale, P. A. *Angew. Chem., Int. Ed.* **2001**, *40*, 486-516 and reference therein.

² Schneider, H.-J.; Werner, F.; Blatter, T. *J. Phys. Org. Chem.* **1993**, *6*, 590-594.

³ Alkorta, I.; Rozas, I.; Elguero, J. *J. Am. Chem. Soc.* **2002**, *124*, 8593-8598.

⁴ Quinonero, D.; Garau, C.; Rotger, Frontera, C. A.; Ballester, P. Costa, A.; Deyà, P. M. *Angew. Chem. Int. Ed.* **2002**, *41*, 3389-3392.

⁵ M. Mascal, M.; Armstrong, A.; Bartberger, M.D. *J. Am. Chem. Soc.* **2002**, *124*, 6274-6276.

Anion- π interactions in light-induced reactions

Anion- π interaction result from a combination of electrostatic and anion-induced polarization contributions.⁶ The electrostatic component of the interaction is related to the permanent quadrupole moment (Q_{zz}) of the aromatic system, a measure of the charge distribution of a molecule relative to a particular axis (Figure IV-1, a). For example, hexafluorobenzene has a large and positive Q_{zz} (due to the strong electron-withdrawing fluorine substituents) while benzene has a large and negative one [$Q_{zz}(\text{C}_6\text{F}_6) = +9.50$ B and $Q_{zz}(\text{C}_6\text{H}_6) = -8.48$ B; 1 B (Buckingham) = 3.336×10^{-40} C m²]. Topological analysis of the electron density in anion- π interaction revealed a strong correlation between the magnitude of Q_{zz} and the electrostatic contribution to the interaction energy, with higher positive quadrupole moment leading to more favorable interaction. Moreover, when Q_{zz} is very high, the electrostatic term is essentially dominating the interaction energy. The anion-induced polarization (Figure IV-1, b) is correlated with the molecular polarizability (α_{\parallel}) and reflects the interaction of the π electron cloud with the anion. Polarizability contribution to the overall energy is higher for aromatic systems with higher α_{\parallel} and prevails over electrostatic for non-electron deficient rings.

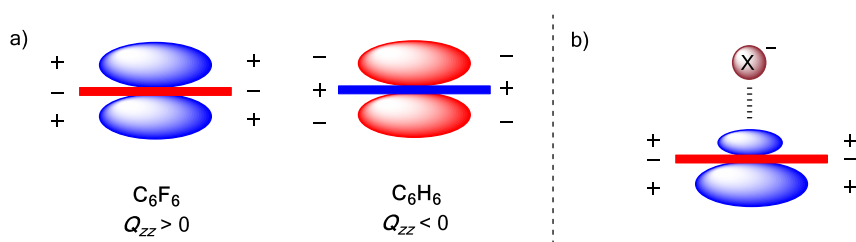


Figure IV-1. a) Representation of the quadrupole moment for hexafluorobenzene and benzene; b) aromatic π -electron density polarizability.

⁶ Garau, C.; Frontera, C. A.; Quinonero, D.; Ballester, P.; Costa, A. Deyà, P. M. *ChemPhysChem* **2003**, *4*, 1344-1348.

IV.1.2. Anion- π catalysis

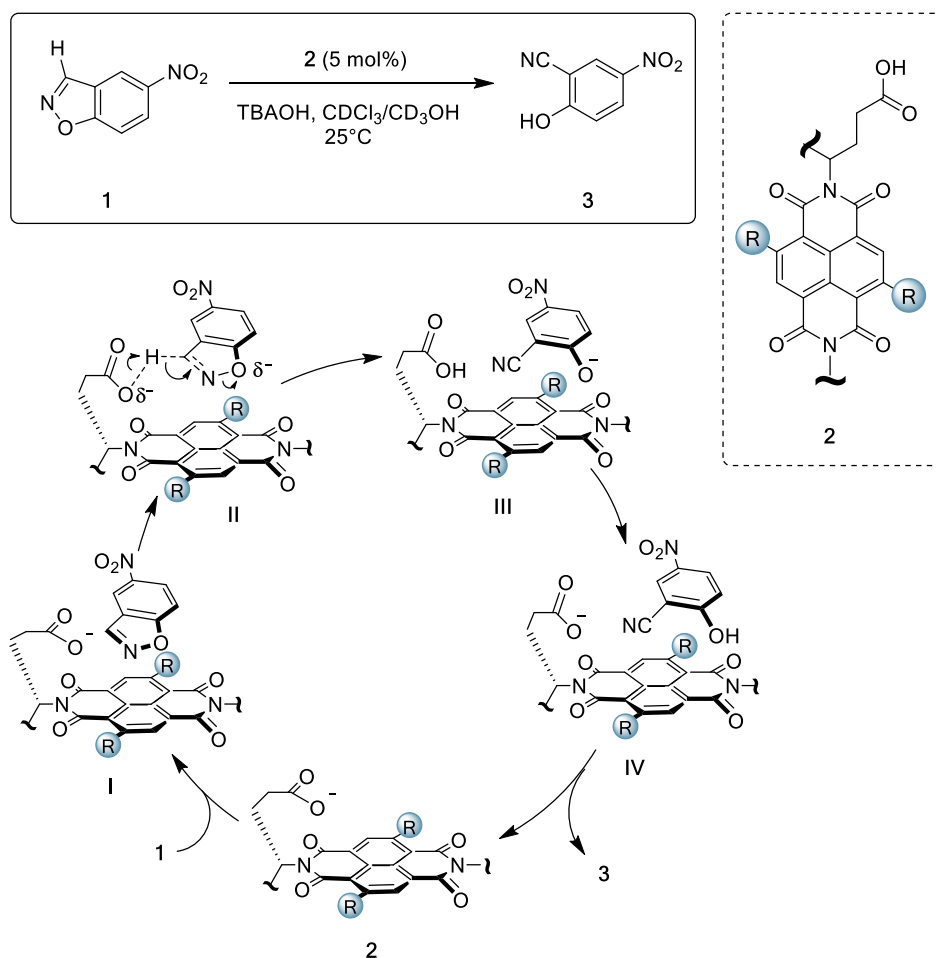
After the explicit recognition of anion- π interactions in 2002, it took eleven years for the exploitation of such forces in catalysis.⁷ In principle, the extension of the ground state stabilization of anions to the stabilization of anionic transition states is conceptually straightforward, but it revealed to be a challenging task. Matile research group focused on naphthalenediimides (NDIs) as privileged scaffold to tackle this task, due to their intrinsic high and easy-to-modulate quadrupole moment. The first reaction chosen as proof of concept was the Kemp elimination, a classical model reaction characterized by a single anionic transition state. The increasing transition-state stabilization with increasing π -acidity of the catalyst furnished strong experimental evidence that anion- π interactions were indeed responsible for the observed rate enhancements. The mechanism for this transformation is depicted in Scheme I-IV. The structural key factor in the design of catalyst **2** is the compresence of a π -acidic surface of a NDI and a carboxylate base. The onset of anion- π interactions between the substrate and the catalyst should coincide with the transfer of a negative charge from the proximal carboxylate to **1**. The translocation of this negative charge through five atoms (**II**) closer to the π -acidic surface is the perfect example of anion- π forces mediated transition state stabilization.

Following this groundbreaking report, the concept of anion- π catalysis has been exploited in several transformations paving the way to the establishment of anion- π catalysis as a general principle in this discipline.⁸

⁷ Zhao, Y.; Domoto, Y.; Orentas, E.; Beuchat, C.; Emery, D.; Mareda, J.; Sakai, N.; Matile, S. *Angew. Chem., Int. Ed.* **2013**, *52*, 9940–9943.

⁸ Zhao, Y.; Cotelle, Y.; Liu, L.; Ljpez-Andarias, J.; Bornhof, A.-B.; Akamatsu, M.; Sakai, N.; Matile, S. *Acc. Chem. Res.* **2018**, *51*, 2255–2263

Anion- π interactions in light-induced reactions



Scheme IV-1. Catalysis of the Kemp elimination with anion- π interactions.

IV.1.3. Nitrogen-centered radicals

Nitrogen-containing functional groups are a ubiquitous in almost all pharmaceuticals, agrochemicals, food additives and materials.⁹ This aspect makes developing methods for C–N bond formation fundamental to our society. General methods are based on ionic strategies taking advantage of the intrinsic nucleophilic polarity of the nitrogen atom, while the possibility of

⁹ Lawrence, S. A. *Amines: Synthesis Properties and Applications* 2008, Cambridge University Press.

exploring alternative pathways is offered by nitrogen-centered radicals (NCRs).¹⁰ Despite these open shell intermediates offer complementary opportunities for C–N bond forging to both ionic and transition-metal-based protocols, nitrogen-radical chemistry has been relatively underutilized from a synthetic perspective. The main factor that has thwarted the development of methodologies in this field is the lack of convenient methods for accessing these radical species.¹¹

Traditionally, two approaches for generating NCRs have been used. The more general route involves the cleavage of a weak N–X bond, where X is a halogen (except fluorine), a nitrogen, an oxygen or a sulfur moiety. Also included in this category are the direct oxidation reactions, where a N–H bond is ultimately broken. The second strategy is indirect and based on radical addition to unsaturated nitrogen moieties such as a nitrile, an imine, an oxime, a hydrazine or an azide. The advent of visible-light-mediated photoredox catalysis has allowed to overcome the limitations associated with these strategies (harsh reaction conditions and use of toxic reagents) contributing to the renaissance of the chemistry of nitrogen radicals.

A NCRs classification can be proposed according to the different electronic configuration which results in peculiar philicity and finally in reactivity (Figure IV-2). Iminyl radicals have a σ configuration, the unpaired electron populating a sp^2 -orbital, and show weak nucleophilicity like that of carbon-centered radicals.¹² Instead, neutral aminyl radicals have a π configuration with the electron occupying a p-orbital but still possess nucleophilic character. Lack of lone pair repulsion in combination with permanent positive charge make π aminium radicals the most electrophilic of the

¹⁰ Zard, S. Z. *Chem. Soc. Rev.* **2008**, *37*, 1603-1618.

¹¹ a) Neale, R. S. *Synthesis* **1971**, 1–15; b) Bowman, W. R.; Fletcher, A. J.; Potts, G. B. S. *J. Chem. Soc. Perkin Trans. 1* **2002**, 2747–2762.

¹² Walton, J. C. *Acc. Chem. Res.* **2014**, *47*, 1406-1416

Anion- π interactions in light-induced reactions

family.¹³ Albeit due to a different reason (delocalization of the unpaired electron through the carbonyl lowers the energy of the single-occupied orbital),¹⁴ amidyl radicals also show marked electrophilicity. The behavior of other NCRs bearing different *N*-substituents capable of electron delocalization (e.g., *N*-sulfonyl radicals) is consistent with the behavior of amidyl radicals.

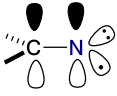
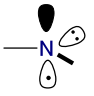
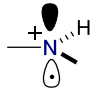
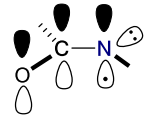
NCR	Iminyl	Aminyl	Aminium	Amidyl
Configuration	σ	π	π	π
Structure				
Philicity	Nucleophilic	Nucleophilic	Electrophilic	Electrophilic

Figure IV-2. Nitrogen-centered radicals classification.

NCRs can undergo four main classes of reactions (Figure IV-3): a) intramolecular cyclization onto alkenes (or alkynes); b) intramolecular hydrogen atom abstraction; c) Norrish type-I fragmentation and d) intermolecular addition to unsaturated systems. It is noteworthy that not all the classes of nitrogen radicals share the same set of reaction modes, due to their different electronic configuration and consequently different ability in the stabilization of the corresponding transition states.

¹³ Chow, Y. L.; Danen, W. C.; Nelsen, S. F.; Rosenblatt, D. H. *Chem. Rev.* **1978**, *78*, 243-274

¹⁴ Lessard, J.; Griller, D.; Ingold, K. U. *J. Am. Chem. Soc.* **1980**, *102*, 3262-3264

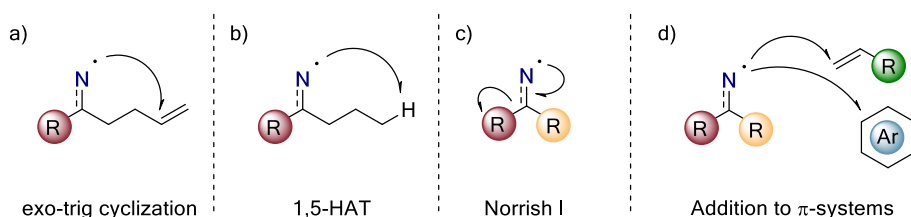


Figure IV-3. Nitrogen-centered radicals general reactivities.

IV.1.4. Amidyl Radicals

Recent developments in the field of visible light photocatalysis have opened new pathways for the catalytic, mild and selective generation of nitrogen centered radicals. In particular, application of photoredox catalysis has allowed the generation of amidyl radicals (Figure IV-4), able to promote various conceptually challenging synthetic transformations.^{15,16}

A very attractive possibility offered by photoredox catalysis is the generation of amidyl radicals *via* N–H bond cleavage. The formal hydrogen atom abstraction of amides has been rarely reported in the past due to typically high bond strength (BDE N–H >100 kcalmol⁻¹) that required the use of strong oxidizing reagents and high temperatures.¹⁷

¹⁵ Chen, J. R.; Hu, X.-Q.; Lu, L.-Q.; Xiao, W.-J. *Chem. Soc. Rev.* **2016**, *45*, 2044-2056; b) Kärkäs, M. D. *ACS Catal.* **2017**, *7*, 4999-5022.

¹⁶ Imidyl and sulfonamidyl radical generation and reactivity are not included in this discussion. An exhaustive survey of literature can be found in Ref. 15.

¹⁷ Forrester, A. R.; Ingram, A. S.; Thomson, R. H. *J. Chem. Soc., Perkin Trans. 1*, **1972**, 2847-2853.

Anion- π interactions in light-induced reactions

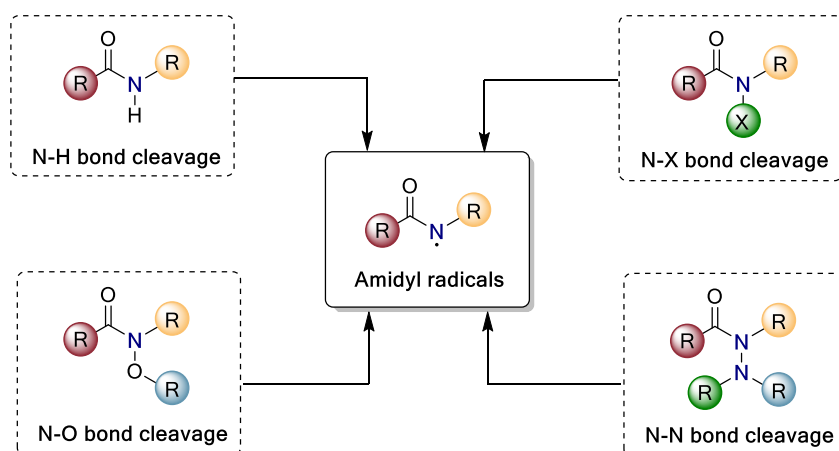
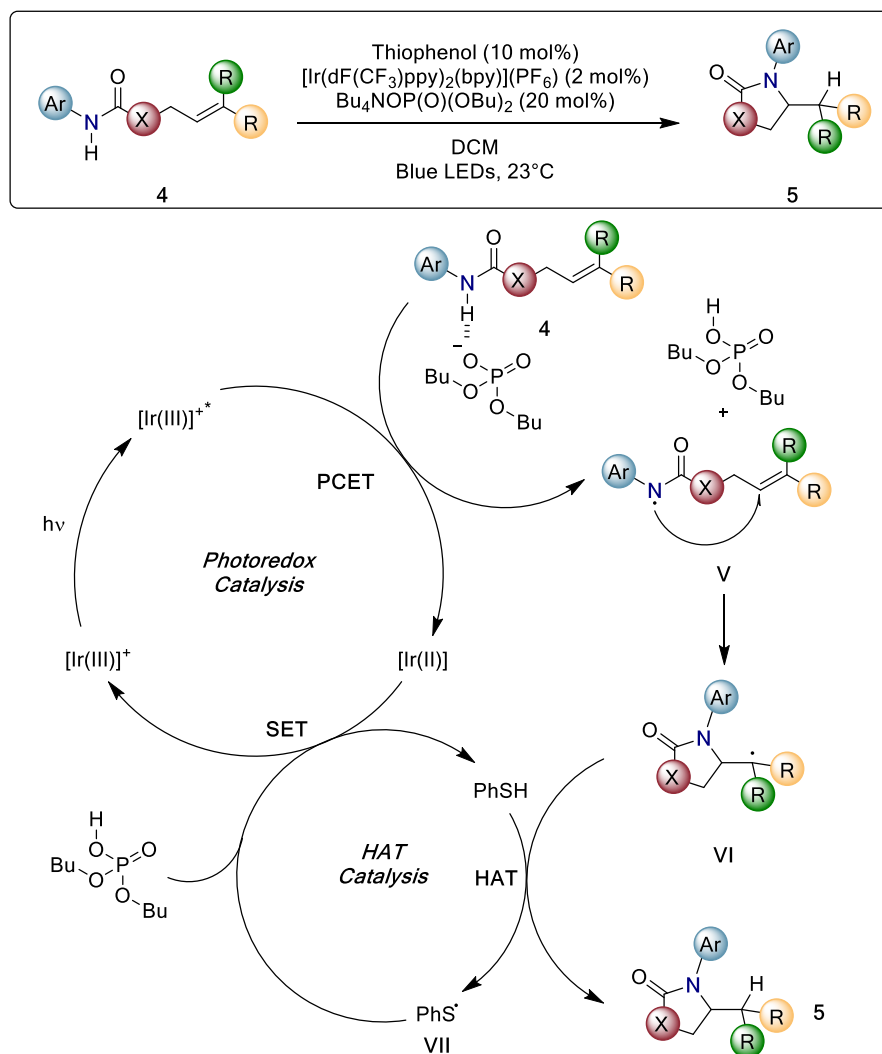


Figure IV-4. Strategies for the visible light-mediated formation of amidyl radicals.

The Knowles group has developed catalytic transformations relying on proton-coupled electron transfer (PCET) for the activation of N–H bonds towards formal homolysis.¹⁸ Photoredox and Brønsted base cooperative catalysis gave access to a previously inaccessible pathway, allowing the transfer of a proton and an electron from a single donor to two independent acceptors in a concerted process. The reaction depicted in Scheme IV-2 is the first example of such strategy applied to the intramolecular hydroamination of olefins.^{18a} The mechanistic proposal is based on PCET mediated amide activation, resulting in N–H bond homolysis and generation of amidyl radical **V**. Radical addition to the pendant double bond affords carbon centered radical **IV** able to abstract a hydrogen from thiophenol delivering product **5**. Next, SET from the reduced Ir(II) photocatalyst (resulting from reductive quenching exerted by the amide) to the thiophenyl radical **VII** regenerates the HAT catalyst. The Knowles group has also applied this PCET activation strategy to alkene carboamination.^{18b}

¹⁸ a) Miller, D. C.; Choi, G. J.; Orbe, H. S.; Knowles, R. R. *J. Am. Chem. Soc.* **2015**, *137*, 13492–13495; b) Choi, G. J.; Knowles, R. R. *J. Am. Chem. Soc.* **2015**, *137*, 9226–9229.



Scheme IV-2. Visible light-mediated alkene hydroamination enabled by proton coupled electron transfer.

Recently, several research groups have reported how hydroxylamine derivatives can efficiently serve as nitrogen-centered radical precursors owing to their weak N–O bond.¹⁹ The common strategy adopted to achieve photoredox mediated N–O bond homolysis is based on installation of

¹⁹ Davies, J.; Morcillo, S. P.; Douglas, J. J.; Leonori, D. *Chem. Eur. J.* **2018**, *24*, 12154–12163.

Anion- π interactions in light-induced reactions

appropriate electrophores on O atom (Figure IV-5). Depending on the nature of these functionalities, amidyl radicals have been generated *via* reductive or oxidative SET exerted by excited photocatalysts. Electron poor *O*-aryl and *O*-acyl hydroxylamines ($\pi^* + \sigma^*$ electrophores), upon SET reduction, form stable anion radicals (aryl and ketyl, respectively) leading ultimately to N–O bond homolysis (Figure IV-5, a and b). Instead, α -*N*-oxyacids ($n + \sigma + \sigma$ electrophores) undergo SET oxidation of the carboxylate triggering two β -scissions, forming the NCR (Figure IV-5, c).

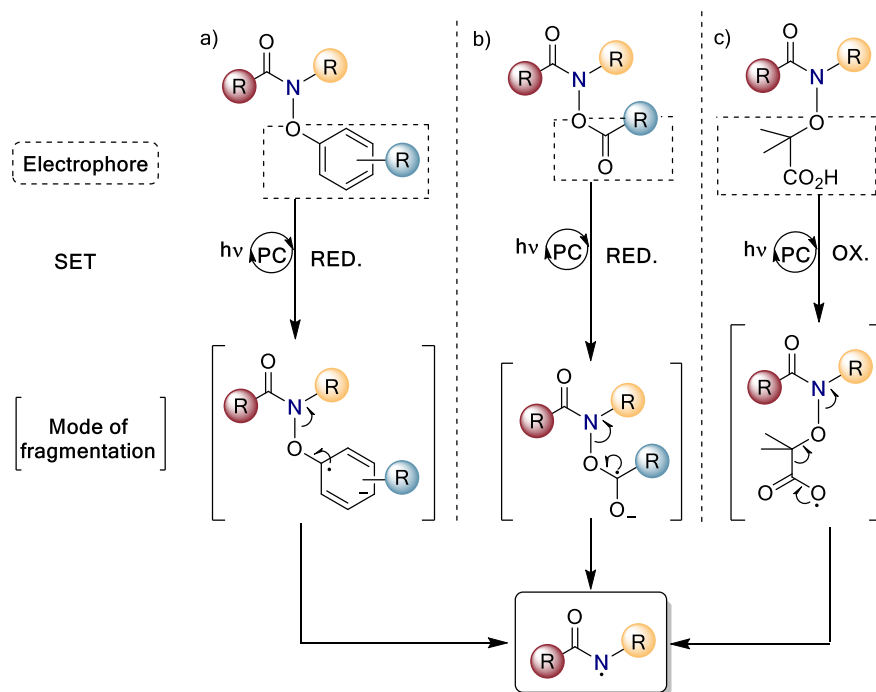
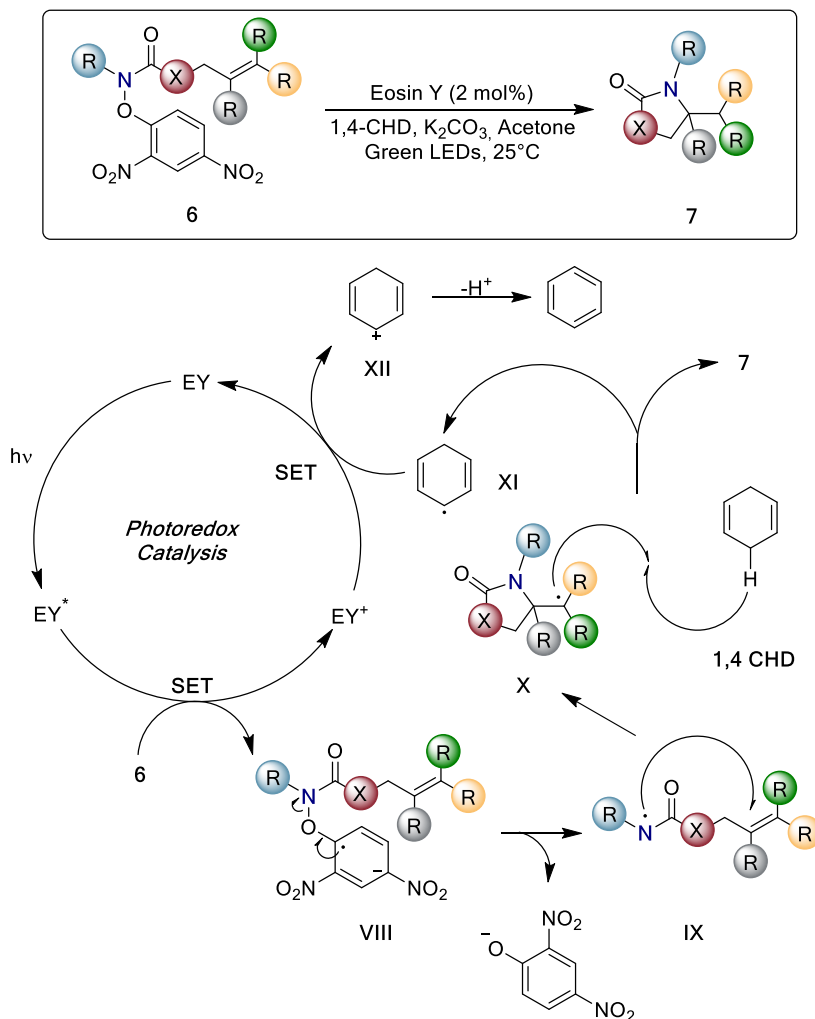


Figure IV-5. Formation of amidyl radicals from hydroxylamines derivatives.

In 2016 Leonori applied the first mentioned activation strategy to the intramolecular cyclization of amidyl radicals derived from aryloxy amides

(Scheme IV-3).²⁰ Guided by DFT and electrochemical studies, aryloxy amides **6** were chosen due to their ease of synthesis and favorable reduction potential. Using Eosin Y as photocatalyst, 1,4-cyclohexadiene and K_2CO_3 as base under green LEDs irradiation the synthesis of cyclization product **7** was accomplished.



Scheme IV-3. Transition metal-free hydroamination of aryloxy amides.

²⁰ Davies, J.; Svejstrup, T. D.; Fernandez Reina, D.; Sheikh, N. S.; Leonori, D. *J. Am. Chem. Soc.* **2016**, *138*, 8092–8095.

Anion- π interactions in light-induced reactions

The developed transformation was assumed to commence with SET reduction of **6** by photoexcited Eosin Y that triggers N–O bond homolysis affording amidyl radical **IX**. This radical undergoes 5-*exo*-trig cyclization producing intermediate **X**. Concomitant hydrogen atom abstraction from 1,4-CHD affords the hydroamination product **7** and radical **XI** that can be oxidized by EY^+ closing the photoredox cycle. In the same work was reported the possibility to extend the developed activation of amides to intermolecular *N*-arylation employing electron-rich (hetero)aromatics.

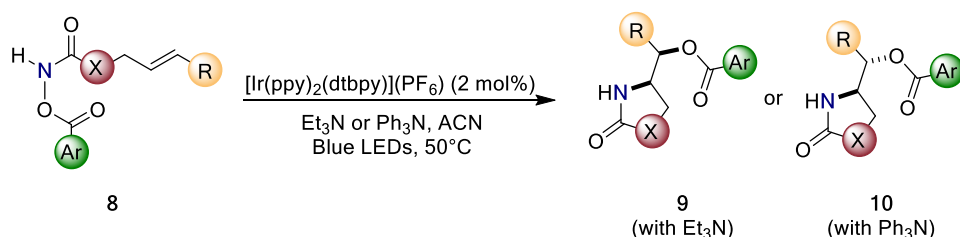
Xie, Xu and Lu demonstrated the feasibility of reductive generation of amidyl radicals from *O*-benzoyl hydroxyl amines (**8**) in the stereodivergent oxy-amination of olefins (Scheme I-IV, a).²¹ The transformation affords 5-*exo*-trig cyclization product **9** when triethylamine was used as base and stoichiometric electron donor, while in the presence of triphenylamine the other diastereomer **10** was selectively obtained. The same activation strategy was applied by Yu in the intermolecular reaction of amidyl radicals (formed from precursor **11**) with styrenes **12** (Scheme I-IV, b).²² Divergent assembly of functionalized carbamates is achieved according to the solvent used: acetonitrile is utilized for obtaining 1,2-diamines **13**, while α -amino ketones **14** are delivered in the presence of dimethyl sulfoxide.

The oxidative generation of amidyl radicals (Figure IV-5, c) has been relatively less explored. However, this strategy offers an advantage in comparison with reductive manifolds consisting in the possibility of remote functionalization with polarized SOMOphiles. Typically, these species bear an electrophilic “Z” group that ensures an efficient homolytic substitution but thwarts a mechanism in which a SET reduction of the photocatalyst is required for its turnover.

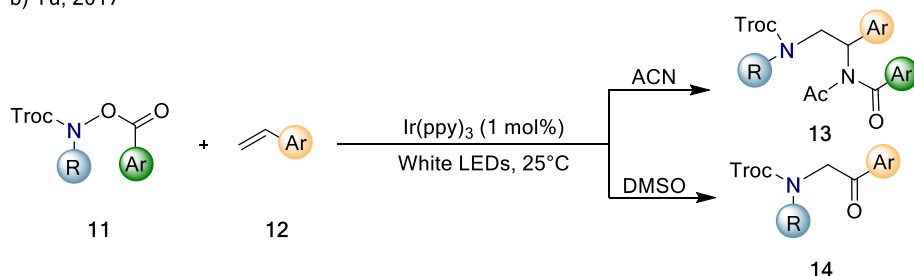
²¹ Ren, X.; Q. Guo, Q.; J. Chen, J.; Xie, H.; Xu, Q.; Lu, Z. *Chem. Eur. J.* **2016**, *22*, 18695-18699.

²² Qin, Q.; Han, Y.-Y.; Jiao, Y.-Y.; He, Y.; Yu, S. *Org. Lett.* **2017**, *19*, 2909-2912.

a) Xie, Xu and Lu 2018



b) Yu, 2017

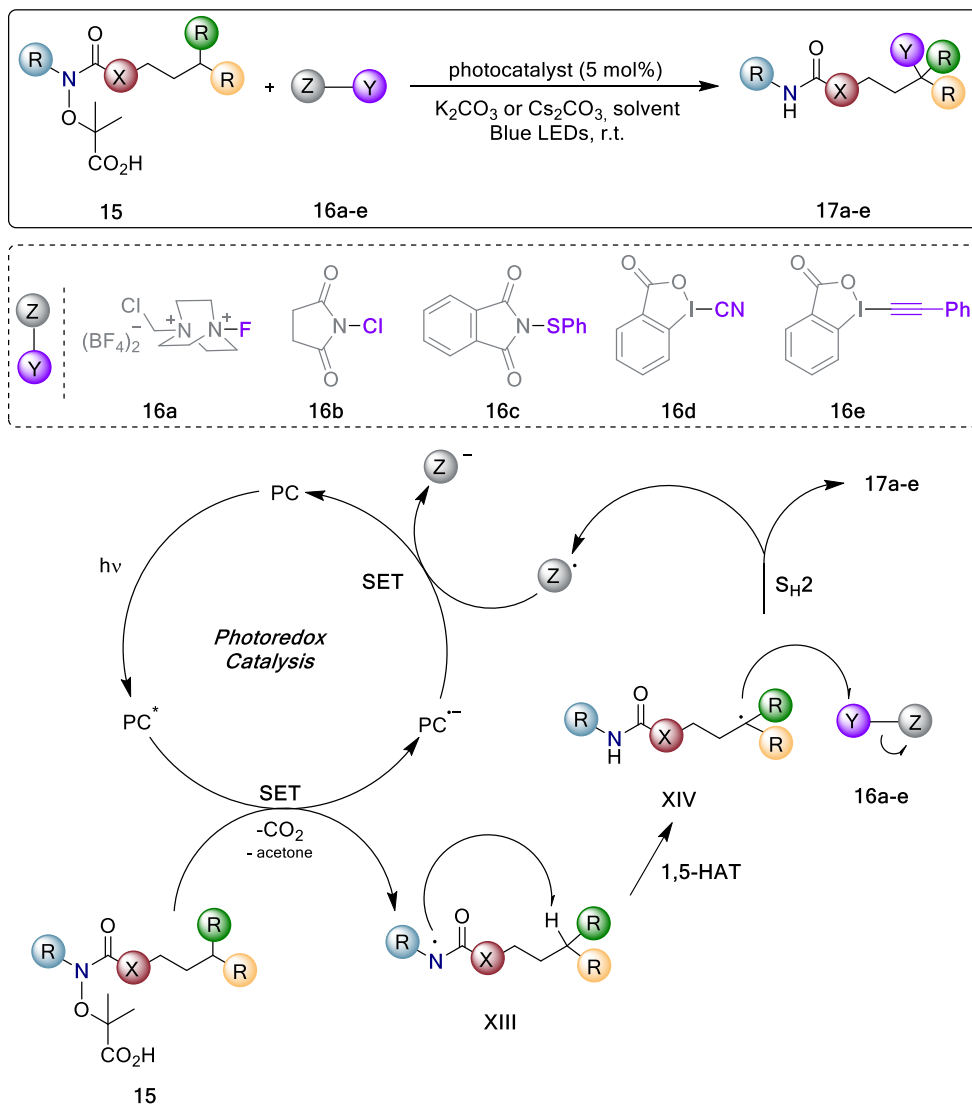


Scheme IV-4. Diastereodivergent intramolecular aminohydroxylation; b) divergent functionalizations of styrenes using nitrogen radicals.

Addressing this redox mismatch is possible when α -N-oxycarboxylic acids are used as NCR precursors. An implementation of this strategy, allowing the remote functionalization of amides and amines, has been reported by Leonori (Scheme IV-5).²³ Employing **15** as an amidyl radical source, five different γ -functionalization with SOMOphiles (**16a-e**) were accomplished. The mechanistic proposal shown in Scheme IV-5 is centered on reductive quenching of the excited photocatalyst by **15** affording (after fragmentation through decarboxylation and loss of acetone) radical **XIII**. Then, 1,5-HAT delivers the distal radical **XIV** which engages polarized SOMOphiles (**16a-e**) in homolytic atom/group transfer, furnishing the targeted amides **17a-e** as well as an electron-poor radical Z^\cdot . This intermediate then oxidizes the reduced photocatalyst, closing the photoredox cycle.

²³ Morcillo, S. P.; Dauncey, E. M.; Kim, J. H.; Douglas, J. J.; Sheikh, N. S.; Leonori, D. *Angew. Chem. Int. Ed.* **2018**, *57*, 12945-12949.

Anion- π interactions in light-induced reactions



Scheme IV-5. Remote functionalization of amides using amidyl radicals. Photocatalyst = $[Ir(dF(CF_3)ppy)_2(bpy)](PF_6)$ for **16a**; 4CzIPN for **16b-e**. Solvent = ACN/H₂O for **16a**; ACN for **16b**; DCM for **16c-e**.

IV.2. Objective

Despite the importance anion- π interactions have in supramolecular chemistry²⁴ as well as in biological processes,²⁵ their role in photocatalysis remains largely unexplored. However, it is straightforward that strong anion- π interactions can result in charge transfer complex leading ultimately to electron transfer events. Initial applications of this concept were mostly in the design of anion-sensing receptors. For example, Dunbar reported chromogenic anion- π and charge transfer interactions involving halides and electron deficient aromatic rings in organic solvents.²⁶ Following this report, Saha in 2010 presented a new strategy for F⁻ ion sensing involving p-acidic NDI receptors (Figure IV-6).²⁷

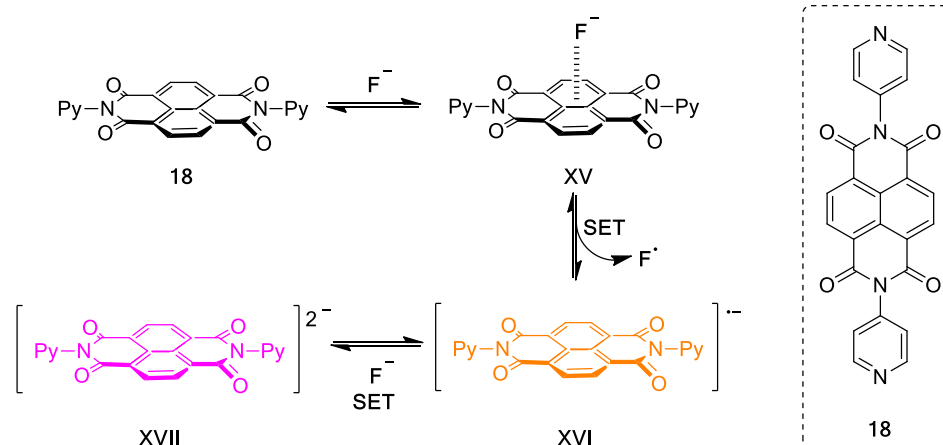


Figure IV-6. Graphical illustrations of anion- π and CT interactions between F⁻ and NDI receptor, generating fluorochromogenic response *via* SET event.

²⁴ a) Garau, C.; Quiñero, D.; Frontera, A.; Ballester, P.; Costa, A.; Deyà, P. M. *J. Phys. Chem. A* **2005**, *109*, 9341-9345; b) Gamez, P.; Mooibroek, T. J.; Teat, S. J.; Reedijk, J. *Chem. Res.* **2007**, *40*, 435-444.

²⁵ Estarellas, C.; Frontera, A.; Quiñero, D.; Deyà, P. M. *Angew. Chem. Int. Ed.* **2011**, *50*, 415-418.

²⁶ Chifotides, H. T.; Schottel, B. L.; Dunbar, K. R. *Angew. Chem., Int. Ed.* **2010**, *49*, 7202-7207.

²⁷ Guha, S.; Saha, S. *J. Am. Chem. Soc.* **2010**, *132*, 17674-17677.

Anion- π interactions in light-induced reactions

Interactions between lone-pairs electrons of fluoride and π^* -orbitals of NDI **18** lead to the formation of anion- π complex **XV**. A subsequent electron transfer event produces an orange colored NDI radical anion **XVI** and fluorine radical. Further reduction of **XVI** by another F^- ion affords a pink colored NDI^{2-} dianion **XVII**, rendering NDI a colorimetric F^- sensor.

These examples, even if not oriented towards organic synthesis, show a strong resemblance with the photochemistry of EDA complexes, recently emerged as the basis of a powerful enabling strategy for the generation of open-shell intermediates (See Section I.3).

Fundamental to define our strategy was finding a suitable π -acidic aromatic system able to elicit an anion- π complex. Moreover, this complex should depict a charge transfer band in the visible region so that irradiation could trigger an electron-transfer event leading ultimately to the formation of radical species able to be engaged productively in organic processes.

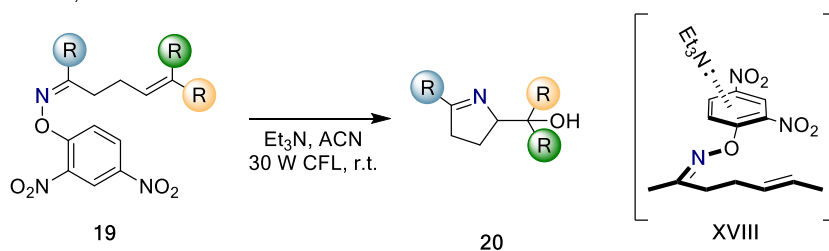
As described in Section IV.1.4, hydroxylamine derivatives work efficiently as nitrogen-centered radical precursors in photo-chemical transformations. We turned our attention to two reports in which these processes are not mediated by exogenous photocatalysts. In the first of them, the formation of EDA complex **XVIII** between oxime **19** and Et_3N allows, under visible light irradiation, the synthesis of pyrroline alcohol **20** (Scheme IV-6, a).²⁸ The second one describes a photochemical intramolecular cyclization affording 5-methylenepyrrolidine **22** via 5-*exo*-dig cyclization of the amidyl radical generated from *N*-aryloxyamide **21** (Scheme IV-6, a).²⁹ These two examples made us wonder whether an anion- π interaction might enable the light-mediated formation of amidyl radicals from electron-poor *N*-aryloxyamides. Conceptuality and practicality aside, this new activation mode might offer a new opportunity to harness the synthetic applicability of

²⁸ Davies, J.; Booth, S. G.; Essafi, S.; R. W. A. Dryfe; Leonori, D. *Angew. Chem., Int. Ed.* **2015**, *54*, 14017-14021.

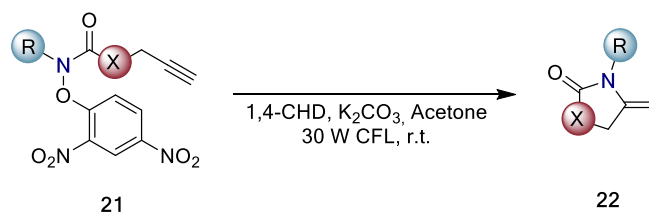
²⁹ Fernandez Reina, D.; Dauncey, E. M.; Morcillo, S. P.; Svejstrup, T. D.; Popescu, M. V.; Douglas, J. J.; Sheikh, N. S.; Leonori, D. *Eur. J. Org. Chem.* **2017**, 2108-2111.

amidyl radicals for building up molecular complexity. Therefore, the aims of this project are to demonstrate (i) the formation of an anion- π complex between inorganic anions and an electron-poor *N*-aryloxyamide, (ii) the weakening of the N-O bond resulting from this interaction and (iii) the direct cleavage of this bond after single electron transfer (SET) induced by visible light, resulting in an amidyl radical that can be trapped in either intermolecular or intramolecular fashion by electron-rich aromatic substrates.

a) Leonori, 2015



b) Leonori, 2017



Scheme IV-6. a) Photochemical generation of iminyl radicals *via* EDA complex: iminohydroxylation reactions; b) visible-light-mediated 5-*exo*-dig cyclizations of amidyl radicals.

Anion- π interactions in light-induced reactions

IV.3. Anion- π interactions driven amidation of aromatic systems

IV.3.1. Preliminary studies and optimization

As the first test of our hypothesis, we studied the behavior of the 2,4-dinitro substituted aryloxy amide **1a** in the presence of K_2CO_3 in acetonitrile (ACN) solution. Interestingly, the UV-visible spectra showed the appearance of a dramatic enhancement in the absorption between 425 and 450 nm (Figure IV-7, red trace).³⁰

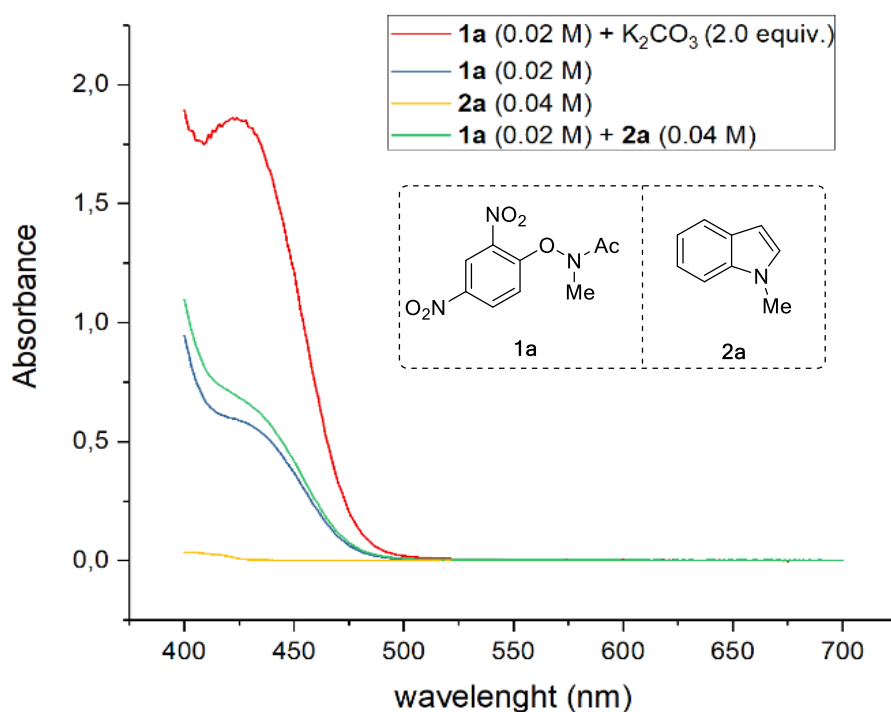
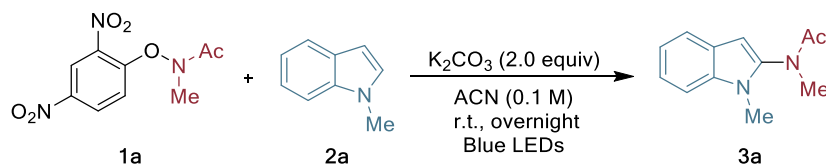


Figure IV-7. UV-visible absorption studies.

³⁰ The project discussed in this Chapter has been conducted in collaboration with Dr. Laura Buglioni and Prof. Antonio Frontera.

We next studied the light-promoted reaction (4.5 W blue LED, emission centered at 460 nm, see Section IV.4.2) between **1a** and *N*-methyl indole (**2a**) in the presence of K_2CO_3 as the sole additive (Table IV-1).



Entry	Variation from standard conditions ^[a]	Yield (%) ^[b]
1	None	75
2	Acetone instead of ACN	63
3	DMSO instead of ACN	68
4	1.5 equiv. of 2a	72
5	23 W CFL instead of blue LEDs	<5 ^[c]
6	Green LEDs instead of blue LEDs	29 ^[d]
7	White LEDs instead of blue LEDs	37 ^[d]
8	No K_2CO_3 , 48 h	18 ^[d]
9	No light	<5 ^[c]
10	NaH_2PO_4 instead of K_2CO_3	25 ^[d]
11	$Na(PhO)_2PO_2$ instead of K_2CO_3	31 ^[d]
12	$(NEt_4)HCO_3$ instead of K_2CO_3	15
13	K_2HPO_4 instead of K_2CO_3	75
14	$Na_2(PhO)PO_3$ instead of K_2CO_3	75
15	K_3PO_4 instead of K_2CO_3	75
16	Et_3N instead of K_2CO_3	7
17	Cs_2CO_3 in acetone instead of K_2CO_3	50

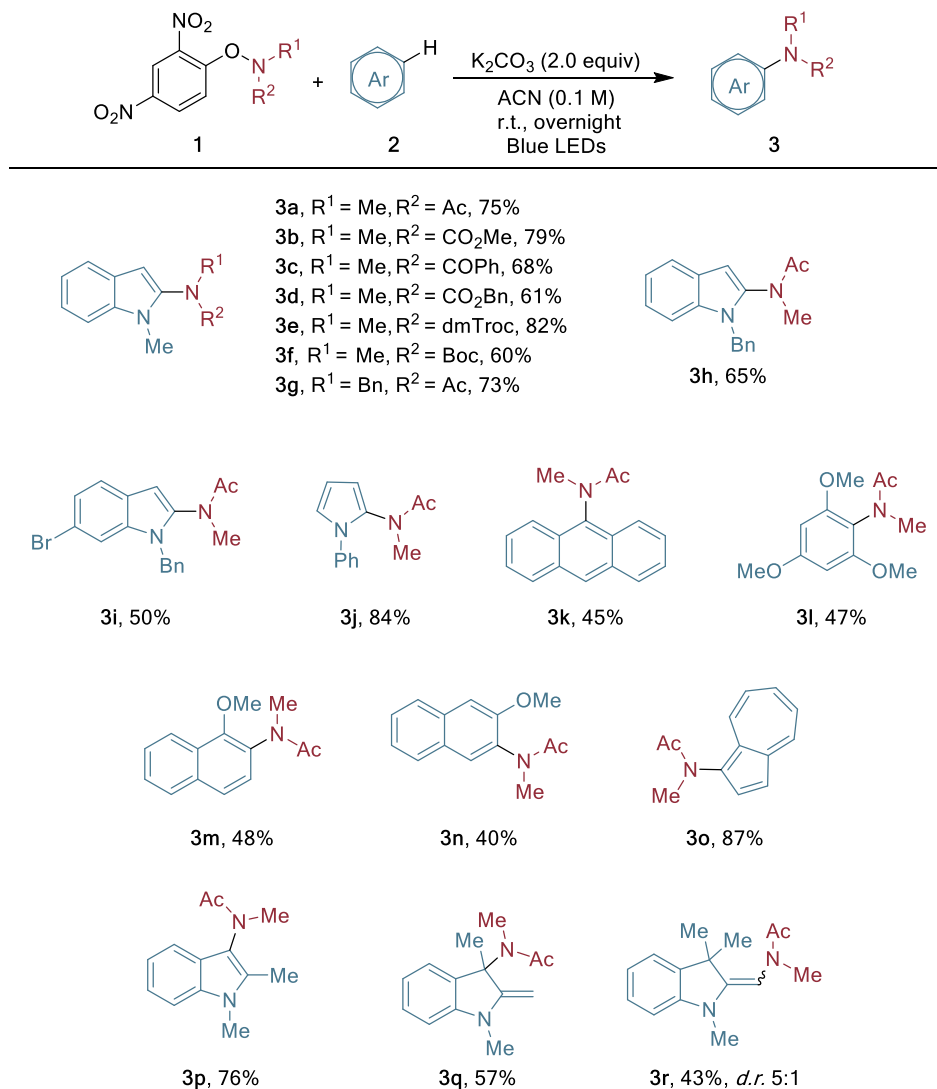
Table IV-1. Screening and optimization of reaction conditions for the amidation of *N*-methylindole (**2a**) with **1a**. ^[a]Standard conditions: **1a** (0.2 mmol), **2a** (0.4 mmol), K_2CO_3 (0.4 mmol), ACN (2.0 mL) blue LEDs, r.t., overnight. ^[b]After flash column chromatography. ^[c]By 1H NMR of the crude reaction mixture. ^[d]Incomplete reaction (30% conversion).

Anion- π interactions in light-induced reactions

We were pleased to observe that working under the standard conditions of Table VI-1 the reaction proceeded to completion overnight, affording the amidated indole **3a** in 75% yield (entry 1). The substitution of acetonitrile with other solvents such as acetone (entry 2) or DMSO (entry 3) lowered the yield (63 and 68%, respectively). Decreasing the ratio between **1a** and **2a** led to a slight erosion of the yield, as well (entry 4). The nature of the light source proved crucial for the outcome of the transformation. In fact, when either a compact fluorescence lamp (CFL), or green or white LEDs were employed, the reaction became much slower with consequent lower yields (entries 5, 6 and 7). Importantly, both the presence of carbonate and of a light source proved to be necessary for the success of the transformation. (entries 8 and 9, respectively).

IV.3.2. Reaction scope

The scope of this transformation was next investigated under the optimal reaction conditions (Scheme IV-7). Modifying the substituents of either the amide in **1** or of the *N*-substituted indole did not affect the reaction outcome. In fact, the corresponding amidated products **3a-3i** were isolated in good to high yields, and the same stands for **3j**, derived from *N*-phenylpyrrole. When switching to different aromatic carbocycles as partners, a decrease in yield was generally observed (**3k-3n**), with the notable exception of azulene, which afforded the amidated product **3o** in high yield. Starting from 1,2-dimethyl indole and 1,2,3-trimethyl indole, the light-promoted amidation proceeds efficiently at C-3 (products **3p** and **3q**), leading in the second case to dearomatization. When 1,3,3-trimethyl-2-methyleneindoline (Fischer base) is used as radical acceptor, the amidation took place at the *exo* double bond, affording **3r** in moderate yield and good diastereoselectivity.

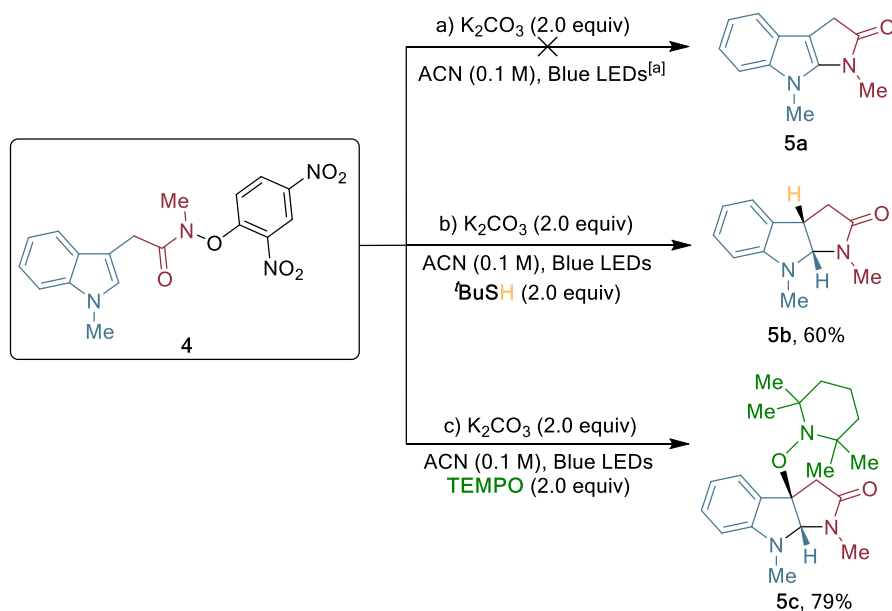


Scheme IV-7. Intermolecular light-promoted amidation.

We next explored the possibility of an intramolecular version of the light-promoted amidation reaction, which would afford pharmaceutically valuable

Anion- π interactions in light-induced reactions

pyrroloindoline motifs **5** (Scheme IV-8).³¹ Inspired by a previous work by Wang and co-workers,³² we synthesized compound **4**, which was irradiated with blue LEDs in the sole presence of potassium carbonate (Scheme IV-7, a). Although complete consumption of the starting material was observed, the desired compound **5a** was not obtained. This experiment strongly suggests that the putative tertiary radical intermediate that could be originated by N-O cleavage from **4** is not able to reduce the starting material and, thus, the radical chain propagation step cannot take place. To circumvent this limitation, *tert*-butyl thiol and TEMPO were added to the reaction mixture as radical trapping reagents, affording the desired cyclized products **5b** and **5c** in 60% and 79% yield, respectively (Scheme IV-7, b and c).



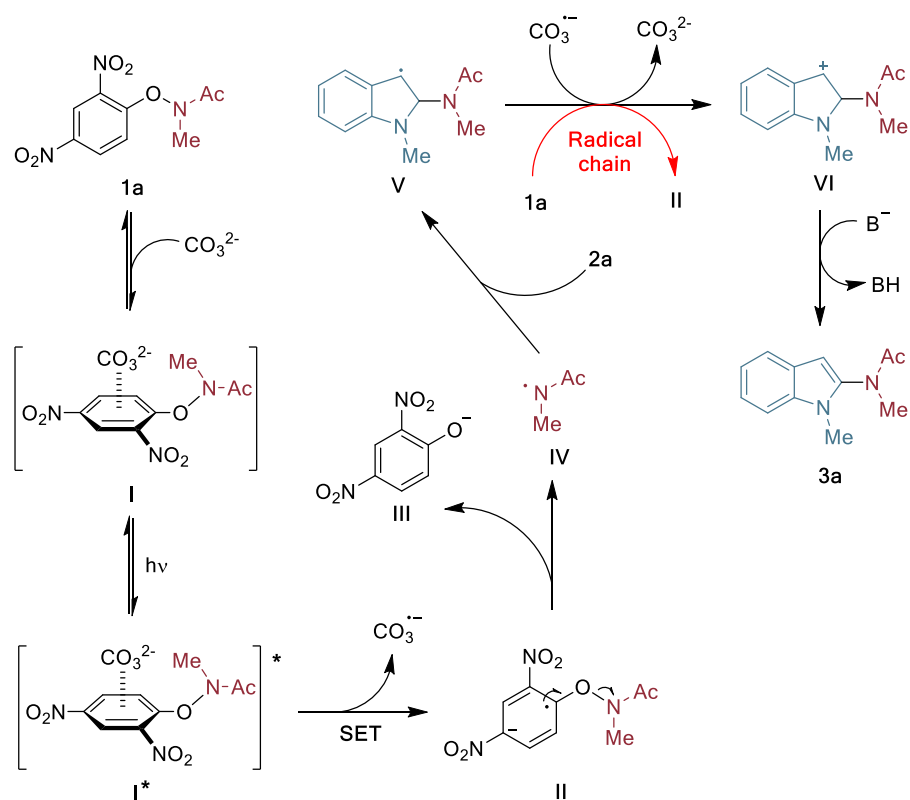
Scheme IV-8. Intramolecular light-promoted amidation. Reaction conditions: blue LEDs, r.t., overnight. Yields measured after column chromatography. ^[a]The only isolated product was 1-Methylindole-3-carboxaldehyde (20% yield).

³¹ a) Zheng, C. J.; Kim, C. J.; Bae, K. S.; Kim, Y. H.; Kim, W. G. *J. Nat. Prod.* **2006**, *69*, 1816-1819; b) Varoglu, M.; Corbett, T. H.; Valeriotte, F. A.; Crew, P. *J. Org. Chem.* **1997**, *62*, 7078-7079.

³² a) Wu, K.; Du, Y.; Wang, T. *Org. Lett.* **2017**, *19*, 5669-5672; b) Wu, K.; Du, Y.; Wei, Z.; Wang, T. *Chem. Commun.* **2018**, *54*, 7443-7446.

IV.3.3. Mechanistic investigation

The tentative mechanistic proposal shown in Scheme IV-9 was formulated for an anion- π driven, light-induced amidation. Complex I, an anion- π complex generated by the interaction of the electron poor aryloxy amide **1a** with K_2CO_3 , can be excited to I^* by irradiation with blue light (Figure IV-7). This excited state can then undergo an intramolecular SET event, leading to disassembly of the complex and generation of the radical anion **II**, which readily fragments into the amidyl radical **IV** and the phenolate **III**. The former can attack the N-methyl indole, affording radical **V**. The latter can be protonated to give **3a**.

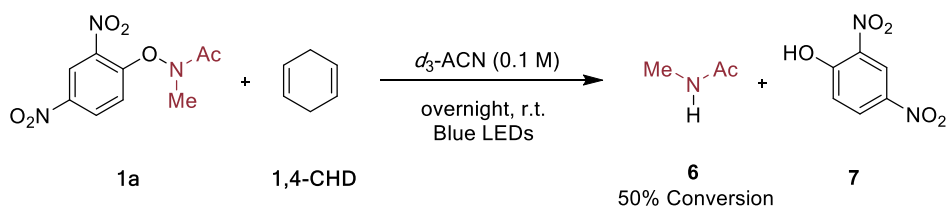


Scheme IV-9. Proposed mechanism of the anion- π driven photo-amidation.

Anion- π interactions in light-induced reactions

This radical can contribute to the chain propagation³³ by reducing **1a** ($E_{\text{red}} = -0.26$ V vs. SCE) to the readily cleavable intermediate **II** and giving rise to the carbocation species **VI**, base-induced deprotonation of which leads to the amidated product **3a**. Another intriguing possibility involves the reduction of carbonate radical anion, which affords **VI** from **V**, regenerating the carbonate species.³⁴

Although the anion- π interaction appears to be very relevant for the outcome of this transformation, an alternative mechanism could, in principle, also be operative in the observed transformation, involving homolytic cleavage of the N–O bond in **1a** due to the absorption of light of the appropriate wavelength (see Section IV.4.4). The possible light-induced homolysis of **1a** was tested (Scheme IV-9) by irradiating **1a** under the standard conditions of this study (blue LED, 4.5 W) and in the presence of 1,4-cyclohexadiene. Formation of the homolysis products **6** and **7** under these conditions was observed by NMR, proving that homolytic cleavage could also have some relevance in the reaction outcome.



Scheme IV-10. Study on the homolytic fragmentation of **1a**. Reaction conditions: **1a** (0.2 mmol), **1,4-CHD** (1.0 mmol), deuterated-acetonitrile (2.0 mL), blue LEDs, r.t., overnight. The conversion was measured by ^1H NMR.

³³ The quantum yield could not be measured because of the heterogeneity of the system.

³⁴ This possibility could be realistic as the oxidation potential of **B** is 2.1 V, as reported in: Mandal, P.C.; Bardhan, D.; Sarkar, S.; Bhattacharyya, S. N. *J. Chem. Soc. Dalton Trans.* **1991**, 6, 1457-1461.

However, it is important to note that the possible contribution of this initiation mode may be relatively minor, as shown by the results of the amidation reaction performed in the absence of base (Table IV-1, entry 8), whereby only an 18% yield of **3a** was obtained after reaction for 48 h.

At this point, it became important to assess the influence of the base used in the amidation reaction, considering its fundamental role in the generation of the anion- π complex. From observation of the results summarized in Table IV-1, entries 10-16, we can deduce that:

- i) the use of a neutral base, such as triethylamine, is deleterious for the transformation (entry 16);
- ii) the use of singly-charged anions has a negative effect on the outcome of the reaction (entries 10-12);
- iii) doubly- or triply-charged anions are those giving the best results (entries 13-15).

Interestingly, these observations perfectly correlate with the expected strengths of the anion- π interactions. In an attempt to perform photochemical studies on **I**, which would be facilitated by a high concentration of the complex, soluble tetrabutylammonium phosphate was used as the anionic component, since the use of caesium carbonate in acetone proved to be unfavorable (entry 17). However, when solutions of **1a** and $(\text{Bu}_4\text{N})_3\text{PO}_4$ in acetonitrile were mixed in an inert environment (glovebox), as well as in the dark, immediate and complete decomposition of **1a** took place, suggesting extreme photochemical and thermal lability of **I**. To confirm these qualitative observations on the formation and lability of anion- π complex **I**, the abilities of different bases to form complexes with the substrate **1a** were analyzed by DFT calculations at the B3LYP-D/6-311+G* level of theory.³⁵ Firstly, the molecular electrostatic potential (MEP) was computed and plotted on the Van der Waals surface in order to

³⁵ Calculations have been performed by Prof. Antonio Frontera.

Anion- π interactions in light-induced reactions

ascertain the most electrophilic and nucleophilic parts of the substrate (Figure IV-8). The most negative region corresponds to the O atom of the carbonyl group ($-30 \text{ kcal mol}^{-1}$, colored red). On the other hand, the electrostatic potential over the aromatic ring is positive ($+23.8 \text{ kcal mol}^{-1}$, colored blue) due to the electron-withdrawing effect of the two nitro groups. Therefore, the substrate is well suited for establishing anion- π interactions.

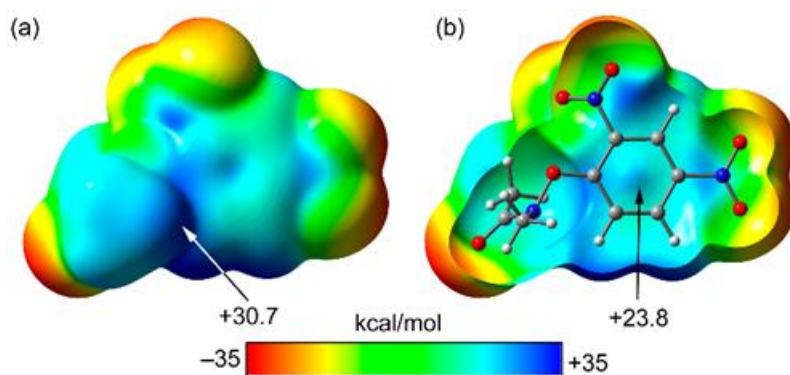


Figure IV-8. Closed a) and open b) MEP surfaces of **1a**.

Moreover, the H atom of the *N*-bonded methyl group that is directed towards the aromatic surface also exhibits a large and positive MEP ($+30.7 \text{ kcal mol}^{-1}$; see Figure IV-8, a). In summary, this MEP analysis implies that anionic bases will interact with the substrate through a combination of H-bonding and anion- π interactions.

Next, the EDA complexes of **1a** with monoanionic (hydrogencarbonate) and dianionic (carbonate) bases were computed both in the gas phase and taking into consideration solvent effects (using a polarized continuum model).³⁶ Key geometric features of the optimized geometries and

³⁶ The influence of the counteraction in the calculations was not considered because it was assumed that in acetonitrile solvent-separated ion pairs are present. The large differences between interaction energies in the gas phase and in acetonitrile arise from the fact that in the gas phase the energy needed to desolvate the anion is not taken into consideration.

interaction energies of the CT complexes are shown in Figure IV-9. As predicted by the MEP analysis, the complexes are stabilized by the concurrent formation of anion- π and H-bonding interactions in all cases (see Section IV.4.3.2). The corresponding equilibrium distances are shorter for the dianionic molecules because the electrostatic forces are stronger. Consequently, the interaction energies are significantly greater in absolute value for the dianionic bases. Thus, for all of the monoanionic complexes, the interaction energies in acetonitrile range from -1.7 to -0.9 kcal mol $^{-1}$, whereas for the dianionic complexes the interaction energies are all very similar (around -5 kcal mol $^{-1}$).

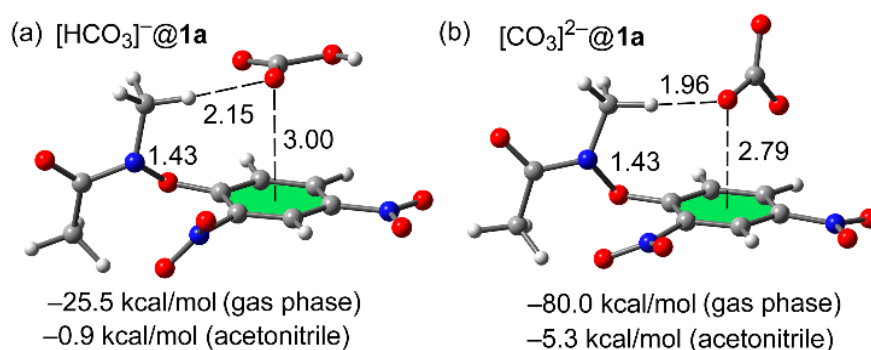


Figure IV-9. B3LYP-D/6-311+G* optimized geometries and energies of the hydrogencarbonate (a) and carbonate (b) complexes of **1a**. Distances in Å.

Interestingly, this correlates well with the ability of the different bases (Table IV-1) to promote the light-induced amidation and, in particular, with the observation that essentially the same yield (ca. 75%) was recorded for all of the studied dianionic bases. From a geometrical point of view, it is important to remark that the N–O distance increases upon formation of the EDA complex. The N–O distance in **1a** is 1.42 Å, and this increases to 1.43 Å in all the EDA complexes, thus revealing a weakening of the N–O bond upon complexation.

Anion- π interactions in light-induced reactions

A key point in our mechanistic hypothesis is the absorption of one photon by complex I leading to generation of the excited state I^* , in which an internal SET can take place. Analyzing the frontier orbitals of complex I, it is evident (Figure IV-10) that the HOMO is located in the anion region (a), while the LUMO is concentrated on the nitro groups and one carbon atom of the aromatic group.

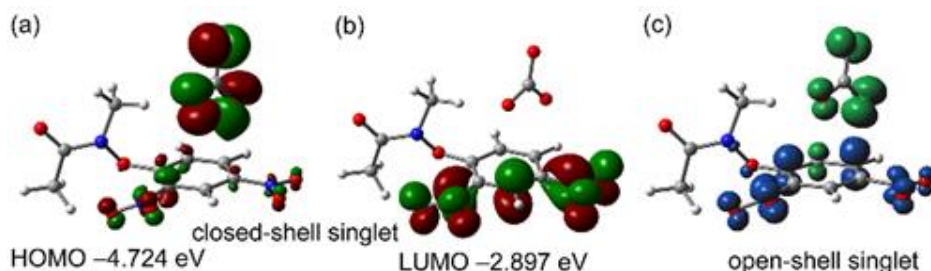


Figure IV-10. Plots of the HOMO (a) and LUMO (b) of complex I. (c) Spin density plot of the biradical open singlet configuration of I.

The very small computed HOMO-LUMO difference (1.83 eV) implies that low-lying excited states are accessible for this structure, and that internal SET should be quite feasible.

Moreover, since small HOMO-LUMO gaps are indicative of biradical or biradicaloid character, we examined the presence of such character in I. To do so, the electronic structure of the complex was recalculated using an open-shell singlet configuration, which led to an energy drop of 1.4 kcal mol⁻¹ (i.e., the biradical is predicted to be more stable than the closed-shell system). A spin density plot of this configuration is depicted in Figure IV-10 c, which clearly shows that the alpha electron (blue) is essentially located on the aromatic ring and nitro groups, whereas the beta electron is located on the carbonate. This corresponds to a situation in which an internal SET has taken place from the putative complex I^* . It is worthy of mention that attempted geometrical optimization of this configuration led to dissociation of the complex because of the mutual electrostatic repulsion of two negative

charges $[\text{CO}_3^{2-} \cdots \mathbf{1a}^{\cdot-}]$. Interestingly, the optimized structure of **II** exhibits an elongation of the N–O bond with respect to that in **1a** (Figure IV-11).

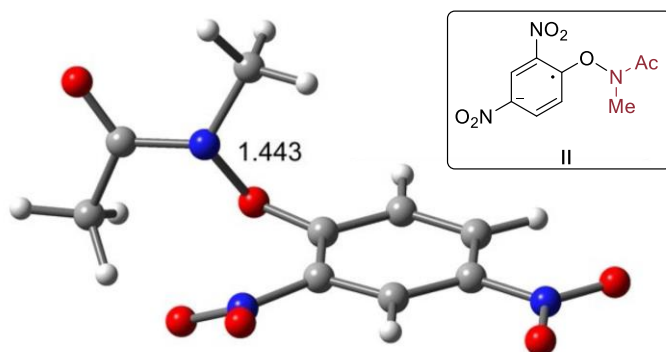
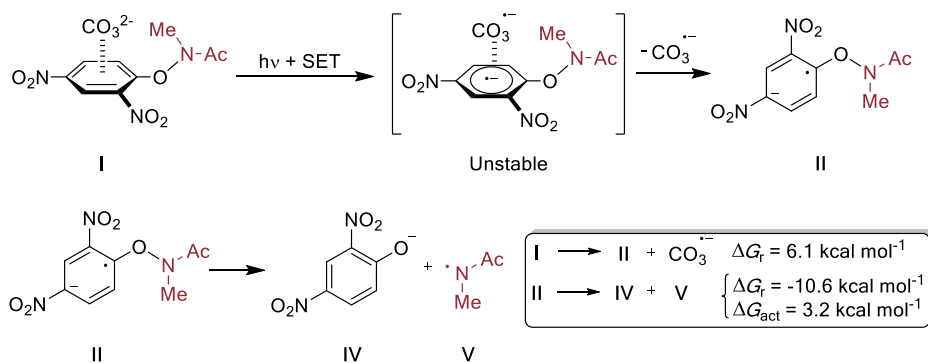


Figure IV-11. Optimized structure of **II**. Distances in Å.

Additional data from two different origins further confirmed the relevance of the anion- π complex in the light-mediated cleavage of **1a**. First, the results of time-dependent DFT calculations showed that the presence in **I** of the anion interacting with the π -system of **1a** increases the probability of excitation and decreases the absorption energy (see Section IV.4.3.2). Second, when homolysis of the N–O bond required for generation of the amidyl radical **IV** is considered (Scheme IV-10), it is found that direct homolysis of **I** yielding carbonate dianion and radicals **IV** and 2,4-dinitrophenoxyl radical is not energetically favorable ($\Delta G = 52.2 \text{ kcal mol}^{-1}$), this energy being almost identical to that calculated for **1a** ($\Delta G = 54.7 \text{ kcal mol}^{-1}$, See Section IV.4.3.2). In contrast, the transformation of **I** to **II** with the concomitant formation of CO_3^{2-} is more achievable [$\Delta G_r(\text{I} \rightarrow \text{II}) = 6.1 \text{ kcal/mol}$] and, remarkably, the subsequent homolysis of the transient intermediate **II**, yielding **IV** and **V** is predicted to be exergonic [$\Delta G_r(\text{II} \rightarrow \text{IV} + \text{V}) = -10.6 \text{ kcal mol}^{-1}$]. The calculated activation energy for this homolysis step is very low, $\Delta G_{\text{act}} = 3.2 \text{ kcal mol}^{-1}$, thus confirming the feasibility of this mechanistic route.

Anion- π interactions in light-induced reactions



Scheme IV-11. Energetics of the calculated generation of amidyl radical **IV** from anion- π complex **I**.

IV.3.4. Conclusions

In conclusion, anion- π interactions have been identified for the first time as an enabling phenomenon in light-mediated processes. Anion- π interactions involving carbonate anion have been described by spectroscopic and theoretical methods as the enabling step in the light-promoted amidation of arenes with activated aryloxy amides. The available evidence supports the hypothesis that π -interactions between carbonate and the electron-poor aryloxy amide facilitate the absorption of visible light, promoting the generation of a low-lying excited state that spontaneously undergoes internal SET and disintegration of the complex, providing a low-energy pathway for generation of the highly reactive amidyl radical.

Our results suggest that other poorly understood light-promoted processes involving the use of inorganic bases may also be reliant on hitherto overlooked anion- π interactions.

IV.4. Supporting Information C

IV.4.1. Table of contents

IV.4.2. General information	258
IV.4.3. Computational studies	260
IV.4.3.1. Theoretical methods	260
IV.4.3.2. Computational results	260
IV.4.4. Studies on the homolytic cleavage of the N–O bond in 1a	264
IV.4.5. Experimental procedures	268
IV.4.6. Product characterization	270
IV.4.7. References	279

Anion- π interactions in light-induced reactions

IV.4.2. General information

If not specified, all reagents were purchased and used without any further purification. All the light-induced reactions were degassed before irradiation, with 10 min flow of argon. The reaction progress was checked by thin layer chromatography (TLC). Therefore aluminium-foil backed silica TLC plates with a fluorescent indicator (TLC Silica gel 60 F254) from Merck were employed. Compounds were detected either with a UV lamp ($\lambda = 254$ nm) or by employing a p-anisaldehyde stain in sulfuric acid, acetic acid and ethanol. For column chromatography, Aldrich flash grade silica gel (230-400 mesh) was used as a stationary phase. UV-Vis measurements were carried out on a Shimadzu UV-2401PC spectrophotometer equipped with a photomultiplier detector, double beam optics and D2 and W light sources.

Fluorescence measurements were carried out on a Fluorolog Horiba Jobin Yvon spectrofluorimeter equipped with photomultiplier detector, double monochromator and Xenon light source.

High-resolution mass spectra (HRMS) was carried out using High Resolution Mass Spectrometry on Waters GCT gas chromatograph coupled time-of-flight mass spectrometer (GC/MS-TOF) with electron ionization (EI).

NMR spectra were recorded at 25°C on a Bruker Avance 400 or Bruker Avance 500 Ultrashield for ^1H NMR, 101 or 126 MHz for ^{13}C NMR in CDCl_3 , having the solvent resonance as internal standard. The chemical shifts (δ) were given in ppm and the coupling constants (J) are reported in Hz. Multiplicities were abbreviated by s (singlet), d (doublet), t (triplet) and m (multiplet). All products that are known were characterized by comparison of their physical and spectroscopic properties with those described in the literature.

The measured emission intensity of the blue LEDs at 700 mA is 75 mW/cm². LEDs were purchased from Digi-Key

(https://www.digikey.com/products/en?WT.z_cid=sp_1537_buynow&site=us&mpart=LZ4-40B208-0000).

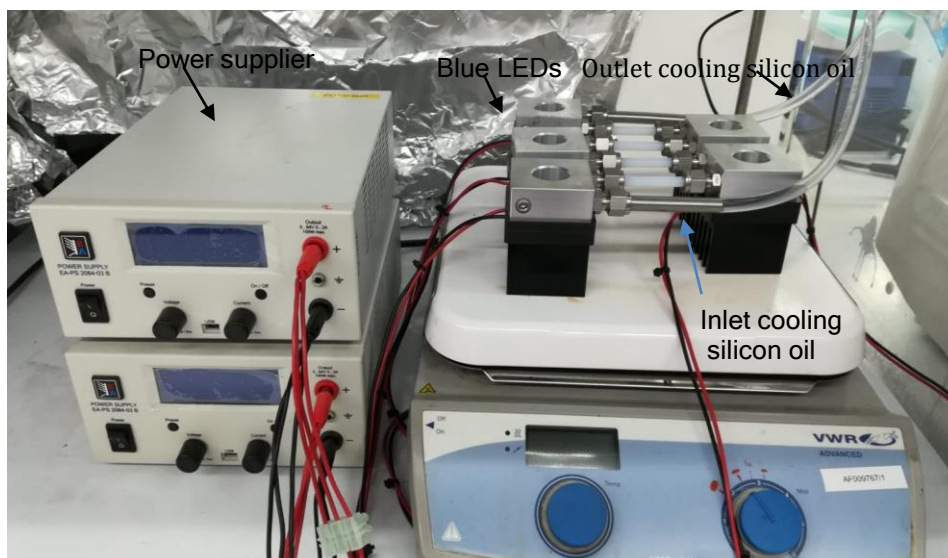


Figure IV-12. Set up of the light-induced amidation of aromatics.

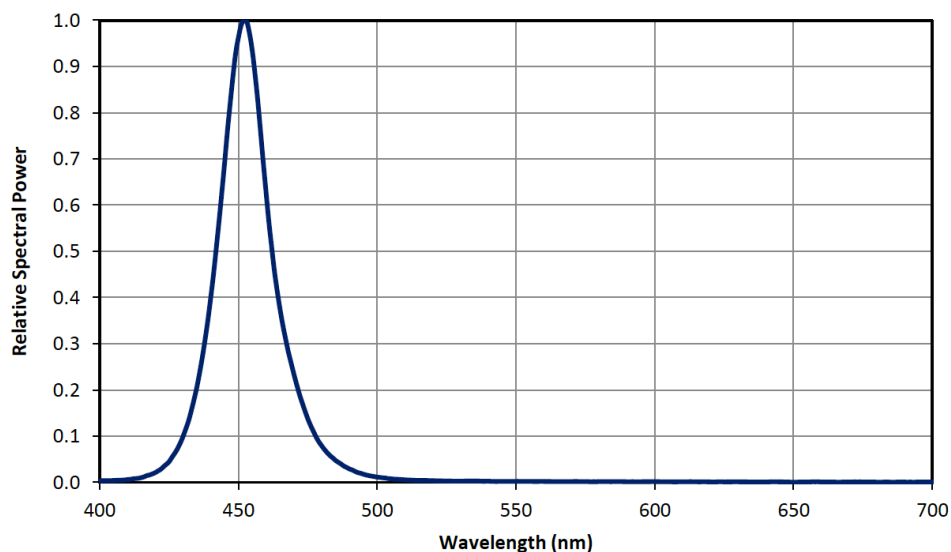


Chart IV-1. Typical relative spectral power vs. wavelength @ TC= 25°C (taken from LZ4-00B208 Product Datasheet 1.5 -11/19/2018 © 2018 LED ENGIN.ALL RIGHTS RESERVED).

IV.4.3. Computational studies

IV.4.3.1. Theoretical methods

The calculations have been performed using the B3LYP functional¹ adding Grimme's dispersion correction² and combined with the 6-311+G* basis set,³ which is a good compromise between the size of the system and the accuracy of the results. We have taken into consideration solvent effects (acetonitrile) using a polarized continuum model (PCM)⁴ as implemented in Gaussian-09.⁵ It uses the integral equation formalism model (IEFPCM).⁴ The molecular electrostatic potential surfaces have been computed at the same level of theory using the 0.001 isosurface as a good estimate of the Van der Waals surface. The geometries have been fully optimized without symmetry constrictions. In the anion- π complexes with dianions, a nucleophilic attack is in some cases observed. In these cases, we have preserved the planarity of the ring in the calculations. The transition states have been characterized using the standard procedure and in all cases, they present only one negative frequency connecting reactant and product.

IV.4.3.2. Computational results

As for the structures reported in Section IV.3.3, the interaction energies given in Figures IV-8 and IV-9 have been computed both in the gas phase and taking into consideration solvent effects (using a polarized continuum model) and the energies are considerably smaller in acetonitrile than in the gas phase, which are very large because the energy needed to desolvate the anion is not taken into consideration. As already stated, it is possible to observe that the interaction energies in acetonitrile are similar (varying from -1.7 to -0.9 kcal/mol) for all monoanionic complexes. For the dianionic complexes the interaction energies are also very similar (around -5 kcal/mol), in agreement with the experimental yield that is equivalent for all dianionic bases.

In conclusion, the dianionic bases form stronger anion- π complexes with the substrate than the monoanionic ones, which can be related with higher experimental yield obtained for the former.

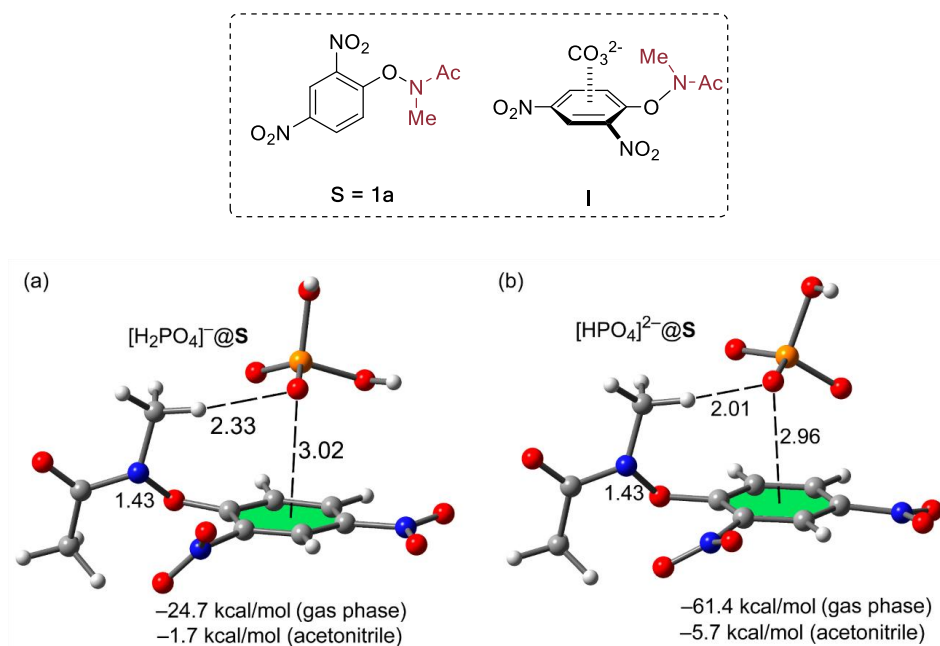


Figure IV-13. B3LYP-D/6-311+G* optimized geometries and energies of dihydrogenphosphate (a) and hydrogenphosphate (b) complexes. Distances in Å. (**S=1a**).

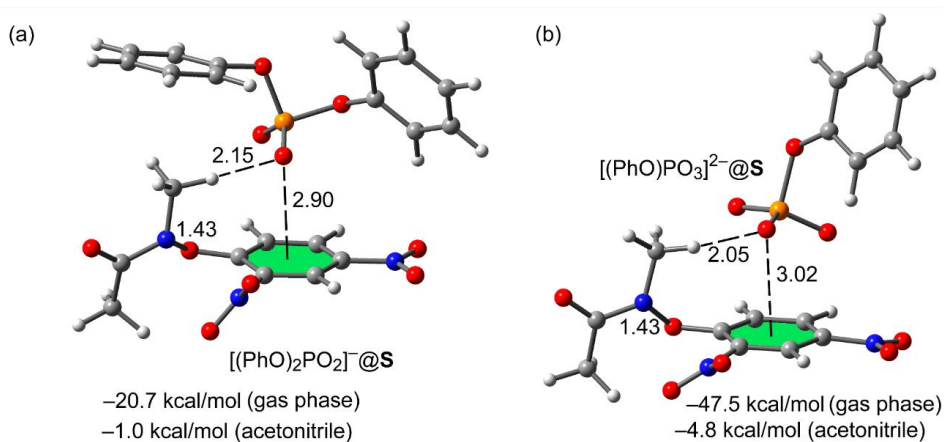


Figure IV-14. B3LYP-D/6-311+G* optimized geometries and energies of $[(\text{PhO})_2\text{PO}_2]^-$ (a) and $[(\text{PhO})\text{PO}_3]^{2-}$ (b) complexes. Distances in Å. (**S=1a**).

Anion- π interactions in light-induced reactions

In Figure IV-15, we show the Et₃N@S complex (with and without the H-atoms, S being **1a**) and also the X-ray structure of SEJCOZ,⁶ that we have used as starting point for the calculations (changing the *p*-Cl-phenyl ring by a methyl). In the optimized complex, the amine interacts with **1a** via an H-bonding contact with one aromatic H-atom at 2.39 Å. Moreover, some ancillary interactions between the O-atoms of the nitro groups and the H-atoms of the ethyl groups are also formed (not marked in the figure for clarity). In fact, the nitro group in ortho rotates (with respect to the X-ray structure) to facilitate these additional interactions. Using triethylamine, the electron transfer becomes difficult due to the location of the N-atom that is far from the π -system.

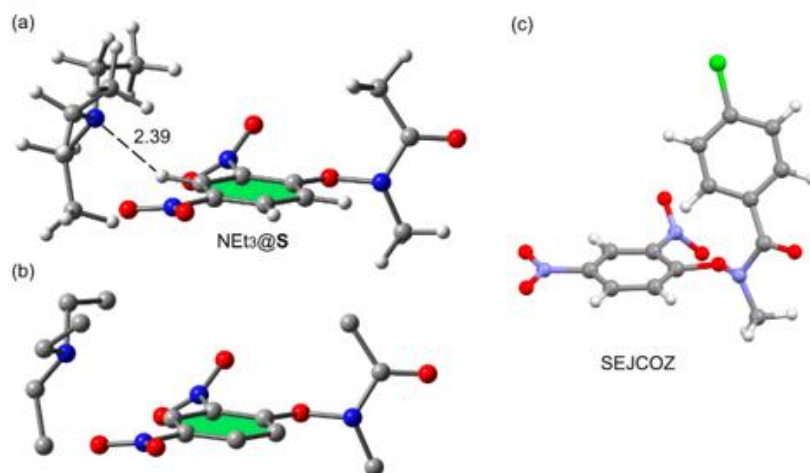


Figure IV-15. Optimized geometry of the complex of Et₃N with substrate S (S=**1a**), represented with (a) and without (b) the H-atoms. (c) X-ray structure of CSD refcode SEJCOZ.

We have performed TD-DFT calculations in compound **1a** and in the anion- π complex **I** to compare the transition energies. The results are gathered in Tables IV-2 and IV-3. In **1a** the first two excitations (3.4 eV and 3.7 eV for S₀→S₁ and S₀→S₂, respectively) require larger absorption energies than those in the anion- π complex (1.3 eV and 1.8 eV for S₀→S₁ and S₀→S₂,

respectively). Moreover, it is interesting to remark that the oscillator strength (probability of absorption) is very low for both transition of compound **1a** and the first transition of **I**. However, the probability of adsorption corresponding to the $S_0 \rightarrow S_2$ transition in the anion- π complex is high ($f = 0.1384$). Consequently, the presence of the anion interacting with the π -system increases the probability of excitation and decreases the absorption energy.

Excitations	Orbital transitions	Energy	Oscillator strength
$S_0 \rightarrow S_1$	HOMO-2 \rightarrow LUMO+1	3.4054 eV (364.08 nm)	$f = 0.0026$
	HOMO-1 \rightarrow LUMO+1		
	HOMO \rightarrow LUMO		
	HOMO \rightarrow LUMO+1		
$S_0 \rightarrow S_2$	HOMO-2 \rightarrow LUMO+1	3.7120 eV (334.01 nm)	$f = 0.0246$
	HOMO-1 \rightarrow LUMO		
	HOMO-1 \rightarrow LUMO+1		
	HOMO \rightarrow LUMO		

Table IV-2. Transitions, orbitals, Excitation energies and oscillator strengths in **1a** at the TD-B3LYP/6-311+G* (acetonitrile).

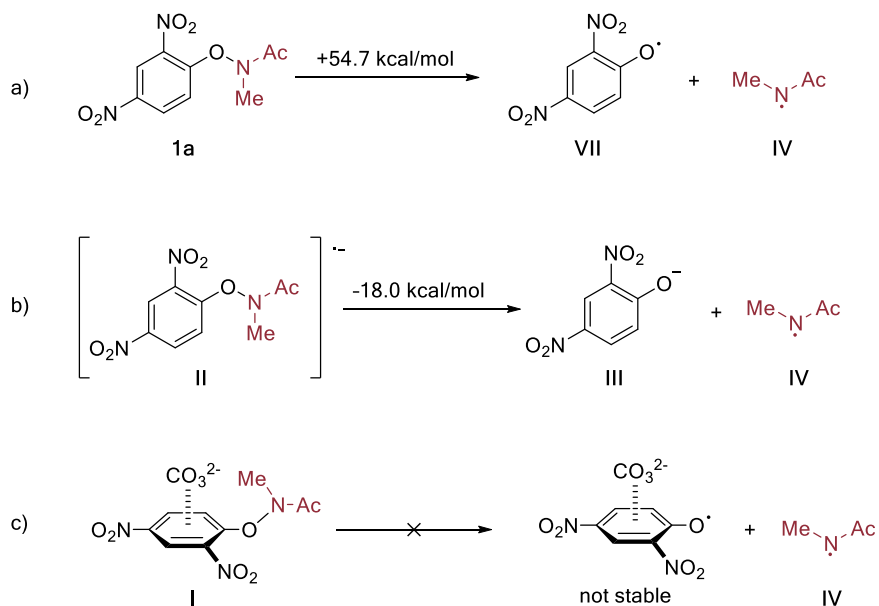
Excitation	Orbital transitions	Energy	Oscillator strength
$S_0 \rightarrow S_1$	HOMO \rightarrow LUMO	1.2945 eV (957.74 nm)	$f = 0.0178$
	HOMO \rightarrow LUMO+1		
$S_0 \rightarrow S_2$	HOMO-2 \rightarrow LUMO+1	1.7880 eV (693.43 nm)	$f = 0.1384$
	HOMO \rightarrow LUMO		
	HOMO \rightarrow LUMO+1		

Table IV-3. Transitions, orbitals, Excitation energies and oscillator strengths in **I** at the TD-B3LYP/6-311+G* (acetonitrile).

Moreover, we have analyzed several possibilities for the fragmentation of the N-O bond in different situations. The results are gathered in Scheme IV-12. The energy required to fragment the N-O bond in compound **1a** is calculated to be 54.7 kcal/mol, which is similar to the experimental dissociation energy of the N-O bond (48 kcal/mol)⁷ and, consequently, it is not energetically favored. In sharp contrast, the dissociation is thermodynamically favored (-18 kcal/mol) when it occurs in intermediate **II**.

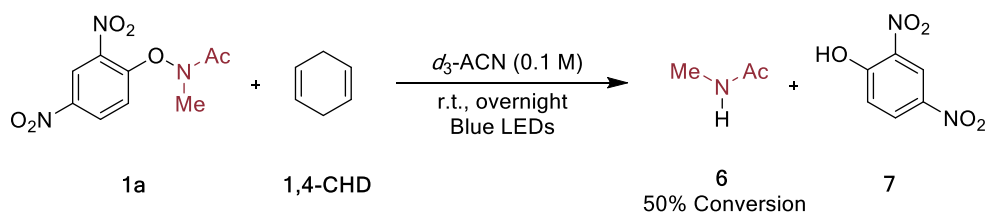
Anion- π interactions in light-induced reactions

If the homolytic process occurs directly from the anion- π complex, the supramolecular complex spontaneously dissociates and it is not stable (stationary point not found).



Scheme IV-12. Energetic study at the UB3LYP-D/6-311+G* level of theory in acetonitrile.

IV.4.4. Studies on the homolytic cleavage of the N–O bond in **1a**



Scheme IV-13. Study on the homolytic fragmentation of **1a**. Reaction conditions: **1a** (0.2 mmol), **1,4-CHD** (1.0 mmol), deuterated-acetonitrile (2.0 mL), blue LEDs, r.t., overnight. The conversion was measured by ^1H NMR.

Here, we report the ^1H NMR spectra in deuterated acetonitrile of compounds **1a**, **1,4-CHD** and **7** of the reaction reported in Scheme IV-13. At the end, we also report the comparison among the NMR spectra. It is possible to see that, although **1a** is not totally consumed yet, *N*-methyl acetamide (**7**) was formed.

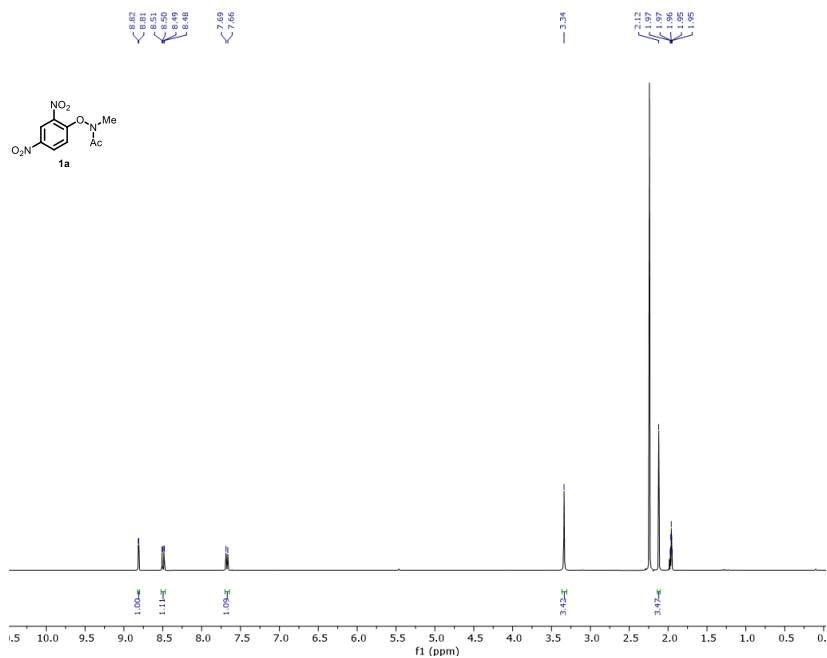


Figure IV-16. ^1H NMR of **1a** in d_3 -acetonitrile.

Anion- π interactions in light-induced reactions

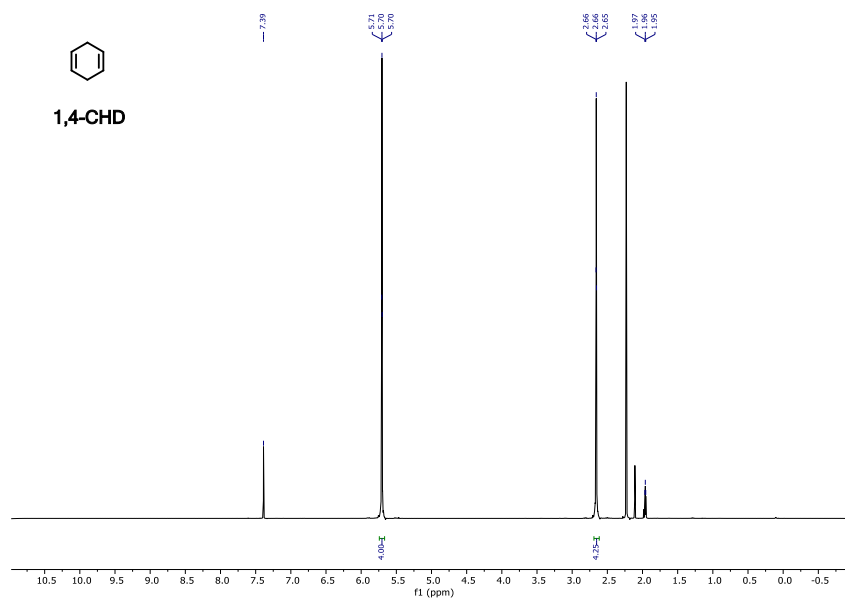


Figure IV-17. ^1H NMR of 1,4-CHD in d_3 -acetonitrile.

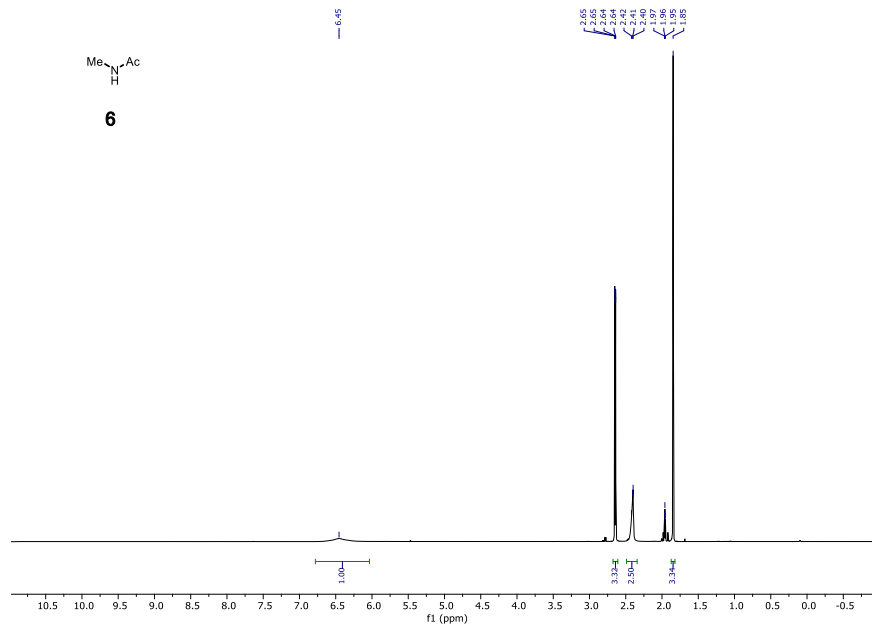


Figure IV-18. ^1H NMR of 6 in d_3 -acetonitrile.

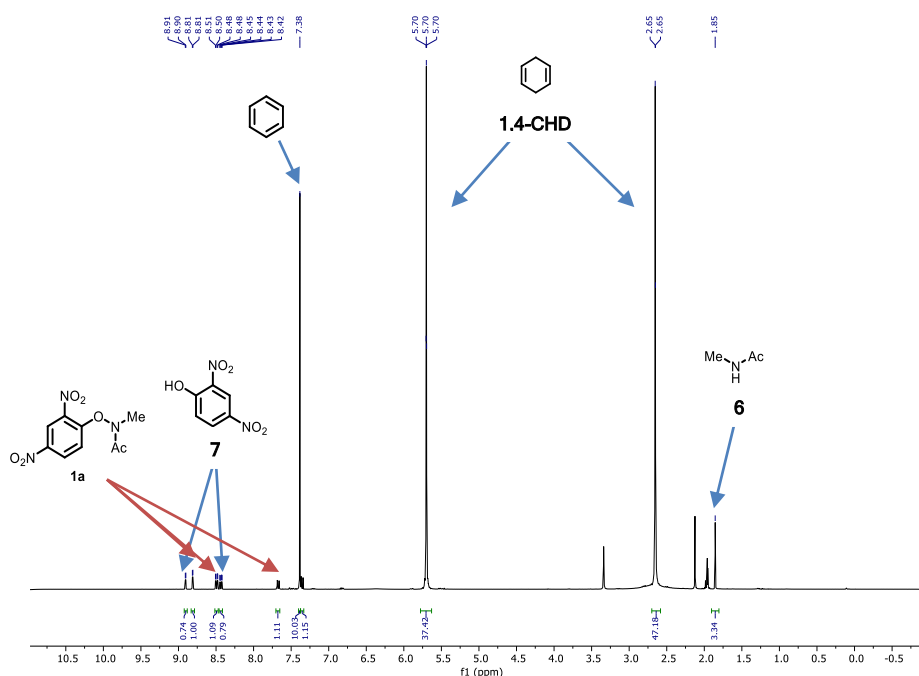
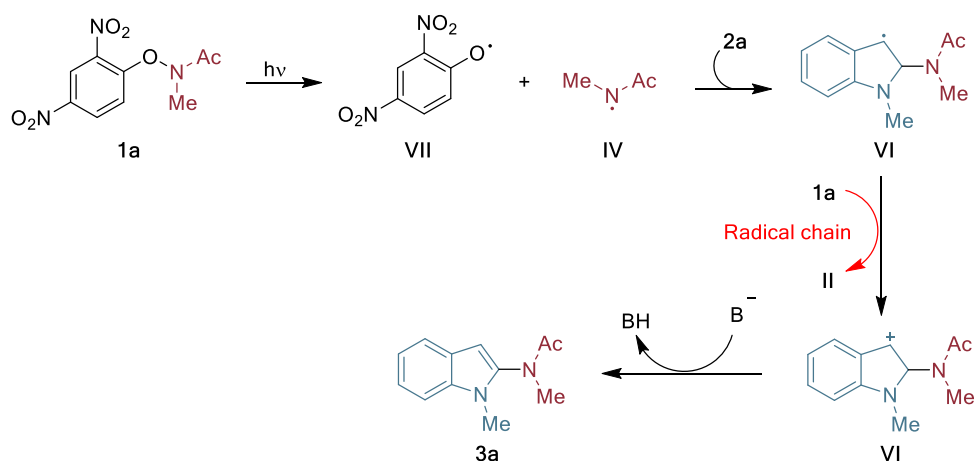


Figure IV-19. ^1H NMR of the reaction mixture in d_3 -acetonitrile.

Taking into account this experiment, we can propose a mechanism as the one reported in Scheme IV-14. Irradiation with the proper wavelength provokes the homolysis of the N-O bond in **1a**, which produces the amidyl radicals **IV** and **VII**. **IV** attacks the *N*-methyl indole affording **V**. This radical can reduce **1a** contributing to the radical chain propagation, so the carbocation **VI** is formed. The desired product **3a** is obtained either by deprotonation of **VI** or by hydrogen atom abstraction (HAT) on **V** exerted by **VII**. Although the homolysis contributes to the outcome of the reaction, it is worth to remind that the low conversion and yield observed when potassium carbonate is not employed indicates that this is not the main possibility.

Anion- π interactions in light-induced reactions



Scheme IV-14. Proposed mechanism of the light-promoted amidation initiated by the homolysis of **1a**.

IV.4.5. Experimental procedures

All the aryloxyamides **1a-1f** used as starting materials were prepared as described in literature,⁸ as well as the starting material **4**.⁹ Here, we report only the full characterization of **1g**, which was not previously described.

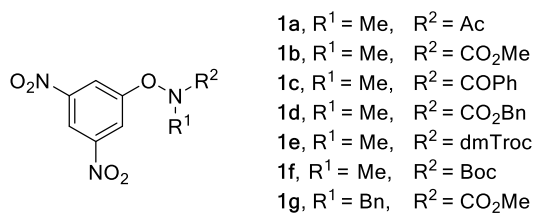
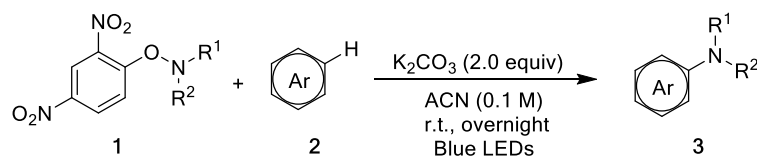


Figure IV-20. Synthesized starting materials.

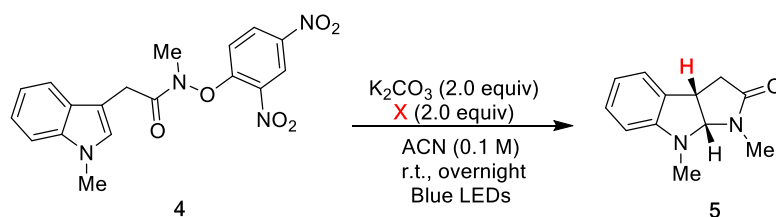
- **General procedure for the amidation reaction (GP1)**



Scheme IV-15. Amidation reaction.

The corresponding aryloxyamide (0.2 mmol) was mixed in a 10 mL vial with K_2CO_3 (0.4 mmol, 55 mg) and an aromatic compound (if solid) (0.4 mmol). Then the vial was sealed and three cycles of vacuum-refill with Ar were performed. After adding acetonitrile (2.0 mL) and degassing with a flow of argon for 10 minutes, the aromatic compound (0.4 mmol) was added with a syringe (when liquid) and the mixture was stirred under blue LEDs irradiation overnight. Afterward, it was washed with water (5.0 mL), extracted with EtOAc (3 x 4.0 mL) and dried over $MgSO_4$. The reaction mixture was then filtered and concentrated under vacuum. The desired product was purified by silica gel column chromatography (Petroleum ether/EtOAc 9:1 to 4:1).

- **General procedure for the cyclization reaction (GP2)**



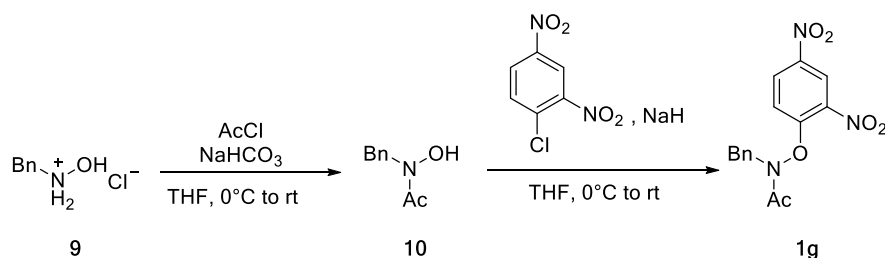
Scheme IV-16. Cyclization reaction. X = Radical trapping reagent.

Compound **4** (0.2 mmol) was mixed in a 10 mL vial with K_2CO_3 (0.4 mmol, 55 mg) and a radical scavenger (if solid) (0.4 mmol). Then the vial was sealed and three cycles of vacuum-refill with Ar were performed. After

Anion- π interactions in light-induced reactions

adding acetonitrile (2.0 mL) and degassing with a flow of argon for 10 minutes, the aromatic compound (0.4 mmol) (if liquid) was added with a syringe mixture was stirred under blue LEDs irradiation overnight. Afterward, it was washed with water (5.0 mL), extracted with EtOAc (3x4.0 mL) and dried over MgSO_4 . The reaction mixture was then filtered and concentrated under vacuum. The desired product was purified by silica gel column chromatography (Petroleum ether/EtOAc 9:1 to 4:1).

IV.4.6. Product characterization

Methyl benzyl(3,5-dinitrophenoxy)carbamate (**1g**)

Scheme IV-17. Preparation of starting material **1g**.

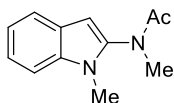
Compound **1g** was prepared following the procedure already reported in the literature and shown in Scheme 7.⁴ Starting from *N*-benzylhydroxylamine hydrochloride (**9**) (1.5 g, 9.40 mmol), **10** was obtained and used without further purification in the next step. After the second step, **1g** was obtained as a slightly yellow solid (2.5 g, 80% yield).

^1H NMR (400 MHz, CDCl_3) δ 8.79 (d, $J = 2.7$ Hz, 1H), 8.27 (dd, $J = 9.3, 2.7$ Hz, 1H), 7.37 - 7.25 (m, 6H), 4.94 (s, 2H), 2.20 (s, 3H).

^{13}C NMR (101 MHz, CDCl_3) δ 174.7, 156.5, 142.2, 136.7, 133.7, 129.6, 129.1, 129.0, 128.8, 122.2, 115.8, 53.8, 21.3.

HRMS (ESI) m/z calculated for $(\text{C}_{15}\text{H}_{13}\text{N}_3\text{NaO}_6)$ $[\text{M}+\text{Na}]^+$ 354.0697; found 354.0700.

N-methyl-*N*-(1-methyl-1*H*-indol-2-yl)acetamide (**3a**)⁸

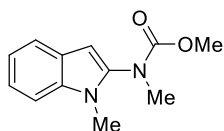


Following GP1, **3a** was prepared starting from **1a** (0.2 mmol, 51 mg) and 1-methyl indole (**2a**) (0.4 mmol, 52 mg) and it was isolated as an oil (30 mg, 75% yield).

¹H NMR (400 MHz, CDCl₃) δ 7.59 (dt, *J* = 7.9, 1.0 Hz, 1H), 7.34 - 7.22 (m, 2H), 7.13 (ddd, *J* = 8.0, 6.9, 1.2 Hz, 1H), 6.33 (d, *J* = 0.8 Hz, 1H), 3.72 (br s, 3H), 3.57 (s, 3H), 3.33 (s, 3H).

¹³C NMR (101 MHz, CDCl₃) δ 156.6, 134.9, 126.5, 122.1, 120.9, 120.0, 109.5, 96.0, 53.5, 38.9, 28.8.

Methyl methyl(1-methyl-1*H*-indol-2-yl)carbamate (**3b**)



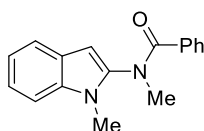
Following GP1, **3b** was prepared starting from **1b** (0.2 mmol, 54 mg) and 1-methyl indole (**2a**) (0.4 mmol, 52 mg) and it was isolated as oil (34 mg, 79% yield).

¹H NMR (400 MHz, CDCl₃) δ 7.59 (dt, *J* = 7.9, 1.0 Hz, 1H), 7.33 - 7.30 (m, 1H), 7.28 - 7.24 (m, 1H), 7.13 (ddd, *J* = 8.0, 6.9, 1.2 Hz, 1H), 6.33 (br s, 1H), 3.72 (s, 3H) 3.57 (s, 3H), 3.33 (s, 3H).

¹³C NMR (101 MHz, CDCl₃) δ 156.6, 134.9, 126.5, 122.1, 120.9, 120.0, 109.5, 96.0, 53.5, 39.0, 28.8.

HRMS (ESI) *m/z* calculated for (C₁₂H₁₅N₂O₂) [M+H]⁺ 219.1128; found 219.1125.

N-methyl-*N*-(1-methyl-1*H*-indol-2-yl)benzamide (**3c**)⁸

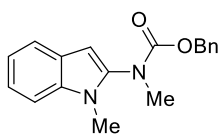


Following GP1, **3c** was prepared starting from **1c** (0.2 mmol, 63 mg) and 1-methyl indole (**2a**) (0.4 mmol, 52 mg) and it was isolated an oil (36 mg, 68% yield).

Anion- π interactions in light-induced reactions

^1H NMR (400 MHz, CDCl_3) δ 7.50 (d, $J = 7.9$ Hz, 1H), 7.38 (d, $J = 7.6$ Hz, 2H), 7.28 - 7.05 (m, 6H), 6.22 (s, 1H), 3.54 (s, 3H), 3.47 (s, 3H).

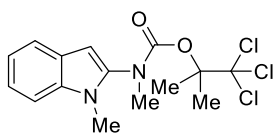
^{13}C NMR (101 MHz, CDCl_3) δ 171.1, 139.2, 135.1, 134.8, 130.4, 128.0 (2xC), 126.5, 122.2, 121.0 (2xC), 120.2, 109.6 (2xC), 98.2, 38.8, 29.0.

Benzyl methyl(1-methyl-1*H*-indol-2-yl)carbamate (**3d**)⁸

Following GP1, **3d** was prepared starting from **1d** (0.2 mmol, 69 mg) and 1-methyl indole (**2a**) (0.4 mmol, 52 mg) and it was isolated as an oil (36 mg, 61% yield).

^1H NMR (500 MHz, CDCl_3) δ 7.59 (dt, $J = 7.9, 1.0$ Hz, 1H), 7.39 - 7.18 (m, 7H), 7.13 (ddd, $J = 8.0, 6.7, 1.4$ Hz, 1H), 6.34 (s, 1H), 5.16 (br s, 2H), 3.46 (br s, 3H), 3.33 (s, 3H).

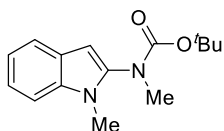
^{13}C NMR (126 MHz, CDCl_3) δ 156.0, 136.4, 134.9, 128.6, 128.2, 128.1, 126.5, 122.0, 120.9 (2xC), 119.9, 109.5 (2xC), 96.2, 67.8, 38.9, 29.8, 11.3.

1,1,1-trichloro-2-methylpropan-2-yl methyl(1-methyl-1*H*-indol-2-yl)carbamate (**3e**)⁸

Following GP1, **3e** was prepared starting from **1e** (0.2 mmol, 83 mg) and 1-methyl indole (**2a**) (0.4 mmol, 52 mg) and it was isolated as an oil (60 mg, 82% yield).

^1H NMR (400 MHz, CDCl_3) δ 7.78 (d, $J = 7.9$ Hz, 1H), 7.58 - 7.42 (m, 2H), 7.33 (ddd, $J = 8.0, 6.6, 1.4$ Hz, 1H), 6.54 (br s, 1H), 3.83 (s, 3H), 3.52 (br s, 3H), 2.15 (br s, 6H).

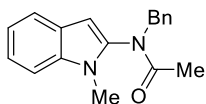
^{13}C NMR (101 MHz, CDCl_3) δ 153.6, 135.0, 126.5, 122.0, 120.9, 119.8, 109.4, 96.4, 89.4, 60.5, 53.5, 38.3, 28.7, 27.0, 21.7.

***tert*-butyl methyl(1-methyl-1*H*-indol-2-yl)carbamate (3f)⁸**

Following GP1, **3f** was prepared starting from **1f** (0.2 mmol, 63 mg) and 1-methyl indole (**2a**) (0.4 mmol, 52 mg) and it was isolated as an oil (31 mg, 60% yield).

¹H NMR (400 MHz, CDCl₃) δ 7.58 (dt, *J* = 7.8, 1.0 Hz, 1H), 7.33 - 7.27 (m, 1H), 7.24 (dd, *J* = 7.0, 1.2 Hz, 1H), 7.15 - 7.08 (m, 1H), 6.29 (s, 1H), 3.58 (s, 3H), 3.27 (s, 3H), 1.43 (br s, 9H).

¹³C NMR (101 MHz, CDCl₃) δ 155.1, 139.0, 134.8, 126.7, 121.6, 120.7, 119.7, 109.4, 95.5, 81.0, 38.5, 28.9, 28.4 (3xC).

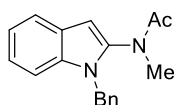
Methyl benzyl (1-methyl-1*H*-indol-2-yl)carbamate (3g)

Following GP1, **3g** was prepared starting from **1g** (0.2 mmol, 66 mg) and 1-methyl indole (**2a**) (0.4 mmol, 52 mg) and it was isolated as an oil (41 mg, 73% yield).

¹H NMR (500 MHz, CDCl₃) δ 7.56 (dt, *J* = 7.9, 1.0 Hz, 1H), 7.28 - 7.20 (m, 7H), 7.13 (ddd, *J* = 8.0, 5.4, 2.7 Hz, 1H), 6.20 (s, 1H), 4.92 (d, *J* = 13.9 Hz, 1H), 4.79 (d, *J* = 13.9 Hz, 1H), 3.25 (s, 3H), 1.87 (s, 3H).

¹³C NMR (126 MHz, CDCl₃) δ 171.7, 137.3, 137.0, 135.2, 129.3 (2xC), 128.6 (2xC), 127.9, 126.4, 122.5, 121.2, 120.3, 109.8, 98.9, 52.9, 28.4, 22.1.

HRMS (ESI) *m/z* calculated for (C₁₈H₁₈N₂NaO) 301.1311 [M+Na]⁺; found 301.1317.

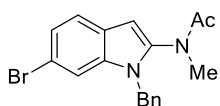
***N*-(1-benzyl-1*H*-indol-2-yl)-*N*-methylacetamide (3h)⁸**

Following GP1, **3h** was prepared starting from **1a** (0.2 mmol, 51 mg) and 1-benzyl indole (**2b**) (0.4 mmol, 83 mg) and it was isolated as an oil (36 mg, 65% yield).

Anion- π interactions in light-induced reactions

^1H NMR (500 MHz, CDCl_3) δ 7.64 (dt, $J = 7.9, 1.0$ Hz, 1H), 7.33 - 7.21 (m, 5H), 7.17 (ddd, $J = 8.1, 6.9, 1.2$ Hz, 1H), 7.08 - 7.00 (m, 2H), 6.41 (d, $J = 0.8$ Hz, 1H), 5.26 - 5.14 (m, 2H), 3.09 (s, 3H), 1.74 (s, 3H).

^{13}C NMR (126 MHz, CDCl_3) δ 172.2, 138.9, 136.9, 135.1, 129.0, 127.8, 126.6 (2xC), 126.5 (2xC), 123.0, 121.3, 120.6, 110.4, 98.7, 46.1, 37.1, 21.7.

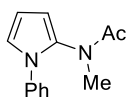
***N*-(1-benzyl-6-bromo-1*H*-indol-2-yl)-*N*-methylacetamide (3i)**

Following GP1, **3i** was prepared starting from **1a** (0.2 mmol, 51 mg) and 1-benzyl-6-bromo-1*H*-indole (**2c**) (0.4 mmol, 114 mg) and it was isolated as a yellow solid (36 mg, 50% yield).

^1H NMR (500 MHz, CDCl_3) δ 7.78 - 7.66 (m, 1H), 7.31 - 7.19 (m, 4H), 7.11 (dt, $J = 8.8, 0.7$ Hz, 1H), 7.02 - 6.91 (m, 2H), 6.33 (s, 1H), 5.22 - 5.12 (m, 2H), 3.05 (s, 3H), 1.69 (s, 3H).

^{13}C NMR (126 MHz, CDCl_3) δ 171.9, 139.8, 136.4, 133.7, 129.1 (2xC), 128.1, 128.0 (2xC), 126.4, 126.0, 123.8, 113.8, 112.0, 98.4, 46.3, 37.1, 21.7.

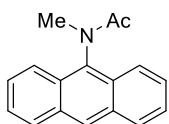
HRMS (ESI) m/z calculated for ($\text{C}_{18}\text{H}_{18}\text{BrN}_2\text{O}$) 357.0597 [$\text{M}+\text{H}$] $^+$; found 357.0597.

***N*-methyl-*N*-(1-phenyl-1*H*-pyrrol-2-yl)acetamide (3j)⁸**

Following GP1, **3j** was prepared starting from **1a** (0.2 mmol, 51 mg) and 1-phenyl pyrrole (**2d**) (0.4 mmol, 57 mg) and it was isolated as an oil (36 mg, 84% yield).

^1H NMR (500 MHz, CDCl_3) δ 7.44 - 7.40 (m, 2H), 7.37 - 7.31 (m, 1H), 7.23 - 7.18 (m, 2H), 6.79 (dd, $J = 3.2, 1.9$ Hz, 1H), 6.24 (t, $J = 3.4$ Hz, 1H), 6.10 (dd, $J = 3.7, 1.9$ Hz, 1H), 3.04 (s, 3H), 1.82 (s, 3H).

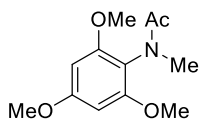
^{13}C NMR (126 MHz, CDCl_3) δ 172.5, 138.5, 132.4, 129.7 (2xC), 127.5, 124.6 (2xC), 120.3, 108.3, 106.2, 37.4, 21.9.

***N*-(anthracen-9-yl)-*N*-methylacetamide (3k)⁸**

Following GP1, 3k was prepared starting from **1a** (0.2 mmol, 51 mg) and anthracene (**2e**) (0.4 mmol, 71 mg) and it was isolated as a solid (22 mg, 45% yield).

¹H NMR (400 MHz, CDCl₃) δ 8.51 (s, 1H), 8.08 (ddt, *J* = 8.3, 1.4, 0.7 Hz, 2H), 7.95 (dq, *J* = 8.7, 1.0 Hz, 2H), 7.60 (ddd, *J* = 8.7, 6.6, 1.3 Hz, 2H), 7.53 (ddd, *J* = 8.0, 6.6, 1.3 Hz, 2H), 3.47 (s, 3H), 1.66 (s, 3H).

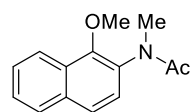
¹³C NMR (101 MHz, CDCl₃) δ 172.3, 135.5, 132.2, 129.1 (2xC), 128.4, 127.7 (2xC), 127.7 (2xC), 125.9 (2xC), 122.6 (2xC), 36.5, 21.8.

***N*-methyl-*N*-(2,4,6-trimethoxyphenyl)acetamide (3l)⁸**

Following GP1, **3l** was prepared starting from **1a** (0.2 mmol, 51 mg) and 1,3,5-trimethoxybenzene (**2f**) (0.4 mmol, 67 mg) and it was isolated as solid (22 mg, 47% yield).

¹H NMR (400 MHz, CDCl₃) δ 6.13 (s, 2H), 3.82 (s, 3H), 3.79 (s, 6H), 3.04 (s, 3H), 1.74 (s, 3H).

¹³C NMR (126 MHz, CDCl₃) δ 172.5, 160.7, 156.9 (2xC), 115.1, 90.8 (2xC), 55.9 (2xC), 55.6, 34.9, 21.1.

***N*-(1-methoxynaphthalen-2-yl)-*N*-methylacetamide (3m)⁸**

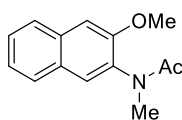
Following GP1, **3m** was prepared starting from **1a** (0.2 mmol, 51 mg) and 1-methoxynaphthalene (**2g**) (0.4 mmol, 63 mg) and it was isolated as an oil (22 mg, 48% yield).

¹H NMR (500 MHz, CDCl₃) δ 8.31 (ddd, *J* = 8.2, 1.4, 0.7 Hz, 1H), 7.70 (ddd, *J* = 8.3, 1.4, 0.7 Hz, 1H), 7.57 (ddd, *J* = 8.3, 6.8, 1.4 Hz, 1H), 7.52 (ddd, *J* =

Anion- π interactions in light-induced reactions

8.2, 6.8, 1.4 Hz, 1H), 7.24 (s, 1H), 6.78 (d, J = 8.1 Hz, 1H), 4.02 (s, 3H), 3.31 (s, 3H), 1.75 (s, 3H).

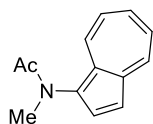
^{13}C NMR (126 MHz, CDCl_3) δ 172.0, 155.5, 133.7, 130.9, 128.0, 126.6, 126.1, 125.5, 123.0, 122.2, 103.4, 55.8, 37.2, 22.1.

***N*-(3-methoxynaphthalen-2-yl)-*N*-methylacetamide (3n)⁸**

Following GP1, **3n** was prepared starting from **1a** (0.2 mmol, 51 mg) and 2-methoxynaphthalene (**2h**) (0.4 mmol, 63 mg) and it was isolated as an oil (18 mg, 40% yield) .

^1H NMR (400 MHz, CDCl_3) δ 7.88 (br d, J = 9.1 Hz, 1H), 7.86 - 7.83 (m, 1H), 7.75 - 7.73 (m, 1H), 7.55 (ddd, J = 8.4, 6.8, 1.3 Hz, 1H), 7.41 (ddd, J = 8.4, 6.8, 1.3 Hz, 1H), 7.34 (d, J = 9.1 Hz, 1H), 3.98 (s, 3H), 3.24 (s, 3H), 1.72 (s, 3H).

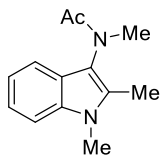
^{13}C NMR (101 MHz, CDCl_3) δ 172.4, 152.7, 131.4, 129.9, 129.4, 128.4, 128.1, 125.9, 124.4, 121.6, 113.4, 56.4, 35.2, 21.5.

***N*-(azulen-1-yl)-*N*-methylacetamide (3o)⁸**

Following GP1, **3o** was prepared starting from **1a** (0.2 mmol, 51 mg) and azulene (**2i**) (0.4 mmol, 51 mg) and it was isolated as a blue oil (35 mg, 87% yield).

^1H NMR (400 MHz, CDCl_3) δ 8.34 (d, J = 9.5 Hz, 1H), 8.13 (d, J = 9.7 Hz, 1H), 7.73 - 7.63 (m, 2H), 7.33 (d, J = 4.1 Hz, 1H), 7.27 - 7.18 (m, 2H), 3.38 (s, 3H), 1.77 (s, 3H).

^{13}C NMR (101 MHz, CDCl_3) δ 172.4, 138.9, 138.7, 138.4, 134.2, 133.0, 132.8, 131.7, 124.1, 123.5, 115.7, 37.9, 22.1.

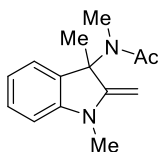
***N*-(1,2-dimethyl-1H-indol-3-yl)-*N*-methylacetamide (3p)**

Following GP1, **3p** was prepared starting from **1a** (0.2 mmol, 51 mg) and 1,2-dimethylindole (**2j**) (0.4 mmol, 58 mg) and it was isolated as a white solid (33 mg, 76% yield).

^1H NMR (500 MHz, CDCl_3) δ 7.39 (dt, $J = 7.8, 0.9$ Hz, 1H), 7.32 (dt, $J = 8.1, 0.9$ Hz, 1H), 7.22 (ddd, $J = 8.2, 7.0, 1.2$ Hz, 1H), 7.14 (ddd, $J = 7.9, 7.0, 1.0$ Hz, 1H), 3.70 (s, 3H), 3.26 (s, 3H), 2.32 (s, 3H), 1.84 (s, 3H).

^{13}C NMR (126 MHz, CDCl_3) δ 173.0, 135.4, 132.3, 123.6, 121.8, 120.2, 118.0, 116.9, 109.2, 36.5, 29.8, 21.6, 9.5.

HRMS (ESI) m/z calculated for ($\text{C}_{13}\text{H}_{17}\text{N}_2\text{O}$) 217.1335 $[\text{M}+\text{H}]^+$; found 217.1339.

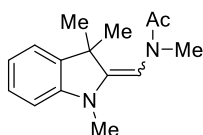
***N*-(1,3-dimethyl-2-methyleneindolin-3-yl)-*N*-methylacetamide (3q)**

Following GP1, **3q** was prepared starting from **1a** (0.2 mmol, 51 mg) and 1,2,3-trimethylindole (**2k**) (0.4 mmol, 64 mg) and it was isolated as an oil (26 mg, 57% yield).

^1H NMR (400 MHz, CDCl_3) δ 7.56 (dt, $J = 7.8, 1.0$ Hz, 1H), 7.30 - 7.27 (dt, $J = 8.1, 1.1$ Hz, 1H), 7.23 (ddd, $J = 8.2, 6.8, 1.2$ Hz, 1H), 7.12 (ddd, $J = 7.9, 6.8, 1.3$ Hz, 1H), 4.83 (s, 2H), 3.65 (s, 3H), 2.79 (s, 3H), 2.36 (s, 3H), 2.15 (s, 3H).

^{13}C NMR (101 MHz, CDCl_3) δ 170.5, 137.3, 130.9, 128.0, 122.1, 119.0, 118.8, 110.7, 109.1, 39.1, 33.9, 30.0, 22.2, 8.99.

HRMS (ESI) m/z calculated for ($\text{C}_{14}\text{H}_{18}\text{N}_2\text{NaO}$) 253.1311 $[\text{M}+\text{Na}]^+$; found 253.1310.

Anion- π interactions in light-induced reactions***N*-methyl-*N*-((1,3,3-trimethylindolin-2-ylidene)methyl)acetamide (**3r**)**

Following GP1, **3r** was prepared starting from **1a** (0.2 mmol, 51 mg) and 1,3,3-trimethyl-2-methyleneindoline (**2l**) (0.4 mmol, 69 mg) and it was isolated as an oil (21 mg, 43% yield).

Major diastereoisomer (*Z*): ^1H NMR (500 MHz, CDCl_3) δ 7.17 (td, $J = 7.7$, 1.3 Hz, 1H), 7.10 (ddd, $J = 7.3$, 1.3, 0.5 Hz, 1H), 6.85 (td, $J = 7.4$, 0.9 Hz, 1H), 6.62 (d, $J = 7.9$ Hz, 1H), 5.18 (s, 1H), 3.16 (s, 3H), 3.04 (s, 3H), 2.08 (s, 3H), 1.37 (s, 6H).

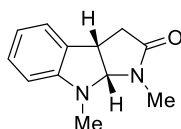
^{13}C NMR (126 MHz, CDCl_3) δ 172.5, 153.7, 146.9, 137.2, 128.0, 121.9, 119.9, 106.2, 98.6, 44.6, 37.4, 31.2, 30.2, 22.4.

Minor diastereoisomer (*E*): ^1H NMR (500 MHz, CDCl_3) δ 7.16 - 7.12 (m, 1H), 7.07 - 7.05 (m, 1H), 6.80 (dd, $J = 7.4$, 1.0 Hz, 1H), 6.56 (d, $J = 7.8$ Hz, 1H), 5.39 (s, 1H), 3.11 (s, 3H), 3.04 (s, 3H), 2.12 (s, 3H), 1.48 (s, 6H).

^{13}C NMR (126 MHz, CDCl_3) δ 174.3, 156.6, 145.7, 137.6, 128.0, 121.5, 119.2, 105.4, 101.7, 45.5, 39.9, 29.5, 27.4, 22.9.

HRMS (ESI) m/z calculated for ($\text{C}_{15}\text{H}_{21}\text{N}_2\text{O}$) 245.1648 $[\text{M}+\text{H}]^+$; found 245.1651.

The assignation of the *E*- and *Z*-diastereoisomer was made through ^1H NOESY experiment.

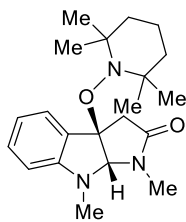
(3*aS*,8*aS*)-1,8-dimethyl-3,3*a*,8,8*a*-tetrahydropyrrolo[2,3-*b*]indol-2(1*H*)-one (5b**)⁹**

Following GP2, **5b** was prepared starting from **4** (0.2 mmol, 77 mg) and *tert*-butylthiol (0.4 mmol, 36 mg) and it was isolated as a white solid (24 mg, 60% yield).

^1H NMR (500 MHz, CDCl_3) δ 7.14 (tt, J = 7.7, 1.1 Hz, 1H), 7.05 (dq, J = 7.3, 1.1 Hz, 1H), 6.73 (td, J = 7.4, 1.0 Hz, 1H), 6.46 (d, J = 7.8 Hz, 1H), 5.07 (d, J = 8.0 Hz, 1H), 4.02 (m, 1H), 3.07 (s, 3H), 2.94 (d, J = 0.7 Hz, 3H), 2.93 - 2.85 (m, 1H), 2.59 (ddd, J = 17.2, 3.4, 0.8 Hz, 1H).

^{13}C NMR (126 MHz, CDCl_3) δ 173.6, 150.4, 131.2, 128.8, 124.2, 118.9, 107.6, 85.9, 38.7, 36.9, 35.8, 28.6.

(3a*R*,8a*S*)-1,8-dimethyl-3a-((2,2,6,6-tetramethylpiperidin-1-yl)oxy)-3,3a,8,8a-tetrahydropyrrolo[2,3-*b*]indol-2(1*H*)-one (5c)⁹



Following GP2, **5a** was prepared starting from **4** (0.2 mmol, 77 mg) and TEMPO (0.4 mmol, 62 mg) and it was isolated as a white solid (56 mg, 79% yield).

^1H NMR (300 MHz, CDCl_3) δ 7.30 - 7.23 (m, 1H), 7.18 (td, J = 7.7, 1.3 Hz, 1H), 6.78 (td, J = 7.5, 0.9 Hz, 1H), 6.45 (d, J = 8.0 Hz, 1H), 5.76 (s, 1H), 3.07 (dd, J = 104.2, 18.0 Hz, 2H), 3.08 (s, 3H), 2.98 (s, 3H), 1.53 - 1.38 (m, 6H), 1.12 (s, 3H), 0.99 (s, 3H), 0.93 (s, 3H), 0.37 (s, 3H).

^{13}C NMR (126 MHz, CDCl_3) δ 172.6, 150.8, 132.9, 130.0, 124.2, 119.0, 108.2, 88.2, 86.9, 60.1, 59.4, 46.8, 40.9, 40.4, 36.8, 33.4, 33.0, 28.4, 20.7, 20.4, 17.0.

IV.4.7. References

- Becke, A. D. *J. Chem. Phys.*, **1993**, *98*, 5648-52.
- Hehre, W. J.; Ditchfield, R.; Pople, J. A. *J. Chem. Phys.*, **1972**, *56*, 2257.
- Grimme, S. *J. Comp. Chem.*, **2006**, *27*, 1787-99.
- Scalmani G.; Frisch, M. J. *J. Chem. Phys.*, **2010**, *132*, 114110.

Anion- π interactions in light-induced reactions

⁵ Gaussian 09, Revision D.01, Frisch, M. J.; Trucks, G. W.; Schlegel, H. B.; Scuseria, G. E.; Robb, M. A.; Cheeseman, J. R.; Scalmani, G.; Barone, V.; Mennucci, B.; Petersson, G. A.; Nakatsuji, H.; Caricato, M.; Li, X.; Hratchian, H. P.; Izmaylov, A. F.; Bloino, J.; Zheng, G.; Sonnenberg, J. L.; Hada, M.; Ehara, M.; Toyota, K.; Fukuda, R.; Hasegawa, J.; Ishida, M.; Nakajima, T.; Honda, Y.; Kitao, O.; Nakai, H.; Vreven, T.; Montgomery, J. A., Jr.; Peralta, J. E.; Ogliaro, F.; Bearpark, M.; Heyd, J. J.; Brothers, E.; Kudin, K. N.; Staroverov, V. N.; Kobayashi, R.; Normand, J.; Raghavachari, K.; Rendell, A.; Burant, J. C.; Iyengar, S. S.; Tomasi, J.; Cossi, M.; Rega, N.; Millam, J. M.; Klene, M.; Knox, J. E.; Cross, J. B.; Bakken, V.; Adamo, C.; Jaramillo, J.; Gomperts, R.; Stratmann, R. E.; Yazyev, O.; Austin, A. J.; Cammi, R.; Pomelli, C.; Ochterski, J. W.; Martin, R. L.; Morokuma, K.; Zakrzewski, V. G.; Voth, G. A.; Salvador, P.; Dannenberg, J. J.; Dapprich, S.; Daniels, A. D.; Farkas, Ö.; Foresman, J. B.; Ortiz, J. V.; Cioslowski, J.; Fox, D. J. Gaussian, Inc., Wallingford CT, 2009.

⁶ Baughman, R. G.; Fountain, K. R.; Fountain, D. P.; Tappmeyer A. M. *J. Org. Chem.* **1989**, *54*, 5819-5821.

⁷ T.L. Cottrell, "The Strengths of Chemical Bonds" 2nd ed., Butterworths, London, **1958**.

⁸ Davies, J.; Svejstrup, T. D.; Reina, D. F.; Sheikh, N. S.; Leonori, D. *J. Am. Chem. Soc.* **2016**, *138*, 8092-8095.

⁹ Wu, K.; Du, Y.; Wei, Z.; Wang, T. *Chem. Commun.*, **2018**, *54*, 7443-7446

CHAPTER V

Conclusions

UNIVERSITAT ROVIRA I VIRGILI

Harnessing Visible Light for the Development of Novel Synthetic Strategies

Marco Michele Mastandrea

CHAPTER V

Conclusions

This PhD thesis was aimed to develop photochemical processes for the implementation of new synthetic methodologies. In this regard, approaches involving cooperative photoredox organo- and metal catalysis have been considered. In addition, the involvement of non-bonding interactions, such as anion- π forces, in photoredox transformations has been spotlighted. Consequently, three projects have been disclosed in the present thesis.

As described in Chapter II, the asymmetric cross-dehydrogenative coupling of aldehydes and xanthenes can be successfully accomplished through a hitherto unexplored strategy. The key feature of this approach lies in the two-step process employed to oxidize xanthenes to their corresponding carbocations. The mildness and selectivity enabled by photoredox catalysis allows to reach high level of stereocontrol, good yields and wide functional group tolerance. Moreover, non-symmetrical xanthenes are suitable substrates for the transformation, affording the corresponding products with high diastereoselectivity. A detailed DFT mechanistic study, supported by experimental data, suggests that hydrogen atom abstraction is the rate-limiting step and coupling of enamine and carbocation the selectivity-determining one.

Conclusions

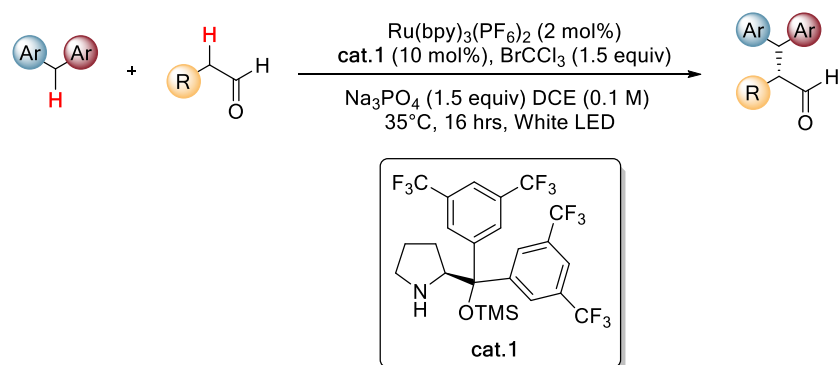


Figure V-1. Chapter II: asymmetric cross-dehydrogenative coupling of aldehydes with xanthenes.

In Chapter III, our research has been focused on the development of a catalytic method for the intermolecular hydroalkylation of terminal alkynes with carboxylic acids. The success of this transformation is due to the activation of alkynes towards radical addition in presence of a stable copper catalyst and visible light irradiation. Another key feature consists in the use of an organic photocatalyst for generating alkyl radicals *via* SET oxidation and isomerizing the alkenes, resulting from the reaction, to their *Z* isomer. Interestingly, HTE screening of reaction conditions revealed that the proper choice of ligand and base allows for a switch in the stereochemical outcome of the reaction. Moreover, practical advantageous aspects, consisting in the low cost and availability of the starting materials as well as catalysts, made this synthetic methodology a robust alternative to other photoredox hydroalkylation reactions.

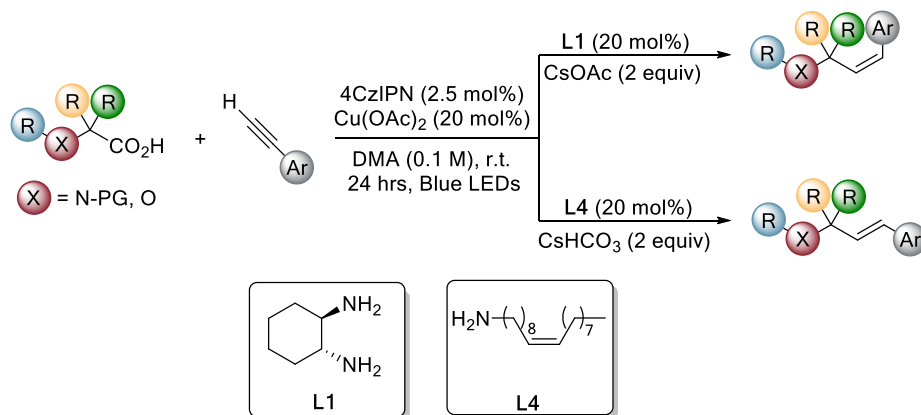


Figure V-2. Chapter III: decarboxylative hydroalkylation of alkynes.

Lastly, the participation of anion- π interactions in light-induced reactions has been described in Chapter IV. Anion- π interactions established by carbonate anion have been identified by spectroscopic and theoretical methods as the key forces involved in the light-promoted amidation of aromatic systems with activated aryloxy amides. The available evidence supports the hypothesis that an anion π -complex between carbonate and the electron-poor aryloxy is elicited, facilitating, in turn, the absorption of visible light. Upon visible light irradiation, electron excitation to a low-lying excited state triggers a spontaneous internal SET leading ultimately to the generation of amidyl radicals. These radicals have been efficiently trapped by electron-rich (hetero)arenes, affording the corresponding amidated products.

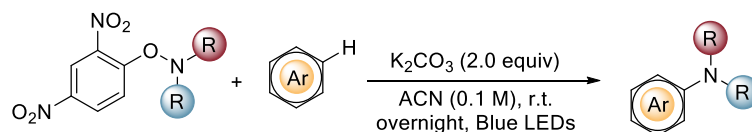


Figure V-3. Chapter IV: anion- π interactions in light-induced reactions.

UNIVERSITAT ROVIRA I VIRGILI

Harnessing Visible Light for the Development of Novel Synthetic Strategies

Marco Michele Mastandrea

UNIVERSITAT ROVIRA I VIRGILI

Harnessing Visible Light for the Development of Novel Synthetic Strategies

Marco Michele Mastandrea

UNIVERSITAT ROVIRA I VIRGILI

Harnessing Visible Light for the Development of Novel Synthetic Strategies

Marco Michele Mastandrea



UNIVERSITAT
ROVIRA i VIRGILI



Institut
Català
d'Investigació
Química